A UNITED STATES DEPARTMENT OF COMMERCE PUBLICATION

SECTION A

JOURNAL OF RESEARCH

of the NATIONAL BUREAU OF STANDARDS

JNBAAR 78A (1) 1-94, Jan.-Feb. 1974

Physics and Chemistry

U.S. DEPARTMENT OF COMMERCE
National Bureau of Standards

Journal of Research

of the

National Bureau of Standards

A. Physics and Chemistry

Jan.–Feb. • 1974

VOLUME • 78A

NUMBER • 1

Editor: C. W. Beckett

Associate Editor: D. D. Wagman

Publication dates:
Feb. 1, Apr. 1, June 1, Aug. 1, Oct. 1, Dec. 1, 1974

J. Res. Nat. Bur. Stand. (U.S.), A

JOURNAL OF RESEARCH

The National Bureau of Standards Journal of Research reports research and development in the fields of activity shown at right. Also included from time to time are survey articles on topics closely related to the Bureau's scientific and technical program.

The Journal is published in two separate sections as follows:

A. Physics and Chemistry

Contains papers of interest primarily to scientists working in these fields. Issued six times a year. Annual subscription: domestic, $17.00; foreign $21.25. Single copy, varies.

B. Mathematical Sciences

Presents studies and compilations designed mainly for the mathematician and the theoretical physicist. Issued quarterly. Annual subscription: domestic, $9.00; foreign, $11.25. Single copy, $2.25.

The National Bureau of Standards[1] was established by an act of Congress March 3, 1901. The Bureau's overall goal is to strengthen and advance the Nation's science and technology and facilitate their effective application for public benefit. To this end, the Bureau conducts research and provides: (1) a basis for the Nation's physical measurement system, (2) scientific and technological services for industry and government, (3) a technical basis for equity in trade, and (4) technical services to promote public safety. The Bureau consists of the Institute for Basic Standards, the Institute for Materials Research, the Institute for Applied Technology, the Institute for Computer Sciences and Technology, and the Office for Information Programs.

THE INSTITUTE FOR BASIC STANDARDS provides the central basis within the United States of a complete and consistent system of physical measurement; coordinates that system with measurement systems of other nations; and furnishes essential services leading to accurate and uniform physical measurements throughout the Nation's scientific community, industry, and commerce. The Institute consists of a Center for Radiation Research, an Office of Measurement Services and the following divisions:

Applied Mathematics — Electricity — Mechanics — Heat — Optical Physics — Nuclear Sciences[2] — Applied Radiation[2] — Quantum Electronics[3] — Electromagnetics[3] — Time and Frequency[3] — Laboratory Astrophysics[3] — Cryogenics[3].

THE INSTITUTE FOR MATERIALS RESEARCH conducts materials research leading to improved methods of measurement, standards, and data on the properties of well-characterized materials needed by industry, commerce, educational institutions, and Government; provides advisory and research services to other Government agencies; and develops, produces, and distributes standard reference materials. The Institute consists of the Office of Standard Reference Materials and the following divisions:

Analytical Chemistry — Polymers — Metallurgy — Inorganic Materials — Reactor Radiation — Physical Chemistry.

THE INSTITUTE FOR APPLIED TECHNOLOGY provides technical services to promote the use of available technology and to facilitate technological innovation in industry and Government; cooperates with public and private organizations leading to the development of technological standards (including mandatory safety standards), codes and methods of test; and provides technical advice and services to Government agencies upon request. The Institute consists of a Center for Building Technology and the following divisions and offices:

Engineering and Product Standards — Weights and Measures — Invention and Innovation — Product Evaluation Technology — Electronic Technology — Technical Analysis — Measurement Engineering — Structures, Materials, and Life Safety[4] — Building Environment[4] — Technical Evaluation and Application[4] — Fire Technology.

THE INSTITUTE FOR COMPUTER SCIENCES AND TECHNOLOGY conducts research and provides technical services designed to aid Government agencies in improving cost effectiveness in the conduct of their programs through the selection, acquisition, and effective utilization of automatic data processing equipment; and serves as the principal focus within the executive branch for the development of Federal standards for automatic data processing equipment, techniques, and computer languages. The Center consists of the following offices and divisions:

Information Processing Standards — Computer Information — Computer Services — Systems Development — Information Processing Technology.

THE OFFICE FOR INFORMATION PROGRAMS promotes optimum dissemination and accessibility of scientific information generated within NBS and other agencies of the Federal Government; promotes the development of the National Standard Reference Data System and a system of information analysis centers dealing with the broader aspects of the National Measurement System; provides appropriate services to ensure that the NBS staff has optimum accessibility to the scientific information of the world. The Office consists of the following organizational units:

Office of Standard Reference Data — Office of Technical Information and Publications — Library — Office of International Relations.

---

[1] Headquarters and Laboratories at Gaithersburg, Maryland, unless otherwise noted; mailing address Washington, D.C. 20234.
[2] Part of the Center for Radiation Research.
[3] Located at Boulder, Colorado 80302.
[4] Part of the Center for Building Technology.

U.S. DEPARTMENT OF COMMERCE
Frederick B. Dent, Secretary
NATIONAL BUREAU OF STANDARDS
Richard W. Roberts, Director

Order all publications from the Superintendent of Documents
U.S. Government Printing Office, Washington, D.C. 20402

The Secretary of Commerce has determined that the publication of this periodical is necessary in the transaction of the public business required by law of this Department. Use of funds for printing this periodical has been approved by the Director of the Office of Management and Budget through June 30, 1976.

JOURNAL OF RESEARCH of the National Bureau of Standards—A. Physics and Chemistry
Vol. 78A, No. 1, January–February 1974

Thermophysical Measurements on Iron Above 1500 K Using a Transient (Subsecond) Technique

Ared Cezairliyan and J. L. McClure

Institute for Materials Research, National Bureau of Standards, Washington, DC 20234

(September 11, 1973)

Simultaneous measurements of heat capacity, electrical resistivity and hemispherical total emittance of iron (99.9% pure) in the temperature range 1500 to 1800 K, and the melting point of iron by a subsecond duration, transient technique are described. The measurements indicate increases in heat capacity and electrical resistivity as the result of the solid-solid phase transformation ($\gamma \rightarrow \delta$) in iron. The measured value of the hemispherical total emittance at 1720 K is 0.33. The average of the results of two experiments yield a value of 1808 K for the melting point of iron. Estimated inaccuracies of measured properties are: 3 percent for heat capacity and emittance, 1 percent for electrical resistivity, and 5 K for the melting point.

Key words: Electrical resistivity; emittance; heat capacity; high-speed measurements; high temperature; iron; melting point; phase transformation; thermodynamics; thermophysical properties.

1. Introduction

Most of the reliable measurements of thermophysical and related properties of iron reported in the literature were performed at temperatures below 1500 K. Even at these temperatures, considerable disagreements exist between the results of various investigations. To a large extent, these disagreements may be attributed to difficulties associated with the magnetic and allotropic transformations in iron. The objective of the present work is to measure selected properties (heat capacity, electrical resistivity, hemispherical total emittance, and melting point) of iron above 1500 K using a transient technique.

The method is based on rapid resistive self-heating of the specimen from room temperature to high temperatures in less than one second by the passage of an electrical current pulse through it; and on measuring with millisecond resolution, such experimental quantities as current through the specimen, potential drop accross the specimen, and specimen temperature. Details regarding the construction and operation of the measurement system, the formulation of relations for the properties, the methods of measuring experimental quantities, and other pertinent information are given in earlier publications [1, 2] [1].

2. Measurements

Specimens: The specimens were tubes fabricated from rods[2] by removing the center portion using an electro-erosion technique. The nominal dimensions of the specimens were: length, 102 mm; outside diameter, 6.3 mm; and wall thickness, 0.5 mm. The outer surfaces of the specimens were polished to reduce heat loss due to thermal radiation.

Procedure: Because of the $\gamma \rightarrow \delta$ phase transformation in iron, the measurements were performed in the following two ranges: low (1500–1660 K), and high (1700–1800 K). Four experiments were conducted on two specimens; two experiments in the low range and two experiments in the high range. The duration of the current pulses in the experiments ranged from 500 to 900 ms, and the heating rate ranged from 2000 to 3500 $K \cdot s^{-1}$. Radiative heat loss from the specimen was, in all cases, less than 2 percent at 1500 K and less than 4 percent at 1800 K of the input power. All the experiments were conducted with the specimen in a vacuum environment of approximately 10^{-5} torr.

3. Experimental Results

The properties reported in this paper are based on the International Practical Temperature Scale of 1968 [3]. In all computations, the geometrical quantities are based on their room temperature (298 K) dimensions. The experimental results for the heat capacity and the electrical resistivity of iron (for each phase) are presented as linear functions in temperature. These functions were obtained by least squares approximation of the individual points corresponding to the measurements on the two specimens. The final values of the properties at 20 degree temperature intervals computed from these functions are presented in table 1. The results of individual experiments are given in the appendix.

[1] Figures in brackets indicate the literature references at the end of this paper.
[2] The specimens in rod form were furnished by the Office of Standard Reference Materials (OSRM) of NBS (Standard Reference Material 734–S, Electrolytic Iron, 99.9 % pure). The details regarding the impurities are documented by OSRM.

TABLE 1. *Heat capacity and electrical resistivity of iron*

Phase	Temperature (K)	c_p(J·mol^{-1}·K^{-1})	ρ($10^{-8}\Omega$·m)
γ-iron	1500	36.12	120.66
	1520	36.37	121.10
	1540	36.61	121.54
	1560	36.86	121.98
	1580	37.11	122.42
	1600	37.35	122.86
	1620	37.60	123.29
	1640	37.84	123.73
	1660	38.09	124.17
δ-iron	1700	41.46	125.35
	1720	42.09	125.65
	1740	42.72	125.96
	1760	43.35	126.26
	1780	43.99	126.57
	1800	44.62	126.87

Heat Capacity: Heat capacity was computed from data taken during the heating period. A correction for power loss due to thermal radiation was made using the single measured value of hemispherical total emittance in conjunction with the slope of emittance versus temperature function obtained from the literature [4].

The functions for heat capacity are:
In the temperature range 1500 to 1660 K (γ-iron),

$$c_p = 17.64 + 1.232 \times 10^{-2} T \qquad (1)$$

In the temperature range 1700 to 1800 K (δ-iron),

$$c_p = -12.28 + 3.161 \times 10^{-2} T \qquad (2)$$

where T is in K, and c_p is in J·mol^{-1}·K^{-1}. The standard deviation of experimental data from equations (1) and (2) is 0.4 percent. In the computations of heat capacity, the atomic weight of iron was taken as 55.85.

Electrical Resistivity: The electrical resistivity was determined from the same experiments that were used to calculate the heat capacity.

The functions for electrical resistivity are:
In the temperature range 1500 to 1660 K (γ-iron),

$$\rho = 87.72 + 2.196 \times 10^{-2} T \qquad (3)$$

In the temperature range 1700 to 1800 K (δ-iron),

$$\rho = 99.37 + 1.528 \times 10^{-2} T \qquad (4)$$

where T is in K and ρ is in $10^{-8}\Omega$·m. The standard deviation of experimental data from equations (3) and (4) is 0.5 percent. The electrical resistivity of one of the specimens measured at 293 K using a Kelvin bridge was $10.2 \times 10^{-8}\Omega$·m.

Hemispherical Total Emittance: In one of the experiments in the low temperature range, data were taken during the initial cooling period of the specimen which followed the heating period. The results yielded a value of 0.33 for the hemispherical total emittance at 1720 K.

Melting Point: The melting point of a specimen is manifested by a plateau in the temperature versus time function (fig. 1). The melting point of the specimen was determined by averaging the temperature points at the plateau. The results for two specimens (fig. 2) yielded the values 1807.5 K and 1808.6 K, with standard deviations of 0.2 K and 0.4 K, respectively. It may be concluded that the melting point of iron is 1808 K.

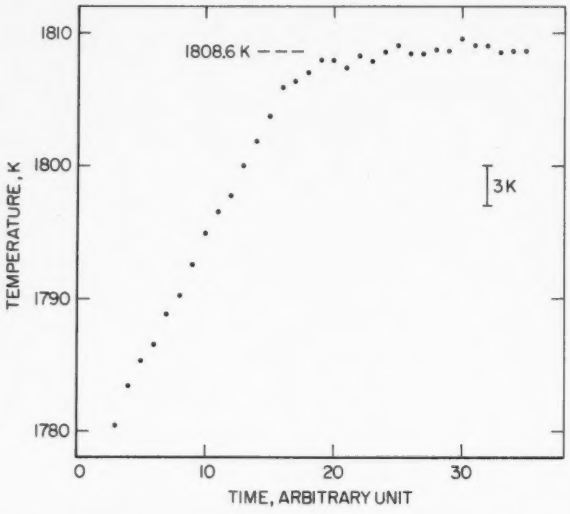

FIGURE 1. *Variation of temperature of iron (specimen 2) as a function of time near and at the melting point (1 time unit= 0.833 ms).*

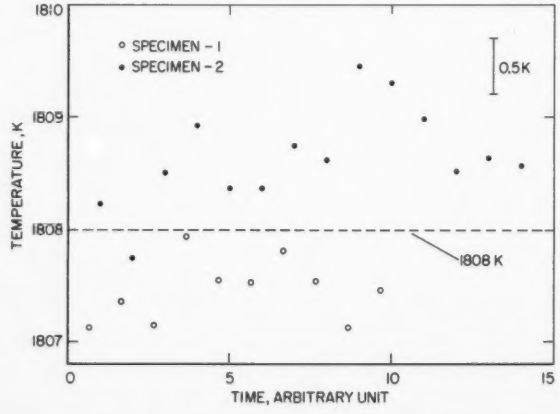

FIGURE 2. *Variation of temperatures of two iron specimens as a function of time at the melting point (1 time unit=0.833 ms).*

Estimate of Errors: The details for estimating errors in measured and computed quantities using the

present measurement system are given in an earlier publication [2]. In this paper, the specific items were recomputed whenever the present conditions differed from those in the earlier publication.

The results for imprecision[3] and inaccuracy[4] in the properties are: 0.6 percent and 3 percent for heat capacity, 0.5 percent and 1 percent for electrical resistivity, 0.5 K and 5 K for the melting point. The inaccuracy in the hemispherical total emittance is estimated to be 3 percent.

4. Discussion

The heat capacity and electrical resistivity results of this work are compared graphically with those in the literature in figures 3 and 4, respectively.

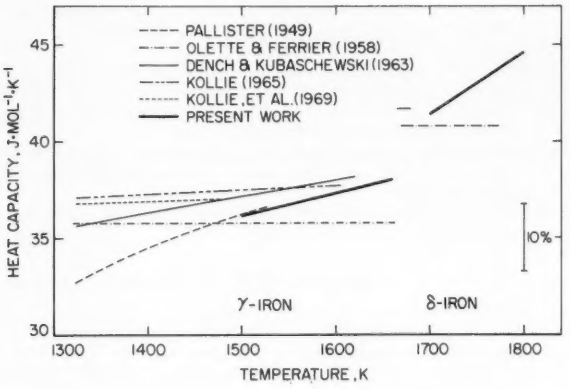

FIGURE 3. *Heat capacity of iron reported in the literature.*

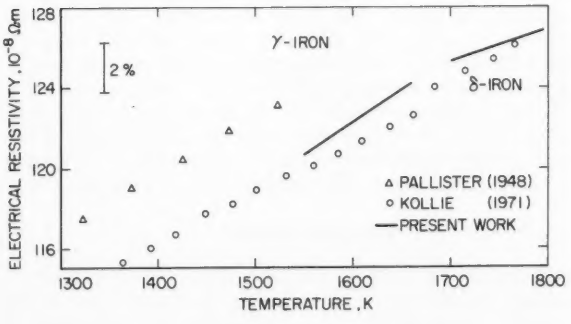

FIGURE 4. *Electrical resistivity of iron reported in the literature.*

From figure 3 it may be seen that at 1300 K considerable disagreements (up to approximately 10%) exist in the heat capacity values reported in the literature; however, immediately below the $\gamma \rightarrow \delta$ transformation the disagreements (especially between the results of recent investigations) are reduced to a value less than 3 percent. In contrast to the constant values for the heat capacity of δ-iron reported in the literature, the results of the present work show that heat capacity increases with temperature as the melting point is approached.

Figures 3 and 4 show that the heat capacity and electrical resistivity are discontinuous at the transformation point. Extrapolation of the properties to the transformation temperature (1683 K, based on preliminary measurements in this laboratory) indicates increases of approximately 7 percent in the heat capacity and 0.3 percent in the electrical resistivity during the $\gamma \rightarrow \delta$ transformation. Since the time resolution of the experiments was longer than the time required for the transformation, it is not likely that the high values for heat capacity above the transformation point were due to any residual transformation energy. The actual increase in the electrical resistivity is likely to be larger than the value given above because the expansion that occurs in iron during the $\gamma \rightarrow \delta$ transformation was not included in the electrical resistivity computations.

The melting point of iron reported in the literature is given in table 2. All the tabulated values are within 6 K of each other. The maximum difference of the present value from the values reported by other investigators is 4 K.

TABLE 2. *Melting point of iron*

Investigator	Reference	Year	Melting point* (K)
Bristow	11	1939	1806±5
Chipman & Marshall	12	1940	1807
Roeser & Wensel	13	1942	1812±1
Schofield & Bacon	14	1953	1810±10
Present work	...	...	1808±5

*All temperatures are corrected to the IPTS 1968.

The authors express their gratitude to C. W. Beckett for his encouragement of research in high-speed thermophysical measurements and to M. S. Morse for his help with the electronic instrumentation.

[3] Imprecision refers to the standard deviation of an individual point as computed from the difference between measured value and that from the smooth function obtained by the least squares method.

[4] Inaccuracy refers to the estimated total error (random and systematic).

5. Appendix

TABLE A–1. *Experimental results on heat capacity and electrical resistivity of iron**

Phase	Temperature K	Specimen 1		Specimen 2	
		c_p	ρ	c_p	ρ
γ-iron	1500	35.87	121.12	36.38	120.13
	1520	36.12	121.59	36.62	120.59
	1540	36.37	122.05	36.85	121.04
	1560	36.62	122.51	37.08	121.49
	1580	36.88	122.95	37.31	121.92
	1600	37.14	123.39	37.54	122.35
	1620	37.40	123.82	37.78	122.76
	1640	37.67	124.25	38.01	123.17
	1660	37.94	124.66	38.27	123.56
δ-iron	1700	41.37	125.80	41.66	124.87
	1720	41.95	126.13	42.22	125.22
	1740	42.58	126.45	42.83	125.54
	1760	43.18	126.71	43.48	125.83
	1780	43.81	127.07	44.13	126.08
	1800	44.51	127.38	44.86	126.30

*Heat capacity in $J \cdot mol^{-1} \cdot K^{-1}$, electrical resistivity in $10^{-8}\,\Omega \cdot m$.

6. References

[1] Cezairliyan, A., Design and operational characteristics of a high-speed (millisecond) system for the measurement of thermophysical properties at high temperatures, J. Res. Nat. Bur. Stand. (U.S.), **75C** (Eng. and Instr.), No. 1, 7 (Jan.–Mar. 1971).

[2] Cezairliyan, A., Morse, M. S., Berman, H. A., and Beckett, C. W., High-speed (subsecond) measurement of heat capacity, electrical resistivity, and thermal radiation properties of molybdenum in the range 1900 to 2800 K. J. Res. Nat. Bur. Stand. (U.S.), **75A** (Phys. and Chem.), No. 1, 65 (Jan.–Feb. 1970).

[3] International Practical Temperature Scale of 1968, Metrologia, **5**, 35 (1969).

[4] Touloukian, Y. S., and DeWitt, D. P., Thermal radiative properties-metallic elements and alloys, Thermophysical Properties of Matter, Vol. 7 (Plenum Press Inc., New York, 1970).

[5] Pallister, P. R., The specific heat and resistivity of high-purity iron up to 1250° C. J. Iron Steel Inst. (London), **161**, 87 (1949).

[6] Olette, M., and Ferrier, A., High temperature enthalpy of gamma and delta pure iron, NPL Symposium No. 9, Vol. 2, Paper 4 H (1958).

[7] Dench, W. A., and Kubaschewski, O., Heat capacity of iron at 800° to 1420° C. J. Iron Steel Inst. (London), **201**, 140 (1963).

[8] Kollie, T. G., M. S. Thesis, University of Tennessee (1965).

[9] Kollie, T. G., Barisoni, M., McElroy, D. L., and Brooks, C. R., Pulse calorimetry using a digital voltmeter for transient data acquisition, High Temp.-High Press., **1**, 167 (1969).

[10] Kollie, T. G., Private Communication, 1971.

[11] Bristow, C. A., Iron Steel Inst. Spec. Rep., No. 24, 1 (1939).

[12] Chipman, J., and Marshall, S., The equilibrium $FeO + H_2 = Fe + H_2O$ at temperatures up to the melting point of iron, J. Am. Chem. Soc. **62**, 299 (1940).

[13] Roeser, Wm. F., and Wensel, H. T., Freezing temperatures of high-purity iron and some steels, J. Research NBS **26**, 273 (1941)RP1375.

[14] Schofield, T. H., and Bacon, A. E., The melting point of titanium, J. Inst. Metals, **82**, 167 (1953).

(Paper 78A1–798)

JOURNAL OF RESEARCH of the National Bureau of Standards—A. Physics and Chemistry
Vol. 78A, No. 1, January–February 1974

Measurement of Melting Point, Normal Spectral Emittance (at Melting Point) and Electrical Resistivity (Near Melting Point) of Some Refractory Alloys*

Ared Cezairliyan

Institute for Materials Research, National Bureau of Standards, Washington, D.C. 20234

(October 23, 1973)

A subsecond duration pulse heating method is used to measure the melting point, normal spectral emittance (at the melting point, corresponding to 650 nm), and electrical resistivity (near the melting point) of the following refractory alloys: 90 Ta–10 W, 99 Nb–1 Zr, and 80 Nb–10 Ta–10 W (numbers indicate nominal composition in percentage by weight). The melting point and the normal spectral emittance are: 3286 ± 15 K and 0.396 for 90 Ta–10 W, 2737 ± 10 K and 0.351 for 99 Nb–1 Zr, and 2814 ± 10 K and 0.333 for 80 Nb–10 Ta–10 W. The inaccuracy of the normal spectral emittance and electrical resistivity results is estimated to be 3 percent and 0.5 percent, respectively.

Key words: Alloys; electrical resistivity; high temperature; melting point; normal spectral emittance; refractory materials; thermophysics.

1. Introduction

A millisecond resolution pulse heating technique was used earlier for the measurement of the melting point, normal spectral emittance (at the melting point), and electrical resistivity (near the melting point) of niobium [1][1]. In the present study, the same technique is used for similar measurements on the refractory alloys: 90 Ta–10 W, 99 Nb–1 Zr, and 80 Nb–10 Ta–10 W (numbers indicate nominal composition in percentage by weight).

The technique is based on resistive self-heating of the specimen from room temperature to its melting point in less than one second and measuring current through the specimen, potential difference across the specimen, and specimen temperature. These quantities are measured and recorded digitally every 0.4 ms with a full-scale signal resolution of approximately 1 part in 8000. The details regarding the construction and operational characteristics of the measurement system are given in an earlier publication [2].

2. Measurements

Melting point and electrical resistivity measurements were performed on specimens in the form of tubes having the following nominal dimensions: length, 102 mm; outside diameter, 6.3 mm; and thickness, 0.5 mm. A small rectangular hole (0.5 × 1 mm) fabricated in the wall at the middle of the specimen approximated blackbody conditions for temperature measurements. Normal spectral emittance measurements were performed on specimens in the form of rods having the following nominal dimensions: length 76 mm; diameter, 3.1 mm. The surfaces of all specimens were polished. The composition of the alloys is given in table 1.

TABLE 1. *Composition of the alloys*

Alloy	Major constituents (% by weight)	Total impurities (% by weight)
90 Ta–10 W	Ta, 90.45; W, 9.45	0.10
99 Nb–1 Zr	Nb, 98.78; Zr, 1.05	0.17
80 Nb–10 Ta–10 W	Nb, 80.94; Ta, 9.70; W, 9.30	0.06

Before starting the experiments, the specimens were heat treated by subjecting them to 30 heating pulses in the temperature range 2200 to 3000 K. The experiments were conducted in a vacuum environment of 10^{-4} to 10^{-5} torr. Duration of current pulses (duration for the specimen to heat from room temperature to its melting point) was in the range 380 to 750 ms.

For each alloy two experiments were performed for the determination of the melting point and one experiment was performed for the determination of normal spectral emittance and electrical resistivity. Designation of the specimens and the results of some of the

*This work was supported in part by the U.S. Air Force Office of Scientific Research.

[1] Figures in brackets indicate the literature references at the end of this paper.

measurements are given in table 2. All measurements reported in this paper are based on the International Practical Temperature Scale of 1968 [3].

specimen was obtained by averaging the temperature points on the plateau. The results are presented in table 2. The standard deviation of an individual point

TABLE 2. *Specimen designations and the results of individual experiments*

Specimen number	Substance	Geometry	Pulse length (ms)	Melting point			Radiance temp. at melting point		
				Number of temp.	Melting point (K)	Stand. dev. (K)	Number of temp.	Rad. temp. (K)	Stand. dev. (K)
1	90 Ta–10 W	tube	480	12	3287.0	1.3			
2	90 Ta–10 W	tube	750	15	3285.1	0.8			
3	90 Ta–10 W	rod	600				26	2888.7	0.4
4	99 Nb–1 Zr	tube	380	23	2737.0	1.9			
5	99 Nb–1 Zr	tube	390	24	2737.6	1.3			
6	99 Nb–1 Zr	rod	380				21	2423.2	0.8
7	80 Nb–10 Ta–10 W	tube	630	21	2816.1	0.3			
8	80 Nb–10 Ta–10 W	tube	660	30	2812.8	0.6			
9	80 Nb–10 Ta–10 W	rod	610				8	2469.2	0.2

2.1. Melting Point

Temperature of the tubular specimens was measured near and during the initial melting period. A plateau in temperature indicated the transition from solid to liquid phase. Measured temperatures at the plateau for specimens are shown in figure 1. The melting point for each

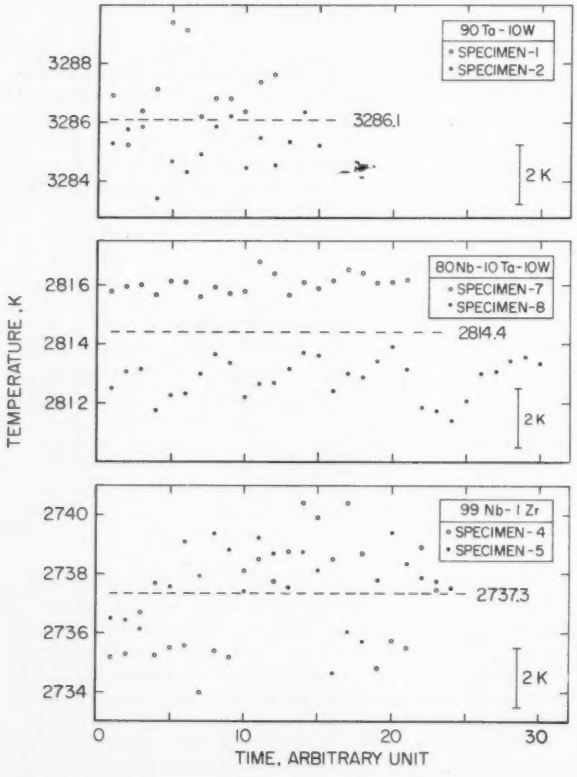

FIGURE 1. *Variation of the temperature of various refractory alloys as a function of time at their respective melting points (1 time unit = 0.833 ms).*

was in the range 0.3 to 1.9 K. As may be seen in table 2, the difference between the results for the two specimens of the same alloy was in the range 0.6 to 3.3 K. The average melting points of the alloys are given in table 3.

TABLE 3. *Melting point (T_m), radiance temperature (T_s) at the melting point, and normal spectral emittance (ϵ) at the melting point of some refractory alloys*

Substance	T_m(K)	T_s(K) (at 650 nm)	ϵ (at 650 nm)
90 Ta–10 W	3286	2889	0.396
99 Nb–1 Zr	2737	2423	0.351
80 Nb–10 Ta–10 W	2814	2469	0.333

2.2. Normal Spectral Emittance

Normal spectral emittance at the melting point of each alloy was determined from the measurements of the radiance temperature of the specimen (in rod form) and the average melting point obtained from the measurements on the tubular specimens. Based on the Wien radiation equation, the relation between emittance and temperature is

$$\epsilon = \frac{1}{\exp\left[\frac{c_2}{\lambda}\left(\frac{1}{T_s}-\frac{1}{T_m}\right)\right]}$$

where ϵ is the normal spectral emittance, T_m the melting point, T_s the radiance temperature, c_2 the second radiation constant (1.4388×10^{-2} m K), and λ the effective wavelength of the optical system. The measurements were performed at 650 nm which corresponds to the effective wavelength of the pyrometer's interference filter. The bandwith of the filter was 10 nm. The circular area viewed by the pyrometer was 0.2 mm in diameter.

The experimental results of the radiance temperature of 90 Ta–10 W and 99 Nb–1 Zr alloys near

and at the respective melting points are shown in figure 2. Similar results for the alloy 80 Nb–10 Ta–10 W are shown in figure 3. It may be seen (figure 2) that both 90 Ta–10 W and 99 Nb–1 Zr samples behaved normally, that is, radiance temperature increased and exhibited a plateau upon melting. However, 80 Nb–10 Ta–10 W results (figure 3) do not indicate the existence of any well-defined plateau, with the exception of a short segment immediately after reaching the melting point. The results of radiance temperature at the melting point of the alloys and corresponding values for the normal spectral emittance are given in table 3.

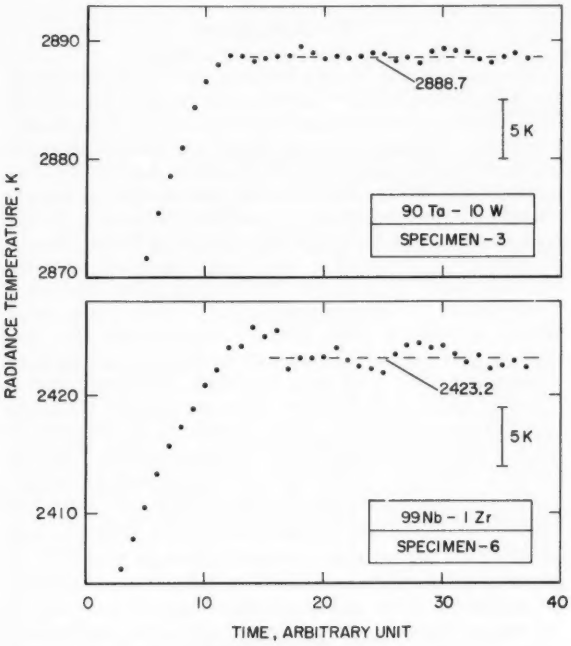

FIGURE 2. *Variation of the radiance temperature (at 650 nm) of the alloys* 90 Ta–10 W *and* 99 Nb–1 Zr *as a function of time near and at their respective melting points (1 time unit = 0.833 ms).*

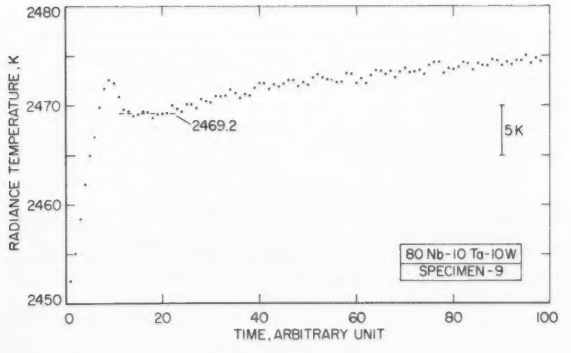

FIGURE 3. *Variation of the radiance temperature (at 650 nm) of the alloy* 80 Nb–10 Ta–10 W *as a function of time near and at its melting point (1 time unit = 0.833 ms).*

2.3. Electrical Resistivity

Electrical resistivity of the tubular specimens was calculated using the relation $\rho = RA/L$, where R is the resistance, A the cross-sectional area, and L the length of the specimen between the potential probes. The dimensions were based on their room temperature values; the cross-sectional area was determined from the measurement of weight and density. The results for the electrical resistivity of the alloys near and at their respective melting points are shown in figures 4, 5, and 6. The values for the 100 K range below the melting points are given in table 4. The results indicate that electrical resistivity of the alloys 90 Ta–10 W (figure 4) and 99 Nb–1 Zr (figure 5) changed almost abruptly at the start of melting. However, in the case of the alloy 80 Nb–10 Ta–10 W (figure 6) the change in the electrical resistivity was gradual, starting approximately 15 K below the melting point. Below the melting point electrical resistivity for each alloy was fitted, using the least squares method, to a linear function in temperature. In all cases, the standard deviation of an individual point from the smooth function was less than 0.06 percent.

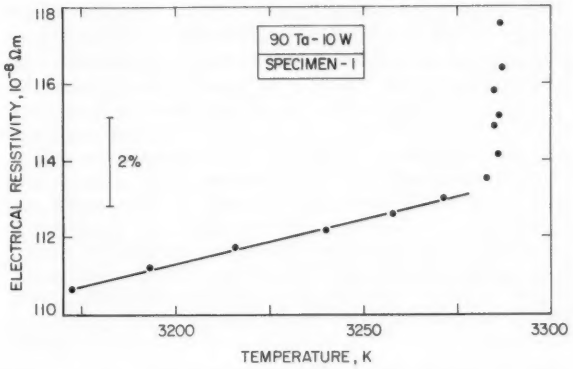

FIGURE 4. *Electrical resistivity of the alloy* 90 Ta–10 W *near and at its melting point.*

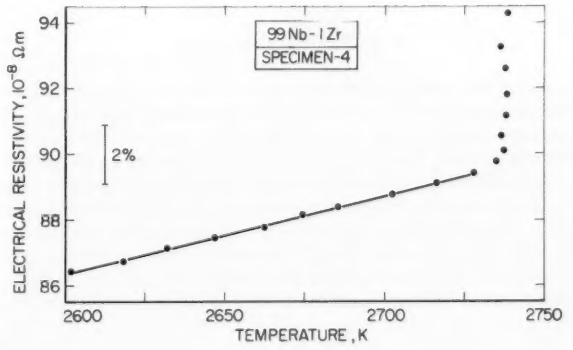

FIGURE 5. *Electrical resistivity of the alloy* 99 Nb–1 Zr *near and at its melting point.*

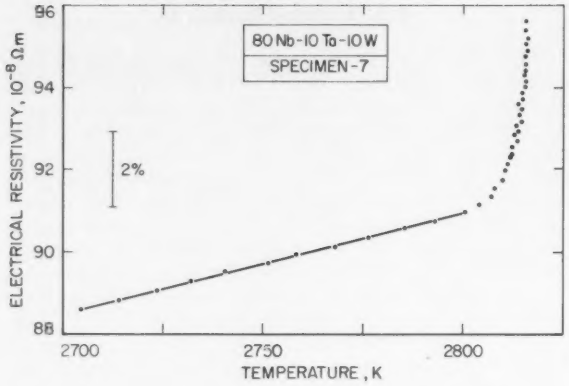

FIGURE 6. *Electrical resistivity of the alloy* 80 Nb–10 Ta–10 W *near and at its melting point.*

TABLE 4. *Electrical resistivity of some refractory alloys near their melting points*

Alloy	Temp. (K)	Elec. res.* (10^{-8} Ω m)
90 Ta–10 W	3180	110.88
	3230	112.03
	3280	113.17
99 Nb–1 Zr	2630	87.06
	2680	88.25
	2730	89.43
80 Nb–10 Ta–10 W	2700	88.49
	2750	89.70
	2800	90.92

*Based on ambient temperature (298 K) dimensions.

2.4. Estimate of Errors

Sources and estimates of errors in experiments similar to the ones conducted in this study are given in earlier publications [4, 5]. Specific items in the error analysis were recomputed whenever the present conditions differed from those in the earlier publications.

As it may be seen from table 2, the imprecision[2] of true (blackbody) and radiance temperature measurements was 0.3–1.9 K and 0.2–0.8 K, respectively. A somewhat higher imprecision in the case of the blackbody temperature measurements may be attributed to the movements of the sighting hole in the specimen during melting. The inaccuracy[3] of the melting points is estimated to be approximately 10 K for the alloys 99 Nb–1 Zr and 80 Nb–10 Ta–10 W, and 15 K for 90 Ta–10 W.

The combination of inaccuracies in the temperature measurements, taking into account likely common errors in both blackbody and radiance temperature measurements, indicates that the inaccuracy in the normal spectral emittance is approximately 3 percent.

The imprecision of the electrical resistivity results is 0.05 percent and the estimated inaccuracy is 0.5 percent.

3. Discussion

The agreement of the melting points of the specimens of the same alloy were in the range 0.6 to 3.3 K, indicating reasonably good reproducibility of the measurements. Radiance temperature and electrical resistivity of the binary alloys 90 Ta–10 W and 99 Nb–1 Zr behaved normally, that is exhibited an almost abrupt change at the beginning of melting. However, in the case of the ternary alloy 80 Nb–10 Ta–10 W the change in electrical resistivity was more gradual, starting approximately 15 K below the melting point. Radiance temperature of the ternary alloy exhibited a peak before melting, a short plateau immediately after the start of melting, and a continuous increase as melting progressed. The peak may be due to the roughness of the solid surface, and the increase in radiance temperature during melting may be attributed to the increase of the normal spectral emittance during melting. With the present system it was not possible to follow the entire melting process because the specimens collapsed and opened the electrical circuit prior to the completion of melting.

4. References

[1] Cezairliyan, A., Measurement of melting point, normal spectral emittance (at melting point), and electrical resistivity (above 2650 K) of niobium by a pulse heating method, High Temperatures – High Pressures, **4**, 453 (1972).

[2] Cezairliyan, A., Design and operational characteristics of a high-speed (millisecond) system for the measurement of thermophysical properties at high temperatures, J. Res. Nat. Bur. Stand. (U.S.), **75C** (Eng. and Instr.), 7 (1971).

[3] International Practical Temperature Scale of 1968, Metrologia, **5**, 35 (1969).

[4] Cezairliyan, A., Morse, M. S., Berman, H. A., and Beckett, C. W., High-speed (subsecond) measurement of heat capacity, electrical resistivity, and thermal radiation properties of molybdenum in the range 1900 to 2800 K, J. Res. Nat. Bur. Stand. (U.S.), **74A** (Phys. and Chem.), 65 (1970).

[5] Cezairliyan, A., Morse, M. S., and Beckett, C. W., Measurement of melting point and electrical resistivity (above 2840 K) of molybdenum by a pulse heating method, Rev. Int. Hautes Tempér. et Réfract., **7**, 382 (1970).

(Paper 78A1–799)

[2] Imprecision refers to the standard deviation of an individual point as computed from the difference between measured value and that from the smooth function obtained by the least squares method.

[3] Inaccuracy refers to the estimated total error (random and systematic).

JOURNAL OF RESEARCH of the National Bureau of Standards—A. Physics and Chemistry
Vol. 78A, No. 1, January–February 1974

Comparative Density Measurements for Solid Specimens Weighing a Few Milligrams

A. D. Franklin and J. R. Donaldson

Institute for Materials Research, National Bureau of Standards, Washington, D.C. 20234

(September 18, 1973)

A density comparison technique previously described has been used to compare the densities of tungsten wires weighing about 1.3 mg to within a few percent error. For larger, less dense specimens the expected random error of a few parts in 10^4 was confirmed by comparing the known densities of Si and CaF_2.

Key words: CaF_2; density; measurement technique; Si; tungsten wires.

1. Introduction

In this laboratory we have recently been using a new technique [1][1] for the comparison, to moderately high precision, of the densities of solid specimens weighing less than 100 mg. In reference [1] we showed that the technique compared the densities of pure and lightly-doped CaF_2 (density, 3.2 g/cm^3) to about 3 parts in 10^4. The densities of all of these specimens differed among themselves by less than 1 percent, and were not too different from the density (1.8 g/cm^3) of the flotation liquid used in the determinations, so that as an example of the use of the technique this work presented a particularly favorable case. In the present paper we report the application of the technique to two less favorable cases:

(i) A comparison of the densities of pure CaF_2 and Si, with results again precise to about 3 parts in 10^4.

(ii) A comparison of the densities of one group of 1 mg tungsten wires to that of another group as comparison standards. The precision attained was about 2 to 7 parts in 10^2. The degradation in precision arises from the small specimen size and also from the very high density of tungsten (19.2 g/cm^3) relative to that of the flotation liquid.

2. Experimental Details

The experimental technique and the constants of the density apparatus were as described in reference [1], except that a more sophisticated temperature bath was employed, so that the temperature was held to within 0.05 °C during the course of a run. The upper liquid used was water containing a few tenths percent ethylene glycol. The lower liquid was a proprietary fluorocarbon marketed by the 3M Company under the designation FC75.[2] Its density at 25 °C is 1.767 g/cm^3.

The ratio (ρ_u/ρ_s) of the density of an unknown to that of a set of comparison standards is found by measuring the differences in float position when the unknown is substituted for each of the comparison standards. These differences are linear in the masses of the comparison standards, and if the intercept and slope of a plot of difference against mass are designated by a and b, the density ratio can be computed using eq (4) of reference [1].

$$\rho_u/\rho_s = [Q + (\rho_s/\rho_2)(1-Q)]^{-1}, \qquad (1)$$

where ρ_u, ρ_s, and ρ_2 are the densities of the unknown, the comparison standards, and the (lower) flotation liquid, and Q is given by

$$Q = (-a/b)/M_u$$

where M_u is the mass of the unknown.

The mass values for the density measurements were computed from direct comparisons of the unknown object with items of known mass determined by the Mass, Length, and Volume Section of the National Bureau of Standards. The uncertainty of each value involves both a systematic error (the total uncertainty of the mass value of the mass standards used) and a random error (taken here to be one standard deviation of the weighing process).

The uncertainty in the measurement of a density ratio can also be taken as the sum of a random part and a systematic part. If the uncertainty relative to the value itself be designated by the symbol Δ, then the random part can be estimated using a generalization of the equation given in reference [1].

[1] Figures in brackets indicate the literature references at the end of this paper.

[2] Certain commercial products are identified in this paper in order to specify adequately the experimental procedure. In no case does such identification imply recommendation or endorsement by the National Bureau of Standards, nor does it imply that the products identified are necessarily the best available for the purpose.

$$\Delta_r = (\rho_u/\rho_2 - 1)\left\{\frac{V_{a/b}}{(-a/b)^2} + \left[\frac{\Delta_R M_u}{M_u}\right]^2\right\}^{1/2} \quad (2)$$

where $V_{a/b}$ is the variance in the ratio a/b determined directly from the float positions and masses of the comparison standard specimens,[3] the $\Delta_R M_u$ is one standard deviation of the process determining the mass of the unknown. There is no contribution in eq (2) from the random error in the masses of the comparison standard specimens because this is already contained in the observed variance, $V_{a/b}$, of the ratio a/b. Note that because the random error in the masses of the comparison standards is much smaller than the scatter in the float position, a simple least-squares fit to the data assuming no error in the masses was used.

The systematic part of the uncertainty arises from two sources: the systematic errors in the masses of the specimens, and the error in the ratio, ρ_s/ρ_2, of the density of the comparison standards to that of the flotation liquid. If we assume these make independently additive contributions to the overall uncertainty, these contributions are:

$$\text{Unknown mass: } \Delta_m = \left|(\rho_u/\rho_2 - 1)\left(\frac{\Delta_s M_u}{M_u}\right)\right| \quad (3)$$

$$\text{Density ratio: } \Delta_\rho = \left|(\rho_u/\rho_s - 1)\left(\frac{\Delta(\rho_s/\rho_2)}{(\rho_s/\rho_2 - 1)}\right)\right| \quad (4)$$

where $\Delta_s M_u$ is the systematic error in M_u and $\Delta(\rho_s/\rho_2)$ is the uncertainty in the ratio ρ_s/ρ_2.

The systematic errors in the masses of the comparison standard specimens may or may not contribute explicitly to the overall uncertainty. If unrelated systematic errors occur for the comparison standards, then these behave like random errors in the computation of a/b, and are contained in the variance of a/b, thus making no explicit contribution. If the comparison standards have the same systematic error, there will be a contribution to the overall uncertainty, given by

$$\Delta'_m = \left|(1 - \rho_u/\rho_2)\frac{\Delta_s M_s}{(-a/b)}\right|. \quad (5)$$

The uncertainties reported here will be given as the random error [one standard deviation, eq (2)] and the various systematic errors [eqs (3), (4), and (5)].

2.1. Comparison of Densities of Si and CaF_2

Using the same set of CaF_2 comparison standards as used in the work reported in reference [1], with masses near 34 mg, the ratio of the density of a very pure specimen of Si to that of CaF_2 was determined at 27.4 °C. The mass of the Si specimen, 62.793 mg, was chosen to produce about the same weight in the flotation (lower) liquid as the CaF_2 comparison standards. These masses were determined as described above. The uncertainties in the measurements of mass were:

	CaF_2 comparison standards	Si, unknown
Random $\Delta_R M$	0.7 μg	4.0 μg
Systematic $\Delta_s M$	1.0 μg	0.6 μg

The density of the Si was [2] 2.32900 ± 0.00001 g/cm³ at 25 °C, almost in agreement with the measurement of Smakula and Sils [3]. The measured value of Q was 0.54709. If we adopt also Smakula and Sils's values for the density of CaF_2 at 25.0 °C (3.17934 g/cm³), and use values for the linear thermal expansion coefficients of Si (2.61×10^{-6}) and CaF_2 (1.9×10^{-5}), then we calculate the density ratio at 27.4 °C to be 0.73263. The measured value was 0.73285, so that the difference between the measured and calculated values amounts to only 3 parts in 10^4.

In the random error, eq (2), only the variance in $(-a/b)$ makes an appreciable contribution. Among the systematic errors, only that involving the ratio ρ_s/ρ_2 of the density of the CaF_2 comparison standards to that of the (lower) flotation liquid is nonnegligible. The density of this liquid at the temperature of measurement was 1.761 ± 0.001 g/cm³. The calculated uncertainties were:

$$\text{Random: } \Delta_r = 1.9 \times 10^{-4}$$

$$\text{Systematic: } \Delta_\rho = 3.4 \times 10^{-4}$$

Thus the measured and calculated density ratios agree within the limits of uncertainty in the measurement. Note that the systematic error above could be reduced by choosing comparison standards of the same density as the unknown.

2.2. Comparison of Densities of Tungsten Wires

A group of four short (about 1 cm long) pieces were cut from a tungsten filament wire (diameter approximately 0.003 in) that had been given a severe heat treatment. These pieces, which served as unknowns, are listed as specimens 1 thorugh 4 in table 1. An additional group (A through E) were cut from a filament not given the heat treatment but otherwise presumably identical, and served as comparison standards. One comparison standard, C, was compared as an unknown against the other comparison standards as a check upon the internal consistency.

[3] There is an error in eq (6) of reference [1], which gives an expression for $V_{a/b}$. The quantity $\left[n\sum_i m_{si}^2 - \left(\sum_i m_{si}\right)^2\right]$ belongs in the denominator and should have been written with −1 as an exponent.

TABLE 1. *Density measurements on tungsten wires*

Wire	Set	Masses			Density ratios, ρ_u/ρ_s				
		Values (μg)	Uncertainties, μg		Values	Uncertainties, percent			
			$\Delta_R M$	$\Delta_s M$		Δ_r	Δ_m	Δ_ρ	G*(g/cm)
1.....	Unknown.....	1301.8	0.4 (0.03%)	1.2 (0.09%)	0.97_4	3.3	0.9	0.02	6.4×10^{-4}
2.....	Unknown.....	1261.4	0.4 (0.03%)	0.6 (0.05%)	0.99_0	2.8	0.5	0.02	6.7×10^{-4}
3.....	Unknown.....	1344.9	0.4 (0.03%)	0.6 (0.04%)	0.97_7	1.5	0.5	0.02	6.3×10^{-4}
4.....	Unknown.....	1382.6	0.4 (0.03%)	1.2 (0.09%)	0.98_4	6.5	0.8	0.02	5.9×10^{-4}
A.....	Standard.....	1228.8	0.4 (0.03%)	0.7 (0.06%)					
B.....	Standard.....	1173.2	0.4 (0.03%)	0.7 (0.06%)					
C.....	Standard.....	1225.8	0.4 (0.03%)	0.7 (0.06%)	1.008	1.2	0.6	0.02	6.4×10^{-4}
D.....	Standard.....	1298.0	0.4 (0.03%)	1.2 (0.09%)					
E.....	Standard.....	1404.5	0.4 (0.03%)	0.9 (0.06%)					

*G multiplied by the acceleration due to gravity is the buoyant force gradient experienced by the float, as obtained from the density measurement itself. Cf. reference [1].

The masses of the wires are listed in column 3 of table 1, and their uncertainties in columns 4 and 5. They have been measured as described under section 2, Experimental Details. Due to the limited range of the balance used, the wires were not all compared to the same combination of mass standards. This is reflected in the variation of the systematic errors of the wires, from 0.64 μg to 1.18 μg. Because different mass standards were used to compute the masses of the wires, the systematic portion of the uncertainty in the masses of the comparison standards appears as a random scattering of the mass values in conjunction with the density measurements, and is included in $V_{a/b}$.

The measured values of the ratios of the densities of the unknown wires to that of the comparison standards are given in column 6, followed by the percentage uncertainties calculated with eqs (2), (3), and (4). The values of Q were all unity to within 0.3 percent.

In the last column is the buoyant force gradient calculated, as in reference [1], in the course of the density measurements themselves. If the upper liquid were perfectly homogeneous, with no density gradients, then the buoyant force gradient would be the product of the cross-sectional area of the suspension wire (8×10^{-4} cm^2) and the difference in density of the upper and lower liquids (0.76 g/cm^3). This product is 6.1×10^{-4} g/cm, very close to the observed values listed in table 1. The agreement between the expected and observed buoyant force gradient is very much better than it was in the work reported in reference [1], and probably reflects the use of water rather than benzene as the upper liquid. The negligible solubility in water of the fluorinated hydrocarbon used as a lower liquid precludes formation of concentration, and therefore density, gradients at the float.

To within the estimated experimental uncertainty, all values of the density ratio of the unknown to known tungsten wires are equal. The values for all four unknown wires, No. 1 through No. 4, lie slightly below unity, which may reflect the special heat treatment given this filament. The difference from unity of the mean value for the unknowns is statistically significant, being 5.2 times the estimated standard deviation of the mean. The measured density of wire C is the same as that of the other comparison standards well within the experimental error.

Most of the relative errors in determining the density ratios of these wires, shown also in columns 6, 7, and 8 of table 1, are larger by as much as two orders of magnitude than they were for the measurements on CaF_2 (ref [1]) or Si above. This increase arises from two causes, which can be understood on the basis of eqs (2) and (3):

(i) The square root in eq (2) was about 10 times larger for the tungsten wires than it was for CaF_2. Equations (1), (2), and (6) of reference [1] show that a/b should be about 30 times smaller for the tungsten wires, and that $V_{a/b}$, which under the conditions of the experiments reported here is roughly proportional to b^{-2}, should be about 10 times smaller. These changes result from the smaller masses (×30) and weights in the lower liquid (×15) for the tungsten wires.

(ii) The initial factor in eqs (2) and (3) is about 12 times larger for the tungsten wires than it was for the CaF_2, because of the very large tungsten density (19.2 g/cm^3) compared to that (3.2 g/cm^3) for CaF_2 and for the lower liquid (1.8 g/cm^3).

On the other hand, the uncertainty Δ_ρ (eq 4) arising from errors in the ratio ρ_s/ρ_2 of the density of the comparison standards to that of the flotation liquid was much smaller for the tungsten wires than for the

Si/CaF_2 ratio. In the former case the unknown and comparison standard densities were almost the same, making the first factor in eq (4) small, and the density of the comparison standards was much larger than that of the flotation liquid, making the denominator of the second factor larger. These changes were more than enough to offset an increase in the uncertainty in the ratio ρ_s/ρ_2 itself because of the rather large uncertainty ($\pm$ 0.1 g/cm^3) in the actual density ρ_s of the tungsten.

3. Summary and Conclusions

The density comparison technique described in reference [1] has been used to compare the densities of very small (1.3 mg) tungsten wires (density 19.2 g/cm^3), with errors in the range 2 to 7 percent. It was shown that both the very small size of these specimens and their very high density contribute to produce this rather high error.

On the other hand, a check upon the method wa. obtained by comparing the density of very pure (63 mg specimen, density 2.3 g/cm^3) Si to that of pure CaF_2. The ratio obtained agreed with measurements in the literature to within 3 parts in 10^4, confirming the expected precision of the density comparison method.

The authors would like to thank Dr. George Comenetz, Westinghouse Research Laboratories, for providing all of the tungsten wires, and Dr. W. Horton for a very careful and helpful reading of the manuscript.

4. References

[1] Franklin, A. D., and Spal, R. D., Rev. Sci. Instr., **42**, 1827 (1971).
[2] Deslattes, R. D., private communication.
[3] Smakula, A., and Sils, V., Phys. Rev., **99**, 1744 (1955).

(Paper 78A1–800)

JOURNAL OF RESEARCH of the National Bureau of Standards—A. Physics and Chemistry
Vol. 78A, No. 1, January–February 1974

A Density Scale Based on Solid Objects

Horace A. Bowman, Randall M. Schoonover, and C. Leon Carroll

Institute for Basic Standards, National Bureau of Standards, Washington, D.C. 20234

(October 15, 1973)

We have determined the density of four pieces of single crystal silicon in terms of universally accepted standards of mass and length. These four objects will be used as a working density standard to which all future density work in the United States will be referred. Using these crystals as standards, NBS can calibrate other objects as density standards for associated laboratories.

The work was accomplished with the assistance of an interferometer, developed especially for the task, which measures the diameter of commercially available steel balls. From measured diameters ball volumes are calculated. The volumetric information contained in the balls is transferred to the silicon crystals in a newly designed hydrostatic weighing experiment.

We have made three independent density determinations on each of the four crystals, and the presently accepted values of the density of each crystal is the average of the three determinations. The random component of uncertainty (3 standard deviations) of these four averages is 0.7 ppm. The systematic error is estimated to be about 0.7 ppm.

Key words: Density standard; hydrostatic weighing; perfect sphere; silicon; spherical interferometer; spherical volume; volume standard.

Contents

	Page
1. Introduction	13
1.1. Background	14
1.2. Modern developments	14
1.3. Dissemination of density information	15
2. The working standard of density	15
2.1. Material for density standards	15
2.2. Sizes of crystals	16
2.3. Mass measurements	16
2.4. Verification of volumes	16
2.4.1. Objects of perfect geometry	16
2.4.2. Diametric measurements	16
2.4.2.1. The interferometer configuration	16
2.4.2.2. The etalon-ball assembly	17
2.4.2.3. Interferometer temperature measurements	17
2.4.2.4. Etalon length measurements	20
2.4.2.5. Ball diameter measurements	20
2.4.2.6. The temperature coefficients of linear expansion of the balls	22
2.5 Hydrostatic transfer of volumetric information from the spheres to the crystals	29
2.5.1. The hydrostatic system	29
2.5.1.1. The hydrostatic suspension	29
2.5.1.2. The hydrostatic liquid	29
2.5.1.3. The immersed pan loading assembly—redundancy	29
2.5.1.4. The hydrostatic balance and its calibration	30
2.5.2. Hydrostatic weighing on a direct-reading balance	31
2.5.3. Hydrostatic weighing format—the 4–1 ratio series	32
2.6. Final calculation of crystal volumes and densities	33
3. References	40

1. Introduction

In the early 1960's NBS began receiving inquiries as to the practicability of making density measurements to an uncertainty of a part or two in a million. This was of particular interest to oceanographers and crystalographers. Cook, NPL, [1, 2],[1] had satisfied the requirements of workers in gas thermodynamics by his determination of the density of mercury to about a part in a million and he had made a generous supply available to NBS. We made several efforts to transfer the density information from this mercury into various objects but this is a difficult experiment and we were rarely able to achieve reproducibility of independent measurements to less than three parts per million. We had some immediate "in house" requirements for density knowledge to a part per million in the field

[1] Figures in brackets indicate the literature references at the end of this paper.

of fundamental constants [3, 4] and, as a long range objective, an improvement of the mass standard.

In 1965 we announced [5] that NBS would undertake to devise a density measurement procedure and the necessary associated standards tied directly to the universally recognized standards of mass and length so that interested experimenters could make such density determinations. We had already demonstrated that the densities of solid objects could be compared to a precision of $1:10^7$ or better [6] so we stated that the proposed measurement system would be based upon a group of solid objects, and we outlined the procedures we would use in the development. Numerous experimental failures have required us to alter our techniques and methods, but every experiment has reinforced our original conclusion that solid density standards are far more practical than any liquid standard which has come to our attention.

Section 2 of this paper outlines the laboratory procedures we used in the development of the system and the results we obtained.

1.1. Background

All density determinations require two measurements, one to find the mass of the unknown and a second to find its volume. Mass may be adequately measured by well understood procedures. Volume may be calculated from linear measurements, but it is ordinarily calculated from observed data on buoyant forces in hydrostatic weighing tests in water of some tabulated value of density.

Cook's determination on mercury was in response to a well-defined problem of very widespread interest, and NPL expended a great deal of effort in accomplishing this excellent measurement to about a part in a million.

The suggestion has frequently been made that if NBS would determine the density of well characterized water from a reproducible source, that other groups could use this type of water, after preparation by a well-defined recipe, for 1 ppm density measurements. Nothing could be further from the truth. While such a determination by NBS might remove some of the uncertainty associated with the use of water as a density standard, no prudent experimenter would claim such accuracy because such a claim would necessarily have to be based upon four assumptions—none of which are subject to proof:

1. That the published value of the density of water applied *without correction* to the particular sample used in his measurement.
2. That the official recipe for preparation of water contained no hidden errors when applied to his particular sample.
3. That no blunders were made during preparation of his sample.
4. That no contamination occurred between the preparation and use of his sample.

There are two additional practical reasons for choosing a solid-based density scale in preference to water: (1) It is possible to compare the densities of two solids to a precision in excess of that which is achievable in the comparison of a solid with water. (2) The density of an unknown liquid may be determined much more easily from a solid standard than from water.

1.2. Modern Developments

There have been numerous technical developments in the past two decades which greatly facilitate the task of developing a solid-based density scale. We utilized five of these developments:

a. The inexpensive commercial availability of single-crystal silicon.
b. The commercial availability at reasonable cost of steel spheres of near-perfect geometry.
c. A new type interferometer designed by J. B. Saunders, NBS [8].
d. The commercial availability of Lamb dip stabilized lasers and techniques for their ready calibration with reference to universally recognized spectral standards [7]. This made the above interferometer configuration practical.
e. A completely redesigned hydrostatic weighing experiment.

Due to the enormous requirements of the electronics industry, single crystal silicon is now mass-produced in sizes much greater than necessary for practical density standards. The virtues of this remarkable material as density standards will be discussed in section 2, but its primary value in such service is its homogeneity and density stability.

A major difficulty facing a laboratory about to embark on a fundamental density measurement is the fabrication of an object of such geometric perfection that its volume may be calculated from linear measurements.

We avoided facing this problem directly by using commercially available steel balls about 6.3 cm in diameter. The difference between the maximum diameters and the minimum diameters of such spheres is rarely greater than about 1 ppm.

The virtues of spherical objects have long been recognized, but there has been no practical method of measuring spherical diameters without introducing uncertainties (such as contact deformation) several times the magnitude of the desirable level of uncertainty. This problem was resolved by the development of the noncontacting interferometer mentioned above.

Volumes calculated from such measured diameters are not indefinitely stable because steel balls are easily damaged by scratches, corrosion, rough handling, etc., so it was desirable to transfer the volumetric knowledge from the spheres to objects of better stability and homogeneity in density. This transfer is performed hydrostatically.

The classical hydrostatic weighing experiment is quite imprecise and most wasteful of density knowl-

edge. In order to get the precision of this operation below 1 ppm we made four changes:

1. The use of a fluorocarbon instead of water.
2. The use of four comparison objects instead of one.
3. The use of direct reading, damped balances instead of free swinging instruments.
4. The employment of a measurement procedure designed for the determination of volumetric ratios rather than densities.

The foregoing remarks suggest the apparatus and procedures we used in developing our working density standard. The work described in this report, outlined in figure 1, was largely exploratory, and we have found that equipment and procedural modifications will provide data of equal or better quality at much less cost in the future.

2. The Working Standard of Density

Inasmuch as density is defined in terms of mass and length, both of which are basic in the SI System, it would be inappropriate to speak of a density standard in the context in which the word "standard" is generally understood. On the other hand, "working" standards are ordinarily thought of as convenience items whose accepted values are obtained by calibration either directly or indirectly against fundamental standards.

For this reason, we have chosen to refer to our group of silicon crystals as a "working" standard. The accepted density values of the individual crystals in this group are not invariantly fixed, but only represent our best estimate of the true value based upon previous calibration experience. As additional measurement

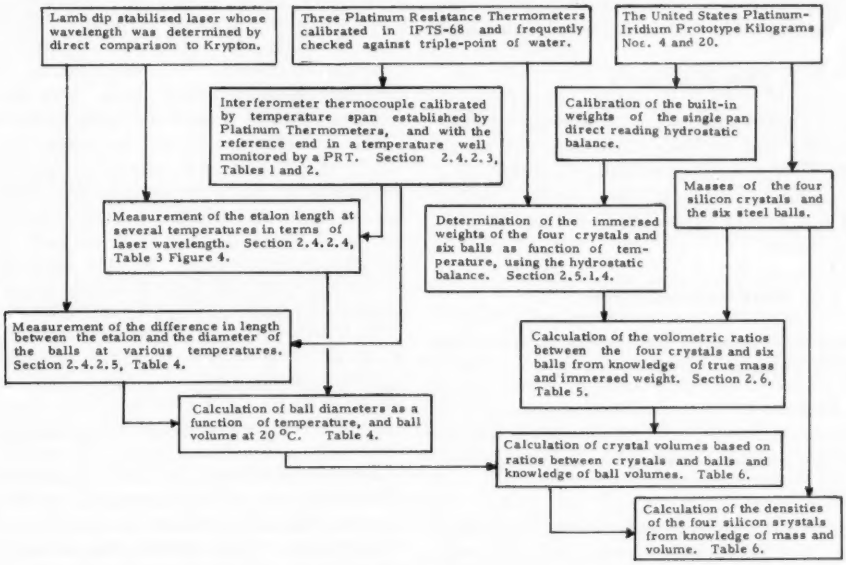
Lamb dip stabilized laser whose wavelength was determined by direct comparison to Krypton.
Three Platinum Resistance Thermometers calibrated in IPTS-68 and frequently checked against triple-point of water.
The United States Platinum-Iridium Prototype Kilograms Nos. 4 and 20.
Interferometer thermocouple calibrated by temperature span established by Platinum Thermometers, and with the reference end in a temperature well monitored by a PRT. Section 2.4.2.3, Tables 1 and 2.
Calibration of the built-in weights of the single pan direct reading hydrostatic balance.
Masses of the four silicon crystals and the six steel balls.
Measurement of the etalon length at several temperatures in terms of laser wavelength. Section 2.4.2.4, Table 3 Figure 4.
Determination of the immersed weights of the four crystals and six balls as function of temperature, using the hydrostatic balance. Section 2.5.1.4.
Measurement of the difference in length between the etalon and the diameter of the balls at various temperatures. Section 2.4.2.5, Table 4.
Calculation of the volometric ratios between the four crystals and six balls from knowledge of true mass and immersed weight. Section 2.6, Table 5.
Calculation of ball diameters as a function of temperature, and ball volume at 20 °C. Table 4.
Calculation of crystal volumes based on ratios between crystals and balls and knowledge of ball volumes. Table 6.
Calculation of the densities of the four silicon srystals from knowledge of mass and volume. Table 6.

FIGURE 1

Additional work on these crystals and balls will be performed as a continuing NBS project, and will be reported on from time to time.

1.3. Dissemination of Density Information

By hydrostatic transfer from our crystals or balls, we are now in a position to calibrate solid standards for use by other laboratories.

If other groups choose to enter the field of fundamental volumetric (density) measurements (we have heard of two such organizations), it will be possible to exchange solid density standards to assure consistency.

The use of solid standards makes comparison of density scales to assure consistency a practical procedure.

effort is expended, the accepted values may be slightly modified. The present accepted values of our crystals are based upon the average of three independent determinations.

2.1. Material for Density Standards

The most important characteristics of an artifact standard of a physical property are:

1. Temporal stability with respect to the physical property it represents.
2. Adaptability to practical measurement methods.
3. Of such a nature that the response of a measurement system is primarily due to the characteristic of interest.

Single crystal silicon meets all of the above requirements to a far greater degree than any of the other materials we considered. It is among the most homogeneous materials available so that chipping or abrasion in use cause equal percentages of loss of mass and volume (density constant). It has a highly stable surface in that the oxide film is formed in a minute or so—thereafter changes occur at a rate estimated to be such that the gross density of the crystal varies by about (worst case) $\frac{1}{10}$ ppm/year [9]. Its oxide has a density very nearly equal to that of the parent material. It has sufficient electrical conductivity so that, with care, electrostatic charges do not interfere with weighing. Its temperature coefficient of expansion is only 2.5 ppm/°C (linear). It is inert in most liquids. It is easily fabricated into desirable shapes and sizes. There are many commercial sources of supply at moderate cost. Inexpensive lightly doped transistor grades are quite adequate in this application. The pieces of silicon used in our working standard were cut from a reject boule given to us by the Fairchild Semiconductor Company.

2.2. Sizes of Crystals

Our working density standard is made up of four silicon crystals cut from a $2\frac{1}{2}$-in diam boule in slices about 1-in thick. They were ground down to about 205 g each and then trimmed to about 200 g by HF etching which exposed the parent crystal lattice surface with work damage removed.

2.3. Mass Measurements

Our measurements required knowledge of the mass of three groups of objects:

1. The steel balls
2. The silicon crystals
3. The built-in weights from our direct-reading balance.

The mass of the balls and crystals were determined in conventional "4–1" weighing series[2] commencing with our national standard of mass to which BIPM had assigned a value. The balance weights were removed from the balance and were worked down from the national standard in weighing series especially designed for the purpose. Uncertainty in the mass of the balls was about 64 μ-grams, in the crystals about 45 μ-grams, and about 12 μ-grams per hundred grams for the balance weights.

2.4. Verification of Volumes

2.4.1. Objects of Perfect Geometry

While it would have been possible within the present day state-of-the-art to fabricate our crystals into perfect geometric forms and calculate their volumes from linear measurements, this would have been prohibitively costly. As pointed out in the introduction, we intend to continue our program of mass and volume measurements on our crystals for an indefinite period. Under these circumstances, if a crystal became chipped, its geometric perfection would be destroyed and volumetric surveillance would necessarily have to stop. The fabrication of any geometrically perfect object is a major undertaking—it was a real problem for NPL during their mercury work, BIPM during their work on water and for Hart and Morgan [10] on silicon.

We were fortunate to discover that nearly perfect spheres of 52100 steel [11] were available from at least two companies supplying the needs of groups working in inertial navigation. These spheres were 6.35 cm in diameter. Our spherical profile instruments could not detect lobing down to about 1 ppm of diameter. Daniel P. Johnson, NBS, has demonstrated (see companion paper in this issue at NBS J. Res.) that the true volumes of such spheres differ insignificantly from the volumes calculated on the basis of the true average diameter. We attempt to obtain a close approximation to this true average diameter by making "many" diametric measurements.

We initially obtained four balls, A, B, C, and D. When the experiment was in progress it became evident that six balls were desirable. Rather than delay the experiment while awaiting two additional balls we used balls A and B a second time in another density determination. In this second determination in which balls A and B were employed, we have referred to them as balls E and F.

Hereafter, in this report, we will refer to six balls, A, B, C, D, E, and F, although, in fact, there are only four. This is justified in section 2.6.

2.4.2. Diametric Measurements

The conventional method of measuring spherical diameters is by comparison with stacks of gage blocks in mechanical contacting devices. This involves deformation errors which are directly additive with gage block and ringing film errors. A most careful search of the literature did not disclose a convenient noncontacting interferometer configuration for this task.

Our interferometer specialist, J. B. Saunders, was persuaded to delay his retirement until he had developed such an instrument. In less than 1 year he presented us with a laboratory device. This configuration is given in detail elsewhere [8], but it will be briefly described below.

2.4.2.1. The Interferometer Configuration

This instrument is an etalon device whose major components are laid out as illustrated in figure 2. Laser light enters face 1 of a conventional beam-splitter prism where it is split into two beams, L and R, leaving the prism through faces 2 and 3 respectively. These two beams are directed by mirrors into the opposite

[2] Designs involving measurements of the $n(n-1)/2$ distinct differences among n objects are referred to in this paper as "$n-1$" designs.

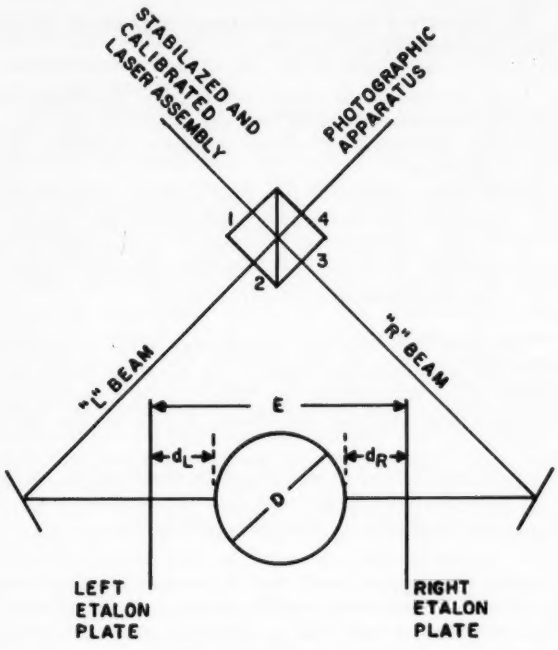

FIGURE 2. *A schmetic diagram of principal members of the Saunders ball and cylinder interferometer*

ends of an etalon, the L beam striking the left etalon plate normally and the R beam striking the right plate. A ball is placed in the etalon and oriented so that the two beams are directed toward the center of the ball. The L beam and the R beam are used one at a time, the undesired beam being masked off by a screen near the prism. With the R beam masked, the L beam strikes the left etalon face which reflects part of the light back toward the prism. The balance of light passes through the left etalon plate and strikes the spherical ball surface, which reflects it back toward the prism. These two reflected beams interfere with one another in a bull's-eye pattern (since one beam is divergent) which is photographed by a camera placed opposite face 4 of the prism. When this photo has been taken, the operator masks off the L beam and photographs the pattern caused by interference between R beam light reflected from the right etalon plate and the right side of the ball. This is a fast operation using 1/15 second exposures on 35 mm film. For high contrast interferograms, the two interfering beams should be of about equal intensity. With one reflected beam coming from a quartz surface and the other from a highly polished steel surface, this requirement is not met. Saunders overcame this difficulty by backing the camera away from the prism. The (approximately collimated) beam of low intensity reflected from the quartz etalon plate was about constant in intensity regardless of the camera position, however, the (divergent) beam of high intensity reflected from the highly polished steel spherical surface became attenuated (due to divergence) as the distance between the prism and camera increased. The photographs were made with the film placed in the plane of equal intensity, so the interferograms were of extremely high contrast. The two interferograms are associated with distances d_L and d_R on the sketch. It is obvious that if E is the etalon length, the ball diameter, D, is given by

$$D = E - d_L - d_R.$$

2.4.2.2. The Etalon-Ball Assembly

The etalon consists of two quartz flats about 1-cm thick separated by an internal distance of 68 mm (millimeters). The spheres are a maximum of about 63 mm in diameter so they are easily inserted and removed from the etalon. The two flats are held rigidly by two quartz plates, above and below, by epoxy cement. Each plate has a 7-cm hole through the center. The hole through the upper plate allows various balls to be inserted in the etalon, and the rotating ball holder comes up from below through the hole in the lower plate.

The ball rests on three rollers arranged so that it may be rotated about two axes 90° apart by remote controls. This makes it possible to measure the diameter through any set of latitudes and longitudes on the ball surface. In practice we made measurements on 10 diameters (20 photos) normal to the faces of an inscribed duodecahedron, and gave each measured diameter equal weight in the calculation of the average.

2.4.2.3. Interferometer Temperature Measurements

Due to the small size of the temperature coefficients involved, temperature measurements of adequate accuracy are easily attainable during etalon measurement tests. Two such coefficients are of importance—the temperature coefficient of wavelength, +1 ppm/°C, and the temperature coefficient of expansion of the etalon, about +.5 ppm/°C. Since these coefficients have the same algebraic sign, they are opposed in their effect on the etalon measurement, adding to about −0.5 ppm/°C to the effective etalon length.

On the other hand, the temperature coefficient of expansion of the 52100 steel balls is in excess of 12 ppm/°C (which amounts to 36 ppm/°C in volume), so that ball temperatures must be measured to the best possible accuracy.

The etalon assembly, described in the previous section, is housed in a double wall chamber with thermostat water circulating in the walls, base, and cover. There are four thermal leaks in this isothermal shield. We have 2 windows about 2 cm in diameter in the walls to permit entrance of the two measuring light beams. The ball rotation control column enters through a 5-cm diameter hole in the floor, and the measuring thermocouple penetrates the shield through a 2-cm diameter hole in the cover. We initially hoped that the thermostat shield would be strong enough to define the temperatures of the steel ball and etalon to a level less than 0.01 °C so that a temperature measurement on the thermostat liquid would satisfy all requirements. However, in developmental

525-013 O - 74 - 2

experiments, we found that the difference between the ball temperature and the thermostat water varied randomly over a range of about ± 0.02 °C at periods of 1 to 3 minutes.

This required that we measure the ball temperature directly. We constructed a measuring thermocouple in the form of a copper-constantan thermopile with six pairs of junctions. The six reference junctions were soaked in a temperature well which was monitored by a platinum resistance thermometer. Each of the six measuring junctions entered the interferometer chamber through the hole in the top and were held in physical contact with the steel ball by the springiness of the wire leads. Each measuring junction was covered by a thin layer of epoxy to prevent their electrical short-circuiting through the ball. Both the lightness of the physical contact between the ball and the measuring junctions and the epoxy coating mitigated against good thermal contact between them.

The indication of a potentiometer-thermocouple combination is a function of the difference in temperature between the junctions of the thermocouple. To make meaningful measurements one must make every effort to assure that the thermal contact between the measuring junction and the object of interest is such that the temperature of the junction is equal to the temperature of the object of interest. Failing this, an evaluation must be made of the difference in temperature if such difference exists.

To calibrate a temperature measuring system of this type requires two experiments:

1. A determination of the relationship between the potentiometer output and the difference between the temperatures of the opposite thermocouple junctions.
2. A determination of the difference in temperature between the measuring junctions of the thermocouple and that of the object of interest as a function of whatever perturbing influence causes this difference to depart from zero.

The data from the first experiment, table 1, showed that the potentiometer output (in nominal millivolts) was a linear function of the difference in temperature between the opposite junctions. A line of the form

$\Delta T = \alpha\ (\text{emf}) + \beta$ was fitted to the data to obtain
$\alpha = 4.12069$ °C/mv (std. dev. $= 0.00589$)
$\beta = 0.000585$ °C (std. dev. $= 0.00149$).

During this experiment, the reference junction was kept in the temperature well employed during the ball diameter tests, and the measuring junctions were deeply immersed in a liquid bath. Platinum resistance thermometers monitored each temperature, and triple point of water measurements by these two ther-

TABLE 1

Date–time		Temperature of bath	Temperature of reference well	ΔT	Potentiometer observation emf
12–15–72	0845	20.053	19.944	0.109	0.026
	1230	20.012	19.947	.065	.016
12–18–72	0840	19.806	19.949	(−) .143	(−) .036
	1630	20.082	19.819	.263	.066
12–19–72	0835	20.090	19.672	.418	.102
	0930	20.089	19.670	.419	.103
	1105	20.096	19.668	.428	.104
	1520	20.093	19.674	.419	.101
12–20–72	0830	19.467	19.713	(−) .246	(−) .061
	0910	19.460	19.714	(−) .254	(−) .0625
	1100	21.366	19.720	1.646	.398
	1335	21.366	19.734	1.632	.396
	1530	21.899	19.742	2.157	.523
12–21–72	0855	21.824	19.756	2.068	.502

This data was taken with good thermal contact between the calibrating ambients and the two ends of the thermocouple. The reference end was in the temperature well used during measurements, and the working junctions were in a thermostat bath. Both the bath and well were monitored by platinum resistance thermometers. Triple-point of water measurement histories on the two thermometers indicate that maximum errors in observed values of ΔT are no greater than 0.0014 °C.

This data fits a straight line of the form

$$\Delta T = \alpha(\text{EMF}) + \beta$$

where

$\alpha = 4.120693$ (standard deviation $= 0.00589$)
$\beta = 0.000585048$ (standard deviation $= 0.00149$).

mometers indicated that the temperature span in the thermocouple calibration experiment was defined to no worse than 0.001 °C.

Having obtained a good measure of the potentiometer output as a function of the difference between junction temperatures, we turned our attention to obtaining a measure of the difference between the true ball temperature and the temperature of the measuring junction of the thermocouple. This second experiment was performed on a ball and thermocouple nominally identical to those used in the ball diameter measuring tests. In this experiment the reference junctions of the thermocouple were cemented to the ball surface with several centimeters of lead wire held against this surface by insulating tape—the intent was to insure that the reference junction was in excellent thermal contact with the ball so that the junction temperature was equal to the ball temperature. The thermocouple wires were led away from the reference junction and passed through the interferometer wall (into the room) through one of the windows in the side of the thermostat chamber. The measuring junctions of this thermocouple were reinserted into the interferometer through the opening in the top cover and held in light contact with the ball by the springiness of the lead wires in exactly the same manner as the measuring junctions of the thermocouple used in ball diameter tests. Assuming that there were negligible thermal gradients in the steel ball and that the reference junction was in adequate thermal contact with the ball surface, we concluded that the output of this thermocouple indicated the difference between the true temperature of the ball and that of the measuring junction.

The test showed that the temperature of the measuring junction was higher than the ball temperature when the room temperature was higher and vice versa. The data, table 2 and figure 3, were fitted to the equation

$$Z = A_2q^2 + A_1q + A_0$$

where

$A_2 = 8.718 \times 10^{-4}$

$A_1 = 1.652 \times 10^{-2}$

$A_0 = 3.038 \times 19^{-3}$

q = The difference in temperature between the room temperature and the ball temperature

Z = the difference in temperature between the ball and the measuring junction.

TABLE 2

Date–time		ΔT indicated by thermocouple	Room temperature	Thermostat temperature
11- 2-72	0845	−0.025 °C	19.50 °C	21.00
11- 3-72	1155	+.022	19.50	18.40
11- 6-72	0820	+.009	19.49	19.39
11- 7-72	1320	−.025	19.40	21.40
11- 8-72	1315	−.044	19.50	22.81
11- 9-72	1621	.000	19.50	19.63
11-10-72	1100	+.025	20.71	19.68
11-13-72	1500	+.028	20.73	19.40
11-14-72	0836	+.019	20.80	19.70
11-15-72	0834	−.019	20.80	22.10
11-16-72	0814	−.016	20.8	22.1
11-17-72	1534	+.047	20.8	18.41
11-20-72	0840	−.031	20.88	23.25
11-21-72		+.050	20.77	18.21
11-24-72	1200	−.031	20.8	23.25
11-27-72	0900	−.044	19.4	23.1

This data was taken with the reference junctions of the thermocouple held in good thermal contact with a dummy steel ball by epoxy cement. The measuring junctions were in only moderate thermal contact (simulating that which existed during the ball diameter tests).

This data fits a curve of the form

$$Z = A_2q^2 + A_1q + A_0$$

where

$A_0 = 3.038\ 263 \times 10^{-3}$
$A_1 = 1.652\ 534 \times 10^{-2}$
$A_2 = 8.718\ 282 + 10^{-4}$
Z = Error in thermocouple indication due to (presumably) lead losses.
q = (Room Temp)−(Thermostat Temp).

During this experiment we used the temperature of the water in the interferometer walls as the criterion for judging true ball temperature. It was previously pointed out that this was false to the extent of about ±0.02 °C but an error of this magnitude has negligible effect on the coefficients shown above.

We feel quite certain that the major perturbation on the ball temperature indicated by the thermocouple was heat flow in the thermocouple leads, but we do not understand why there is a slight quadratic bend in our data, nor why our data does not pass through zero ($A_0 = 0$). We believe that heat flow in the ball rotation control column may cause nonlinear data. Failure of the data to pass through the origin may indicate some perturbing influence we have not found.

Ball temperatures reported during the interferometric tests on their diameters were calculated as follows:

1. The temperature span of the thermocouple was calculated from $\Delta T = 4.12069$ (emf) + 0.000585.
2. The value of ΔT, calculated thus, was algebraically added to the *PRT* indication of the temperature inside of the temperature well. This provided us with the temperature of the measuring junction.
3. The difference between the room temperature and the temperature of the measuring junction

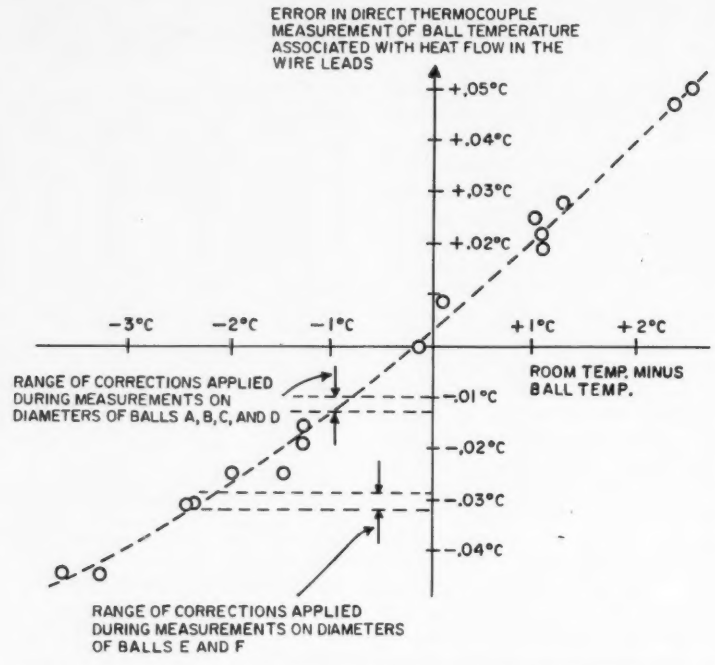

FIGURE 3. *This is a plot of data taken during measurements on the errors in temperature observations caused by heat flow in the thermocouple leads.*

The horizontal axis is labelled "Room temp. minus ball tem.". The data is actually based on room temperature minus thermostat temperature, however, as pointed out in the text, ball temperature and thermostat temperature do not separate by more than about ±.03 °C, so errors in the plot from this assumption are negligible. The dotted line is only a visual estimate. The coefficients of the quadratic fit are given in the text.

was taken to be an adequate indication of q (above), and the temperature of the measuring junction was corrected by the factor

$$8.718\times10^{-4}\times q^2+1.652\times10^{-2}\times q+3.038\times10^{-3}$$

We believe that the reported ball temperatures are uncertain by no more than 0.009 °C.

2.4.2.4. Etalon Length Measurements

The detailed procedure for measuring the length of the etalon is given in Saunder's paper. It consists of modifying the basic configuration of the instrument so that interference occurs between beams of light reflected from the two etalon surfaces. One beam results from an internal reflection so that its phase is shifted by 180°. Our fringe fractions are calculated from measurements on rings of constructive interference and we assume that the phase shift in the shifted beam is a *retardation*. Under this assumption, the length of the etalon is given by

$$E=\frac{\lambda N_E-0.316}{2}$$

where E is the etalon length, N_E the total fringe count, integral plus fractional, and λ the wavelength of the laser light. The -0.316 in the numerator is the 180° phase shift correction mentioned above ($\lambda=0.6328\mu$).

Our Lamb dip stabilized laser has been calibrated three times as follows:

1970	0.632991408 μm
1971	.632991409 μm
1972	.632991411 μm

Our measurements were made between the second two calibrations, and we assume that the vacuum wavelength was 0.632991410μ during ball measurements.

We made six measurements on our etalon length at six different temperatures. The data is shown in table 3 and figure 4. It was found to fit a straight line of slope 0.036259μ/ °C. From these tests we calculate the temperature coefficient of linear expansion to be 0.000 000 537, with a standard deviation of 0.000 000 016. The NBS group specializing in this work estimated the coefficient of the quartz to be 0.000 000 540 (± .000 000 03).

2.4.2.5. Ball Diameter Measurements

As previously mentioned, the ball diameter, D, is given by $D=E-d_L-d_R$, figure 2. The measurement of E was discussed in the previous section. We are concerned here with the measurements of d_L and d_R. It is well known that the phase of light reflected from a steel surface is *retarded* with respect to light reflected from an equidistant quartz surface. This retardation has most recently been measured by

TABLE 3

Resume of raw data taken during Etalon measurements. Tests ET–5 and ET–6 at the elevated temperature were made for use with the high temperature determination of ball diameters and volumetric ratios in Determination E–F. Fringes were photographed with the interfering light beams travelling in both directions through the interferometer. If there is a systematic difference, depending upon light beam direction, it is below our ability to measure it reliably. When all six observations on etalon length at the various temperatures are fitted to a straight line, the slope of the line is such that the temperature coefficient of linear expansion is 0.000 000 537. The six points fit the line to a correlation coefficient of 0.998.

Test number Test date		ET–1 6–27–72	ET–2 6–29–72	ET–3 6–30–72	ET–4 6–30–72	ET–5 7–11–72	ET–6 7–12–72
Parameters required for the Calculation of Temperature of test:							
Room temperature	°C	20.88	19.40	19.40	19.40	21.00	21.00
Potentiometer obs'n	emf	0.0412	0.0293	0.2955	0.2974	0.5490	0.5940
Plat. res. thermometer	°C	20.541	19.171	19.181	19.186	20.560	20.652
Parameters required for the calculation of effective wavelength:							
Vacuum wavelength	μ	.632991410	.632991410	.632991410	.632991410	.632991410	.632991410
Calc. temp. of test	°C	20.706	19.287	20.412	20.414	22.847	23.128
Barometric pressure	mm-Hg	748.66	745.26	743.66	743.06	757.61	756.36
Relative humidity	%	39.3	48.5	47.5	46.9	38.3	42.5
Effective wavelength ($=\lambda$)	μ	.632822643	.632822616	.632823649	.632823782	.632821898	.632822377
Observed fringe fractions:							
left-to-right		Illegible	.561	.366	.292	.216	.076
right-to-left		Illegible	.560	.343	.307	.185	.078
left-to-right		.679	.541	.341	.296	.202	.090
right-to-left		.701	.551	.338	.280	.201	.074
Total fringe count ($=N$)		213240.690	213240.553	213240.347	213240.293	213241.201	213241.079
Etalon length at temperature of the test $=((N\times\lambda)-0.316)/2$	μ	67471.610	67471.564	67471.609	67471.606	67471.692	67471.705
Average values used in ball diameter measurements		Determination A–B		Determination C–D		Determination E–F	
Etalon length	μ	67471.5870		67471.6075		67371.6985	
Temperature	°C	19.996		20.413		22.987	

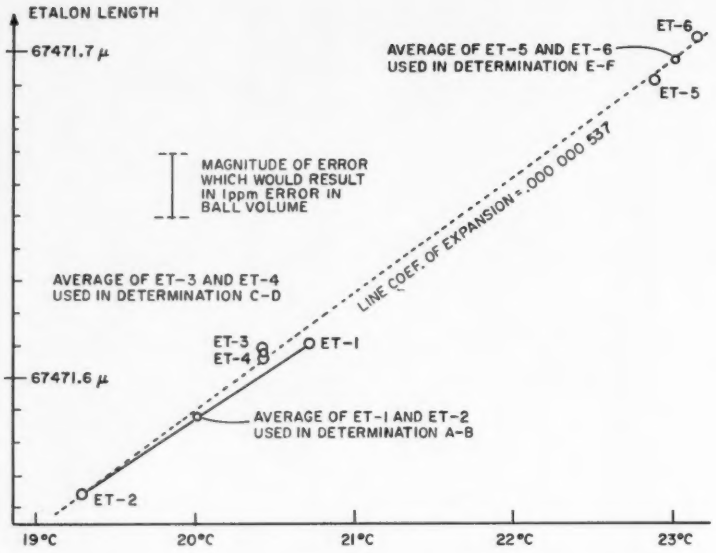

FIGURE 4. *This is a plot of the measurements made on the etalon at various temperatures.*

Raw data are presented in table 3 from the data presented here the temperature coefficient of linear expansion is indicated to be 0.000 000 537.

Bennet [12] and we have used her value of 22° in our calculations. Inasmuch as we assume the 180° phase shift from a quartz reflector to be a *retardation*, we must for consistency assume the phase shift from a steel surface to be 202° (180°+22°) retardation. This is 0.355 μm in the case of light whose wavelength is 0.6328μm.

As pointed out previously we make two interference photographs, one associated with d_L, the other with d_R. Then

$$d_L = \frac{(n_1 + L)\,\lambda - 0.355}{2}$$

$$d_R = \frac{(n_2 + R)\,\lambda - 0.355}{2}$$

where n_1 and n_2 are the integral orders in the two interferograms and L and R the fractional orders. Adding the above two equations and letting $n_1+n_2=N_B$ we get

$$d_L + d_R = \frac{(N_B + L + R)\,\lambda - 0.710}{2}.$$

We have made four diametric measurements on each of our six balls. Each measurement is the average of 10 diameters (pairs of interferograms) taken uniformly over the spherical surface. The data are shown in table 4. The values of L, R and $L+R$ are shown. The sum, d_L+d_R, is the mechanical path difference (M.P.D.) and average values at average temperatures are shown in the caption. The temperatures in the four measurements are averaged as are the four final calculated diameters for use in calculating coef. of expansion and the average values are shown in the caption. These four diameters at various temperatures are reduced to values at 20 °C to provide a criterion for estimating the interferometric precision. The justification for the value of the temperature coefficient of linear expansion used in this reduction is given in the following section.

From the average diameter at 20 °C the volume of the ball at 20 °C is calculated. These two average values are also given in the caption to table 4.

2.4.2.6. The Temperature Coefficients of Linear Expansion of the Balls

In its present form our ball interferometer must be readjusted whenever its temperature is changed more than a few tenths of a degree. For this reason, it is not practical to insert a ball and vary the temperature to get data for a temperature-diameter slope. We have tried this, and the calculated slopes are unrealistically high.

Our interferometer experiment provides us with a value of M.P.D., that is, the difference between the length of the etalon and the diameter of the ball at the temperature of the test. An acceptable estimate of the coefficient can be obtained by dividing the diameter-temperature slope (Δdia/Δtemp) by the average diameter of the ball over this range, 6.3501 cm. The slope may be calculated from the relationship

$$\frac{(\text{MPD} @ t_1) - (\text{MPD} @ t_2) + (\text{expansion of etalon})}{t_2 - t_1}$$

TABLE 4a. *Resume of raw data taken during interferometric tests on Ball A*

Average test temperature = 20.2375 °C
Averaged measured diameter = 63500.2966 μ
Averaged measured MPD = 3971.2991 μ

Data reduction is based upon an assumed etalon length of 67471.5870 microns at 19.996 °C based upon the average values obtained in Etalon tests ET−1 and ET−2. The temperature coefficient of linear expansion of the etalon is assumed to be 0.000 000 537 and of the steel ball, 0.000 012 272. The values of the diameter of the ball at 20 °C reproduce in the four tests to a standard deviation of the mean of 0.0070 microns. Average Values at 20 °C: Dia 6.350 011 16 cm; Vol. 134.067 062 cm^3

		Date of test											
		2-17-72			2-28-72			3-3-72			3-6-72		
Potentiometer Indication of thermocouple output (millivolts nominal)	1st	.			.288			.286			.292		
	2nd	.			.288			.287			.292		
	3rd	.			.288			.286			.292		
	4th	.		Avg.	.288		Avg.	.286		Avg.	.291		Avg.
	5th	.		.2628	.287		.2878	.285		.2860	.291		.2916
Room temperature	°C	19.32			19.25			19.30			19.40		
Thermocouple span	°C	1.084			1.187			1.179			1.202		
Reference temperature well−PRT	°C	19.182			19.017			19.048			19.006		
Correction for lead losses	°C	.012			.012			.011			.010		
Temperature of ball diameter test	°C	20.278			20.216			20.238			20.218		
Barometric pressure	°C	748.66			750.01			742.19			755.86		
Relative humidity	mm-Hg	21.4			25.2			33.3			14.7		
Effective wavelength (λ)	μ	.6328 22277			.6328 21958			.6328 23789			.6328 20572		
R = Right fraction L = Left fraction		L	R	L+R	L	R	L+R	L	R	L+R	L	R	L+R
Fringe fractions calculated from measurements made on interferometer negatives (constructive interference)	1st	.872	.238	.110	.370	.984	.354	.795	.422	.217	.364	.921	.285
	2nd	.514	.639	.153	.649	.634	.283	.293	.783	.076	.192	.038	.230
	3rd	.893	.156	.049	.632	.631	.263	.491	.535	.026	.923	.194	.117
	4th	.528	.563	.091	.769	.564	.333	.313	.803	.116	.197	.053	.250
	5th	.694	.453	.147	.477	.841	.318	.192	.054	.246	.868	.363	.231
	6th	.425	.668	.093	.046	.276	.322	.103	.068	.171	.972	.360	.332
	7th	.414	.700	.114	.286	.014	.300	.176	.888	.064	.144	.110	.254
	8th	.855	.307	.162	.445	.823	.268	.681	.411	.092	.036	.148	.184
	9th	.395	.738	.133	.	.	.	.211	.894	.105	.915	.318	.233
	10th	.672	.436	.108	.	.	.	.351	.707	.058	.163	.219	.382
	Average			.116			.305			.117			.250
Total fringe count (N)		12552.116			12552.305			12552.117			12552.250		
((N × λ)−0.710)/2 = MPD	μ	3971.2743			3971.3321			3971.2841			3971.3060		
Etalon length at test temperature	μ	67471.5972			67471.5950			67471.5957			67471.5950		
Ball diameter at test temperature	μ	63500.3229			63500.2629			63500.3116			63500.2890		
Ball diameter at 20 °C	μ	63500.1063			63500.0946			63500.1262			63500.1191		

TABLE 4b. *Resume of raw data taken during interferometric tests on Ball B*

Average test temperature = 20.2275 °C
Averaged measured diameter = 63500.2614 μ
Averaged Measured MPD = 3971.3340 μ

Data reduction is based upon an assumed etalon length of 67471.5870 microns at 19.996 °C based upon the average values obtained in Etalon tests ET−1 and ET−2. The temperature coefficient of linear expansion of the etalon is assumed to be 0.000 000 537 and of the steel ball, 0.000012272. The values of the diameter of the ball at 20 °C reproduce in the four tests to a standard deviation of the mean of 0.0040 microns. Average Values: Dia @ 20 °C = 6.350 0084 cm Vol. @ 20 °C = 134.066 888 cm^3

		Date of test											
		2–18–72			2–29–72			3–7–72			3–8–72		
Potentiometer indication of thermocouple output (millivolts nominal)	1st	.			.274			.293			.290		
	2nd	.			.274			.293			.291		
	3rd	.			.273			.294			.290		
	4th	.		Avg.	.274		Avg.	.293		Avg.	.289		Avg.
	5th	.		.2526	.		.2737	.		.2932	.		.2900
Room temperature	°C	19.30			19.30			19.30			19.30		
Thermocouple span	°C	1.042			1.128			1.209			1.196		
Reference temperature well − PRT	°C	19.194			19.095			18.995			19.006		
Correction for lead losses	°C	.012			.011			.011			.011		
Temperature of ball diameter test	°C	20.248			20.234			20.215			20.213		
Barometric pressure	mm-Hg	749.56			748.46			751.74			747.09		
Relative humidity	%	25.5			30.2			20.1			24.5		
Effective wavelength (λ)	μ	.6328 22081			.6328 22350			.6328 21535			.6328 22612		
R = Right fraction L = Left fraction		L	R	L+R	L	R	L+R	L	R	L+R	L	R	L+R
Fringe fractions calculated from Measurements made on interferometer negatives (constructive interference)	1st	.711	.705	.416	.157	.186	.343	.216	.174	.390	.645	.780	.425
	2nd	.047	.254	.301	.628	.563	.191	.676	.697	.373	.361	.031	.392
	3rd	.443	.808	.251	.934	.316	.250	.128	.039	.167	.500	.803	.303
	4th	.113	.136	.249	.679	.624	.303	.342	.940	.282	.495	.782	.277
	5th	.353	.852	.205	.043	.237	.280	.468	.861	.329	.902	.428	.330
	6th	.034	.251	.285	.658	.682	.340	.060	.201	.261	.199	.132	.331
	7th	.112	.123	.235	.264	.995	.259	.058	.281	.339	.557	.905	.462
	8th	.798	.517	.315	.470	.778	.248	.293	.091	.384	.622	.826	.448
	9th	.975	.297	.272	.439	.793	.232	.267	.054	.321	.532	.717	.249
	10th	.946	.282	.228	.916	.459	.375	.362	.948	.310	.525	.810	.335
	Average			.276			.282			.316			.355
Total fringe count (N)		12552.276			12552.282			12552.316			12552.355		
$((N \times \lambda) - 0.710)/2 =$ MPD	μ	3971.3237			3971.3273			3971.3329			3971.3520		
Etalon length at test temperature	μ	67471.5961			67471.5956			67471.5949			67471.5948		
Ball diameter at test temperature	μ	63500.2724			63500.2683			63500.2620			63500.2428		
Ball diameter at 20 °C	μ	63500.0792			63500.0860			63500.0945			63500.0769		

TABLE 4c. *Resume of raw data taken during interferometric tests on Ball C*

Average test temperature = 20.2653 °C
Averaged measured diameter = 63500.1918 μ
Averaged Measured MPD = 3971.4104 μ

Data reduction is based upon an assumed etalon length of 67471.6075 microns at 20.413 °C based upon the average values obtained in Etalon tests ET–3 and ET–4. The temperature coefficient of linear expansion of the etalon is assumed to be 0.000 000 537 and of the steel ball, 0.0000 12272. The values of the diameter of the ball at 20 °C reproduce in the four tests to a standard deviation of the mean of 0.0060 micron. Average Values: Dia @ 20 °C = 6.349 9985 cm Vol @ 20 °C = 134.066 261 cm^3

		Date of test											
		3–13–72			3–15–72			3–17–72			3–20–72		
Potentiometer indication of thermocouple output (millivolts nominal)	1st	.289			.286			.287			.285		
	2nd	.289			.285			.287			.286		
	3rd	.288			.286			.287			.285		
	4th	.288		Avg.	.285		Avg.	.287		Avg.	.285		Avg.
	5th	.		.2885	.		.2855	.		.2870	.		.2852
Room temperature	°C	19.30			19.32			19.20			19.30		
Thermocouple span	°C	1.189			1.177			1.183			1.176		
Reference temperature well – PRT	°C	19.065			19.073			19.066			19.084		
Correction for lead losses	°C	.012			.011			.013			.012		
Temperature of ball diameter test	°C	20.266			20.261			20.262			20.272		
Barometric pressure	mm-Hg	755.14			749.04			732.68			758.36		
Relative humidity	%	33.4			28.3			35.4			21.3		
Effective wavelength (λ)	μ	.6328 208 78			.6328 222 23			.6328 259 67			.6328 200 79		
R = Right fraction L = Left fraction		L	R	L+R	L	R	L+R	L	R	L+R	L	R	L+R
Fringe fractions calculated from measurements made on interferometer negatives (constructive interference)	1st	.608	.942	.550	.116	.427	.543	.337	.157	.534	.393	.163	.556
	2nd	.715	.942	.657	.402	.095	.497	.967	.692	.659	.103	.553	.656
	3rd	.564	.007	.571	.882	.715	.597	.483	.919	.402	.380	.262	.642
	4th	.418	.965	.383	.440	.103	.543	.732	.804	.536	.866	.928	.794
	5th	.222	.175	.397	.017	.444	.461	.146	.328	.474	.901	.673	.574
	6th	.998	.504	.502	.890	.654	.544	.796	.848	.644	.006	.494	.500
	7th	.748	.850	.598	.353	.202	.555	.655	.743	.398	.587	.996	.583
	8th	.965	.681	.646	.569	.133	.702	.794	.663	.457	.380	.054	.434
	9th	.332	.089	.421	.812	.788	.590	.171	.319	.490	.353	.124	.477
	10th	.031	.434	.465	.994	.721	.715	.526	.025	.551	.635	.899	.534
	Average			.519			.575			.515			.575
Total fringe count (N)		12552.519			12552.575			12552.515			12552.575		
$((N \times \lambda) - 0.710)/2 = \text{MPD}$	μ	3971.3930			3971.4192			3971.4237			3971.4058		
Etalon length at test temperature	μ	67471.6022			67471.6020			67471.6020			67471.6024		
Ball diameter at test temperature	μ	63500.2092			63500.1828			63500.1783			63500.1967		
Ball diameter at 20 °C	μ	63500.0019			63499.9795			63499.9741			63499.9848		

TABLE 4d. *Resume of raw data taken during interferometric tests on Ball D*

Average test temperature = 20.2678 °C
Averaged measured diameter = 63500.3969 μ
Averaged Measured MPD = 3971.2054 μ

Data reduction is based upon an assumed etalon length 67471.6075 microns at 20.413 °C based upon the average values obtained in Etalon tests ET−3 and ET−4. The temperature coefficient of linear expansion of the etalon is assumed to be 0.000 000 537 and of the steel ball, 0.0000 12272. The values of the diameter of the ball at 20 °C reproduced in the four tests to a standard deviation of the mean of 0.0041 micron. Average Values: Dia @ 20 °C = 6.350 018 8 cm Vol @ 20 °C = 134.067 547 cm³

		Date of test											
		3-14-72			3-16-72			3-21-72			3-22-72		
Potentiometer indication of thermocouple output (millivolts nominal)	1st	.287			.289			.287			.286		
	2nd	.287			.289			.287			.		
	3rd	.287			.290			.287			.		
	4th	.287		Avg.	.289		Avg.	.286		Avg.	.		Avg.
	5th	.		.2870	.		.2893	.		.2867	.		.286
Room temperature	°C	19.32			19.30			19.30			19.30		
Thermocouple span	°C	1.183			1.193			1.182			1.179		
Reference temperature well−PRT	°C	19.071			19.055			19.079			19.081		
Correction for lead losses	°C	.012			.012			.012			.012		
Temperature of ball diameter test	°C	20.266			20.260			20.273			20.272		
Barometric pressure	mm-Hg	750.28			744.16			756.01			737.16		
Relative humidity	%	32.4			29.7			31.9			38.7		
Effective wavelength (λ)	μ	.6328 219 71			.6328 233 35			.6328 206 76			.6328 249 81		
R = Right fraction L = Left fraction		L	R	L+R	L	R	L+R	L	R	L+R	L	R	L+R
Fringe fractions calculated from measurements made on interferometer negatives (constructive interference)	1st	.236	.768	.004	.799	.423	.222	.246	.591	.837	.096	.652	.748
	2nd	.765	.274	.039	.393	.562	.955	.675	.207	.882	.463	.454	.917
	3rd	.430	.368	.798	.831	.083	.914	.806	.142	.948	.011	.753	.764
	4th	.012	.807	.819	.991	.070	.061	.935	.957	.892	.332	.456	.788
	5th	.703	.076	.779	.772	.017	.789	.140	.730	.870	.534	.406	.940
	6th	.063	.913	.976	.530	.285	.815	.900	.935	.835	.555	.253	.808
	7th	.944	.874	.818	.746	.215	.961	.675	.258	.933	.122	.737	.859
	8th	.890	.907	.797	.794	.178	.972	.077	.016	.093	.587	.322	.909
	9th	.371	.664	.035	.194	.659	.853	.720	.100	.820	.881	.854	.735
	10th	.355	.691	.046	.459	.306	.765	.962	.907	.869	.310	.386	.696
	Average			.911			.931			.898			.816
Total Fringe Count (N)		12551.911			12551.931			12551.898			12551.816		
$((N \times \lambda) - 0.710)/2 = \text{MPD}$	μ	3971.2075			3971.2224			3971.1953			3971.1964		
Etalon length at test temperature	μ	67471.6022			67471.6020			67471.6024			67471.6024		
Ball diameter at test temperature	μ	63500.3947			63500.3796			63500.4071			63500.4060		
Ball diameter at 20 °C	μ	63500.1874			63500.1770			63500.1944			63500.1941		

TABLE 4e. *Resume of raw data taken during interferometric tests on Ball E*

Average test temperature = 22.8835 °C
Averaged measured diameter = 63502.3533 μ
Averaged Measured MPD = 3969.3415 μ

Data reduction is based upon an assumed etalon length of 67471.6985 microns at 22.987 °C based upon the average values obtained in Etalon tests ET−5 and ET−6. The temperature coefficient of linear expansion of the etalon is assumed to be 0.000 000 537 and of the steel ball, 0.000012272. The values of the diameter of the ball at 20 °C reproduce in the four tests to a standard deviation of the mean of 0.0054 microns. Average Values: Dia @ 20 °C = 6.350 010 6 cm Vol @ 20 °C = 134.067 028 cm³

		Date of test											
		5–3–72			5–8–72			5–11–72			5–11–72		
Potentiometer indication of thermocouple output (millivolts nominal)	1st	.614			.615			.598			.594		
	2nd	.614			.614			.599			.595		
	3rd	.615			.614			.599			.595		
	4th	.614		Avg.	.614		Avg.	.599		Avg.	.594		Avg.
	5th	.		.6142	.		.6142	.		.5987	.		.5945
Room temperature	°C	20.60			20.50			20.58			20.60		
Thermocouple span	°C	2.532			2.532			2.468			2.450		
Reference temperature well−PRT	°C	20.379			20.361			20.341			20.351		
Correction for lead losses	°C	.030			.032			.029			.029		
Temperature of ball diameter test	°C	22.941			22.925			22.838			22.830		
Barometric pressure	mm-Hg	745.61			747.91			759.11			758.66		
Relative humidity	%	42.2			41.7			23.9			22.4		
Effective wavelength (λ)	μ	.6328 24672			.6328 24143			.6328 21449			.6328 21534		
R = Right fraction L = Left fraction		L	R	L+R	L	R	L+R	L	R	L+R	L	R	L+R
Fringe fractions calculated from Measurements made on interferometer negatives (constructive interference)	1st	.505	.316	.821	.946	.992	.938	.989	.155	.144	.230	.988	.218
	2nd	.708	.115	.823	.992	.795	.787	.666	.520	.186	.544	.569	.113
	3rd	.064	.723	.787	.699	.193	.892	.917	.273	.190	.807	.348	.155
	4th	.225	.563	.788	.690	.239	.929	.825	.320	.145	.982	.116	.098
	5th	.954	.838	.792	.131	.749	.880	.414	.720	.134	.178	.993	.171
	6th	.054	.752	.806	.614	.280	.894	.321	.859	.180	.935	.199	.134
	7th	.534	.200	.734	.824	.106	.930	.650	.448	.098	.853	.317	.170
	8th	.290	.451	.741	.758	.172	.930	.653	.557	.210	.565	.566	.131
	9th	.874	.894	.768	.682	.209	.891	.868	.244	.112	.359	.790	.149
	10th	.246	.458	.704	.094	.782	.876	.290	.863	.153	.183	.982	.165
	Average			.776			.895			.156			.150
Total fringe count (N)		12545.776			12545.895			12546.156			12546.150		
$((N \times \lambda) - 0.710)/2 =$ MPD	μ	3969.2833			3969.3176			3969.3833			3969.3819		
Etalon length at test temperature	μ	67471.6969			67471.6963			67471.6931			67471.6928		
Ball diameter at test temperature	μ	63502.4136			63502.3787			63502.3098			63502.3109		
Ball diameter at 20°C	μ	63500.1217			63500.0993			63500.0982			63500.1055		

TABLE 4f. *Resume of raw data taken during interferometric tests on Ball F*

Average test temperature = 22.9153 °C
Averaged measured diameter = 63502.3682 μ
Averaged Measured MPD = 3969.3278 μ

Data reduction is based upon an assumed etalon length of 67471.6985 microns at 22.987 °C based upon the average values obtained in Etalon tests ET−5 and ET−6. The temperature coefficient of linear expansion of the etalon is assumed to be .000 000 537 and of the steel ball, .0000 12272. The values of the diameter of the ball of 20 °C reproduce in the four tests to a standard deviation of the mean of 0.0064 microns. Average Values: Dia @ 20 °C = 6.350 0096 cm Vol @ 20 °C = 134.066 966 cm³

		Date of test											
		5-2-72			5-2-72			5-4-72			5-10-72		
Potentiometer indication of thermocouple output (millivolts nominal)	1st	.604			.604			.616			.596		
	2nd	.604			.604			.616			.596		
	3rd	.605			.604			.616			.596		
	4th	.604		Avg.	.604		Avg.	.616		Avg.	.596		Avg.
	5th	.		.6042	.		6040	.		.6160	.		.5960
Room temperature	°C	20.70			20.70			20.50			20.60		
Thermocouple span	°C	2.490			2.489			2.539			2.456		
Reference temperature well − PRT	°C	20.421			20.421			20.369			20.357		
Correction for lead losses	°C	.029			.029			.032			.029		
Temperature of ball diameter test	°C	22.940			22.939			22.940			22.842		
Barometric pressure	mm-Hg	748.21			748.11			746.98			754.06		
Relative humidity	%	42.3			41.6			36.5			32.0		
Effective wavelength (λ)	μ	.6328 24089			.6328 24106			.6328 24321			.6328 22643		
R = Right fraction L = Left fraction		L	R	L+R	L	R	L+R	L	R	L+R	L	R	L+R
Fringe fractions calculated from measurements made on interferometer negatives (constructive interference)	1st	.747	.183	.930	.609	.224	.833	.595	.332	.927	.477	.772	.249
	2nd	.139	.727	.866	.796	.107	.903	.054	.848	.902	.482	.744	.226
	3rd	.441	.432	.873	.293	.521	.814	.465	.365	.830	.077	.086	.163
	4th	.285	.527	.812	.401	.475	.876	.969	.951	.920	.663	.523	.186
	5th	.947	.853	.800	.535	.223	.758	.853	.013	.866	.201	.980	.181
	6th	.126	.579	.705	.280	.591	.871	.901	.006	.907	.632	.582	.214
	7th	.244	.547	.791	.379	.395	.774	.130	.721	.851	.150	.941	.091
	8th	.090	.866	.956	.560	.207	.767	.689	.173	.862	.834	.409	.243
	9th	.658	.166	.824	.960	.964	.924	.351	.490	.841	.910	.189	.099
	10th	.866	.011	.877	.424	.388	.812	.341	.388	.929	.002	.102	.104
	Average			.843			.833			.884			.176
Total fringe count (*N*)		12545.843			12545.833			12545.884			12546.176		
$((N \times \lambda) - 0.710)/2 = \text{MPD}$	μ	3969.3008			3969.2978			3969.3153			3969.3971		
Etalon length at test temperature	μ	67471.6968			67471.6968			67471.6968			67471.6933		
Ball diameter at test temperature	μ	63502.3960			63502.3990			63502.3815			63502.2962		
Ball diameter at 20°C	μ	63500.1050			63500.1086			63500.0904			63500.0814		

where t_1 is the lower temperature and t_2 the higher. We have measured the MPD of balls A and B at about 20.2 °C and (under the names E and F) at about 23 °C and presented the data in table 4. By this procedure we estimate the coefficient of A to be 0.000 012 220 and B to be 0.000 012 324.

The manufacturer believes the coefficients of the balls (whatever their magnitude) to be about equal because they were from the same metallurgical stock, subjected to the same heat treatment and same mechanical surface work. Accordingly, we have averaged the above two values and applied this average, 000 012 272 to all balls.

2.5. Hydrostatic Transfer of Volumetric Information from the Spheres to the Crystals

Several years ago, BIPM circulated a one-kilogram metal object among the major national metrology laboratories for a density determination. The spread of data among this very sophisticated group amounted to about 14 ppm. Although part of this spread could most certainly be ascribed to differences in density of the water samples used, we have always believed (without proof) that this was another demonstration of the basic imprecision of the classical hydrostatic weighing experiment. In spite of the shortcomings of this experiment, nobody has suggested a more precise procedure for routine density comparisons. Although the thermal Cartesian Diver of Spaepen [13] and the pressure Cartesian Diver of Bowman and Schoonover [6] are about two orders more precise than ordinary hydrostatic weighing, the complexity of such systems immediately eliminates them from the "routine" category.

The volumetric information contained in our spheres was too dear to us to dissipate unnecessarily in the imprecision of a classical hydrostatic transfer experiment, so we had previously devoted a great deal of effort to improving this precision. We have found it expedient to modify both the hydrostatic system and the experimental philosophy.

2.5.1. The Hydrostatic System

There are four components of the hydrostatic weighing system: (1) the suspension, (2) the liquid, (3) the immersed pan loading assembly, and (4) the hydrostatic balance. Each component contributes to imprecision; but if choices are made with care, total variability may be restricted to reasonable bounds.

2.5.1.1. The Hydrostatic Suspension

This is the member which delivers the load from the immersed structure to the balance. Its most critical component is the suspension wire which passes through the air-liquid interface. Inasmuch as we have already published [14] a procedure for reducing variability from this source to a few micrograms it will not be commented upon here.

2.5.1.2. The Hydrostatic Liquid

The intent of the hydrostatic weighing experiment is accomplished by observing the buoyant force exerted on the object of interest by the liquid. The liquid exerts two independent effects on the precision of the experiment. The greater its density, the greater is the magnitude of the buoyant force exerted by the liquid, and the easier it is to measure in the presence of many small perturbing forces. The liquid we have chosen is a fluorocarbon whose density (1.8g/cm^3) is almost twice that of water so that precision is almost doubled. This substance has been used in this service for many years by atomic reactor experimenters and it has proved to be an excellent choice.

One of the major perturbing forces associated with the use of water arises from its large and variable surface tension. The penetration wire minimizes most of these effects when it is skillfully prepared. The fluorocarbon we use has a surface tension only about one fifth that of water (15 versus 75 dyn/cm) which has the effect of improving wire performance even if incorrectly or sloppily prepared.

An additional major advantage of this liquid is its vast appetite for absorbing gas. This gives a great deal of protection against variability associated with surface bound tiny bubbles on immersed loads.

2.5.1.3. The Immersed Pan Loading Assembly – Redundancy

A time honored technique for minimizing random variability in a process is to make "many" independent observations.

In comparing two quantities the experimenter has available only *one* comparison combination. In working with three quantities he has only *three* combinations. When he works with four quantities he has *six* combinations, and under these circumstances he has the redundancy necessary to make a meaningful reduction in random variability.

Figure 5 is a schematic sketch of our immersed pan loading assembly, from which it is obvious that we

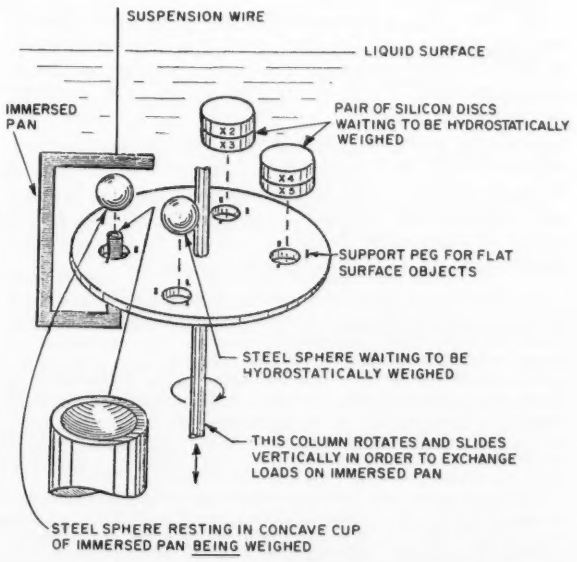
SUSPENSION WIRE
LIQUID SURFACE
IMMERSED PAN
PAIR OF SILICON DISCS WAITING TO BE HYDROSTATICALLY WEIGHED
X2
X3
X4
X5
SUPPORT PEG FOR FLAT SURFACE OBJECTS
STEEL SPHERE WAITING TO BE HYDROSTATICALLY WEIGHED
THIS COLUMN ROTATES AND SLIDES VERTICALLY IN ORDER TO EXCHANGE LOADS ON IMMERSED PAN
STEEL SPHERE RESTING IN CONCAVE CUP OF IMMERSED PAN BEING WEIGHED

FIGURE 5. *Immersed pan loading mechanism.*

are able to compare four different loads in a single experiment. The sketch shows two of the loading trays carrying two silicon crystals each, a third tray carrying ball B and the fourth tray (which normally carries ball A) empty, inasmuch as ball A is on the immersed pan.

With the apparatus loaded as illustrated we may compare the four loads (two balls and two *pairs* of silicon crystals) in all six combinations. This comparison format is called a 4−1 series and is the format used throughout this work. It should be noted that by varying the combinations of loading that many different 4−1 series may be conducted on the same two balls and four crystals. We utilized the four combinations shown below:

TRAY 1	TRAY 2	TRAY 3	TRAY 4
BALL A	BALL B	X2+X3	X4+X5
BALL A	BALL B	X2+X4	X3+X5
BALL A	BALL B	X2+X5	X3+X4
X2	X3	X4	X5

2.5.1.4. The Hydrostatic Balance and Its Calibration

Other factors being equal, the data spread among independently measured densities decreases with increasing sample size. In our 1967 paper on hydrostatic weighing in water, we demonstrated that a single-pan, damped, direct-reading balance would provide density values spreading by 3 ppm (worse case) for 10 cubic centimeter samples. This was significantly better than our previous work using a free-swinging, equal-arm balance. For this reason, and others mentioned in that paper, we abandoned the conventional balance, and since that time, all critical density work at NBS has been performed on single-pan, direct-reading instruments.

In 1967 we recommended the single-pan direct-reading balance as the best available instrument and, to date, we have found no evidence to suggest a change in this position. We have used two balances of this type in the work reported here. In the earlier paper we speculated upon the ideal hydrostatic balance (servo-driven-to-null) and we have commenced development of such a device. We feel confident that this balance will improve the hydrostatic experiment by about an order of magnitude. Until this device is complete we shall continue use of the simple instrument.

In informal and unreported experiments on conventional free-swinging equal-arm balances we found several modifications which would improve their hydrostatic precision. The application of strong vertical temperature gradients in the balance case as described by Macurdy, NBS, [15] reduced random variability. The application of external damping was even more effective. Reducing sensitivity (by lowering the gravity knob) to the point where readability and reproducibility were about equal actually improved the latter. The use of a large-volume hydrostatic chamber appeared to give higher precision data than small chambers.

We believe that the vertical oscillations of an immersed load suspended from a free-swinging balance are damped by the viscous action of the liquid on the load. During this process, momentum is transferred from the oscillating system to the liquid where it manifests itself as turbulence. This turbulence results in faulty "turning point" data. We believe that system damping should be such that momentum is removed completely from the hydrostatic system such as is true for damping by air or magnetic eddy currents and the heavier this damping, up to near critical, the better because the quicker the oscillations are damped to zero, the less the turbulence in the liquid.

We believe that by the judicious use of the techniques mentioned above and perhaps some others, hydrostatic work on the free swinging balance could be significantly improved. Considering the relative ease of achieving ppm results with a direct-reading balance, it is questionable whether the required expenditure of effort would be justified.

In the single-arm direct-reading damped balance, the maximum vertical motion of the suspension is about 3 millimeters, and the motion is quickly damped externally to near zero. In a balance of this type, built-in balance weights may be added to or removed from the suspension by remote control dials which cause only slight motion being induced in the bath.

Commercially available single-pan direct-reading balances are intended for use in the air weighings mode, and in such service they satisfy most weighing requirements. When they are put to use in the hydrostatic mode it is necessary that the direct-reading data be interpreted in a slightly different manner in the data reduction process. The data are obtained from the balance by means of two devices—the numbers engraved on the weight changing dial(s) and the numbers projected on a screen from a highly magnified view of a small reticle attached to the beam counterweight system.

1. SCREEN READINGS. The manufacturer of the balance assigns mass designations to the screen readings which are appropriate for use in the air weighing mode. These designations are based upon assumptions regarding the density of the objects to be weighed and that the only screen-related force in the system is associated with beam-angle moments. In the hydrostatic mode there must necessarily be a wire penetrating the liquid surface. The dip section of this wire (the section which is sometimes immersed in the bath and sometimes exposed to air) exerts two forces on the suspension system—a constant force and also a force which is directly proportional to the screen reading. Although neither of these forces have to be evaluated independently, as will be shown in the section following, the screen-related force demands that we interpret the screen readings *merely as numbers* indicating the angle of the beam counterweight system. This interpretation satisfies all requirements of the double substitution force comparison solution given in the next section.

2. THE DIAL READINGS. The numbers engraved on the weight manipulation dials are intended for use in direct-weighing in air of loads placed on the weighing pan. In the air weighing situation they indicate (in units of apparent mass versus brass [16]) the mass of balance weights *removed from* the suspension. In the calibration procedure it is necessary to determine the true mass of weights actually loading the suspension for each dial reading to make a true comparison between the forces associated with an immersed load and those associated with the built-in balance weights (in air). There are two methods of obtaining a calibration. The easiest is by weighing standard weights on

the pan of the balance. This was discussed in our 1967 paper. The other technique is to remove the weights from the balance and calibrate them in the same manner that one would use in the calibration of any other standard weight.

A requirement of a direct-reading balance to be used in hydrostatic work is that the major weights of the balance have densities equal to a few parts in 10^4. Most manufacturers meet this requirement. We verified by experiment that this requirement was satisfied in the balances used in our work.

When the hydrostatic balance is to be used in the most critical work, the built-in weights should be calibrated in two steps:

1. All weights should be removed from the balance and the total mass (of the summation) should be determined. Out of this test we obtain a value of the correction to the nominal value of the summation and an estimate of the uncertainty in this value.
2. The balance weights should then be intercompared in combinations which permit a calculation of the fraction of the summation mass contained in each individual balance weight.

2.5.2. Hydrostatic Weighing on a Direct-Reading Balance

Our objective in hydrostatically weighing an object is to obtain a value of I, defined as

$$I = M - \rho_L V$$

where M and V are the mass and volume respectively of the object and ρ_L the density of the liquid.

For several years we have determined I from a double substitution comparison between the (unknown) force associated with the immersed load and the (known) force associated with the built-in weights of a single-arm direct-reading balance. The format which we use in making this comparison consists of five balance observations under various load conditions. The entire comparison requires four minutes because, we have found, results are most reproducible when there is a one minute interval between observations. The five load conditions are:

1. With the immersed pan empty
2. With the immersed pan loaded by the object of interest
3. With the sensitivity weight added (in air)
4. With the load removed from the immersed pan
5. With the sensitivity weight removed—the first and fifth load conditions are the same.

Each observation requires the recording of two data (1) the dial reading which indicates the combination of the built-in balance weights which are in place and loading the suspension, (2) the screen reading which is taken as a number indicating the beam-counterweight angle with respect to some fixed reference. As pointed out in the previous section, this *is not* the interpretation placed on direct-reading balance data in the ordinary weighing situation.

In the first, fourth and fifth observations, taken with the immersed pan empty, the dial readings will be the same ($D_i = D_0$), and in the second and third, with the immersed pan loaded ($D_i = D_L$). The five screen readings, s_1 to s_5, are usually different. The balance data are therefore of the form

$$\begin{array}{l} D_0,\ s_1 \\ D_L,\ s_2 \\ D_L,\ s_3 \\ D_0,\ s_4 \\ D_0,\ s_5 \end{array}$$

In our 1967 paper [14] on hydrostatic weighing we presented a detailed discussion of the linearity between the beam angle and changes in the total suspension force. We described how the linearity may be evaluated in a simple experiment and how to correct observed data if linearity was judged to be inadequate. Since the date of that paper, we have evaluated several single-arm, direct-reading balances, and we have not found any to be inadequately linear for hydrostatic work.

Subject to the following assumptions, we may write equations associated with suspension forces under each of the five load conditions listed above:

1. That the beam angle, as defined by screen readings, is a linear indicator of the difference between the total suspension force and a fixed reference force associated with the counter-weight system.
2. That prior calibration effort has provided us with knowledge of the true mass and density of each of the three balance weights involved in the double-substitution comparison. These three weights are:

   a. D_0—the combination of balance weights loading the suspension when the dial reads D_0.
   b. D_L—the combination of balance weights loading the suspension when the dial reads D_L.
   c. S—the sensitivity weight.

3. That the density, ρ_B, of these three weights is equal.
4. That the following parameters are constant during the four minute observation interval:

   a. The air density, ρ_A, in the balance case.
   b. The bath density, ρ_L.
   c. The volume and density of the meniscus.

5. That there are no perturbing turbulent forces.
6. That the drift in the system is linear with time.

The five observation equations to be written consist of various combinations of forces. With the exception of the unknown force exerted by the immersed load, Ig (where g is the acceleration due to gravity at the immersed pan level) these forces fall into three classes:

1. Forces which are constant over the observation interval. These forces need not be evaluated because they are eliminated during the solution of the system

of observation equations. They may be added directly and the value of C assigned to their sum. These forces are:

a. The force exerted by the portion of the suspension which is *never* immersed in the bath.
b. The forces exerted by the portion of the suspension which is *always* immersed.
c. The constant component of force exerted by the dip section of the suspension wire.
d. The reference force.
e. The meniscus force.

2. Forces which are linearily related to the beam angle (and hence the screen reading). There are two such forces:

a. $K_1 s_i$, where K_1 is the proportionality constant between the screen reading, s_i, and the difference between the constant reference force and the total suspension force.
b. $K_2 s_i$, where K_2 is the proportionality constant between the screen reading, s_i, and the component of force exerted by the dip section of the suspension wire which is screen related.

These two forces need not be previously evaluated because they are added together as

$$Ks_i = K_1 s_i + K_2 s_i$$

and are evaluated (as a sum) during the solution of the system of observation equations.

3. The forces which are exerted by the three balance weights involved in the comparison. These three forces are:

$$F_{D0} = M_{D0}\left[1 - \frac{\rho_A}{\rho_B}\right] g_1$$

$$F_{DL} = M_{DL}\left[1 - \frac{\rho_A}{\rho_B}\right] g_1$$

$$F_S = M_S \left[1 - \frac{\rho_A}{\rho_B}\right] g_1$$

where g_1 is the acceleration due to gravity at the vertical level in the balance case in which the balance weights are loaded on the suspension.

The five observation equations and a method of solving them for the value of I are as follows:

1. $C + F_{D0} = s_1 K$
2. $C + F_{DL} + Ig = s_2 K$
3. $C + F_{DL} + Ig + F_S = s_3 K$
4. $C + F_{D0} + F_S = s_4 K$
5. $C + F_{D0} = s_5 K$

Subtracting eq (1) from eq (2) gives us a value of Ig in terms of K. Subtracting eq (2) from eq (3) provides us with a value of K so that we may write our first value of Ig from the double substitution force comparison

$$I'g = F_{D0} - F_{DL} + F_S\left[\frac{s_2 - s_1}{s_3 - s_2}\right].$$

A similar manipulation of eqs (3), (4), and (5) gives us the second value

$$I''g = F_{D0} - F_{DL} + F_S\left[\frac{s_3 - s_4}{s_4 - s_5}\right]$$

Letting

$$s = \frac{\dfrac{s_2 - s_1}{s_3 - s_2} + \dfrac{s_3 - s_4}{s_4 - s_5}}{2}$$

we may write the average value of Ig which is used during data reduction

$$Ig = \frac{I'g + I''g}{2} = F_{D0} - F_{DL} + F_S s.$$

Replacing the right member force terms by their calibration data gives us the numerical value of I which the experiment is designed to provide

$$I = [M_{D0} - M_{DL} + M_S s]\left[1 - \frac{\rho_A}{\rho_B}\right]\left[\frac{g_1}{g}\right]$$

An adequate value of g_1 is obtained from geometric measurements on the system and assumed values of g and the vertical gradient in g. As pointed out in the previous section, there are two methods of calibrating a direct-reading balance. If the weights are *removed from* the balance for calibration, g_1 is the value of the acceleration due to gravity at the level in the suspension where the weights actually load it. On the other hand, if the weights are calibrated in place by weighing standard weights on the load pan of the balance, the effective level at which g_1 should be calculated is the level of the load pan in the weighing chamber of the balance.

In the foregoing solution for I, we initially obtain two values of Ig, namely $I'g$ and $I''g$. These two values should be very nearly equal. A wide separation of the two values probably indicates failure to meet the six assumptions upon which the solution depends. We believe the $I'g - I''g$ may be an excellent quality control signal, but we have not yet had the long experience with our system which is necessary to evaluate it as such.

2.5.3. Hydrostatic Weighing Format—The 4–1 Ratio Series

The equation

$$I_A = M_A - \rho_L V_A$$

where the subscript A indicates that object A is under test, is classically solved for V_A based upon measured values of I_A and M_A and a tabulated value of ρ_L.

This is not our intent. By use of the immersed pan loading assembly, 2.5.1.3, we remove object A from the immersed pan and replace it with object B. This results in violent turbulence in the bath, so we wait 10 minutes for the bath motion to subside, after which we perform the 5 observations required to obtain a value of

$$I_B = M_B - \rho_L V_B.$$

These two equations may be combined to provide us with a value of the volumetric ratio of object A to object B

$$\frac{V_A}{V_B} = \frac{M_A - I_A}{M_B - I_B}.$$

Combining the hydrostatically measured values of I_A and I_B with previously determined values of M_A and M_B yields a numerical value of the volumetric ratio at the temperature of the experiment. The validity of the ratio is primarily limited by the nonlinear drift in the system. The linear component is accounted for by performing the hydrostatic weighings in a time-symmetrical A–B–A format.

Inasmuch as our immersed pan loading assembly will manipulate 4 objects, we may compare them in six combinations. This requires 15 hydrostatic weighings taken in the following order:

A–B–A–C–A–D–A–B–C–B–D–B–C–D–C.

This is not a perfectly balanced series because object D is weighed only three times while all other objects are weighed four times; however it is adequate to define the six ratios in A–B–A type formats.

A 4–1 series ordinarily provides us with six differences. In the case at hand we obtain six ratios, and in this case, the series is referred to as a 4–1 ratio series.

The 15 weighings to be performed are then calculated as six 1–2–1 comparisons of volumes.

A–B–A gives us the volumetric ratio $\frac{A}{B}$

A–C–A gives us the volumetric ratio $\frac{A}{C}$

A–D–A gives us the volumetric ratio $\frac{A}{D}$

B–C–B gives us the volumetric ratio $\frac{B}{C}$

B–D–B gives us the volumetric ratio $\frac{B}{D}$

C–D–C gives us the volumetric ratio $\frac{C}{D}$

This procedure may be interrupted at any time *between* 1–2–1 comparisons, however this usually requires one additional observation to maintain the time symmetrical properties of each comparison.

In actual practice, all 15 tests which make up the 4–1 ratio series are conducted at slightly different temperatures. Unless the objects under volumetric comparison have the same temperature coefficients of expansion, their ratio will be a function of the temperature of observation. Therefore, before proceeding with the least-squares adjustment of this series, we reduce the observed ratio at the temperature of the test to the ratio which would exist at 20 °C by appropriate application of the temperature coefficients of expansion of the objects.

We use the method of Connor and Youden, NBS, [17] for least-squares adjustment. They noted that the products of the observed ratios

$$\frac{A}{B} X \frac{B}{C} X \frac{C}{A}$$

$$\frac{A}{B} X \frac{B}{D} X \frac{D}{A}$$

$$\frac{A}{C} X \frac{C}{D} X \frac{D}{A}$$

$$\frac{B}{C} X \frac{C}{D} X \frac{D}{B}$$

as well as some four-ratio-products would be exactly equal to unity if the series were performed without error. These observed ratios may be adjusted by least squares to values which actually do have unity products by their formula of the form

$$\frac{\hat{A}}{\hat{B}} = \sqrt[4]{\left[\frac{A}{B}\right]^2 \left[\frac{A}{C} X \frac{C}{B}\right] \left[\frac{A}{D} X \frac{D}{B}\right]}$$

where the overlined values, eg., $\frac{\hat{A}}{\hat{B}}$, are adjusted ratios.

The absolute sum of the six residual differences between the observed and adjusted ratios is a measure of the precision of the conduct of the 4–1 ratio series.

As pointed out in 2.5.1.3 we are able to conduct four different 4–1 ratio series on the two standard balls and four crystals. The observed ratios, 24 in all, are presented in tables 5. Also shown in the table are the ratios reduced to 20 °C, their adjusted values from the Connor-Youden procedure, and the sum of the residuals.

In 2.5.2 it was shown that the mass of the objects enters the calculation of the volumetric ratios, so the assumed values of the masses and coefficients of expansion of the six objects are given in the caption to the tables 5.

2.6. Final Calculation of Crystal Volumes and Densities

The 24 ratios shown in the last column of table 5 may each be used in writing an equation expressing the relative volume between various members of the

525-013 O - 74 - 3

TABLE 5a

This table presents the volumetric ratios between the four silicon crystals and the two steel balls employed in Determination AB. As pointed out in the test the "ratios at test temperature" are calculated from the previously measured mass value and the weight in liquid measured hydrostatically. The ratios at 20 °C involve assumed values of temperature coefficients of expansion. These assumed masses and coefficients are given below. These ratios at 20 °C are submitted (in groups of six) to the Connor-Youden least square adjustment procedure, and the adjusted ratios are given in the last column with the sum of residuals.

	Measured mass (grams)	Lin. coef. exp.
Ball A	1043. 352 056	0.000 012 272
Ball B	1043. 482 802	.000 012 272
X2	200. 420 689	.000 002 56
X3	199. 763 734	.000 002 56
X4	200. 010 795	.000 002 56
X5	199. 932 675	.000 002 56

Sum of volumes of the 2 balls = 268.073 950 cm³ at 20 °C.

Test No.	Ratio under test	Avg test temp	Observed ratio at test temp	Ratio reduced to 20 °C	L.S. adjusted ratio
1	A:B	20.3187	1.0000028601	1.0000028442	1.0000028767
2	A:X2 + X3	20.3183	.7802953318	.7802881037	.7802877510
3	A:X4 + X5	20.3168	.7807629276	.7807556860	.7807560134
4	B:X2 + X3	20.3194	.7802923978	.7802851145	.7802855064
5	B:X4 + X5	20.3205	.7807614394	.7807541343	.7807537675
6	X2 + X3:X4 + X5	20.3176	1.0006000685	1.0006000647	1.0006001151
				Absolute sum of residuals =	.00000515217
7	A:B	20.3361	1.0000023160	1.0000023107	1.0000014007
8	A:X2 + X4	20.3370	.7798135876	.7798059447	.7798063201
9	A:X3 + X5	20.3370	.7812466828	.7812390037	.7812393385
10	B:X2 + X4	20.3359	.7798135609	.7798059199	.7798052278
11	B:X3 + X5	20.3346	.7812458895	.7812382618	.7812382442
12	X2 + X4:X3 + X5	20.3336	1.0018380683	1.0018380664	1.0018376594
				Absolute sum of residuals =	.0000027368
13	A:B	20.3533	1.0000013838	1.0000014360	1.0000004250
14	A:X2 + X5	20.3519	.7799632731	.7799553009	.7799560148
15	A:X3 + X4	20.3501	.7810926282	.7810846634	.7810847381
16	B:X2 + X5	20.3482	.7799633471	.7799554589	.7799556833
17	B:X3 + X4	20.3470	.7810933265	.7810854207	.7810844062
18	X2 + X5:X3 + X4	20.3474	1.0014459694	1.0014459580	1.0014471628
				Absolute sum of residuals =	.0000042435
19	X2:X3	20.3157	1.0032860536	1.0032860446	1.0032863403
20	X2:X4	20.3168	1.0020459883	1.0020459770	1.0020468304
21	X2:X5	20.3169	1.0024388963	1.0024388959	1.0024377467
22	X3:X4	20.3186	.9987632820	.9987632796	.9987645502
23	X3:X5	20.3163	.9991551669	.9991551626	.9991541860
24	X4:X5	20.3170	1.0003879913	1.0003879932	1.0003901178
				Absolute sum of residuals =	.0000066700

TABLE 5b

This table presents the volumetric ratios between the four silicon crystals and the two steel balls employed in Determination CD. As pointed out in the text the "ratios at test temperature" are calculated from the previously measured mass value and the weight in liquid measured hydrostatically. The ratios at 20 °C involve assumed values of temperature coefficients of expansion. These assumed masses and coefficients are given below. These ratios at 20 °C are submitted (in groups of six) to the Connor-Youden least square adjustment procedure, and the adjusted ratios are given in the last column with the sum of residuals.

	Measured mass (grams)	Lin. coef. exp.
Ball C	1043. 941 406	0.000 012 272
Ball D	1042. 909 214	.000 012 272
X2	200. 420 653	.000 002 56
X3	199. 763 663	.000 002 56
X4	200. 010 763	.000 002 56
X5	199. 932 620	.000 002 56

Sum of volumes of the 2 balls = 268.073 808 cm^3 at 20 °C

Test No.	Ratio under test	Avg test temp	Observed ratio at test temp	Ratio reduced to 20 °C	L.S. adjusted ratio
1	C:D	19.1941	0.9999902719	0.9999903218	0.9999899545
2	C:X2+X3	19.1931	.7802638204	.7802821681	.7802820581
3	C:X4+X5	19.1925	.7807321977	.7807505575	.7807509544
4	D:X2+X3	19.1933	.7802711575	.7802895033	.7802898965
5	D:X4+X5	19.1928	.7807411148	.7807594778	.7807587975
6	X2+X3:X4+X5	19.1913	1.0006005705	1.0006005686	1.0006009318
				Absolute sum of residuals =	0.0000023109
7	C:D	19.1742	.9999902037	0.9999902105	.9999903037
8	C:X2+X4	19.1748	.7797814847	.7798002324	.7798001020
9	C:X3+X5	19.1758	.7812152264	.7812340008	.7812340586
10	D:X2+X4	19.1770	.7797887982	.7798074949	.7798076632
11	D:X3+X5	19.1781	.7812230169	.7812417295	.7812416338
12	X2+X4:X3+X5	19.1774	1.0018388271	1.0018388285	1.0018388772
				Absolute sum of residuals =	0.0000005943
13	C:D	19.1771	0.9999898783	0.9999898601	.9999899070
14	C:X2+X5	19.1764	.7799335893	.7799523068	.7799524297
15	C:X3+X4	19.1763	.7810629297	.7810816678	.7810815082
16	D:X2+X5	19.1753	.7799418941	.7799606345	.7799603018
17	D:X3+X4	19.1755	.7810702651	.7810890220	.7810893917
18	X2+X5:X3+X4	19.1754	1.0014478970	1.0014478942	1.0014476248
				Absolute sum of residuals =	0.0000013011
19	X2:X3	19.1674	1.0032889403	1.0032889517	1.0032884305
20	X2:X4	19.1661	1.0020461432	1.0020461603	1.0020461508
21	X2:X5	19.1669	1.0024379242	1.0024379280	1.0024384582
22	X3:X4	19.1703	0.9987618535	0.9987618281	0.9987617920
23	X3:X5	19.1687	.9991533078	.9991532965	.9991528136
24	X4:X5	19.1701	1.0003915491	1.0003915520	1.0003915063
				Absolute sum of residuals =	0.0000016255

TABLE 5c

This table presents the volumetric ratios between the four silicon crystals and the two steel balls employed in Determination EF. As pointed out in the text the "ratios at test temperature" are calculated from the previously measured mass value and the weight in liquid measured hydrostatically. The ratios at 20 °C involve assumed values of temperature coefficients of expansion. These assumed masses and coefficients are given below. These ratios at 20 °C are submitted (in groups of six) to the Connor-Youden least square adjustment procedure, and the adjusted ratios are given in the last column with the sum of residuals.

	Measured mass (grams)	Lin. coef. exp.
Ball E	1043.351 968	0.000 012 272
Ball F	1043.482 847	.000 012 272
X2	200.420 679	.000 002 56
X3	199.763 687	.000 002 56
X4	200.010 802	.000 002 56
X5	199.932 659	.000 002 56

Sum of volumes of the 2 balls = 134.073 994 cm^3 at 20 °C.

Test No.	Ratio under test	Avg test temp	Observed ratio at test temp	Ratio reduced to 20 °C	L.S. adjusted ratio
1	E : F	23.4340	1.0000017166	1.0000016894	1.0000012132
2	E : X2 + X3	23.4346	0.7803650384	0.7802869637	0.7802869783
3	E : X4 + X5	23.4336	.7808337796	.7807556737	.7807560308
4	F : X2 + X3	23.4304	.7803630492	.7802850701	.7802860317
5	F : X4 + X5	23.4291	.7808344232	.7807564176	.7807550837
6	X2 + X3 : X4 + X5	23.4303	1.0005998798	1.0005998765	1.0006011283
				Absolute sum of residuals =	.0000043952
7	E : F	23.4300	1.0000007342	1.0000007115	1.0000010387
8	E : X2 + X4	23.4296	0.7798820731	0.7798041460	0.7798046139
9	E : X3 + X5	23.4313	.7813169195	.7812388476	.7812381233
10	F : X2 + X4	23.4307	.7798821909	.7798041925	.7798038039
11	F : X3 + X5	23.4312	.7813147650	.7812366668	.7812373118
12	X2 + X4 : X3 + X5	23.4313	1.0018381973	1.0018381912	1.0018382930
				Absolute sum of residuals =	.0000026549
13	E : F	23.4300	1.0000013369	1.0000012869	1.0000013539
14	E : X2 + X5	23.4289	0.7800351105	0.7799571782	0.7799574605
15	E : X3 + X4	23.4220	.7811638859	.7810859896	.7810856546
16	F : X2 + X5	23.4278	.7800351625	.7799572923	.7799564044
17	F : X3 + X4	23.4267	.7811616473	.7810836555	.7810845970
18	X2 + X5 : X3 + X4	23.4266	1.0014472596	1.0014472591	1.0014464816
				Absolute sum of residuals =	.0000032913
19	X2 : X3	23.3973	1.0032875312	1.0032875421	1.0032877488
20	X2 : X4	23.3970	1.0020470576	1.0020470528	1.0020463889
21	X2 : X5	23.3951	1.0024373288	1.0024373259	1.0024377836
22	X3 : X4	23.3969	0.9987618333	0.9987618238	0.9987627079
23	X3 : X5	23.3977	.9991535001	.9991534986	.9991528200
24	X4 : X5	23.3963	1.0003903684	1.0003903727	1.0003905954
				Absolute sum of residuals =	.0000031138

six objects (four crystals and two balls) used in the hydrostatic tests. For example, the first three equations are:

$$\frac{A}{B} = 1.000\ 002\ 8767$$

$$\frac{A}{X2+X3} = 0.780\ 287\ 7510$$

$$\frac{A}{X4+X5} = 0.780\ 756\ 0134 \qquad \text{etc.}$$

These 24 equations all express *relative* volumetric information. To this system of equations we add a 25th which expresses absolute volumetric information—namely the *sum* of the volumes of the two steel balls used in the tests. This sum is obtained by adding the values of the two ball volumes at 20 °C given in the captions to tables 4 which are based upon direct interferometric measurement.

These 25 equations are solved for six unknowns, namely the volumes of four crystals and two balls, by the method of least squares. Two possible criticisms may be raised to the calculation of volumes by this method:

1. The data have been smoothed twice, once within the six ratios, and again in the 4 sets of ratios,
2. the observed data appear in the coefficients of the observational equations rather than as a separate term.

We have not evaluated the effect of the above, but have calculated the volumes in another way for comparison.

Treating each set of six adjusted ratios separately with the sum of volumes of steel balls, we calculate, for example, the volumes of X2+X3 and X4+X5. Then the individual volumes are solved by adding two appropriate measured ratios of the crystals in the fourth set. Thus three sets of volumes are obtained for each set of ball-temperature combinations.

The differences in volumes from the two methods of computation are found to be negligible, and we decided to use values resulting from least squares fitting. The least squares estimate of the volumes of each of the four crystals and two balls are given in table 6. This table has four columns. The first three columns show the six volumes obtained in each of the three determinations and the fourth column shows the *average* values which (until additional work is done) will be our presently accepted values of the crystal densities.

their associated temperatures are averaged to provide one value of etalon length at some particular temperature.

b. Four measurements on the average diameter of each of two balls. Each diametric measurement is the average of ten observations as explained in 2.4.2.5. The four average diameters along with their associated temperatures are averaged to provide a single value of the average diameter at some particular temperature. The assumed etalon length employed in this step is obtained from the step a above, and appropriately adjusted by the application of our assumed value of the temperature coefficient of expansion of the etalon.

c. A group of mass measurements on each of the two balls.

TABLE 6

The results of the least squares solution for the volumes of the crystals and the balls are given in this table. Also presented are the assumed mass values of the four crystals used in each determination. At the bottom, the quotient of the assumed mass divided by the least squares estimate of volume (i.e. density) is given for each crystal and each determination. The average density value is the presently "accepted" value.

	Determination AB	Determination CD	Determination EF	Average value of density and standard deviation of the average. This is the accepted value as explained in the text.
Silicon crystal volumes (cm^3)				
X2	86.049 744	86.049 821	86.049 800	
X3	85.767 873	85.767 793	85.767 886	
X4	85.874 004	85.874 036	85.874 058	
X5	85.840 520	85.840 466	85.840 488	
Steel ball volumes (cm^3)				
First Ball	Ball A	Ball C	Ball E	
Least square estimate	134.067 080	134.066 237	134.067 078	
Measured value	134.067 062	134.066 261	134.067 028	
Difference	− 0.000 018	+ 0.000 024	− 0.000 050	
Second Ball	Ball B	Ball D	Ball F	
Least square estimate	134.066 870	134.067 571	134.066 916	
Measured value	134.066 888	134.067 547	134.066 966	
Difference	+ 0.000 018	− 0.000 024	+ 0.000 050	
Crystall mass (grams				
X2	200.420 689	200.420 653	200. 420 679	
X3	199.763 734	199.763 663	199.763 687	
X4	200.010 795	200.010 763	200.010 802	
X5	199.932 675	199.932 620	199.932 659	
Crystal densities (g/cm^3)				
X2	2.329 1259	2.329 1234	2.329 1243	2.329 1245 0.000 0007
X3	2.329 1208	2.329 1221	2.329 1199	2.329 1209 0.000 0006
X4	2.329 1192	2.329 1180	2.329 1179	2.329 1184 0.000 0004
X5	2.329 1177	2.329 1185	2.329 1184	2.329 1182 0.000 0003

2.6.1. Precision and Estimate of System Errors

A single determination on the volumes of our four silicon crystals requires the following measurements.

a. Two measurements on the length of the etalon as described in 2.4.2.4. These two lengths and

d. A group of mass measurements on each of the four silicon crystals.

e. Twenty-four hydrostatic comparisons (in four 4–1 ratio series) between the volumes of the two balls and various combinations of the four crystals.

During the winter of 1970–1 we worked on our redundant hydrostatic weighing process. To check the process precision, we performed the complete hydrostatic comparison between balls A and B and the four silicon crystals at a temperature of about 23.4 °C. We were aware of the crudeness of our knowledge of the temperature coefficients of expansion involved (there is no "good" way to measure a ball's coefficient), and we had no intention of using this experiment in a real volumetric determination—we considered this only as a precision test.

In 1971–2 we performed determinations A–B and C–D at temperatures within one degree of 20 °C. At this time it was pointed out to us by H. H. Ku of our Applied Mathematics Division that our experiments over this very limited temperature range were highly nonrealistic, and that we should make every effort to achieve a determination at a temperature at least $2^1/_2$ °C away from 20.

Our interferometer was designed to operate at a maximum temperature of 22 °C, however we found that, at the sacrifice of some thermostat stability, we could operate marginally at a temperature of 23 °C. Accordingly, we made etalon tests ET–5 and ET–6 at 23 °C and also measured the diameters of balls A and B at this temperature. Additional mass measurements were made. These new data at 23 °C were combined with the early hydrostatic work at 23.4 °C and new crystal volumes were calculated. Although balls A and B were employed, in this high temperature determination we have referred to them as balls E and F. Inasmuch as this work on E and F contains all the elements of a single determination as defined above, we feel justified in claiming three independent determinations.

Our presently "accepted" values of the crystal densities are the average of the three determinations. As stated above, as additional work is done on these four crystals our accepted values will be modified. The standard deviations of these average values of crystal volume are given in table 6. These standard deviations are indicative of the reproducibility of our system in the determination of such volumes.

As pointed out in the previous section, the data presented in table 6 are obtained from a least-squares solution of 25 equations—24 relating the relative volumes of crystals and balls and the 25th stating our best estimate of the sum of the volumes of the two balls. Out of the least squares solution we obtain an estimate of the volumes of each of the four crystals as well as an estimate of the volumes of each of the two balls. A comparison between the least square estimates of the individual ball volumes and our measured values (used in calculating the sum) is indicative of the inconsistency between our interferometric tests and our hydrostatic tests. These differences are shown in table 6.

An examination of the three sets of density values did not reveal any discernible pattern in rank. Statistical analysis of the volume and density data for three sets also supported the contention that a between-set component of error, if any, was negligible. The measured masses of the four silicon crystals, on the other hand, did show that the A–B set was on the average 50 μg, 0.25 ppm, higher than the C–D set, but the effect of this discrepancy on densities was not obvious. A possible explanation could be that these values of masses were used first in the computation of volume ratios and then in the computation of densities. The correlation between the numerator and denominator of the density computation would tend to decrease the effect of any systematic error present in the mass on the density values. Since these measured mass values were assigned to the sets of volume ratio calculations by date, an alternate way of computation could be to use the averages of the three sets of mass values in all density calculations. We will, however, adhere to the present scheme of calculation so that the random component of error can be computed from the three sets of final results as planned.

The standard deviation of density values of each determination was computed to be 0.97 $\mu g/cm^3$ with 8 degrees of freedom. The random component of uncertainty of the averages of density values of three determinations is taken as three standard deviations of these averages, 1.68 $\mu g/cm^3$, or 0.72 ppm.

To the extent that the same array of apparatus and instruments is used in all three determinations, the three determinations are not entirely independent. There are residual uncertainties in the calibrations of such instruments, and when these calibration uncertainties exert the *same effect* on the crystal densities calculated in each determination, they do not increase the data spread shown in table 6, so they are not included in the standard deviation of the mean given in that table.

The major sources of such uncertainties going into each determination are listed in table 7. Alongside of each item of source data (which may be an instrument such as a thermocouple or a process such as a weighing experiment to determine mass) is our estimated bound to the systematic uncertainty in that item.

Also shown is the effect of the error on the calculated crystal density obtained in each of the three determinations. It is noted that the effects of such errors on calculated densities classify the errors into two groups:

a. When the effect of the error on the volumetric calculation is the same in each of the three determinations. This group of errors must be assigned to the *systematic* category.
b. When the effect of the error on the volumetric calculation is different in each of three determinations. This group consists of errors, the effects of which are *temperature dependent*. Inasmuch as the temperature pattern in the various tests was grossly different, this group of errors need not be classed as systematic because their effect is present in the spread of data shown in figure 6.

We have no basis for assigning a value of uncertainty to the 22° phase shift used in interferometer calcula-

TABLE 7

Source data	Estimated magnitude of error in source data	Effect of estimated error on calculated values of crystal densities (g/cm³)		
		Determination AB	Determination CD	Determination EF
Data items in which errors exert *the same effect* in all three determinations and are therefore systematic				
1. Temperature measurement system used inside interferometer on etalon and steel balls	0.0092 °C	7.89×10^{-7}		
2. Calibration errors in system used to calculate effective wavelength of interferometer illumination	2.5×10^{-8} μ	2.67×10^{-7}		
3. Fringe fraction calculated from photographic system	0.001	0.18×10^{-7}		
4. Hydrostatic bath temperature	0.0015 °C	1.02×10^{-7}		
5. Mass of one steel ball	0.000 064 g	6.25×10^{-7}		
6. Mass of two silicon crystals	0.000 090 g	1.62×10^{-7}		
7. Calibration errors in hydrostatic balance	13μg/100 g	9.28×10^{-7}		
Absolute sum of systematic errors (worst case)		$28.91 \times 10^{-7} = 1.25$ ppm		
Realsitic estimate (square root of sum of squares)		$14.10 \times 10^{-7} = 0.60$ ppm		
Data items which are temperature dependent and therefore contribute to random component				
8. Expansion coefficient of etalon	3×10^{-8}	-0.63×10^{-7}	$+0.33 \times 10^{-7}$	$+0.10 \times 10^{-7}$
9. Expansion coefficient of balls	5×10^{-8}	-1.40×10^{-7}	$+3.75 \times 10^{-7}$	-1.72×10^{-7}
10. Expansion coefficient of crystals	9×10^{-8}	$+0.67 \times 10^{-7}$	-1.69×10^{-7}	$+7.20 \times 10^{-7}$

The effect of errors in these seven items of source data are equal in all three determinations.

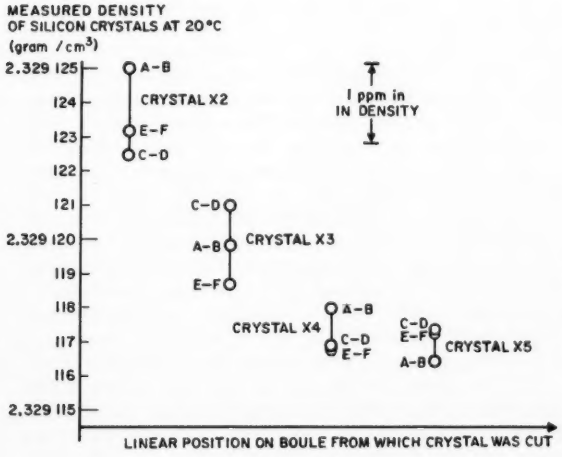

FIGURE 6. *This figure illustrates the spread of density data for each crystal among its three determinations.*

We have made several previous attempts to measure the density gradient in single crystal silicon boules. This graph is the best display of the existence of such a gradient which has come to our attention. We deeply regret that a particularly well-remembered day in history marked the beginning of our utilization of Crystal X1 for the fabrication of fractional-gram silicon weights.

tions. Additionally our estimate of item 9 may be weak. The square root of the sum of the squares of items 1 to 7 indicates a systematic of 0.6 ppm. We believe that 0.7 ppm is a justified and conservative estimate of the total systematics in this work.

The density program described in this report has involved numerous scientists in various divisions of NBS. The following individuals have given generously of their time and talents. D. P. Johnson has been our primary theoretical consultant. He worked out the data taking and reduction procedures for the interferometric part of the experiment on the etalon and balls. He calculated the volumetric uncertainty associated with ball imperfections (given in a companion paper). R. D. Deslattes provided us with adequate values of laser wavelengths and suggested the use of single crystal silicon as a working density standard. J. B. Saunders developed the spherical interferometer at our request. W. H. Gallagher assisted in working out adequate hydrostatic procedures. H. H. Ku played a major role in experiment design and he worked out

the hydrostatic data reduction format. J. L. Riddle gave us guidance in building and evaluating our interferometer temperature measurement system. Geraldine Hailes wrote many computer programs for us especially in the early stages of development when numerical techniques were only hazy ideas.

3. References

[1] Cook, A. H., and Stone, N. W. B., Precise Measurements of Mercury at 20°C-I, Phil. Trans. Roy Soc. **250A** (1957).
[2] Cook, A. H., Precise Measurements of the Density of Mercury at 20°C-II, Phil. Trans. Roy. Soc. **254** (1961–2).
[3] Henins and Bearden, Phys. Rev. **135,** A890 (1964).
[4] Deslattes, R. D., and Sauder, W. C., Intercomparison of Micrometer, Nanometer and Picometer Wavelengths, Proc. 4th Int'l. Conf. on Atomic Masses and Fundamental Constants, Teddington (1971).
[5] Bowman, H. A., Gallagher, W. H., and Schoonover, R. M., Development of a Working Density Standard, Proc. ISA, Los Angeles (1965).
[6] Bowman, H. A., and Schoonover, R. M., The Cartesian Diver as a Density Comparator, J. Res. Nat. Bur. Stand. (U.S.), **69C** (Eng. and Instr.), No. 3, 217–223 (1965).
[7] Deslattes, R. D., Schweitzer, W. G., Layer, H. P., Sidener, C., Whetstone, J. M., and Kessler, E. G., Wavelengths of 633 nm Stabilized Lasers (in process).
[8] Saunders, J. B., Ball and Cylinder Interferometer, J. Res. Nat. Bur. Stand. (U.S.), **76C** (Eng. and Instr.), Nos. 1 and 2 (1972).
[9] Teague, Clayton, NBS Private Communication.
[10] Hart, M, and Morgan, I. G., Lattice Spacing Measurements and Avagadro's Number, Proc. 4th Int'l Conf. on Atomic Masses and Fundamental Constants, Teddington (1971).
[11] Everhart, J. L., Lindlief, W. E., Kanegis, J., Weissler, P. G., and Siegel, F., Mechanical Properties of Metals and Alloys, Nat. Bur. Stand. (U.S.), Circ. 447, 481 pages (1943).
[12] Bennett, J. M., Precise Method for Measuring the Absolute Phase Change on Reflection, Jour. Opt. Soc. Amer. **54,** No. 5, p. 612 (May 1961).
[13] Spaepen, J., Application of the Float Method for Precision Measurement of the Density of Water and for Small Samples of Solids, Mededel. Koninkl. Vlaam. Akad. Wetenschap. Belg. **19,** No. 5 (1957).
[14] Bowman, H. A., and Schoonover, R. M., with appendix by Jones, M. W., Procedure for High Precision Density Determinations by Hydrostatic Weighing, J. Res. Nat. Bur. Stand. (U.S.), **71C** (Eng. and Instr.), No. 3, 179–198 (1967).
[15] Macurdy, L. B., Response of Highly Precise Balances to Thermal Gradients, J. Res. Nat. Bur. Stand. (U.S.), **68C** (Eng. and Instr.). No. 3, 135–140 (1964).
[16] Pontius, P. E., Measurement Philosophy of the Pilot Program for Mass Calibration, Nat. Bur. Stand. (U.S.),Tech. Note 288, 39 pages (May 1966).
[17] Connor, W. S., and Youden, W. J., Part II Comparison of Four National Radium Standards, J. Res. Nat. Bur. Stand. (U.S. 53) (Engr. and Instr.), No. 5, 108 (1954).

(Paper 78A1–801)

JOURNAL OF RESEARCH of the National Bureau of Standards – A. Physics and Chemistry
Vol. 78A, No. 1, January–February 1974

Geometrical Considerations in the Measurement of the Volume of an Approximate Sphere

Daniel P. Johnson

Institute for Basic Standards, National Bureau of Standards, Washington, D.C. 20234

(October 15, 1973)

Expressions are derived for the volume of an approximate sphere in terms of measured breadth, the distance between parallel planes tangent to opposite sides. The difference in volume of a ball and a true sphere of the same average breadth is shown to be of second order, and much smaller than the random and systematic errors in the measurements of the dimension. Thus, a ball commercially available at moderate cost can be used for absolute density measurements of high accuracy. Similar expressions are given for the area of an approximate circle.

Key words: Asphericity correction; density; spherical harmonics; volume of ball.

1. Introduction

The establishment of an absolute density standard, as is described by Bowman et al. in the companion article [1],[1] requires the determination of the volume of some object from its dimensions. The shapes that first come to mind are the cube or rectangular prism used by Cook [2] in the determination of the density of mercury, and the sphere. The latter is attractive because of its symmetry, and its relatively low cost in the form of ball bearings. Of course, no ball is a perfect sphere, and the question is immediately raised as to the importance of the topographic deviations from sphericity. In the following we will examine the determination of the volume from measurable quantities. The discussion will be restricted to objects which are everywhere convex, and free of sharp edges or corners.[2] Commercial ball bearings meet these requirements easily. We will be particularly concerned with features which occupy more than one percent of the surface. Irregularities smaller than a millimeter in extent would produce conspicuous distortions in the interference patterns. The method of measuring the interferograms averages over the irregularities associated with the texture of the surface. The observations with the profilometer and the homogeneous appearance of the ball as an optical surface make it improbable that a significant defect of intermediate size would escape detection. In the following we will show that the correction for asphericity is of the second order, given a good average for the diameter or the breadth of the object, and therefore smaller than first order uncertainties in the measurement. Then we will look at sampling schemes for obtaining that average.

1.1. Description of an Object in Terms of Spherical Coordinates

The volume V of an object is given by the integral,

$$V=\frac{1}{3}\int_s r^3 d\Omega \tag{1}$$

where r is the distance from the origin to the surface element, which subtends a solid angle $d\Omega$ at the origin, and the integration is performed over the full solid angle of 4π steradians. Let r_0 be the mean radius so that $r=r_0+\delta$. Then

$$V=4\pi r_0^3/3+r_0^2\int_s \delta d\Omega+r_0\int_s \delta^2 d\Omega+\int_s \delta^3 d\Omega/3.$$

Since the mean value of δ is zero, and that of δ^3 is very small, we have

$$V=4\pi[r_0^3/3+r_0\sigma_r^2] \tag{2}$$

where σ_r^2 is the mean square variation of the radius. Thus, the correction for irregularities is of the second order. If $\sigma_r/r_0=10^{-4}$ the correction is only 3 parts in 10^8.

But things are not this simple. Measurements with many metrological instruments, from the mechanic's micrometer to the Saunders interferometer [3], do not yield the diameter. Instead, they determine the breadth, that is, the separation of parallel planes

[1] Figures in brackets indicate the literature references at the end of this paper.
[2] This requires that the shape can be described by functions which are single valued and continuous, with single valued and finite first and second derivatives.

tangent to opposite sides of the object. Since the breadth favors the high spots, its average value will be somewhat greater than that of the diameter. In figure 1 let R be a point on a surface, and O be the origin. In general, the tangent plane PT which is normal to OR will not pass through R, but the point of tangency will be at the top of a nearby high spot. The tangential radius $p = \overline{OP}$ is given approximately by

$$p \simeq r + (\nabla r)^2/2R_L \tag{3}$$

where r is the distance OR; $R_L = CT$ the local radius of curvature in the region which includes R and the point of tangency; ∇r is the gradient, or the change of r with respect to the angle subtended at the origin in the direction of most rapid increase, i.e., towards the top of the hill. In the objects of present interest, $R_L \sim r_0$, and the gradient is so small that the difference between sine, angle, and tangent can be neglected. Let $p = p_0 + \Delta p$ where p_0 is the mean value of p,

$$\int_s \Delta p \, d\Omega = 0, \text{ and } 4\pi\sigma_p^2 \simeq \int_s (\Delta p)^2 \, d\Omega.$$

Then

$$r \simeq p_0 + \Delta p - p_0^2 \, (\nabla r)^2/2R_L$$

$$r^3 \simeq p_0^3 + 3p_0^2 \, \Delta p + 3p_0 \, (\Delta p)^2 - 1.5 \, p_0^2 \, (\nabla r)^2/R_L.$$

Then the volume would be given by

$$V = \frac{1}{3}\int_s r^3 d\Omega = 4\pi p_0^3/3 + 4\pi p_0[\sigma_p^2 - \sigma_{\nabla r}^2/2] \tag{4}$$

where

$$4\pi\sigma_{\nabla r}^2 = p_0 \int_s (\nabla r^2/R_L) d\Omega.$$

As before, the topography correction to the volume is of the second order, this time involving the mean square of the gradient ∇r as well as that of the variation in breadth.

In the above we have passed rapidly over several points which require closer examination. (a) It is not obvious that the expression for the volume is independent of the choice of the origin. (b) Equation (4) is in terms of the tangential radius, which cannot be measured since the center of a solid object is not accessible. Rather the measurements yield the breadth, which is the sum of two tangential radii. Therefore it is important to consider the important class of objects which exhibit odd lobing, with a valley opposite a hill. (c) The local radius near the hilltops is systematically less than the mean radius. We have assumed that they are approximately equal so that the difference leads to errors of a higher order than the second. (d) We can expect the gradient ∇p to approximate ∇r, but at this time have no good basis for estimating its magnitude. (e) In order for the terms of the first order to vanish, it is necessary to have a good average value of p experimentally as well as mathematically.

1.2. Description of an Object in Terms of Tangent Planes

We have reached the expression, eq (4), for the volume of an approximate sphere from a description in terms of the usual polar coordinates, r, θ, ϕ. Unfortunately the radius and its derivative with respect to the central angle are not directly measurable. To make the analysis correspond more closely to the measured quantities, we will look at a description of an object as the "envelope" of a set of tangent planes. The analytical description was developed by Meissner [4] in a study of objects of constant breadth. Equivalent graphical methods are used in the design of gears and cams, for example [5, 6]. More recent work has been published by Goldberg [7].

2. Area of an Approximate Circle

Before undertaking the more complex problem of the approximate sphere, let us examine that of the area of a plane figure bounded by the curve S in figure 1. The lines TP and T_1P_1 are two tangents to the curve, which intersect at the point Q between the points of tangency. Let OP and $\overline{OP_1}$ be the perpendiculars from the origin to the two tangents. Let the tangential radius p be expressed as an analytic function of the polar angle θ. Then the distance $\overline{OP} = p(\theta)$, $\overline{OP_1} = p(\theta + \Delta\theta)$, where $POP_1 = PQP_1 = \Delta\theta$. From the

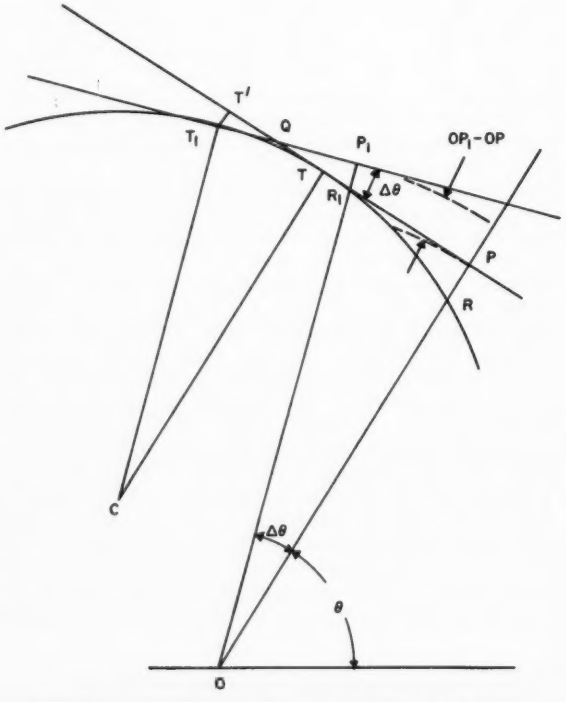

FIGURE 1. *Section normal to a plane tangent to a surface.*

figure it will be seen that the distances $\overline{P_1Q} \cdot \Delta\theta < \Delta p = \overline{OP_1} - \overline{OP} < \overline{PQ} \cdot \Delta\theta$. Divide through by $\Delta\theta$ and let $\Delta\theta \to 0$: $\overline{P_1Q} \to PQ \to \Delta p/\Delta\theta \to dp/d\theta \equiv p'$. Also the intersection Q of the two tangents becomes the point of tangency. Thus, the distance from the foot of the perpendicular to the point of tangency equals the derivative of p with respect to the angle at the origin. Returning to figure 1, we have two tangents PT and P_1T_1, with perpendiculars from the origin OP and OP_1. Let us project onto PT the vectors leading from O to T_1 by way of P and P_1. We have $\overline{OP_1} \sin \Delta\theta + \overline{P_1T_1} \cos \Delta\theta = \overline{PT'} = PT + TT'$. Let the length $\overline{OP} = p(\theta)$, $\overline{OP_1} = p(\theta + \Delta\theta)$; we have already shown that $\overline{PT} = p'(\theta)$, and $\overline{P_1T_1} = p'(\theta + \Delta\theta)$. Making these substitutions we obtain

$$\frac{\overline{TT'}}{\sin \Delta\theta} = p(\theta + \Delta\theta) + \frac{p'(\theta + \Delta\theta) \cos \Delta\theta - p'(\theta)}{\sin \Delta\theta},$$

and as $\Delta\theta \to 0$, $\overline{TT'} \to dS$, the element of arc, so that

$$dS/d\theta = p + p''.$$

The area A enclosed by the curve is given by

$$2A = \int_s p\,dS = \int_0^{2\pi} p^2 d\theta + \int_0^{2\pi} pp''d\theta.$$

Substitute $p = p_0 + \delta p$, where p_0 is the mean value of p, and integrate the last term by parts.

$$2A = \int_0^{2\pi} [p^2 + 2p_0\delta p + (\delta p)^2 - (p')^2]d\theta + |pp'|_0^{2\pi}$$

or, since $\int_0^{2\pi} \delta p = 0$

$$A = \pi[p_0^2 + \sigma_p^2 - \sigma_{p'}^2] \tag{5}$$

where σ_p^2 and $\sigma_{p'}^2$ are mean square values of $p - p_0$ and p'.

There is no problem with the integration if the boundary curve is everywhere convex and free of steps and corners. With these restrictions it is possible to represent $p(\theta)$ by a Fourier series

$$p = p_0 + \sum_n C_n \sin(n\theta + \alpha_n)$$

whence

$$\sigma_p^2 = \sum C_n^2/2,\ \sigma_{p'}^2 = \sum n^2 C_n^2/2$$

and the area will be

$$A = \pi p_0^2 + \frac{\pi}{2} \sum (1 - n^2) C_n^2. \tag{6}$$

The "topography error" in the area is of the second order. Displacement of the origin changes the value of the constants for $n = 1$; because of the factor $(1 - n^2)$, the area is unchanged.

3. Volume of an Approximate Sphere

The problem of the approximate sphere is much more tedious than that of the approximate circle. The reader who is not interested in following the details of the analysis may wish to skip most of this section, stopping only to compare eqs (15) and (5) and eqs (20) and (6), and then to look at the calculation of volume.

The logic is similar to that of the approximate circle: (a) The shape of the object can be described in terms of a set of tangent planes. The position of each plane is defined by a vector $\mathbf{p}$ from the origin to the plane and normal to it. (b) The length p of the normal vector is a function of the polar coordinates θ and ϕ. Note that these coordinates do not refer directly to a point on or within the object but to the coordinates of a reference sphere with its center at the origin of $\mathbf{p}$. If the object has no sharp edges or vertices, each point on its surface defines a single tangent plane and therefore a single point (θ, ϕ), on the reference sphere. If the object is everywhere convex, each point on the reference sphere corresponds to a single point of tangency on the object. (c) We will first determine the vector from the origin to the point of contact between the tangent plane and the surface of the object. Then we will map out the element of the surface which corresponds to the increments $d\theta$ and $d\phi$, and write the expression for the element of volume. (d) In the analytical discussion we will use a series of spherical harmonics, which play the same part on the sphere as does the Fourier series on the circle. The volume integral will contain terms of the first, second, and higher orders in the spherical coordinates. As the first order terms integrate to zero, the main correction for topography will be found in the second order terms, which contain squares and products of the spherical harmonics. A sample calculation will show the magnitude of the second order terms.

3.1. Element of Volume

Figure 2 represents the plane tangent to the object at T and normal to the vector $\mathbf{p}(\theta, \phi)$ which terminates at P. The projections of all meridians of the reference sphere meet at the pole, $\theta = 0$. The intersection with the plane of the equator, $\theta = 90°$, forms the base of the triangle. The projection from the origin of the small circle of constant polar distance θ is a cone; its intersection with the tangent plane is symmetrical with respect to the meridian through P. The plane through P, orthogonal to the tangent and meridian planes, intersects the reference sphere in a great circle tangent to the small circle of constant θ. The angle ψ is measured along this circle.

Let figure 1 represent a meridian plane which contains the normals OP and OP_1 of two planes tangent to the object. T and T_1 are the perpendicular projections onto the plane of the figure of the two points of tangency. The argument proceeds as before, and the projection of PT on the tangent plane is equal to $\partial p/\partial\theta \equiv p_u$.

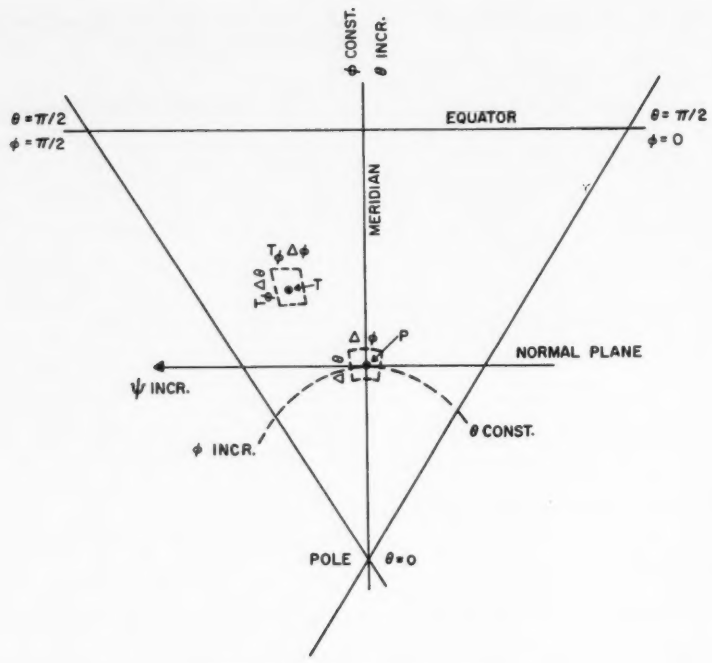

FIGURE 2. *Plane tangent to a surface.*

Now we relabel figure 1, replacing θ with ψ and let it represent projections on the plane normal to the meridian. The projection of PT on this plane is $dp/d\psi \equiv p_\psi$. Since the normal plane is tangent to the cone of constant polar angle θ, we can set $d\psi = \sin\theta d\phi$, and this component of PT, $p_\psi = p_\phi \csc\theta$.

Returning to figure 2 we have the sum of the vectors $\mathbf{p}_\theta$, parallel to the meridian, and $\mathbf{p}_\psi = \mathbf{p}_\phi \csc\theta$, perpendicular to it, connecting the point P to the point of tangency T between the plane and the surface of the object. Then, corresponding to an element $\Delta\theta\Delta\phi$ of the reference sphere, there is on the surface of the object an element whose edges are the vectors $\mathbf{T}_\theta\Delta\theta$ and $\mathbf{T}_\psi\Delta\phi$. The volume element will be a pyramid with this as the base and the origin as the vertex.

Now, let us define three orthogonal unit vectors, which move with the tangential radius vector. In terms of cartesian coordinates associated with the reference sphere $[\theta = 90°, \phi = 0;\ \theta = 90°, \phi = 90°;\ \theta = 0°]$ the components of these are

$\mathbf{u} \equiv (\sin\theta\cos\phi, \sin\theta\sin\phi, \cos\theta)$ along the radius vector,

$\mathbf{v} \equiv (\cos\theta\cos\phi, \cos\theta\sin\phi, -\sin\theta)$ in the meridian plane,

$\mathbf{w} \equiv (-\sin\phi, \cos\phi, 0)$ normal to the meridian plane.

By differentiation of the components the following can be verified:

$$\mathbf{u}_\theta = \mathbf{v} \qquad \mathbf{v}_\theta = -\mathbf{u} \qquad \mathbf{w}_\theta = 0$$

$$\mathbf{u}_\phi = \mathbf{w}\sin\theta \qquad \mathbf{v}_\phi = \mathbf{w}\cos\theta \qquad \mathbf{w}_\phi = -\mathbf{u}\sin\theta - \mathbf{v}\cos\theta$$

Then the tangential radius vector will be $\mathbf{p} = p\,\mathbf{u}$ and the vector to the corresponding point on the object will be:

$$\mathbf{t} = p\mathbf{u} + p_\theta\mathbf{v} + p_\phi \csc\theta\,\mathbf{w}.$$

In differentiating these vectors we must consider changes in both direction and magnitude:

$$\mathbf{t}_\theta = (p + p_{\theta\theta})\mathbf{v} + (p_{\phi\theta} - p_\phi \operatorname{ctn}\theta)\csc\theta\,\mathbf{w}$$

$$\mathbf{t}_\phi = (p_{\theta\phi} - p_\phi \operatorname{ctn}\theta)\mathbf{v} + (p\sin\theta + p_\theta\cos\theta + p_{\phi\phi}\csc\theta)\mathbf{w}.$$

Since no component in the $\mathbf{u}$ direction appears in the expression for $\mathbf{t}_\theta$ and $\mathbf{t}_\phi$, the derivative vectors in the surface of the object also lie in the tangent plane.

The volume element can be expressed in terms of the determinant of the components of $\mathbf{t}$, $\mathbf{t}_\theta$ and $\mathbf{t}_\phi$

$$dV = \begin{vmatrix} p & p_\theta & p_\phi \csc\theta \\ 0 & p + p_{\theta\theta} & (p_{\phi\theta} - p_\phi \operatorname{ctn}\theta)\csc\theta \\ 0 & p_{\phi\theta} - p_\phi \operatorname{ctn}\theta & (p\sin\theta + p_\theta\cos\theta + p_{\phi\phi}\csc\theta) \end{vmatrix} \frac{d\theta d\phi}{3} \tag{10}$$

3.2. Volume Integral

Let p_0 be the average value of p $(4\pi p_0 = \int_s p d\Omega)$, and let Y be the relatively small deviation from the average value, so that $p = p_0 + Y$. Later we will express Y as a linear combination of spherical harmonics. Now let $p = p_0 + Y$ where Y is a linear combination of spherical harmonics. Now we expand the determinant, sort out terms, and start the integration:

$$V = \left\{ \begin{array}{l} 4\pi p_0^3/3 + (p_0^2/3) \iint_s [Y_{\theta\theta} + Y_\theta \mathrm{ctn}\theta + Y_{\phi\phi}\csc^2\theta + 3Y] \sin\theta d\theta d\phi \\ + \dfrac{p_0}{3} \left[\begin{array}{l} \iint_s [2Y_{\theta\theta} + 2Y_\theta \mathrm{ctn}\theta + 2Y_{\phi\phi}\csc^2\theta + 3Y] Y \sin\theta d\theta d\phi \\ + \iint_s \cos\theta (Y_{\theta\theta} Y_\theta d\theta) d\phi + \iint_s (Y_{\theta\theta}\csc\theta)\,(Y_{\phi\phi} d\phi) d\theta \\ - \iint_s Y_{\theta\phi} Y_{\phi\theta} \csc\theta d\theta d\phi + \iint_s Y_{\theta\phi} Y_\phi \mathrm{ctn}\theta \csc\theta d\theta d\phi \\ + \iint_s \mathrm{ctn}\theta \csc\theta (Y_{\phi\theta} T_\phi d\theta) d\phi - \iint_s Y_\phi^2 \mathrm{ctn}^2\theta \csc\theta d\theta d\phi \end{array} \right] \\ + \iint_s [Y^3 \text{ etc}] \sin\theta d\theta d\phi/3 \end{array} \right\} \tag{11}$$

From the outcome of the problem of the approximate circle we expect that the integral of the first order terms in Y will vanish. If the maximum value of Y is small compared to p_0 the terms of the third order in Y will be small compared to those of the second, and may be neglected. In order to get the second order terms into more manageable form we will make a number of integrations by parts, starting with the first term in the second line. With $U = \cos\theta$, $dV = Y_{\theta\theta} Y_\theta d\theta$, integrate by parts, obtaining for the integrand $+ (1/2)(Y_\theta \sin\theta)(Y_\theta d\theta) d\phi$. Again integrate by parts, obtaining $- (1/2)(Y_{\theta\theta} + Y_\theta \mathrm{ctn}\theta) Y \sin\theta d\theta d\phi$. Integrate the next term by parts, obtaining as integrand, $- Y_{\theta\theta\phi} Y_\phi \csc\theta d\phi d\theta$. This combines with the terms in the third line, to form $- d(Y_{\theta\phi} Y_\phi \csc\theta) d\phi$. Integrate by parts the first term of the last line and combine with the final term to obtain $(1/2)(Y_\phi \csc\theta) \times (Y_\phi d\phi) d\theta$. Integrate this by parts to obtain $- (1/2) \times (Y_{\phi\phi} Y \csc\theta d\theta d\phi$. Equation (11) now boils down to

$$V = 4\pi p_0^3/3 + (p_0^2/3) \iint_s [Y_{\theta\theta} + Y_\theta \mathrm{ctn}\theta + Y_{\phi\phi}\csc^2\theta + 3Y] \sin\theta d\theta d\phi + (p_0/2) \iint_s [Y_{\theta\theta} + Y_\Theta \mathrm{ctn}\theta + Y_{\phi\phi}\csc^2\theta) + 2Y] Y \sin\theta d\theta d\phi \tag{12}$$

together with six "*UV*" terms. Later, when Y is expanded in spherical harmonics, we will be able to show that the terms of the first order in Y and the "*UV*" terms reduce to zero.

The record of the radial profilometer is a polar plot of the variations in radius. The amplification, which may be as high as 20000, can be chosen to provide a vivid display of the rate of change q of the tangential radius p as a function of the angular coordinates. A given profile is likely to sample some regions of relatively high relief and other regions of low relief. Therefore one or more profiles, in various orientations, will provide an estimate of the mean square value of the rate of change. If α is the azimuth at a point (θ, ϕ), the rate of change q will be

$$q = p_\theta \cos\alpha + \csc\theta p_\phi \sin\alpha,$$

and the value of q in the direction of its maximum increase is that of the gradient,

$$\nabla p = \mathbf{v} p_\theta + \mathbf{w} \csc\theta p_\phi.$$

At any point on the sphere the value of q^2 averaged with respect to azimuth is

$$\overline{q^2} = \overline{\frac{1}{2}\,[p_\theta^2 + \csc^2\theta p_\phi^2]} = \overline{\frac{1}{2}\,(\nabla p)^2}$$

The average value over the sphere is given by

$$4\pi\sigma_q^2 = \int_s \overline{q^2} d\Omega = (1/2) \iint_s Y_\theta \sin\theta (Y_\theta d\theta) d\phi + (1/2) \iint_s Y_\phi \csc\theta (Y_\phi d\phi) d\theta \tag{13}$$

Integration by parts, with the integrands divided as shown, gives

$$4\pi\sigma^2 \overline{q} = - (1/2) \iint_s (Y_{\theta\theta} + Y_\theta \mathrm{ctn}\theta + Y_{\phi\phi}\csc^2\theta)\ Y \sin\theta d\theta d\phi + \ldots \tag{14}$$

Two "UV" terms will be evaluated later. If we define the mean square variation of p by

$$4\pi\sigma_p^2 = \iint Y^2 \sin\theta d\theta d\phi,$$

we get for the approximate sphere

$$V = 4\pi p_0^2/3 + 4\pi p_0 (\sigma_p^2 - \sigma_q^2). \tag{15}$$

Comparison with eq (2) for the volume based on deviations from the mean radius shows that the mean breadth is slightly larger than the radius,

$$r_0 \simeq p_0 (1-\sigma_q^2/p_0^2)^{1/2}.$$

3.3. Representation in Spherical Harmonics

At this point we will express Y as the sum of spherical harmonics Y_n of degree n. It will then be possible to compute the volume for specific shapes, to evaluate the first order terms in eq (12) and to show that the "*UV*" terms of eqs (12) and (14) reduce to zero. An object as smooth as a ball bearing easily meets the requirements for convergence of a series of spherical harmonics. Summaries of the theory of spherical harmonics will be found in [8] or [9]. We will make use of the following properties:

Each spherical harmonic can be expressed as a linear combination of Laplace functions which are products of Legendre polynomials in $\cos\theta$ and sines or cosines of $m\phi$.

$$Y=\sum_n Y_n=\sum_n\sum_m [A_{n,m}\cos m\phi + B_{n,m}\sin m\phi] P_n^m(\cos\theta). \qquad (16)$$

The Y_n satisfy Legendre's differential equation:

$$(Y_n)_{\theta\theta}+(Y_n)_\theta \operatorname{ctn}\theta+(Y_n)_{\phi\phi}\csc_\theta^2=-n(n+1)Y_n. \qquad (17)$$

Also,

$$\iint_s Y_n \sin\theta d\theta d\phi=0, \iint_s Y_n Y_k \sin\theta d\theta d\phi=0 \text{ if } n\neq k.$$

Letting $x=\cos_\theta$, we can define the Legendre polynomials of degree n and order m:

$$P_n=P_n^0=(2^n n!)^{-1}(d/dx)^n(x^2-1)^n$$

$$P_m^m=(1-x^2)^{m/2}(d/dx)^m P_n.$$

If the shape of an object can be represented by a single spherical harmonic Y_n, the radial profile on the section of greatest relief will show n lobes. The zonal harmonics P_n describe n lobed figures of revolution symmetrical about the polar axis. The sectoral harmonics $P_n^n\cos n\phi$ describe figures with maximum relief along the equator, and with nodal lines along meridians. If n is odd, a valley will be found at the antipodes of every hill, while if n is even a hill will be opposite a hill and a valley opposite a valley.

Any distribution of lobes over the sphere can be described with spherical harmonics. A few examples will illustrate the possibilities:

$$P_3^2\cos 2\phi=(3.75)(\cos\theta-\cos 3\theta)\cos 2\phi$$

has lobes in the directions of the vertices of a tetrahedron oriented so that the polar axis passes through the midpoint of two opposite sides.

$$P_4+(1/168)P_4^4\cos 4\phi$$

has octahedral symmetry with a lobe at each pole and four on the equator.

$$P_6+(1/3960)P_6^5\cos 5\phi$$

has lobes in the direction of the normals to faces of a dodecahedron.

Let $AP\cos m\phi$ be a sample term in the series expansion of Y [if $m=0$, $P\equiv P_n$; if $m\neq 0$, $P\equiv P_n^m$]. Since the variables are separated, the "*UV*" terms from eq (11) can be written:

$$\frac{p_0A^2}{3}\Big\{ (1/2)\Big|P_\theta^2\cos\theta\Big|_0^\pi\int_0^{2\pi}\cos^2 m\phi d\phi + (1/2)\Big|P_\theta P\sin\theta\Big|_0^\pi\int_0^{2\pi}\cos^2 m\phi d\phi + m\Big|\sin m\phi\cos m\phi\Big|_0^{2\pi}\int_0^\pi P_{\theta\theta}P\csc\theta d\theta - m^2\Big|P_\theta P\csc\theta\Big|_0^\pi\int_0^{2\pi}\sin^2 m\phi d\phi (m^2/2)\Big|P^2\operatorname{ctn}\theta\csc\theta\Big|_0^\pi\int_0^{2\pi}\sin^2 m\phi d\phi + (m/2)\Big|\sin m\phi\cos m\phi\Big|_0^{2\pi}\int_0^\pi P^2\csc\theta d\theta\Big\}.$$

If $m=0$ only the first two terms appear. Since $P\equiv P_n$ is a polynomial in $\cos\theta$, $P_\theta=-\sin\theta P_n'$. Therefore, both the terms contain the factor $\sin^2\theta$ which is zero at the limits $\theta=0$ and $\theta=\pi$.

If $m=1$, $P\equiv P_n$, $\sin\theta P_\theta=P_n'\cos\theta-P_n''\sin^2\theta$, and $P_{\theta\theta}=-P_n'\sin\theta-3P_n''\sin\theta\cos\theta+P_n''\sin^3\theta$. For the two terms which contain $\Big|\sin m\phi\cos m\phi\Big|_0^{2\pi}=0$, it is sufficient to note that both $P_{\theta\theta}$ and P contain $\sin\theta$ as a factor, so that the integrals with respect to θ are finite. For the other four terms the ϕ integrals equal π. For these, retaining only the part which is significant at the limits, we have:

$$\frac{\pi p_0A^2}{3}\Big\{(1/2)\Big|(P')^2\cos^3\theta\Big|_0^\pi+1/2\Big|(P')^2\sin^2\theta\cos\theta\Big|_0^\pi - \Big|(P')^2\cos\theta\Big|_0^\pi+1/2\Big|(P')^2\cos\theta\Big|_0^\pi\Big\}=0.$$

For $m>1$, all terms contain $\sin\theta$ in the numerator and reduce to zero at both limits.

The "*UV*" terms from the integration of eq (13) are

$$1/2\int_0^{2\pi}\left|Y_\theta Y\sin\theta\right|_0^{\pi}d\phi-1/2\int_0^{2\pi}\left|Y_\phi Y\csc\theta\right|_0^{2\pi}d\theta$$

both of which occurred in the integration of eq (11) and were shown to vanish for all values of m.

Having justified the omission of the "*UV*" terms from eq (12), let us expand Y in a series of spherical harmonics, then use Legendre's differential equation (17) to eliminate the derivatives of Y_n. The result is

$$V=4\pi p_0^3/3$$

$$+(p_0^2/3)\sum_n(3-n-n^2)\int_0^{2\pi}\int_0^{\pi}Y_n\sin\theta d\theta d\phi$$

$$+(p_0/2)\sum_n\sum_k(2-n-n^2)\int_0^{2\pi}\int_0^{\pi}Y_nY_k\sin\theta d\theta d\phi. \qquad (18)$$

The integrals of Y_n and of the cross products Y_nY_k, $n\neq k$, vanish and we have

$$V=4\pi p_0^3/3-(p_0/2)\sum(n-1)(n+2)\int_0^{2\pi}\int_0^{\pi}Y_n^2\sin\theta d\theta d\phi. \qquad (19)$$

If the standard deviation σ_n of the spherical harmonic of degree n is given by

$$4\pi\sigma_n^2=\int_0^{2\pi}\int_0^{\pi}Y_n^2\sin\theta d\theta d\phi,$$

$$V=4\pi p_0^3/3-2\pi p_0\sum(n-1)(n+2)\sigma_n^2. \qquad (20)$$

3.4. Calculation of Volume

As an example, let us calculate the topography correction for a ball bearing of a type which is produced in quantity by centerless grinding. The radial profiles usually show three or five lobes. The balls are graded on the basis of the tolerance for the difference in diameter of circles inscribed and circumscribed on the lobe pattern. 2.5-inch balls with a 100 microinch tolerance can be bought in small quantities for about $25. The shape of one of these balls might be represented by the formula:

$$p=p_0+A(\cos\theta-\cos^3\theta)\cos 2\phi$$

$$=p_0+(A/15)P_3^2\cos 2\phi$$

where A is the tolerance and p_0 is the half width. This ball would have tetrahedral symmetry, and the radial profile would have three lobes. The standard deviation of p is given by

$$4\pi\sigma_p^2=A^2\int_0^{2\pi}\cos^2 2\phi d\phi\int_0^{\pi}(\cos\theta-\cos^3\theta)^2\sin\theta d\theta$$

or

$$\sigma_p^2=4A^2/105.$$

The volume is

$$V=4\pi p_0^3/3-2\pi p_0(3-1)(3+2)\sigma_p^2$$

$$=(4\pi p_0^3/3)(1-4A^2/7p_0^2)$$

For $A=10^{-4}$ inch and $p_0=1.25$ inch the correction to the volume is about 4 parts in 10^9.

4. Measurement of Mean Breadth

In measuring the object it is desirable to have as large a number of independent observations as practicable, to provide estimates of precision and of topographic variations. There are some advantages in having the directions of measurement distributed systematically so that each can be associated with the same solid angle and therefore have equal weight. It is possible to do this by measuring in directions normal to the faces of a regular polygon. Three orthogonal directions are normal to the faces of a cube, four directions are normal to the faces of an octahedron, six are determined by a dodecahedron and ten by an icosahedron.

Mapped on a sphere, latitudes and longitudes of these sets of directions can be as follows:

	Set of three			
N. Latitude...	90°	0°	0°	
Longitude....	—	0°	90°	
	Set of four			
N. Latitude...	35.264°	35.264°$=\tan^{-1}(\sqrt{2}/2)$		
Longitude....	±45°	±135°		
	Set of six			
N. Latitude...	90°	26.565°	26.565°	26.565°$=\tan^{-1}(1/2)$
Longitude....	—	±36°	±108°	180°
	Set of ten			
Longitude....	0	±72°	±144°	
N. Latitude...	52.623°	52.623°	52.623°$=\tan^{-1}(3+\sqrt{5})/4$	
N. Latitude...	10.812°	10.812°	10.812°$=\tan^{-1}(3-\sqrt{5})/4$	

These orientations are chosen so that each direction of the set of four directions is towards the centroid of a spherical triangle (an octant) determined by the set

of three. Similarly, each direction of the set of 10 is toward the centroid of three adjacent directions of the set of six.

The set of six or the set of 10 directions each corresponds to the locations of the lobes of one of the spherical harmonics of degree six. If the lobe pattern of the ball is represented by spherical harmonics of degree less than six, the observations of either set are distributed over hills and valleys so as to average out the lobe pattern *exactly*, and thus give a correct mean width.

If the ball had lobes distributed like the vertices of a dodecahedron and is oriented just right, it would be possible for the observations of the set of six to fall in the low spots or for those of the set of 10 to fall on the high spots. Either set would yield an erroneous result.

What is more likely is for the ball to have a single feature, such as a dent or abraded patch, covering one or two percent of its surface. Then there would be a chance that this feature would be missed in a set of observations. In this experiment the chance of missing an isolated feature was reduced by making four series of observations in ten directions with the ball relocated at random between series.

An estimate of the magnitude of the even spherical harmonics can be made on the basis of the interferometric measurements. However, this information is incomplete on two counts. First, the breadth is not affected by the odd spherical harmonics, but the volume is. Second, the expression for the volume contains the square of the degree n, and the interferometer provides no information on the number of lobes.

Observations with the radial profilometer are essential in estimating the error due to topography. The profiles show the odd as well as the even harmonics. If a single harmonic dominates the topography the number n of lobes can be counted. If the pattern is irregular, a radial profile provides a sample from which to estimate a mean square rate of change of radius ($\sigma_{\dot{q}}^2$ in eq (15)). The angular resolution of the trace is of the order of a degree, so that the chance of finding a small defect is improved.

5. Summary

We have evaluated the topography correction for the difference between the volume of an approximate sphere and that of a true sphere of the same average breadth. It is of second order in the variations in tangential radius, and therefore much smaller than the random and systematic errors of the measurements which can be made on the object. For example, a commercially available ball bearing of moderate cost can be expected to have a topography correction of a few parts in 10^9. Its mean breadth can be measured to a part in 10^6 corresponding to a few parts in a million in its volume.

In order to have no question as to the integral part of the order of interference, Bowman [1] used balls of much better quality. The manufacturer's nominal tolerances were one or two microinches. The radial profiles appeared to be elliptical ($n=2$) with a difference between the major and minor axes less than one part in a million. Harmonics of degree greater than two were too small to detect. In sixteen sets of interferometric measurements, the greatest and least breadths of a ball in a set of ten differed by less than two parts in a million. If all of this difference resulted from a spherical harmonic of degree two, the correction to the volume would be a few parts in 10^{12}. The effect of harmonics of higher degree and smaller amplitude might be comparable. In any case the topoggraphy corrections are several orders of magnitude smaller than the uncertainties inherent in the interferometer.

6. References

[1] Bowman, H. A., Schoonover, R. M., Carroll, C. L., A Density scale based on solid objects, J. Res. Nat. Bur. Stand. (U.S.), **78A** (Phys. and Chem.) No. 1, (1974).

[2] Cook, A. H., and Stone, N. W. B., Precise measurements of the density of mercury at 20 °C, Phil. Trans. [A] **250,** 279 (1957).

[3] Saunders, J. B., Sr., Ball and cylinder interferometer, J. Res. Nat. Bur. Stand. (U.S.) **76C** (Eng. & Inst.), Nos. 1 & 2, 11–20 (1972).

[4] Meissner, E., Über die durch reguläre Polyeder nicht stützbaren Körper, Vierteljahrsschrift der naturforschenden Gesellschaft, Zürich **63,** 544–551, (1918).

[5] ASTE Handbook Committee, Tool Engineers Handbook, Sect 107, Cams, p. 1759–60 (New York, N.Y., McGraw Hill Book Co. Inc., 1949).

[6] Carmichael, C., Kent's Mechanical Engineer's Handbook, Art 7.4, Cams, p. 7–15, Fig. 39, Cam Profile for Flat Faced Follower (New York, N.Y., John Wiley & Sons, Inc., 1961).

[7] Goldberg, M., Rotors in polygons and polyhedra, mathematical tables and other aids to computation **14,** 71, (1960).

[8] Abramowitz, M., and Stegun, I. A., Handbook of Mathematical Functions, Nat. Bur. Stand. (U.S.), Appl. Math. Ser. **55,** Chs. 8 and 22 (1964). Washington, D.C. 20402 (1964).

[9] Jahnke, E., and Emde, F., Tables of Functions, Ch 7, Legendre Functions (New York, N.Y., Dover, 1945).

(Paper 78A1–802)

JOURNAL OF RESEARCH of the National Bureau of Standards—A. Physics and Chemistry
Vol. 78A, No. 1, January–February 1974

Note on Diffusion of Vapor into Flowing Gas

Daniel P. Johnson

Institute for Basic Standards, National Bureau of Standards, Washington, D.C. 20234

(October 23, 1973)

The theory of diffusion of vapor between the walls of a tube and a stream of gas is applied to a generator of known humidities. The rate of approach to equilibrium is evaluated for gas velocities in the laminar flow range. The effect of pressure drop is examined.

Key words: Diffusion; equilibrium; evaporation; humidity; humidity generator; laminar flow; saturation; water vapor.

The apparatus described by Greenspan, [1][1] as well as others used to generate known humidities, includes a long tube of negligible curvature, down which a carrier gas flows. The walls of the tube are coated with the solid or liquid phase, and the vapor diffuses between the walls and the carrier gas. The length of the tube should be such that the gas should be fully saturated with the vapor at the outlet, or at least, the departure from full saturation should be well known. Precautions should be taken against entrainment of water droplets or ice particles.

With the addition of terms which represent the transport of the vapor, the differential equation for diffusion becomes:

$$D\,\nabla^2 c - \partial c/\partial t - \mathbf{v}\cdot\nabla c - c\ \mathrm{Div}\ \mathbf{v} = 0$$

where c is the vapor concentration, $\mathbf{v}$ the velocity of the carrier gas, and D the coefficient of diffusion for the vapor in the carrier gas. We will consider the case of laminar flow, far enough down the tube that the entry transients are negligible. We will take the channel as circular, of radius a. In the steady state the flow of the gas will be parallel to the axis and the axial velocity at distance r from the axis given by $v = v_0(1 - r^2/a^2)$ where v_0 is the velocity at the axis. Div $\mathbf{v}$ represents the expansion of the gas in consequence of the pressure drop in the tube. If this is small, the acceleration of the gas will produce negligible distortion of the parabolic flow pattern, so that Div $\mathbf{v} = -(v_0/p)(1 - r^2/a^2)\ dp/dz$. After the start-up transients have subsided, the time derivatives are zero. We can now write the differential equation as:

$$\frac{\partial^2 c}{\partial r^2} + \frac{1}{r}\frac{\partial c}{\partial r} + \frac{\partial^2 c}{\partial z^2} + \frac{v_0}{D}\left(1 - \frac{r^2}{a^2}\right)\left[\frac{c}{p}\frac{dp}{dz} - \frac{\partial c}{\partial z}\right] = 0$$

where z is the axial coordinate.

The importance of the velocity effects can be measured by a dimensionless number $b = av_0/D$. For water vapor in air, b is about 1.5 times the Reynolds number.

Let us seek a general solution of the differential equation as the sum of a set of terms each of which can be separated into factors dependent on the axial and on the radial coordinates. Near the outlet the solution will be shown to be dominated by a term which includes the expansion of the carrier gas due to the pressure drop. Upstream, terms will be found which contain factors which decay exponentially with respect to the axial coordinate. We will be concerned particularly with the more persistent of these terms. All terms of the solutions will be finite within the tube, i.e., for $r < a$ and symmetrical about the axis at $r = 0$. At the wall ($r = a$) the solution has a value independent of z; for the terms which decay exponentially the value is zero. Let us try the sum of a number of terms of the form $\phi e^{-\alpha z/a}$, where ϕ is a function only of r, say $\phi = \sum_0^\infty A_n (r^2/a^2)^n$. The requirements of symmetry and finite values are met by restricting n to positive integers. Putting this in the differential equation we get

$$\left[a^2\left(\frac{d^2\phi}{dr^2} + \frac{1}{r}\frac{d\phi}{dr}\right) + \alpha^2\phi + b\left(1 - \frac{r^2}{a^2}\right)(\beta + \alpha)\phi \right] e^{-\alpha z/a} = 0$$

where $\beta = (a/b)(dp/dz)$ is the (taken as constant) fractional loss of pressure in a distance equal to the radius. Substituting for ϕ and performing the differentiations the following relations between coefficients are obtained:

$$4A_1 = -[b(\beta + \alpha) + \alpha^2]A_0$$

[1] Figures in brackets indicate the literature references at the end of this paper.

525-013 O - 74 - 4

$$4n^2 A_n = -[b(\beta+\alpha)+\alpha^2]A_{n-1} + b(\beta+\alpha)A_{n-2}$$

ϕ reduces to zero at $r=a$ for an infinite number of values of α. For $\beta < \alpha \ll b$, the first three of the roots are given by

$$(\alpha+\beta)b = 7.3136,\ 44.608,\ 113.922.$$

The closely related problem of the transfer of heat from a tube to a fluid was examined by Graetz [2] and independently by Nusselt [3]. Their solution was essentially the same as the above, and is summarized in a review article by Drew [4] who also recalculated the roots.

Their interest, and the experimental comparisons, were with relatively short tubes, for which the terms containing the second and third roots were significant, and they omitted the quantities α^2 and β in the differential equation.

Their values for the roots are compared with the values indicated below in the table

Roots of $\phi_j(1)=0$

j	Graetz	Nusselt	Drew	$\sqrt{(\alpha+\beta)b}$
1	2.7043	2.705	2.70436	2.704365
2	6.50	6.66	6.6791	6.67903
3		10.3		10.67337

When ϕ is plotted as a function of the radius the curves corresponding to these roots resemble the Bessel function $J_0(\gamma r/a)$, where $\gamma^2=(\alpha+\beta)b$, for small radii. As $r \to a$, the curve is flattened somewhat. For $r > a$ the function increases in absolute value without limit. This set of functions can be used to fit boundary conditions, such as the humidity distribution of the gas entering the tube, in a manner similar to the Fourier of Bessel series.

The coefficient α^2 in the differential equation represents diffusion in the axial direction. It reduces the value of the root slightly. The conditions of operation to be evaluated in Greenspan's experiment are a mean velocity of 71 cm/s, a radius of 0.4 cm, and a diffusion coefficient of 0.1 cm/s corresponding to -80 °C at atmospheric pressure. Thus $b \sim 530$, $\alpha \sim 0.014$ and the effect is to reduce the value of the first root from $(\alpha+\beta)b = 7.3136$ to 7.3125.

The distance required for a term to decrease by a factor of e equals a/α. For Greenspan's experiment this is 29 cm for the first root, 4.7 cm for the second, and 1.85 cm for the third. The decay distances for higher roots are much smaller. If the tube is long enough these terms will decay to negligible values at the outlet, and the associated transfer of material at the wall is substantially complete.

The effect of pressure drop is indicated by the coefficient β in the differential equation. This may be small compared with the smallest value of α considered above, but significant when $\alpha=0$, corresponding to a distribution of concentration which is uniform over the length of the tube. If βb is small so that $\beta^2 b^2$ can be neglected, only the first three terms of the series are significant and we have

$$A_1 = -\beta b A_0,\ A_2 = (\beta b + \beta^2 b^2)A_0/4 \ldots$$

At radius r

$$C(r) = A_0\,[1 - \beta b\,(r^2/a^2) + (\beta b/4)\,(r^4/a^4) + \beta^2\,(\ldots)]$$

At the wall, $r=a$

$$C(a) = A_0\,[1 - \beta b + \beta b/4 + \beta^2\,(\ldots)]$$

Because of the expansion of the carrier gas there will also be a transfer of gas from the wall to the stream at a uniform rate

$$2\pi a D\left(\frac{-\partial C(a)}{\partial r}\right) = 2\pi D A_0 \beta b \text{ per unit length.}$$

At the outlet, if all other terms have decayed to negligible magnitude, the concentration is

$$\frac{C(r)}{C_w} = \frac{A_0[1-\beta b(r^2/a^2) + (\beta b/4)\,(r^4/a^4) - \beta^2(\ldots)]}{A_0[1-\beta b + (\beta b/4) + \beta^2 \ldots]}$$

by long division, we get

$$C(r)/C_w = 1 + \beta b(1-r^2/a^2) - (\beta b/4)\,(1-r^4/a^4) + \beta^2(\ldots).$$

The quantity of vapor discharged at the outlet is

$$\pi a^2 v_0 \bar{C}/2 = \pi \int_0^{r=a} vC(r)\,d(r^2)$$

$$= \pi a^2 \int_0^{r=a} v_0(1-r^2/a^2)C(r)\,d(r^2/a^2)$$

$$= \pi a^2 v_0 C_w \int_0^{r=a} (1-r^2/a^2)\,[1+\beta b(1-r^2/a^2) - (\beta b/4)\,(1-r^4/a^4) + \ldots]\,d(r^2/a^2)$$

$$= \pi a^2 v_0 C_w \left[\frac{1}{2} + \beta b \int_0^{r=a} \left(1 - \frac{2r^2}{a^2} + \frac{r^4}{a^4}\right) d\left(\frac{r^2}{a^2}\right) - \frac{\beta b}{4} \int_0^{r=a} \left(1 - \frac{r^2}{a^2} - \frac{r^4}{a^4} + \frac{r^6}{a^6}\right) d\left(\frac{r^2}{a^2}\right) + \ldots\right]$$

$$= \pi a^2 v_0 C_w \left[\frac{1}{2} + \beta b(1-1+1/3) - (\beta b/4)\,(1-1/2-1/3+1/4)\ldots\right]$$

$$= \pi a^2 v_0 C_w (1/2 + 11\beta b/48 + \ldots).$$

Therefore

$$(\bar{C}-C_w)/C_w=11\beta b/24.$$

In the apparatus used by Greenspan the pressure drop was measured to be $\beta=(adp/dz)/p_0=-5.2\times10^{-8}$ at atmospheric pressure so that $\beta b=-2.8\times10^{-5}$. The corresponding error in concentration is $(C-C_w)/C_w=-(11/24)\times2.8\times10^{-5}\sim-1.2\times10^{-5}$.

In the above we have taken the vapor concentration at the interface with the condensed phase to be that in equilibrium at the bath temperature. A more complete discussion would take into account the temperature gradient in the wall and the balance at the interface between the latent heat of evaporation and the thermal conduction in the wall and in the gas stream. It should also consider the effect of the partial pressure of the vapor on the conservation equation. These factors can be neglected in Greenspan's experiment since the partial pressure of vapor is 0.1 percent or less, and a rough calculation indicates that the thermal gradient in the wall will change the decay lengths by less than 1 percent at 0 °C and much less at lower temperatures. They cannot be neglected at higher temperatures. There is also the possibility that the rate of evaporation or condensation is affected by a potential barrier in a surface film.

The author thanks Mr. Lewis Greenspan for programming the computations.

References

[1] Greenspan, L., Low frost point humidity generator, J. Res. Nat. Bur. Stand. (U.S.), **77A** (Phys. and Chem.), No. 5, 671–677 (Sept.–Oct. 1973).
[2] Graetz, Ann. der Physik **18**, 79 (1883); ibid **25**, 337 (1885).
[3] Nusselt, W., Zeil Verein deul. Inj. **54**, 1154 (1910).
[4] Drew, T. B. Trans. Am. Inst. Chem. Eng. **26**, 26 (1931).

(Paper 78A1–803)

JOURNAL OF RESEARCH of the National Bureau of Standards—A. Physics and Chemistry
Vol. 78A, No. 1, January–February 1974

Theoretical Analysis of Miscibility Gaps in the Alkali-Borates

Pedro B. Macedo*

Catholic University of America, Washington, D.C. 20017

Joseph H. Simmons

Institute for Materials Research, National Bureau of Standards, Washington, D.C. 20234

(September 5, 1973)

A thermodynamic approach based on the regular solution concept is applied to the description of miscibility gap boundaries in the alkali-borate systems. It is suggested that in each system the structural units which control the entropy of mixing are the stoichiometric compounds at the apparent limit of the alkali-rich edge of the gap, and a complex boron trioxide structure. (The former is inferred by the shape of the gap, and the latter is chosen to fit the regular mixing equation.) The same boron trioxide complex is used for all the systems analyzed. The physical implications of this analysis are discussed.

Key words: Glass; immiscibility; phase separation; thermodynamics of solutions.

1. Introduction

While miscibility gaps have been measured in a large number of systems [1] [1], there have been few attempts to analyze their shape. Concentrating on the oxide glass systems, we find that the majority of these gaps have been observed in complex systems consisting of more than two component oxides. Since it is not clear whether these systems separate into two or more phases [2], and since the exact chemical identities of the coexistent phases have largely escaped definition, a first principle analysis of the thermodynamics of their phase-separation is not possible. There are, however, several binary oxide mixtures which exhibit immiscibility at high glassformer concentrations. These are largely the alkali silicates [3, 4] and borates [5]. Despite this apparent simplification, attempts to describe the shape of the miscibility gap boundaries in these binary systems have not been generally successful [6, 7].

The regular-mixing approach [8] which depends upon balancing the exothermic entropy of mixing and an endothermic enthalpy of mixing results in a coexistence or miscibility gap boundary curve which is symmetric in terms of the relative concentrations of the two immiscible liquids. The alkali-borates and silicates, which represent the major binary oxide systems with miscibility gaps, show highly asymmetric gaps. In the case of the alkali-silicates, the miscibility gap is limited at one branch by silica and at the other by the first stoichiometric crystalline compound encountered as alkali oxide is added. Assuming that the two demixing liquids are SiO_2 and this stoichiometric compound still leads to an asymmetric gap [6]. This behavior has discouraged the use of regular-mixing equations [8] to describe such gaps. The borates pose a more serious problem to this approach, since their miscibility gaps reach beyond several stoichiometric crystal compounds.

The most serious attempt to describe the thermodynamics of phase separation in binary oxide systems was recently presented by R. J. Charles [7]. Assuming that the enthalpy of mixing in the silicates resulted principally from changes of coordination and valence of oxygen ions in the melt and changes in bonding energy at oxygen sites, he was able to show that the enthalpic heat of mixing of transition metal oxide-silica mixtures was endothermic. The addition of this endothermic enthalpy contribution to the exothermic entropy contribution in the Gibbs free energy leads to phase-separation. Following the same considerations, he found that the heat of mixing for the alkali-metal and alkaline-earth oxide mixtures with silica was exothermic thus negating any possibility for phase separation. Since these systems do exhibit phase separation, it was concluded that the partial molar heat of solution of silica, which had been previously overlooked, was a prime candidate for the necessary large endothermic contribution to the heat of mixing. The implications of such an assumption are interesting, since they point to the formation upon phase-separation of a complex

*Work done at Catholic University was supported by Contract Number AF72-2203.

[1] Figures in brackets indicate the literature references at the end of this paper.

silica structure larger than a single SiO_4 tetrahedron.

This hypothesis, proposed by Charles, serves well to introduce the concepts of our model, although the two were developed independently. Below we propose a model to describe the thermodynamic processes which control liquid-liquid immiscibility in the binary oxide glasses. This is based upon the concept that molten oxides are made up of small structural units which control the physical properties of their melts. The configurational entropy of mixing is therefore determined by the possible rearrangements of these units. As a result, the free energy of the system is not expressed in terms of molar concentrations of the component oxides, but rather in terms of the relative concentrations of the dominant structural units. This approach allows the use of the regular mixing equation and replaces the arbitrary assumption that the glass-former, say B_2O_3, mixes as a cell containing two borons and three oxygens, with the more physically acceptable concept that the cell consists of a complex structure, $(B_2O_3)_m$, with m being an integer. In this paper, we will consider the alkali-metal oxide-boric oxide mixtures, since their gaps occur in similar temperature ranges, thus reducing the number of undetermined parameters. The alkali-silicates are covered in a separate paper [3].

2. Structural Units in the Melt

The existence of small stable species made up of several molecules in the melts of oxide glassformers has long been suspected. A number of authors have proposed complex species for various structures in order to describe structural, thermodynamic and kinetic measurements [10–17].

In these various studies it seems clear that the structure of the primary network formers—SiO_2, B_2O_3 and GeO_2—extends well beyond the nearest neighbor coordination, but the definition of a molecule of glassformer is not clear and may easily depend upon the property analyzed.

The smallest unit which retains its identity when two liquids are mixed may be defined in several ways. Following a correlation function approach, a size corresponding to an ordered region may be obtained. A geometrical approach, emphasizing the structural units (e.g., boroxol rings for B_2O_3) may be tested by x-ray diffraction. However, it appears that the different investigators do not agree on the various interpretations of the x-ray data. A thermodynamic approach is also possible, whereby the exact nature of the structural units is not specified and only the thermodynamic behavior of the system is analyzed.

In this paper we will restrict our analysis to thermodynamic concepts, since we are only concerned with investigating the variables which determine the shape of miscibility gaps in the oxide mixtures.

3. Complex Molecule Model for Miscibility Gaps

In considering the thermodynamic properties of binary mixtures, simple mixing between the glass-formers, B_2O_3 or SiO_2, and the alkali oxides, M_2O or MO can be rejected on structural grounds, as done by other authors [6], since it is unlikely that such molecules exist in the melt. Let us analyze, instead, mixing between more complex and hopefully, more realistic structures.

As an example, in the phase diagram of the lithium-borate system it will be assumed that mixing occurs between the network former and a stoichiometric chemical compound whose composition can be obtained by extrapolating the immiscibility or coexistence curve to zero Kelvin. By inspection it appears that the coexistence curve can best be extrapolated to the compound $Li_2O \cdot 4B_2O_3$ at low temperatures. The model which we propose thus considers the $Li_2O \cdot 4B_2O_3$ composition as one of the mixing liquids.

The choice of this stoichiometric compound as one of the mixing liquids is not inconsistent with the existence of a crystalline compound at $Li_2O \cdot 5B_2O_3$, since it is well accepted that borate melts have far different structures than the crystalline states. Thus, it is unlikely that a correspondence would develop between the structures of compounds in the melt and those of crystals, in the high B_2O_3 region of the systems.

The significant contribution presented by this paper involves choosing a complex boron molecule, $[(B_2O_3)_m]$, as the second liquid. The complex molecule is a somewhat stable grouping of boron and oxygen atoms which can be identified as a single species in the entropy calculation. This species, however, once identified for a particular glassformer in a given temperature range, must contribute to the entropy calculations of the other miscibility gaps of that glassformer (i.e., in the alkali-borates) occurring in the same temperature range.

Without committing ourselves as to the geometrical appearance of these species, we propose to use the complex molecules, $[(M_2O \cdot nB_2O_3)]$ and $[(B_2O_3)_m]$, in the calculation of the entropy of mixing. In the alkali-borates only one value of m will be used for all the different alkalis, since the miscibility gaps occur in the same temperature range. The silicates, however, present more difficulty due to the vast temperature differences between their miscibility gaps [3].

The composition of the alkali-borate melt is normally written $xB_2O_3 \cdot yM_2O$, where x and y are the respective molar fractions of B_2O_3 and M_2O. In terms of the new components used here the melt composition will be expressed as $\bar{x}[(B_2O_3)_m] \cdot \bar{y}[M_2O \cdot nB_2O_3]$, where $\bar{x}$ and $\bar{y}$ are the respective mole fractions of $[(B_2O_3)_m]$ and $[M_2O \cdot nB_2O_3]$. It is easily shown that

$$\bar{y} = y/\{y + [1-(n+1)y]/m\}$$
$$\bar{x} = 1-\bar{y} \qquad (1)$$

Once the identities of the two separated liquids are found, then each original composition (molar concentrations) can be converted to relative concentrations of the two separated liquids (i.e., $\bar{x}$ and $\bar{y}$) and then the data can be compared with the ideal mixing equation for the system $[(B_2O_3)_m]$ and $[M_2O \cdot n(B_2O_3)]$.

The value of n in the formula $[M_2O \cdot n(B_2O_3)]$ can be obtained in most instances by visual inspection of the data. The complex glassformer molecule must then be inferred from the data by choosing the value of m necessary to symmetrize the coexistence curve with respect to concentrations of the immiscible liquids. The crucial test then is to see whether all gaps are likewise symmetrized by the same glassformer complex molecule in the alkali-borates.

4. Calculation of the Regular Mixing Equation

The regular mixing equations are well known (see ref. 8, for instance) and we will only review the basic derivation here, for completeness. The free energy of mixing can be expressed in terms of an enthalpy and entropy of mixing. When the enthalpy is positive, phase separation may ultimately occur. The molar enthalpy of mixing is expressed in terms of the two concentrations $\bar{x}$ and $\bar{y}$, and an interaction energy parameter $w (w > 0)$ as follows:

$$\Delta H = \bar{x}\bar{y}w \tag{2}$$

Contributions to the entropy of mixing of two liquids come from two sources. In general, most authors have ignored the effect due to changes in the internal degrees of freedom of each liquid, and have only been concerned with configurational states [6, 9]. Both terms will be examined here. The configurational molar entropy of mixing is written as:

$$\Delta S_1 = -R[\bar{x}\ln\bar{x} + \bar{y}\ln\bar{y}]$$
$$= -R[(1-\bar{y})\ln(1-\bar{y}) + \bar{y}\ln\bar{y}] \tag{3}$$

The molar entropy of mixing arising from changes in the internal degrees of freedom upon mixing is expressed as:

$$\Delta S_2 = \bar{x}\bar{y}\delta S \tag{4}$$

The structural implications of the magnitude of this term will be discussed later. The molar free energy of mixing now becomes:

$$\Delta G = \Delta H - T(\Delta S_1 + \Delta S_2)$$

$$\Delta G = \bar{y}(1-\bar{y})(w - T\delta S)$$
$$+ RT[\bar{y}\ln\bar{y} + (1-\bar{y})\ln(1-\bar{y})] \tag{5}$$

Phase separation is now obtained by minimizing the free energy of mixing with respect to composition:

$$\left(\frac{\partial \Delta G}{\partial \bar{y}}\right)_{P,T} = 0 = (1-2\bar{y})w$$
$$+ RT[\ln\bar{y} - \ln(1-\bar{y}) - (1-2\bar{y})\delta S/R] \tag{6}$$

This condition leads to a temperature-composition relationship which represents the coexistence curve:

$$T_{\text{coex}} = (w/R) \cdot (1-2\bar{y}) \cdot \left\{\ln\left[\frac{(1-\bar{y})}{\bar{y}}\right] + (1-2\bar{y})\,\delta S/R\right\}^{-1} \tag{7}$$

The critical temperature, T_c, corresponding to the top of the miscibility gap is found by maximizing T_{coex}:

$$T_c = (w/R)/(2 + \delta S/R) \tag{8}$$

The dependence of the normalized coexistence temperature on concentration can then be expressed as:

$$T_{\text{coex}}/T_c = (2 + \delta S/R) \cdot (1-2\bar{y})$$
$$\left\{\ln\left[\frac{(1-\bar{y})}{\bar{y}}\right] + (1-2\bar{y})\,\frac{\delta S}{R}\right\}^{-1} \tag{9}$$

Once the coexistence curve has been established, it is of interest to calculate the spinodal curve, by letting the second derivative of the free energy of mixing with respect to composition go to zero:

$$\left(\frac{\partial^2 \Delta G}{\partial \bar{y}^2}\right) = 0 = -2(w - T\delta S) + RT[1/\bar{y} + 1/(1-\bar{y})] \tag{10}$$

The spinodal curve is now written as:

$$T_s = 2(w/R)\left[\frac{1}{\bar{y}(1-\bar{y})} + 2\delta S/R\right]^{-1} \tag{11}$$

$$T_s/T_c = 2\,(2 + \delta S/R)\left[\frac{1}{\bar{y}(1-\bar{y})} + 2\delta S/R\right]^{-1} \tag{12}$$

These results may now be transformed into functions of the usual molar fractions of M_2O (e.g., y) by substituting the expression for $\bar{y}$, eq (1), into the coexistence and spinodal equations (eqs (9) and (12)). These solutions are represented in our subsequent graphs by solid and dashed lines, respectively.

5. Comparison with Data

5.1. Lithium-borate System

The data by Shaw and Uhlmann [5] were used to test the equations obtained above. The phase diagram of the lithium-borate system exhibits a liquid-liquid metastable miscibility gap between 4 and 16 mole percent Li_2O. The maximum of the coexistence curve appears at 10 mole percent Li_2O. The stoichiometric

compound $Li_2O \cdot 4B_2O_3$, therefore, appears to limit the gap in the high alkali region. This then will be one of the immiscible liquids at zero Kelvin.

Let us now consider the immiscible liquid on the borate-rich side of the gap. Assuming regular mixing between $[B_2O_3]$ and $[Li_2O \cdot 4B_2O_3]$ yields a maximum in the coexistence curve at 50 percent (B_2O_3) and 50 percent ($Li_2O \cdot 4B_2O_3$) which corresponds to the 17 mole percent Li_2O concentration. This result disagrees with the measured maximum near 10 percent Li_2O. The choice of a boroxol ring as suggested by Krogh-Moe [18] yields a maximum near 15 mole percent Li_2O, which is also unsatisfactory. The $[B_4O_6]$ cages of Ottar and Ruigh [12] are no more successful with 14 mole percent Li_2O for the maximum. The complex $(B_2O_3)_m$ molecule which allows symmetrization of the gap and leads to a maximum at 10 mole percent Li_2O turns out to be the $[(B_2O_3)_5]$.

While this choice of a complex $[(B_2O_3)_5]$ molecule appears arbitrary in this case, it must be remembered that since the other alkali-borates have miscibility gaps in the same temperature range, we are restricted to the same complex for these other gaps. The data are plotted in terms of concentrations of the two demixing liquids $[(B_2O_3)_5$ and $(Li_2O \cdot 4B_2O_3)]$ in figure 1. The

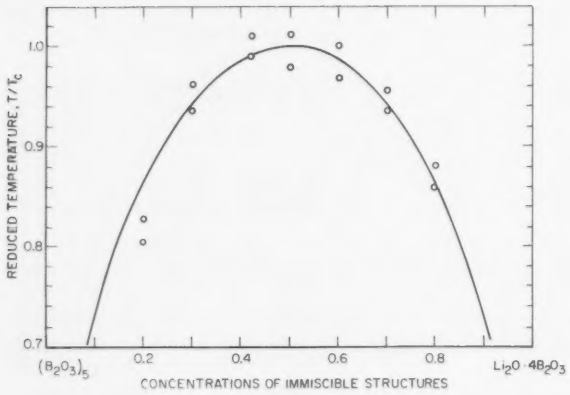

FIGURE 1. *Miscibility gap in the lithium-borate system, plotted in terms of concentrations of the two demixing liquids:* $[(B_2O_3)_5]$ *and* $[(Li_2O \cdot 4B_2O_3)]$.

regular-mixing solution is also plotted, and appears to fit the data well. In this case the entropy contribution from changes in vibrational states of the molecules appears to be negligible ($\Delta S_2 = 0$). A plot of the data and the coexistence and spinodal curves in terms of Li_2O molar concentration is shown in figure 2 and also demonstrates good agreement between the data and the equations.

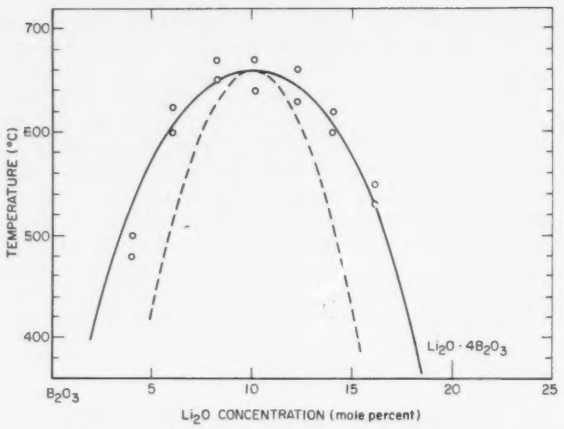

FIGURE 2. *Miscibility gap in the lithium-borate system, plotted in terms of* Li_2O *concentration.*

The solid and dashed lines are the calculated coexistence and spinodal boundary curves, respectively.

5.2. Other Alkali-Metal Oxide-Borate Systems

While we have four adjustable parameters in this analysis, m, n, w and δS, we may only freely adjust δS, in fitting the shape of the coexistence curve in the other alkali-borate systems. The value of maximum coexistence temperature, T_c, in general cannot be adjusted by more than 1 percent and determines w directly. The identities of the two demixing liquids at zero Kelvin (n and m) are fixed by the data at the high-alkali branch, and by the choice of $[(B_2O_3)_5]$ on the boric oxide side.

Shaw and Uhlmann's measurements in the potassium-borate, rubidium-borate and cesium-borate systems show phase separation occurring between 4 and 20 mole percent K_2O, 4 and 14 mole percent Rb_2O, and 4 and 18 mole percent Cs_2O, respectively. The data for the potassium and cesium borate systems indicates that the compound limiting one of the branches of the coexistence curves is at 25 mole percent alkali oxide. A lack of data in the rubidium-borate system prevents a similar analysis, so we assumed that it would follow the same behavior as the other two. Therefore, the demixing liquid at the high-alkali side of the gap is $[M_2O \cdot 3B_2O_3]$, where M_2O stands for the three alkali oxides in question.

A regular mixing between $[M_2O \cdot 3B_2O_3]$ and $[(B_2O_3)_5]$ leads to a maximum in the coexistence curve near 11 percent M_2O. Inspection of the data shows good agreement for the K_2O and Cs_2O mixtures. Figures 3 and 5 show that the data appear symmetric when plotted as a function of concentration of these immiscible liquids. The regular-mixing equation gives a good fit of the data with the vibrational contribution to the entropy, δS, chosen at $+0.5R$ and $-0.8R$ for the K_2O and Cs_2O systems, respectively. The data for the rubidium system show only fair agreement with the model and require a choice of $\delta S = -0.5R$ for the

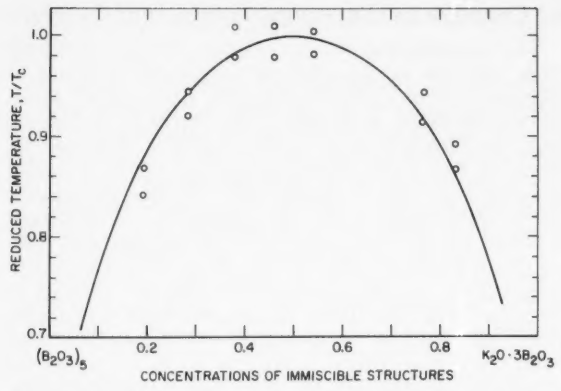

FIGURE 3. *Miscibility gap in the potassium-borate system, plotted in terms of concentrations of the two demixing liquids:* [$(B_2O_3)_5$] *and* [$(K_2O \cdot 3B_2O_3)$].

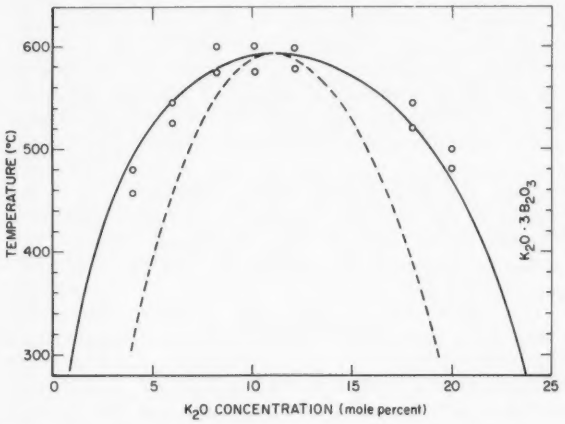

FIGURE 4. *Miscibility gap in the potassium-borate system, plotted in terms of* K_2O *concentration.*

The solid and dashed lines are the calculated coexistence and spinodal boundary curves, respectively.

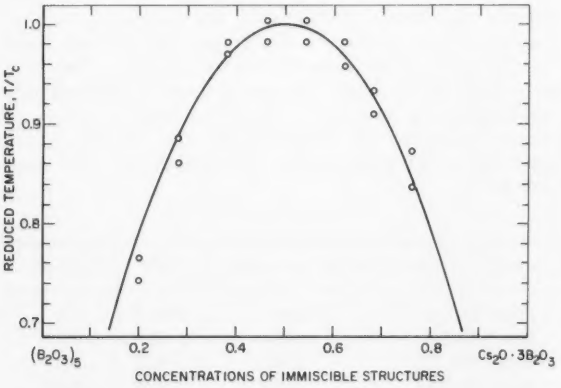

FIGURE 5. *Miscibility gap in the cesium-borate system, plotted in terms of concentrations of the two demixing liquids:* [$(B_2O_3)_5$] *and* [$(Cs_2O \cdot 3B_2O_3)$].

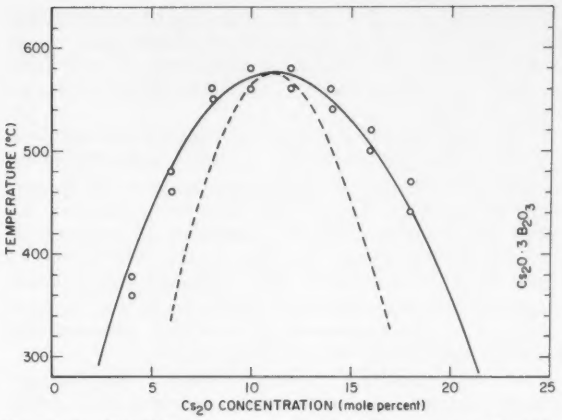

FIGURE 6. *Miscibility gap in the cesium-borate system, plotted in terms of* Cs_2O *concentration.*

The solid and dashed lines are the calculated coexistence and spinodal boundary curves, respectively.

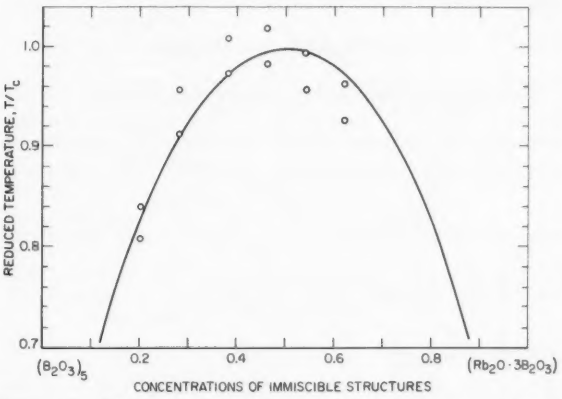

FIGURE 7. *Miscibility gap in the rubidium-borate system, plotted in terms of concentrations of the two demixing liquids:* [$(B_2O_3)_5$]. *and* [$(Rb_2O \cdot 3B_2O_3)$].

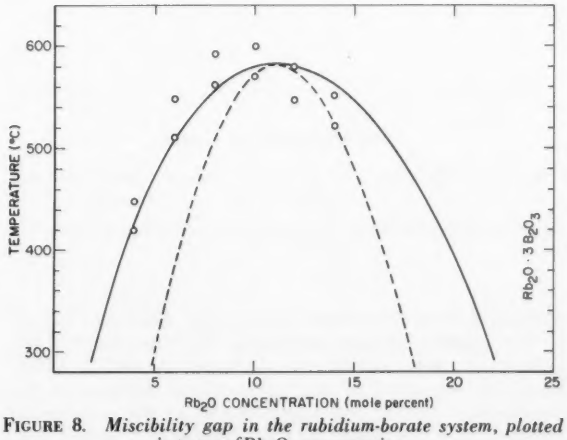

FIGURE 8. *Miscibility gap in the rubidium-borate system, plotted in terms of* Rb_2O *concentration.*

The solid and dashed lines are the calculated coexistence and spinodal boundary curves, respectively.

fit shown (fig. 7). Plots of the data and the coexistence and spinodal curves in terms of alkali-oxide molar concentrations are shown in figures 4, 6, and 8. In general, the model satisfactorily describes the phase-separation data.

The above results confirm our choice of the species: $[(B_2O_3)_5]$ as the molecular complex controlling the configurational entropy of the system over the observable temperature range, and therefore, support the merit of this approach. We see that in addition to describing the shape of the coexistence curve, a calculation of the location of the spinodal region is also possible. This has potential usefulness in the interpretation of measurements on glasses with compositions far from the critical composition.

We have omitted a description of the sodium-borate system, because the data appeared very different from that for the other systems. Attempts to symmetrize the coexistence curve were relatively unsuccessful. An attempt to measure the gap as a check on the data was equally unsuccessful due to the quick hydration of the samples.

5.3. Lead-Borate System

Data for the lead-borate system was reported by two authors [19, 20]. One of us, J. H. Simmons, has also recently reported the results of careful measurements of phase separation in this system [21]. Figure 9,

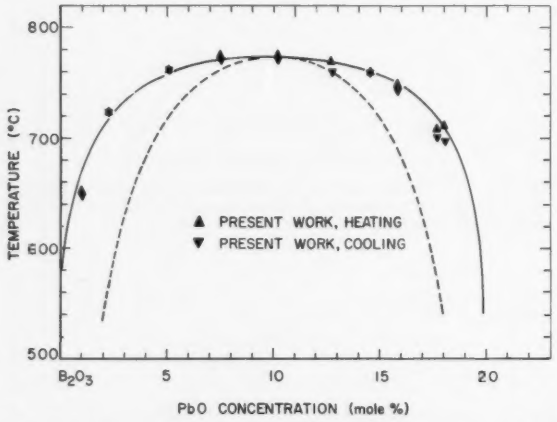

FIGURE 9. *Miscibility gap in the lead-borate system, reprinted from ref* [21].

The solid and dashed lines are the calculated coexistence and spinodal boundary curves, respectively.

reprinted from his paper, shows his data and the fit of the regular-mixing equations. The two immiscible liquids at zero kelvin are $[(B_2O_3)_5]$ and $[(PbO \cdot 4B_2O_3)]$. Because of the pronounced flatness of the coexistence curve, the contribution to the entropy of mixing from changes in the vibrational states was large, $\delta S = +10R$. The implications of this result are discussed in the next section.

6. Changes in the Internal Degrees of Freedom

The contribution to the entropy of mixing arising from changes in the internal degrees of freedom or vibrational states of the immiscible liquids, ΔS_2, is the parameter which most affects the shape of the miscibility gap boundaries in the fits presented above. Its effect on the regular mixing equation serves to either broaden ($\delta S > 0$), or narrow ($\delta S < 0$), the coexistence curve while maintaining symmetry. This is achieved through its effect on the critical temperature, T_c: eq (8). A positive value for the additional entropy corresponds to an increase in the internal degrees of freedom. The additional states developed by mixing thus will tend to suppress phase separation. The evidence is mounting in support of the two-dimensional structural description of pure boron trioxide glass. The addition of alkali-metal oxides tends to convert three-coordinated planar borons to four-coordinated borons. This helps form a three dimensional network. The change is small, however, since only the boron ions are affected. Because of their low valence the alkali ions cannot form cross linking. In addition, however, one must consider the effect of changes in the molecular vibrational states. As a simple example, we may look at the phonon density of states of a linear chain with alternating different masses (mixed state) and compare it with that of two chains with equal masses (phase-separated state). The result is a decrease in the available states or internal degrees of freedom upon mixing. The additional entropy, δS, would be negative thus raising T_c. The effect is more pronounced for the heavier alkali-borate compounds.

The table below lists the various alkali-oxide compounds postulated with their formula weights and the additional entropy terms necessary for fitting the regular mixing equation. The potassium oxide compound is the lightest and it appears that the entropy contribution from the formation of a three dimensional structure dominates. As the mass of the compound increases to the cesium oxide system, the change in vibrational states dominates and the entropy term becomes increasingly negative.

The lead oxide-boric oxide system is also included. Despite its heavy compound, the entropy term is positive. This is due to the large contribution from the change in dimensionality of the system. The lead ions with their high valence become tetrahedrally coordinated in solution and add a large number of internal degrees of freedom to the system. This apparently dominates over the effect of the mass change.

TABLE 1

Immiscible compound	Molecular weight	$\delta S/R$	$[2+\delta S/R]^{-1}$
$[K_2O \cdot 3B_2O_3]$	303	+0.5	0.4
$[Li_2O \cdot 4B_2O_3]$	308	0	0.5
$[Rb_2O \cdot 3B_2O_3]$	396	−0.5	0.67
$[Cs_2O \cdot 3B_2O_3]$	491	−0.8	0.83
$[PbO \cdot 4B_2O_3]$	501	+10.0	0.083
$[(B_2O_3)_5]$	348		

7. Conclusion

We have shown that the thermodynamic equations of regular mixing can be applied to phase separation in the alkali-borate glasses. The concept, which must be introduced to accomplish this, is the assumption that the glassformer phase is structurally represented by a complex molecule and the glassformer-modifier phase by a stoichiometric compound. This transformation symmetrizes the coexistence curve.

The regular mixing equation appears to represent the data well when an additional entropy of mixing arising from changes in the internal degrees of freedom of the system is included in the calculation. Following this approach, five systems were treated successfully. The complex boron trioxide molecule $[(B_2O_3)_5]$ was used in the regular mixing analyses of all the borate systems considered, since the miscibility gaps occurred approximately within the same temperature range.

The implications of such an approach are interesting but not surprising. As mentioned before, by other authors and in some of our other work, the existence of complex glass-former structures in the melt appears to offer a good explanation for the behavior of an increasing number of physical properties of molten oxide glasses.

An actual geometrical description of the complex boron trioxide structure is not accessible to us by this analysis since thermodynamic treatments do not afford structural descriptions.

8. References

[1] Levin, E. M., Liquid Immiscibility in Oxide Systems, Phase Diagrams, Vol. 3 (Academic Press, Inc., New York, 1970).

[2] Haller, W., Blackburn, D. H., Wagstaff, F. E., and Charles, R. J., J. Amer. Ceram. Soc. **53**, 34 (1970).

[3] Haller, W., Blackburn, D. H., and Simmons, J. H., Miscibility gaps in alkali-silicates, J. Am. Ceram. Soc. (to be published, March 1974).

[4] Andreev, N. S., Goganov, D. A., Porai-Koshits, E. A., and Sokolov, Yu G., Proc. Fourth All Union Conf. on Glassy States (Eng. Transl.) p. 45 (Consultants Bureau, New York, 1964).

[4a] Hammel, J. J., VII International Congress on Glass, Brussels, June 1965.

[5] Shaw, R. R., and Uhlmann, D. R., J. Amer. Ceram. Soc. **51**, 377 (1968).

[6] Moriya, Y., Warrington, D. H., and Douglas, R. W., Phys. Chem. Glasses **8**, 19 (1967).

[7] Charles, R. J., Phys. Chem. Glasses **10**, 169 (1969).

[8] Thompson, J. B., Jr., Thermodynamic Properties of Simple Solutions, Researches in Geochemistry, II, P. H. Abelson, Ed., pp. 340–361. (John Wiley & Sons, N.Y., 1967).

[9] Charles, R. J., Phys. Chem. Glasses **10**, 169 (1969).

[10] Warren, B. E., X-ray Structural Determination of Glasses, Amorphous Materials, R. W. Douglas and B. Ellis, Eds., p. 263 (John Wiley & Sons, London, 1972).

[11] Ottar, B., and Ruigh, W. L., Phys. Chem. Glasses **3**, 95 (1962).

[12] Dunlevey, F. M., and Cooper, A. R., Bul. Am. Ceram. Soc. **51**, 374 (1972).

[13] Konnert, J., Karle, J., and Ferguson, G. A., Bul. Am. Ceram. Soc. **51**, 374 (1972).

[14] Fajans, K., and Barber, S. W., J. Am. Chem. Soc. **74**, 2761 (1952).

[15] Mackenzie, J. D., Some Physical Properties and Structure of Liquid Boron Trioxide, General Electric Research Laboratory Report 3550.

[16] Macedo, P. B., Capps, W., and Litovitz, T. A., J. Chem. Phys. **44**, 3357 (1966).

[17] Leidecker, H. W., Simmons, J. H., Litovitz, T. A., and Macedo, P. B., J. Chem. Phys. **55**, 2028 (1971).

[18] Krogh-Moe, J., Phys. Chem. Glasses **3**, 101 (1962).

[19] Leidberg, D. J., Ruderer, C. C., and Bergeron, C. G., J. Am. Ceram. Soc. **48**, 440 (1965).

[20] Zarzycki, J., and Naudin, F., Phys. Chem. Glasses **8**, 11 (1967).

[21] Simmons, J. H., Miscibility gap in the $PbO–B_2O_3$ system, J. Amer. Ceram. Soc. **56**, 284 (1973).

(Paper 78A1–804)

JOURNAL OF RESEARCH of the National Bureau of Standards — A. Physics and Chemistry
Vol. 78A, No. 1, January-February 1974

Publications of the National Bureau of Standards*

Citations with Selected Abstracts

J. Res. Nat. Bur. Stand. (U.S.), **77A** *(Phys. and Chem.)*, No. 6, (Nov.-Dec. 1973), SD Catalog No. C13.22/sec.A:77/6.

Absolute isotopic abundance ratio and atomic weight of a reference sample of rhenium, J. W. Gramlich, T. J. Murphy, E. L. Garner, and W. R. Shields.

Reflection correction for high-accuracy transmittance measurements on filter glasses, K. D. Mielenz and R. Mavrodineanu.

Temperature-pressure phase relationships in niobium pentoxide, J. L. Waring, R. S. Roth, and H. S. Parker.

Nuclear magnetic resonance of ^{113}Cd and ^{199}Hg in Cd-Mg and Cd-Hg solid solutions, V. V. Zhukow, I. D. Weisman, and L. H. Bennett.

Molecular basis of flame inhibition, J. W. Hastie.

The effect of temperature and pressure on the refractive index of some oxide glasses, R. M. Waxler and G. W. Cleek.

The pair correlation function in liquid ^{4}He, R. D. Mountain and H. J. Raveché.

J. Res. Nat. Bur. Stand. (U.S.), **77B** *(Math. Sci.)*, Nos. 3 and 4, SD Catalog No. C13.22/sec.B:77/3&4.

Certification of an algorithm for Bessel functions of complex argument, D. J. Sookne.

Character induced subgroups, R. Merris and W. Watkins.

The characterizations of $(A_0(U))$, M. E. Sheingorn.

An application of Schur's lemma on irreducible sets of matrices in continuum mechanics, J. T. Fong.

Remarks on a problem of Rademacher in the theory of modular forms, M. I. Knopp.

Performance testing of a FORTRAN library of mathematical function routines—A case study in the application of testing techniques, D. W. Lozier, L. C. Maximon, and W. L. Sadowski.

Bessel functions *I* and *J* of complex argument and integer order, D. J. Sookne.

Certification of an algorithm for Bessel functions of real argument, D. J. Sookne.

Triangles generated by powers of triplets on the unit circle, C. R. Johnson and M. Newman.

Tables and graphs of the stable probability density functions, D. R. Holt.

Bessel functions of real argument and integer order, D. J. Sookne.

Monogr. 130. **The divergent beam (Kossel) x-ray method and its uses in measuring strain contours in an individual grain of Fe-3 weight percent Si transformer sheet,** H. Yakowitz, Nat. Bur. Stand. (U.S.), Monogr. 130, 80 pages (Aug. 1973) 95 cents, SD Catalog No. C13.44:130.

Key words: Divergent beam x-ray diffraction; electron probe microanalysis; iron-silicon alloy; Kossel; strain; stress; transformer sheet.

Residual and impressed stresses and strains in Fe-3 wt. pct. Si alloy transformer sheet were studied. Results were obtained by the divergent beam (Kossel) x-ray microdiffraction techniques. The optically opaque Fe-3 wt. pct. Si alloy was mapped for residual and impressed stresses and strains. These maps are roughly analogous to polarized light stress analysis of transparent materials. The results showed that a variable strain distribution existed in the alloy sheet at the time it was ready for insertion into a transformer core. Small applied compressive and tensile loads tended to rearrange this variable strain distribution but not to appreciably alter the total stored elastic energy.

Monogr. 131. **Thermal conductivity of solids at room temperature and below. A review and compilation of the literature,** G. E. Childs, L. J. Ericks, and R. L. Powell, Nat. Bur. Stand. (U.S.), Monogr. 131, 624 pages (Sept. 1973) $7.80, SD Catalog No. C13.44:131.

Key words: Cryogenic thermal conductivity; elements, alloys, commercial metals, semiconductors, semimetals, ionic and valence crystals, minerals, molecular crystals, polymers, glasses, disordered dielectrics, thermal conductivity of; review; thermal conductivity.

An extensive compilation is given of the measured values of thermal conductivity for nearly all solid materials from room temperature down to 0.01 kelvin. The reviewed materials include elements, alloys and commercial metals, semiconductors, semimetals, ionic and valence crystals, minerals, molecular crystals, polymers, glasses, and disordered dielectrics. Excluded are foams, powders, earths, fibers, layers of composites, and similar other heterogeneous solids. Data for temperatures below 1 kelvin are presented separately. The tables and graphs are complete for literature references from 1900 to mid-1971. Experimental methods and physical phenomena are discussed in the text and coded in the tables for references for which curves are shown. Supersedes NBS Circular 556.

Monogr. 134. **Space groups and lattice complexes,** W. Fisher, H. Burzlaff, E. Hellner, and J. D. H. Donnay, Nat. Bur. Stand. (U.S.), Monogr. 134, 184 pages (May 1973) $4.10, SD Catalog No. C13.44:134.

Key words: Crystallography; crystal point groups; crystal structure; lattice complexes; site sets; space groups.

The lattice complex is to the space group what the site set is to the point group—an assemblage of symmetry-related equivalent points. The symbolism introduced by Carl Hermann has been revised and extended. A total of 402 lattice complexes are derived from 67 Weissenberg complexes. The Tables list site sets and lattice complexes in standard and alternate representations. They answer the following questions: What are the coordinates of the points in a given lattice complex? In which space groups can a given lattice complex occur? What are the lattice complexes that can occur in a given space group? The higher the symmetry of the crystal structures is, the more useful the lattice-complex approach should be on the road to the ultimate goal of their classification.

**Publications with prices and SD Catalog numbers may be purchased directly from the Superintendent of Documents, U.S. Government Printing Office, Washington, D.C. 20402 (foreign: one-fourth additional). Microfiche copies are available from the National Technical Information Service (NTIS), Springfield, Va. 22151. Reprints from outside journals and the NBS Journal of Research may often be obtained directly from the authors.*

Monogr. 135. **Properties of glasses in some ternary systems containing BaO and SiO_2,** G. W. Cleek and C. L. Babcock, Nat. Bur. Stand. (U.S.), Monogr. 135, 42 pages (Sept. 1973) 70 cents, SD Catalog No. C13.44:135.

Key words: Barium glasses; barium silicates; glass properties; glass property factors; oxide glasses; silicate substructures; ternary glasses.

The glass forming regions in six ternary oxide systems containing BaO, SiO_2 and a third oxide have been determined. The properties of the resulting glasses were measured and the results are reported. The data on refractive indices, dispersions and specific volumes were evaluated by computer methods in an attempt to identify "substructures" containing the cations present in the glasses.

H112. **Examination procedure outlines for commercial weighing and measuring devices. A manual for weights and measures officials,** O. K. Warnlof, Nat. Bur. Stand. (U.S.), Handb. 112, 89 pages (June 1973) $1.10, SD Catalog No. C13.11:112.

Key words: Codes; examination procedure; inspection; meters; outlines; scales; tests.

This handbook presents an operational guide for the field examination of commercial weighing and measuring devices. It includes inspection and test procedures, with code references to National Bureau of Standards Handbook 44, Fourth Edition, "Specifications, Tolerances, and Technical Requirements for Commercial Weighing and Measuring Devices."

SP260-45. **Standard Reference Materials: Development of NBS Standard Reference Material No. 1579 Powdered Lead-Based Paint,** B. Greifer, E. J. Maienthal, T. C. Rains, and S. D. Rasberry, Nat. Bur. Stand. (U.S.), Spec. Publ. 260-45, 31 pages (Mar. 1973) 50 cents, SD Catalog No. C13.10:260-45.

Key words: Analytical standard; atomic absorption spectrometry; differential cathode ray polarography; electrodeposition; lead-based paint; neutron activation analysis; x-ray fluorescence spectrometry; Standard Reference Material.

The development of NBS Standard Reference Material No. 1579, Powdered Lead-Based Paint is described. This SRM is intended for use in the calibration of apparatus and methods used in determining lead in paint removed from old housing.

Paints scraped from the interior surfaces of old housing were collected, blended, homogenized, and characterized for lead content. The average lead content was found to be 11.87 ± 0.04 percent lead by weight determined by atomic absorption spectrometry and by diferential cathode ray polarography.

The analytical procedures involved sample dissolution by dry ashing in a furnace at 450-550 °C followed by exhaustive extractions of the insoluble residue with acids and with ammonium acetate solution.

SP370. **Research and testing facilities of the Engineering Mechanics Section, National Bureau of Standards, Washington, D.C.,** by the Staff of the NBS Engineering Mechanics Section, D. J. Chwirut, Coordinator, Nat. Bur. Stand. (U.S.), Spec. Publ. 370, 23 pages (Jan. 1973) 55 cents, SD Catalog No. C13.10:370.

Key words: Engineering Mechanics Section; force generating equipment; research facilities; testing machines.

The principal characteristics of the force measuring and generating equipment and related research facilities available in the Engineering Mechanics Section of the National Bureau of Standards are described.

SP374. **Method for determining the resolving power of photographic lenses,** F. E. Washer and I. C. Gardner. Appendix added by C. E. Kuyatt, Nat. Bur. Stand. (U.S.), Spec. Publ. 374, 32 pages (June 1973) $3.00, SD Catalog No. C13.10:374.

Key words: Photographic lenses; resolution test charts; resolving power.

This publication supersedes NBS Circular 533, issued May 20, 1953. It contains the original data and a new appendix describing the NBS Microcopy Resolution Test Charts No. 1010a. It provides the photographer with two sets of charts by which the resolving power of a photographic lens may be numerically measured with respect to a definite scale of values. A detailed description is given of the procedure and technique to be followed in order that comparable values may be obtained by different observers. The test provides an objective method of testing a photographic lens. The six charts of one set are printed in black on a white background to form a high-contrast chart. The six charts of the other set are printed with gray ink on a gray background to form a low-contrast chart. Additional uses of these charts are also described. These uses include the testing of goggle lenses for definition and prismatic power and the testing of telescopes and binoculars for definition. Supersedes NBS Circular 533, issued May 1953.

SP375. **An index of State specifications and standards, covering those standards and specifications issued by State Purchasing Offices of the United States,** L. L. Grossnickle, Editor, Nat. Bur. Stand. (U.S.), Spec. Publ. 375, 394 pages (Sept. 1973) $3.70, SD Catalog No. C13.10:375.

Key words: Index of State specifications and standards; Key-Word-In-Context index of State specifications and standards; purchase specifications and standards, State; specifications, State; standards, State; State specifications and standards.

This computer-produced Index contains the permuted titles of more than 6,000 State purchasing specifications and standards issued by 37 State Purchasing Offices thru 1971. The title of each specification and standard can be found under all the significant key words which it contains. These key words are arranged alphabetically down the center of each page together with their surrounding context. The date of publication or latest revision, the specification or standard number, and an abbreviation for each State appear as part of each entry. A list of these abbreviations and the names and addresses of the State Purchasing Officials are found at the beginning of the Index.

SP377. **Index to the reports of the National Conference on Weights and Measures. From the First to the Fifty-sixth 1905 to 1971,** F. C. Bell, Nat. Bur. Stand. (U.S.), Spec. Publ. 377, 46 pages (Feb. 1973) 75 cents, SD Catalog No. C13.10:377.

Key words: Index; measures; National Conference; reports; weights.

This publication comprises a subject index and a speaker index for the Reports of the National Conference on Weights and Measures from the First (1905) through the Fifty-Sixth (1971). Supersedes Miscellaneous Publication 243.

SP383. **The creative partnership: Government and the professional services,** Proceedings of the Fourth Users-Producers Conference Sponsored by the Technical Analysis Division, Institute for Applied Technology, National Bureau of Standards, in Cooperation with the Center for the Study of Private Enterprise, The American University, held at the National Bureau of Standards, Gaithersburg, Md., January 23, 1973, J. D. Johnson, Ed., Nat. Bur. Stand. (U.S.), Spec. Publ. 383, 142 pages (Aug. 1973) $2.10, SD Catalog No. C13.10:383.

Key words: Creative-partnership; management; operating; procurement; services; Users-Producers.

These proceedings are written for the 4th Users-Producers Conference held at the National Bureau of Standards on January 23, 1973. The Conference was designed to highlight the problems and advantages in our present procurement system when Government utilizes the services of professional and Professions Service firms.

The speakers addressed themselves to the many facets of the procurement process. They represent both the private and Government side and bring their views forward in a clear and concise manner. Speakers are grouped into three panels. The first panel describes the development of the problem, the second panel considers the procurement process, and the third panel discusses managing the project. At the end of each group of panel speeches, there is a general discussion with comments and questions by all attendees.

There is also a separate presentation given by the Honorable James C. Corman, United States Congressman (Calif.), Chairman, Sub-Committee on Government Procurement of Professional Services.
These proceedings include the following papers (indented):

Management information and computer systems, R. M. Davis.
Management consulting, W. P. Sommers.
Architecture and engineering, J. R. Dunn.
Operating level problems in procurement, W. E. Cushen.
Government procurement policy, P. Waterman.
The relationship of private enterprise to Government procurement, R. W. Kreuger.
Legal aspects of Government procurement, G. P. Bond.
A proposed Government system for professional services, J. E. Moriarty.
Government project management, T. F. Noble.
Managing the private contractor, R. A. Walbrecker.
Managing the university research team, R. P. Boynton.

SP384. **Annotated bibliography of the literature on resource sharing computer networks,** R. P. Blanc, I. W. Cotton, T. N. Pyke, Jr., and S. W. Watkins, Nat. Bur. Stand. (U.S.), Spec. Publ. 384, 95 pages (Sept. 1973) $1.25, SD Catalog No. C13.10:384.

Key words: Bibliography; computer network; data communications; resource sharing.

This bibliography consists of references with critical annotations to the literature on computer networks. A classification scheme has been developed to place each annotation in a category reflective of its content. Five indexes to the bibliography are included: author index, corporate author index, network index, key word out of context index, and report number index.

NSRDS-NBS46. **Reactivity of the hydroxyl radical in aqueous solutions,** L. M. Dorfman, G. E. Adams, Nat. Stand. Ref. Data Ser., Nat. Bur. Stand. (U.S.), 46, 72 pages (June 1973) 90 cents, SD Catalog No. C13.48:46.

Key words: Abstraction reactions; addition reactions; aqueous solution; biological molecules; electron transfer reactions; hydroxyl radical; oxide radical ion; radical reactions; rate constants; reference data.

The reaction rate data of the hydroxyl radical in aqueous solution are compiled and evaluated in this critical review. The values are reported in a series of tables covering additon, hydrogen abstraction, inorganic electron transfer and radical reactions. Rate constants for the hydroxyl radical with biological molecules are included. In addition, the rate constant data for the oxide radical ion are given. Physical properties are listed and the experimental methods employed in OH radical chemistry are reviewed. An analysis involving rate constant data comparisons is made.

NSRDS-NBS 50. **Resonances in electron impact on atoms and diatomic molecules,** G. J. Schulz, Nat. Stand. Ref. Data Ser., Nat. Bur. Stand. (U.S.), 50, 118 pages (Oct. 1973) $1.35, SD Catalog No. C13.48:50.

Key words: Atoms; compound states; cross-sections; diatomic molecules; electron impact; energy levels; resonances; temporary negative ions.

Two reviews are presented on the energies, configuration and other properties of resonances in electron impact on atoms and diatomic molecules. Included are discussions of the experimental methods which are useful for studying resonances and of the results obtained by various investigations. Much of the information is presented in the form of tables and energy level diagrams.

BSS45. **Dynamic thermal performance of an experimental masonry building,** B. A. Peavy, F. J. Powell, and D. M. Burch, Nat. Bur. Stand. (U.S.), Bldg. Sci. Ser. 45, 103 pages (July 1973) $1.25, SD Catalog No. C13.29/2:45.

Key words: Building heat transfer; computer programs; dynamic thermal performance; heat flow analysis; heating and cooling loads; temperature predictions; thermal analysis; thermal behavior; transient heat flows.

Measurements of the dynamic heat transfer in an experimental masonry building were made in a large environmental chamber to explore the validity of a computer program developed at NBS, labeled NBSLD, for computing heating and cooling loads, and indoor air temperatures. This study was jointly supported by the National Bureau of Standards and the Department of Housing and Urban Development, and is a part of a broader research program being supported by both agencies to improve performance test procedures and criteria for housing.

The experimental structure was a one-room house 20 ft long 20 ft wide, and 10 ft high with walls of solid concrete blocks and a flat roof made of reinforced precast concrete slabs. During the tests changes were made in fenestration, the amount and location of insulation, and the indoor mass; and the building was exposed to a diurnal temperature cycle.

It was found that the combination of mass in the masonry walls and roof, and insulation placed on the outside of the masonry was very effective in reducing and controlling the variation of indoor air temperature. The NBSLD computer program realistically predicted the heat storage effects, and maximum heating loads during these tests. For five heating tests, the greatest difference between computed maximum heating load and measured values was 8 percent and the average difference was 4.3 percent. It was shown that steady-state methods of heating load calculation could result in oversizing heating equipment by 30 percent or more for this particular building and imposed exterior conditions if the lowest outdoor temperature was selected as the design temperature.

BSS46. **Building practices for disaster mitigation.** Proceedings of a workshop sponsored by The National Science Foundation, Research Applied to National Needs Program, and The National Bureau of Standards, held at the National Bureau of Standards, Boulder, Colo., Aug. 28-Sept. 1, 1972, R. Wright, S. Kramer, and C. Culver, Editors, Nat. Bur. Stand. (U.S.), Bldg. Sci. Ser. 46, 483 pages (Feb. 1973) $5.30, SD Catalog No. C13.29/2:46.

Key words: Building; earthquakes; hazards; land use; structural engineering; wind effects.

The national workshop on building practices for disaster mitigation was concerned with earthquakes, extreme winds, and similar dynamic hazards. These proceedings present recommendations derived at the workshop and addressed to policy makers in government and industry, as well as practitioners in engineering, architecture, land use

planning, and the earth and meteorological sciences. The recommendations evaluate current building practices, define opportunities for improving current practice from documented research findings, and recommend research to fill gaps in knowledge. Recommendations are made for implementation of improved practices at professional and policy levels. The objectives include avoidance of human suffering, reduction of property loss, and maintenance of vital function in buildings under conditions threatening disaster. Fifteen review articles were prepared by experts in the professions and research disciplines to define the state-of-the-art in disaster mitigation and to guide discussions at the workshop. These articles are included in the proceedings as follows:

Workshop Recommendations.
Values and costs, H. Kunreuther.
Approaches to implementation, P. E. Baseler.
Earthquake hazards for buildings, N. C. Donovan.
The problem of seismic zoning, S. T. Algermissen.
Wind hazards for buildings, J. W. Vellozzi and J. J. Healey.
Land use planning and natural disaster mitigation, W. J. Petak, M. McCoy, W. J. Monasch, J. E. Slosson, D. F. Moran, J. H. Wiggins, Jr.
Architectural approaches to hazard mitigation, E. C. Hillman Jr., A. E. Mann.
Procedures and criteria for earthquake resistant design, C. W. Pinkham.
Procedures and criteria for earthquake resistant design, N. M. Newmark and W. J. Hall.
Procedures and criteria for wind resistant design, J. W. Vellozzi and J. J. Healey.
Criteria for building services and furnishings, J. M. Ayres and T.-Y. Sun.
Behavior of structural elements. A review, B. Bresler.
Behavior of structural systems under dynamic loads, R. L. Sharpe, G. Kost, and J. Lord.
Survey and evaluation of existing buildings, F. E. McClure.
Abnormal loading on buildings and progressive collapse, N. F. Somes.

BSS47. **Structural deflections. A literature and state-of-the-art survey,** T. V. Galambos, P. L. Gould, M. K. Ravindra, H. Suryoutomo, and R. A. Crist, Nat. Bur. Stand. (U.S.), Bldg. Sci. Ser. 47, 104 pages (Oct. 1973) $1.25, SD Catalog No. C13.29/2:47.

Key words: Analysis; deflection; design; dynamic; experimental; human sensitivity; loading functions; specifications; static; structural engineering; subsystems; vibration.

A literature survey and state-of-the-art study was compiled using 233 primary source documents, research papers, and texts. Over 800 documents were scanned to arrive at the primary source documents. The problem of structural deflections is discussed and reviewed in its component areas of static and dynamic deflections as related to forcing functions and structural characteristics. Also the interactions of major structural deflections with building structures subsystems and human occupants is reviewed. Emphasis is placed on serviceability limit states of deflections. Detailed comparisons of human response to structural vibrations are also made. This report is broad in scope and covers the areas of analysis, design and experimentation.

FIPS PUB 6-2. **Counties and county equivalents of the states of the United States,** H. E. McEwen, Standards Coordinator, Nat. Bur. Stand. (U.S.), Fed. Info. Process. Stand. Publ. (FIPS Pub) 6-2, 35 pages (1973) 65 cents, SD Catalog No. C13.52:6-2.

Key words: ADP standards; computers; data elements and codes; data processing; Federal Information Processing Standards; geography; information processing standards; information systems; national government; representations and codes; standards; statistical data.

This publication provides names and codes for representing the Counties of the 50 States or county equivalents thereof for use in the interchange of formatted machine sensible data. Also included in the set of codes are the independent cities of Maryland, Missouri, Nevada, and Virginia and the Census Divisions and boroughs of Alaska. Supersedes NBS FIPS Pub 6-1.

FIPS PUB 8-3. **Standard metropolitan statistical areas,** H. E. McEwen, Standards Coordinator, Nat. Bur. Stand. (U.S.), Fed. Info. Process. Stand. Publ. (FIPS PUB) 8-3, 20 pages (1973) 55 cents, SD Catalog No. C13.52:8-3.

Key words: Computers; data processing; Federal Information Processing Standards Publication; representations and codes; Standard Metropolitan Statistical Areas.

This publication provides standard identifications and codes for representing Standard Metropolitan Statistical Areas for the interchange of machine sensible data among agencies. It supersedes FIPS PUB 8-2, Standard Metropolitan Statistical Areas, dated 1972 November 1. The general concept of a Standard Metropolitan Statistical Area, commonly referred to as "SMSA" is one of an integrated economic and social unit with a recognized large population nucleus. The codes are available on Hollerith punched cards. The following data elements are provided: SMSA Title (Name) and SMSA Code. Supersedes FIPS PUB 8-2.

FIPS PUB 23. **Objectives and requirements of the Federal Information Processing Standards Program,** H. S. White, Jr., Nat. Bur. Stand. (U.S.), Fed. Info. Process. Stand. Publ. (FIPS Pub.) 23, 8 pages (1972) 35 cents, SD Catalog No. C13.52:23.

Key words: Computers; data processing; Federal Information Processing Standards; management; standards; U.S. Government.

Public Law 89-306 (the Brooks legislation) was enacted to provide for the economic and efficient purchase, lease, maintenance, operation and utilization of automatic data processing equipment by Federal departments and agencies. Among the other provisions of PL89-306, the Secretary of Commerce is authorized to make appropriate recommendations to the President relating to the establishment of uniform Federal automatic data processing standards. The Federal Information Processing Standards Program was established in response to this part of the legislation. The purpose of this document is to outline the objectives of the Federal Information Processing Standards Program and to identify requirements for specific standards necessary to accomplish these objectives.

FIPS PUB 26. **One-inch perforated paper tape for information interchange,** P. S. Johnson, Standards Coordinator, Nat. Bur. Stand. (U.S.), Fed. Info. Process. Stand. Publ. (FIPS PUB) 26, 4 pages (1973) 20 cents, SD Catalog No. C13.52:26.

Key words: Data processing; Federal Information Processing Standard; information interchange; information processing; paper tape; paper perforator tape.

This standard specifies the physical dimensions and tolerances of one-inch wide paper tape, including the size and location of the perforations used for recording information.

PS54-72. **Body measurements for the sizing of girls' apparel,** C. W. Devereux, II, Technical Standards Coordinator, Nat. Bur. Stand. (U.S.), Prod. Stand. 54-72, 19 pages (July 1973) 30 cents, SD Catalog No. C13.20/54-72.

Key words: Apparel, girls'; body measurements, girls'; classifications, girls' size; grading charts, girls' size; size designations, girls'; span charts, girls' sizing.

This Voluntary Product Standard establishes a nationally recognized sizing system for girls, based on body measurements. The stan-

dard covers three classifications: slims, regulars, and chubbies. In each classification, sizes 7, 8, 10, 12, 14, and 16 are defined by 33 body measurements.

TN627. **Computation of spectral data for a Josephson junction circuit,** E. G. Johnson, Jr. and D. G. McDonald, Nat. Bur. Stand. (U.S.), Tech. Note 627, 63 pages (Nov. 1972) 60 cents, SD Catalog No. C13.46:627.

Key words: Differential equation; fast Fourier transform; Josephson junction; nonlinear integral-differential equation; spline theory.

A computer program has been developed to study power flow between different frequency channels in a Josephson junction circuit. This paper discusses the mathematical assumptions used to get such results. They are the trapezoidal approximation from spline theory and the use of a finite range of frequencies to characterize the frequency spectrum. This paper describes the program and provides the FORTRAN listing, flow charts, and discusses how to use the program. A discussion of possible sources of errors is also included.

TN629. **Superconducting quantum interference devices: An operational guide for rf-biased systems,** D. B. Sullivan, Nat. Bur. Stand. (U.S.), Tech. Note 629, 47 pages (Nov. 1972) 50 cents, SD Catalog No. C13.46:629.

Key words: Electrical measurements; quantum interference devices; superconductivity.

The report discusses a number of practical considerations concerning the operation and application of rf-biased Superconducting QUantum Interference Devices (SQUID's). In the course of routine operation of these devices one amasses a set of operational rules, many of which never reach the open literature. This report is aimed at filling that void. Topics of discussion include: the readout circuitry, operational limits of the SQUID, rf-coupling to the SQUID, flux transformers, and shielding.

TN630. **Developments in cryoelectronics,** R. A. Kamper and D. B. Sullivan, Nat. Bur. Stand. (U.S.), Tech. Note 630, 73 pages (Nov. 1972) 70 cents, SD Catalog No. C13.46:630.

Key words: Electronics; Josephson effect; precise measurements; superconductivity.

This is a survey of progress to date in the development of new electronic instruments taking advantage of the unique properties of superconductors.

TN633. **Critical two-phase flow for cryogenic fluids,** R. V. Smith, K. R. Randall, and R. Epp, Nat. Bur. Stand. (U.S.), Tech. Note 633, 80 pages (Jan. 1973) 70 cents, SD Catalog No. C13.46:633.

Key words: Analyses; analytical models; choking flow; critical flow; cryogenic fluids; helium; hydrogen; oxygen; reviews; two-phase flow.

This work presents a state-of-the-art survey intended to be useful to a designer of equipment involving two-phase flow of cryogenic fluids. It is desirable to assess the probability of critical, or choking, flow in such a system and, if possible, estimate the critical flow rate. The literature is surveyed, primarily since Smith (1963), and the predictive results for several analytical models are evaluated and compared with experimental data. These results are discussed; however, no firm conclusions are reached because, often, the spread of experimental data is equivalent to the predictive results from the models. Finally, computer evaluations are presented for oxygen, hydrogen and helium along with some design recommendations.

TN638. **A synchronous satellite time delay computer,** W. F. Hamilton and D. W. Hanson, Nat. Bur. Stand. (U.S.), Tech. Note 638, 39 pages (July 1973) 45 cents, SD Catalog No. C13.46:638.

Key words: Satellite timing; slant range; synchronous satellites; time delay.

A special purpose slide rule designed to compute the free space propagation delay between a synchronous satellite and points on the earth's surface is discussed. The slide rule was developed to provide users of time information relayed by geostationary satellites a means of computing the propagation delays without dealing directly with the satellite's orbital elements. The delays computed with the slide rule are compared with the values obtained from orbital elements using a high precision digitial computer. The limitations and accuracy of the slide rule are discussed. A sample slide rule which may be cut out and used is included in the report.

TN639. **Publications and services of the National Bureau of Standards, Cryogenics Division, Institute for Basic Standards, Boulder, Colo. 80302, 1953-1972,** J. R. Mendenhall, V. J. Johnson, and N. A. Olien, Nat. Bur. Stand. (U.S.), Tech. Note 639, 82 pages (Aug. 1973) 75 cents, SD Catalog No. C13.46:639.

Key words: Author indexes; bibliography; cryogenics; liquefaction; metrology; properties of fluids; properties of solids; subject indexes; superconductivity; transport processes.

This NBS Technical Note catalogs the publications of the Cryogenics Division, along with author and subject indexes, for the period 1953 through 1972. It also contains a listing of available thermodynamic properties charts, bibliographies, and miscellaneaous reports of cryogenic interest.

A resumé of the activities of and services provided by the Cryogenics Division is also included.

TN640. **Considerations for the precise measurement of amplifier noise,** D. F. Wait, Nat. Bur. Stand. (U.S.), Tech. Note 640, 129 pages (Aug. 1973) $1.25, SD Catalog No. C13.10.46:640.

Key words: Amplifier noise; effective input noise temperature; mismatch error; mismatch uncertainty; noise figure.

For the best accuracy in measuring noise figure, attention needs to be given to the choice of the hot and the cold noise standards and to mismatch problems. Tables and graphs are presented to aid in choosing the proper measurement conditions, and an example is given to demonstrate their use. This paper essentially supplements a previous paper (included in an appendix), treating in more detail topics that become important when state-of-the-art measurements are required.

TN643. **Measurement of rf power and attenuation using superconducting quantum interference devices,** R. A. Kamper, M. B. Simmonds, C. A. Hoer, and R. T. Adair, Nat. Bur. Stand. (U.S.), Tech. Note 643, 93 pages (Aug. 1973) $1.00, SD Catalog No. C13.46:643.

Key words: Josephson effect; quantum interference; rf attenuation; rf measurement; rf power; superconductivity.

This report is the product of the first two years' work on a project to exploit an entirely new principle for the measurement of rf power and attenuation, namely the Superconducting QUantum Interference Device (SQUID). This is a simple circuit of superconducting metal, operating at a very low temperature in a bath of liquid helium. It functions as a sensor of magnetic flux with an almost perfectly periodic response over a wide dynamic range. It may therefore be used to measure dc or rf electrical quantitites such as current, power, attenuation, etc., in circuits inductively coupled to it. Measurements of these quantities can be made by counting off periods in the response of the SQUID (flux quanta) in the same way that we measure length with a laser by counting off wavelengths of light.

This work is partly funded by the CCG under project number 72-72. It has reached the stage of a demonstration that the new principle can indeed be used for precise measurement. We have developed

525-013 O - 74 - 5

and tested prototype systems for measuring power and attenuation as accurately as we can test by the conventional means available to us. A single calibration with dc is required to measure absolute rf power in the range of frequency from 0 to 1 GHz at levels from 10^{-8}W to 10^{-3}W with an uncertainty of ± 0.1 dB at the port of the SQUID. Transferring this measurement to calibrate a source of power would require a proper evaluation of the intervening network over the full range of frequency. We have demonstrated the feasibility of extending our measurements of power to much lower levels. No external calibration is required to measure rf attenuation directly over a dynamic range of 45 dB with an rms deviation of ± 0.002 dB from calibrations performed by the NBS Calibration Service.

After an elementary exposition of the basic principles of our technique, we describe: the SQUIDs themselves; the prototype systems we have developed to measure rf power and attenuation; systematic errors and fundamental limitations of the measurements that can be performed with them; and the obvious and immediate improvements that can be applied to them. We reserve an appendix for detailed drawings and instructions for the fabrication of components.

In order to make this report self-contained, we have included the material from previous reports that has successfully withstood the test of time.

TN748. **An adjoint gamma-ray moments computer code, ADJ-MOM-I,** G. L. Simmons, Nat. Bur. Stand. (U.S.), Tech. Note 748, 23 pages (Feb. 1973) 30 cents, SD Catalog No. C13.46:748.

Key words: Adjoint; buildup factor; dosimetry; gamma-ray transport; moment methods; shielding.

In this paper we discuss a computer code for generating spatial-angular moments of the adjoint gamma-ray flux in an infinite medium. The equation for the flux moments is given and techniques used for the solution are described. Details of the input data and a sample problem are also supplied.

TN751. **Studies of calibration standards used in the Department of Defense Equipment Oil Analysis Program,** D. W. Golightly and J. L. Weber, Nat. Bur. Stand. (U.S.), Tech. Note 751, 48 pages (Jan. 1973) 75 cents, SD Catalog No. C13.46:751.

Key words: Calibration standards; concentration validity; flash point; lubricating oil; pour point; spectrometric analysis; stability; trace elements; viscosity.

At the request of the Naval Systems Air Command, Department of the Navy, studies have been conducted on organo-metallic calibration standards and diluent oil used in the Department of Defense Equipment Oil Analysis Program. Consultation on standards has been provided, and measurements of physical properties of base oil, concentrations of major elements in standards, concentrations of trace contaminants, and stability of solutions have been performed. Results of studies accomplished in fiscal year 1972 are detailed in this report.

TN752. **Directory of law enforcement and criminal justice associations and research centers,** B. J. Latka, Nat. Bur. Stand. (U.S.), Tech. Note 752, 49 pages (June 1973) 80 cents, SD Catalog No. C13.46:752.

Key words: Associations; criminal justice; directory, law enforcement; research centers.

This directory lists national, non-profit professional and volunteer social action associations and research centers which are active in the fields of law enforcement and criminal justice. The International and foreign organizations which are listed either have a large number of American members, have a United States chapter, or are doing work which is applicable to the United States. The local organizations which are listed either cover several states or are of national interest. The organizations are listed alphabetically with a subject index included. The format of an entry is: title of organization; mailing address; officer; telephone number; year when founded; number of members, number of staff; description of purpose and activities; affiliations; publications, meetings.

TN753. **NBS Special Foreign Currency Program in Yugoslavia 1971-72,** H. S. Peiser, S. E. Chappell, E. Horowitz, H. Yakowitz, and D. Bluebond, Nat. Bur. Stand. (U.S.), Tech. Note 753, 72 pages (Jan. 1973) 90 cents, SD Catalog No. C13.46:753.

Key words: Binational research cooperation; international scientific cooperation; physical science research administration; research planning; scientific research abstracts; Special Foreign Currency Program; Yugoslavia science and technology.

An overview is given of grants awarded by the National Bureau of Standards under the Special Foreign Currency Program (SFCP) in Yugoslavia, authorized by Public Law 480 and other legislation. Each grant is identified by title, principal investigator, institution in Yugoslavia, NBS monitor, and the monitor's organizational unit within NBS. The work is then described briefly under the three headings "Summary Description of Project Goals," "Results and Implications to Date" and "List of Publications that Resulted from the Project." To demonstrate the relevance of such grants to the programs of NBS, the grant descriptions are ordered by the elements of that Program Structure. The significance and purpose of the NBS/SFCP grant program are discussed in the Foreword, the Introduction and an Appendix. The NBS monitors and the program manager judge this grant program to have had a high benefit to cost ratio from the viewpoint of NBS.

TN754. **Methods of measurement for semiconductor materials, process control, and devices. Quarterly report July 1 to September 30, 1972,** W. M. Bullis, Editor, Nat. Bur. Stand. (U.S.), Tech. Note 754, 55 pages (Mar. 1973) 80 cents, SD Catalog No. C13.46:754.

Key words: Aluminum wire; base transit time; carrier lifetime; die attachment; electrical properties; epitaxial silicon; gamma-ray detectors; generation centers; germanium; gold-doped silicon; infrared response; methods of measurement; microelectronics; microwave diodes; nuclear radiation detectors; probe techniques (a-c); recombination centers; resistivity; ribbon wire bonding; semiconductor devices; semiconductor materials; semiconductor process control; silicon; thermal resistance; trapping centers; ultrasonic bonding; wire bonds.

This quarterly progress report, seventeenth of a series, describes NBS activities directed toward the development of methods of measurement for semiconductor materials, process control, and devices. Significant accomplishments during this reporting period include design of a plan to provide standard silicon wafers for four-probe resistivity measurements for the industry, publication of a summary report on the photoconductive decay method for measuring carrier lifetime, publication of a comprehensive review of the field of wire bond fabrication and testing, and successful completion of organizational activity leading to the establishment of a new group on quality and hardness assurance in ASTM Committee F-1 on Electronics. Work is continuing on measurement of resistivity of semiconductor crystals; characterization of generation-recombination-trapping centers in silicon; study of gold-doped silicon; development of the infrared response technique; evaluation of wire bonds and die attachment; and measurement of thermal properties of semiconductor devices, delay time and related carrier transport properties in junction devices, and noise properties of microwave diodes. New efforts were initiated in both the die attachment and wire bond evaluation tasks. Supplementary data concerning staff, standards committee activities, technical services, and publications are included as appendixes. A description of breakdown tracks, a primary failure mode of monolithic integrated circuits stressed with voltage pulses, is given in a separate appendix.

TN755. **Some aspects of the setting and hardening of gypsum plaster,** J. R. Clifton, Nat. Bur. Stand. (U.S.), Tech. Note 755, 33 pages (Jan. 1973) 55 cents, SD Catalog No. C13.46:755.

Key words: Colloidal theory; crystallization theory; gypsum; hydration; induction period; plaster of paris; setting mechanisms.

The mechanisms by which gypsum plaster sets and hardens have been investigated and the results generally are consistent with the crystallization theory. No evidence for the presence of colloidal intermediates has been found. The crystallization theory is modified to include, as an intermediate species, solvated calcium sulfate hemihydrate molecules. Evidence is presented that supports the belief that more than one reaction is responsible for the setting and hardening of gypsum plaster.

The roles of accelerators and retarders have been studied by calorimetric, differential thermal analysis, and scanning electron microscopic techniques. The cation is more effective than the anion in accelerating the setting and hardening of gypsum plasters; the catalytic order follows the sequence M^{+} M^{2+} M^{3+}. Small amounts of retarders can severely retard the setting and hardening processes.

Influences of temperature, impurities, and production conditions on the setting rates of gypsum plasters are discussed.

TN757. **The smoke density chamber method for evaluating the potential smoke generation of building materials,** T. G. Lee, Nat. Bur. Stand. (U.S.), Tech. Note 757, 20 pages (Jan. 1973) 45 cents, SD Catalog No. C13.46:757.

Key words: Building materials; fire; fire services; smoke; smoke density chamber; smoke potential; test method; visibility.

The paper reviews the Smoke Density Chamber Test Method and illustrates its use and application to assess smoke generation of building materials in fire situations. It shows how test results may aid the Fire Services and code authorities in evaluating and reducing the potential light-obscuration hazard of smoke in buildings. An example is given for calculating visibility in a simplified fire situation involving material of known smoke generation. The smoke generation of some common interior finish and construction materials is given.

TN759. **The NBS lead paint poisoning project: Housing and other aspects,** H. W. Berger, Nat. Bur. Stand. (U.S.), Tech. Note 759, 25 pages (Feb. 1973) 30 cents, SD Catalog No. C13.46:759.

Key words: Hazard elimination; lead analysis; lead paint; lead poisoning.

The National Bureau of Standards is providing technical support required by the Department of Housing and Urban Development to carry out its research responsibilities under PL 91-695, The Lead Based Paint Poisoning Prevention Act. The program at NBS has involved three major areas of research: (1) an estimation of the numbers of children at risk and with excessive body burdens of lead and the geographical distribution of those children; (2) the capabilities and characteristics of analytical methods for the detection of lead in paint and other building materials; and (3) the identification and evaluation of materials, techniques and systems for removing or eliminating the lead paint hazard from housing. This paper is a brief presentation of the activities and conclusions of NBS in the areas listed above.

TN767. **Microelectronic interconnection bonding with ribbon wire,** H. K. Kessler and A. H. Sher, Nat. Bur. Stand. (U.S.), Tech. Note 767, 31 pages (Apr. 1973) 50 cents, SD Catalog No. C13.46:767.

Key words: Aluminum wire; bonding; fabrication (wire bonds); microelectronics; ribbon wire; round wire; testing (wire bond); ultrasonic bonding; wire bond.

The feasibility of using aluminum ribbon wire for ultrasonic bonding of semiconductor microelectronic interconnections was studied, and several advantages over the use of round wire of equivalent cross-sectional area were found. Ribbon wire bonds exhibited little deformation or heel damage, and a greater percentage of bonds of a certain quality (as judged by pull strength and appearance) could be made over much greater ranges of the bonding machine parameters, time and tool tip displacement, using ribbon wire than was possible with round wire. The ease of positioning ribbon wire was indicated by making multiple ribbon wire bonds side-by-side on a 5-mil square pad, or by stacking up to four bonds one on top of another. However, bonding with harder than normal wire, previously thought to offer certain advantages with respect to higher bond tensile strength, yielded inconsistent results.

TN769. **A rigorous correction procedure for quantitative electron probe microanalysis (COR 2),** J. Hénoc, K. F. J. Heinrich, and R. L. Myklebust, Nat. Bur. Stand. (U.S.), Tech. Note 769, 132 pages (Aug. 1973) $2.10, SD Catalog No. C13.46:769.

Key words: Continuum fluorescence; data reduction; electron probe microanalysis; fluorescence correction; quantitative analysis.

This publication describes a rigorous data reduction procedure for quantitative electron probe microanalysis, which avoids simplifications present in conventional schemes. In addition, the program contains a correction for fluorescence due to the continuum, and separate computation of the fluorescent effects of each exciting primary x-ray line. Constants characteristic of elements are stored in a permanent data file, and the constants and parameters needed for the calculation of mass absorption coefficients are contained in a subprogram. These provisions and decision-making sections in the development of the fluorescence corrections reduce the required input considerably.

TN777. **Cost analysis of blood banking alternatives,** T. Miller, M. King, J. Flannagan, E. Nilsson, and B. Lemieux, Nat. Bur. Stand. (U.S.), Tech. Note 777, 121 pages (Sept. 1973) $1.35, SD Catalog No. C.13.46:777.

Key words: Blood banks; blood utilization statistics; cost benefit analysis; donor profiles; peer review; regulatory activities; sensitivity analysis.

This report provides a description of the current blood banking system and of the collection and derivation of quantitative information concerning system operation and blood cost. A reasonably accurate but somewhat incomplete profile of practices, attitudes, and likely costs of present and alternative systems has been developed. Among the topics presented are: 1) a discussion of the blood collection process including statistics on present use and future needs; 2) information relating to donor motivation, attitudes and incentives; 3) a brief summary of demonstration programs in the U.S. and national blood programs in other countries which provides some insight concerning means for improving blood quality and availability; 4) a description of blood processing, storage and distribution procedures; 5) narrative and statistical information relating to blood utilization practices; 6) discussions of post transfusion reactions and frozen blood programs; 7) a discussion of current governmental and professional standards, regulations and controls which influence many, but not all, concerns involved in blood collection and processing.

This information serves as the basis for the selection of alternatives analyzed in a cost effectiveness analysis of eight apparently viable alternatives to the current system. Because of the possible variation which might be ascribed to many of the parameters used as a basis for costing alternatives, the sensitivity analysis is crucial in the comparison of alternatives.

TN779. **Data communications system throughput performance using high speed terminals on the dial telephone network,** D. S. Grubb, Nat. Bur. Stand. (U.S.), Tech. Note 779, 40 pages (May 1973) 65 cents, SD Catalog C13.46:779.

Key words: Data communications; modems; terminals; throughput; TRIB.

Throughput performance of high speed data terminals using the dial telephone network is calculated for signaling rate of 1200 to 4800 bits per second using the ANSI X3.28-1971 control procedures and measured in terms of the proposed ANSI strand TRIB described in X3S35/80. The performance calculations are shown graphically with TRIB as a function of block length, error rates of the telephone connection, signaling rate and telephone line delays. Error rates are based on a published survey involving several hundred telephone connections to geographically distributed parts of the United States.

TN783. **Durability and maintenance as related to the selection of flooring,** W. C. Wolfe, R. F. Roberts, and M. Russell, Nat. Bur. Stand. (U.S.), Tech. Note 783, 68 pages (Aug. 1973) 90 cents, SD Catalog No. C13.46:783.

Key words: Carpets; durability; economics; field studies; flooring; floor coverings; life-cost; maintenance; user needs.

This report is addressed to the problem of selection and maintenance of flooring to the best advantage in terms of durability, type and severity of service, appearance, comfort, and safety. The selection of flooring is discussed with respect to service life, maintenance, obsolescence, and trade-off advantages. Two articles by maintenance administrators include information and discussion helpful in determining maintenance cost, trade-offs, and selection of flooring for different types of service. Field observations and preliminary field tests by the National Bureau of Standards indicate areas in which research is needed, as in laboratory tests for wear and slip resistance. Observations and field tests are impracticable to use for procurement.

This report is helpful in the selection and maintenance of flooring and floor finishes. More important, it points up areas in which research is needed to develop information for this purpose.

TN785. **Scanning electron microscope examination of wire bonds from high-reliability devices,** K. O. Leedy, Nat. Bur. Stand. (U.S.), Tech. Note 785, 35 pages (Aug. 1973) 55 cents, SD Catalog No. C13.46:785.

Key words: Aluminum wire; high reliability; integrated circuit; metallization; scanning electron microscope; transistor; ultrasonic bonding; wire bonding.

An examination with a scanning electron microscope was made of the wire bonds of over 75 high-reliability microelectronic devices. The device interconnects were ultrasonically bonded aluminum wires. Of primary interest were the bonds themselves; their appearance and its significance are described. Also described is the appearance of the metallization and the wire. Comments and explanations are given where the phenomena are understood. Although the devices studied had passed preliminary electrical tests and pre-encapsulation visual examinations, many potential reliability problems were identified such as weak bonds, electrical shorts and contamination.

TN786. **Methods for testing wire-bond electrical connections,** H. A. Schafft, Nat. Bur. Stand. (U.S.), Tech. Note 786, 23 pages (Nov. 1973) 50 cents, SD Catalog No. C13.46:786.

Key words: Bonding; electrical connection; failure (wire bond); integrated circuits; microelectronics; reliability; semiconductor devices; testing (wire bond); wire bond.

A significant fraction of the failures that occur in integrated circuits are due to failures of the wire-bond electrical connections that are used. Therefore, a critical area for reliability improvement is in the methods for testing and evaluating wire bonds. Several of these methods are surveyed. In particular, analyses with regard to the stress that the test imposes on the wire bond in the pull, centrifuge, mechanical shock, vibration, and temperature cycling tests are presented and used in discussing the capabilities and limitations of these methods.

TN788. **Methods of measurement for semiconductor materials, process control, and devices, quarterly report January 1 to March 31, 1973,** W. M. Bullis, Editor, Nat. Bur. Stand. (U.S.), Tech. Note 788, 79 pages (Aug. 1973) 95 cents, SD Catalog No. C13.46.788.

Key words: Base transit time; carrier lifetime; delay time; die attachment; electrical properties; electronics; epitaxial silicon; four-probe method; generation centers; germanium; gold-doped silicon; infrared response; methods of measurement; microelectronics; microwave diodes; probing techniques (a-c); pull test; recombination centers; resistivity; resistivity standards; semiconductor devices; semiconductor materials; semiconductor process control; silicon; S-parameters; switching transients; thermal resistance; thermally stimulated properties; trapping centers; wire bonds.

This quarterly progress report, nineteenth of a series, describes NBS activities directed toward the development of methods of measurement for semiconductor materials, process control, and devices. Significant accomplishments during this reporting period include (1) development of a comprehensive, large-area test pattern for evaluating planar junction structures, (2) completion of experimental work on the evaluation of the destructive, double-bond pull test for wire bonds, (3) initiation of a scanning electron microscope facility, and (4) completion of the investigation of the mechanism of emitter-base junction reverse breakdown during rapid switching of transistors. Because of the general applicability of the last of these, details are presented in a separate appendix. Work is continuing on measurement of resistivity of semiconductor crystals; characterization of generation-recombination-trapping centers in silicon; study of gold-doped silicon; development of the infrared response technique; evaluation of wire bonds and die attachment; measurement of thermal properties of semiconductor devices; determination of S-parameters, delay time, and related carrier transport properties in junction devices; development of a-c probing techniques; and characterization of noise and conversion loss of microwave detector diodes. Supplementary data concerning staff, standards committee activities, technical services, and publications are included as appendices.

TN789. **Technical options for energy conservation in buildings,** National Conference of States on Building Codes and Standards and National Bureau of Standards Joint Emergency Workshop on Energy Conservation in Buildings held at the U.S. Department of Commerce Washington, D.C., June 19, 1973, Nat. Bur. Stand. (U.S.), Tech. Note 789, 184 pages (July 1973) $2.35, SD Catalog No. C13.46:789.

Key words: Building design; energy conservation; mechanical systems.

The purpose of this report is to provide reference material on the technical options for energy conservation in buildings. It was prepared for the National Conference of States for Building Codes and Standards-National Bureau of Standards Joint Emergency Workshop on Energy Conservation in Buildings held at the U.S. Department of Commerce in Washington, D.C. on June 19, 1973.

This report describes actions pertinent to existing buildings and new buildings. Regarding existing buildings, principal topics include summer cooling, winter heating, and other energy conserving features—i.e., insulation, fenestration, lighting, appliances, domestic

hot water, and human comfort. Suggested actions include those which can be accomplished voluntarily or without expense, and also actions which require some modest effort or expense on the part of the building owner or occupant.

Regarding new buildings, energy conservation actions are described that deal with building design and mechanical systems. The report concludes with a summary of mechanisms for implementation of such actions and criteria for use in evaluation of them.

TN790. **MIDAS modular interactive data acquisition system—description and specification,** C. H. Popenoe and M. S. Campbell, Nat. Bur. Stand. (U.S.), Tech. Note 790, 49 pages (Aug. 1973) 75 cents, SD Catalog No. C13.46:790.

Key words: Computer-controlled experiment; computer interfacing; data acquisition system; digital interface; instrumentation; laboratory automation; MIDAS; programmable controller.

The task of interfacing experiments to computers and data-logging systems should be made as painless as possible for the scientist. With this intent, MIDAS, a user-oriented, modular digital interface system based on CAMAC hardware and USASCII-bus data communication has been developed. MIDAS modules enable the experimenter to set up, program, modify and operate automated or computer-controlled experiments independently of the experts. Salient features of the concept are described and operating configurations discussed both with and without computer control. System interface requirements are specified in sufficient detail to enable one skilled in the art to design and construct modules operable within a MIDAS system.

TN791. **Dose calibrator pilot study,** S. B. Garfinkel and G. J. Hine, Nat. Bur. Stand. (U.S.), Tech. Note 791, 7 pages (Aug. 1973) 30 cents, SD Catalog No. C13.46:791.

Key words: Dose calibrators; indium-113m; molybdenum-99; nuclear medicine; radiopharmaceuticals; technetium-99m; tin-113.

Results of measurements of six sources in dose calibrators used in nuclear medicine facilities at eight hospitals in the Washington metropolitan area are given.

TN792. **Investigation of viscous flow in glass during phase separation,** J. H. Simmons, S. A. Mills, A. Napolitano, D. H. Blackburn, and W. K. Haller, Nat. Bur. Stand. (U.S.), Tech. Note 792, 43 pages (Sept. 1973), 65 cents, SD Catalog No. C13.46:792.

Key words: Glass; microstructure; phase separation; viscosity.

The isothermal viscosity of two borosilicate glasses, of which one is a commercial glass widely used for chemical glassware, shows a large increase (4 to 5 orders of magnitude) with heat-treatment time (ranging up to 100,000 min) near the annealing point. The two glasses have similar compositions, but differ greatly in their phase separation characteristics. Electron micrographs are used to analyze the development of microstructure during the suspected phase separation. In both glasses, it is found that the structure development is primarily responsible for the viscosity increase. An analysis of the data, and a theoretical interpretation of the effect are presented.

TN793. **Development of a procedure for measuring the noise of paper caps,** M. A. Cadoff, D. E. Mathews, and D. S. Blomquist, Nat. Bur. Stand. (U.S.), Tech. Note 793, 23 pages (Oct. 1973) 50 cents, SD Catalog No. C13.46:793.

Key words: Acoustics; cap guns; children; consumer safety; hearing damage; noise; paper caps; standard apparatus; toys.

In recent years, a great concern has been expressed for consumer protection and safety, especially for children. As an outgrowth of this concern, acoustical testing of potentially hazardous noise-producing toys has been carried out at the National Bureau of Standards for the Bureau of Product Safety (FDA) under the authority of the Toy Safety Act of 1969. This paper discusses in detail the testing work carried out on commercial cap guns and caps, which culminated in the development of a standard firing apparatus for testing paper caps. Engineering drawings of the standard apparatus are given as well as a recommended procedure for using this apparatus to test paper caps.

TN795. **Review of network management problems and issues,** A. J. Neumann, Nat. Bur. Stand. (U.S.), Tech. Note 795, 77 pages (Oct. 1973) $1.00, SD Catalog No. C13.46:795.

Key words: Academic computing; networks; network management; regional networks; research computing.

Computer networking is broadly considered including hardware, software, procedures and people. Networking encompasses many activities; such as, creation of network products, distribution processes, user activities, and supporting services like marketing, documentation, information services and maintenance. Network management covers both the establishment of networking operations and actual operation of the network facilities. It includes all management functions performed at such network nodes as computing centers, documentation facilities, and service distribution centers. In order to survey the problems facing development of network management, user requirements and system requirements are outlined in a qualitative manner. Examples of political, economic and legal constraints are summarized, such as the economic impact of extended networks on regional and local computing activities. Critical issues for networking management, and other areas of significant management concern are outlined. Organizational alternatives are conceived in terms of a four layer organization model. Conclusions deal with continuing problem areas, the need for a structural model for network management, critical experiments and tasks to be undertaken to further networking capabilities, and a suggestion to establish planning teams to initiate some of the initial steps required for further networking development.

TN796. **FRAME: An on-line correction procedure for quantitative electron probe microanalysis,** H. Yakowitz, R. L. Myklebust, and K. F. J. Heinrich, Nat. Bur. Stand. (U.S.), Tech. Note 796, 51 pages (Oct. 1973) 80 cents, SD Catalog No. C13.46:796.

Key words: Electron probe; mini-computer; on-line correction; quantitative microanalysis.

A procedure using a mini-computer for on-line correction of x-ray data from electron microprobe analysis has been developed. This program, called FRAME, allows mass fractions to be computed on-line by the ZAF approach. Besides x-ray intensities, the only input data required are the atomic numbers of the elements present, the analytical line being used, and the operating voltage. Other required parameters such as atomic weights and x-ray mass attenuation coefficients are stored or calculated by the program. FRAME is in FORTRAN IV, and requires about 4K of computer core. Results from FRAME are very close to those of COR2, which is considered to be the most accurate program available for quantitative electron probe microanalysis.

TN797. **Static language analysis,** G. Lyon, Nat. Bur. Stand. (U.S.), Tech. Note 797, 23 pages (Oct. 1973) 50 cents, SD Catalog No. C13.46:797.

Key words: Data archives; language use; programming aids; programming languages; source-statement analysis; syntax analysis.

Although many variants of programming languages exist, little information is available on how language features are actually used by programmers. Several data collection schemes are discussed here;

each would provide empirical data on language use. Some internal details are given for analyzers for FORTRAN and COBOL. In addition, a suggestion is made for a special systems option which would allow a compiler to continuously record source statement characteristics or programs given to it.

CIS7. **What About Metric?**, L. E. Barbrow, Nat. Bur. Stand. (U.S.), Consum. Inf. Ser. 7, 16 pages (Oct. 1973) 80 cents, SD Catalog No. C13.53:7.

Key words: Metric system; SI; weights and measures.

The metric system of measurement, how it compares with our customary system, and how it will affect everyday life are described in everyday terms. Examples of computations of the type frequently encountered by the average citizen are included to illustrate the relative simplicity of the metric system. Although extensive use of the metric system in the United States is envisioned to be several years in the future, the reasons for at least becoming acquainted with the system now are discussed. The necessary acquaintanceship for everyday life involves the learning of fewer than ten metric units of measurement.

The following Bibliography Series are available by purchase from the National Technical Information Service (NTIS), Springfield, Va. 22151.

COM-73-10281. **Index and cumulative list of papers on radiation chemistry,** Vol. V, Nos. 27-52, July through Dec. 1972, Radiation Chemistry Data Center, Radiation Laboratory, University of Notre Dame, Jan. 1973, $6.00.

Key words: Biological systems; ESR; hot atom chemistry; luminescence; photochemistry; polymers; radiation chemistry; radiation chemistry theory.

The Radiation Chemistry Data Center, as part of its operations, collects, keywords, and stores literature of fundamental radiation chemistry and several related fields. Since 1968, references to this literature have been stored in computer files. These files have been used for retrospective researches and for the Weekly List of Papers on Radiation Chemistry which has been used as a current-awareness aid by radiation chemists since 1968. This index to and cumulation of entries in the Weekly List of Papers on Radiation Chemistry for the period July through December 1972 is intended as a guide to the recent literature and as a searching tool for those who would find a printed index valuable.

This column lists all outside publications by the NBS staff, as soon after issuance as practical. For completeness, earlier references not previously reported may be included from time to time.

Achenbach, P. R., Phillips, C. W., **Performance characteristics of pressure-actuated water-regulating valves for refrigerant condensers,** (Proc. XII Int. Congress of Refrigeration, Madrid, Spain, 1967), Paper in *Progress in Refrigeration Science and Technology* **2,** 1107-1118 (Gráficas Reunidas, Madrid, Spain, 1969).

Key words: Performance characteristics; refrigeration accessories; valves; water-flow regulation.

Water-regulating valves are used on the condensers of water-cooled refrigerating units to maintain a satisfactory refrigerant condensing pressure and to conserve water. Both pressure-actuated and temperature-actuated valves are used for this purpose. A study was made of three sizes of pressure-actuated water-regulating valves from each of three sources to determine their range of condenser pressure control, the change in condensing pressure required to move the valves from fully-closed to fully-open position, the hysteresis in the control mechanism, and the water-flow characteristics near the fully-closed position. These and other performance characteristics related to water conservation and reliable operation of refrigerating units were investigated to provide guidance to the U.S. Army Natick Laboratories in writing performance specifications. The study revealed that the nominal pipe size of the valves was not a good indication of water-flow capacity, that the sensitivity of the various valves to change in condensing pressure differed widely, and that the difference between opening and closing pressure was in excess of 10 psi (0.7 kg/cm^2) in some valves. Moreover, the condensing pressure at 90 percent maximum water flow rate ranged from 118 to 172 psig (8.3 to 12.1 kg/cm^2) for the several valves when the opening pressure was set at 80 psig (5.6 kg/cm^2).

Acquisita, N., Abramowitz, S., **Vibrational spectrum of MoF_5,** *J. Chem. Phys.* **58,** No. 12, 5484-5488 (June 15, 1973).

Key words: Infrared; matrix isolation; MoF_5; Raman spectroscopy.

The infrared spectrum of matrix isolated MoF_5 as well as the Raman spectra of the liquid and polycrystalline species have been observed. The use of double boiler Knudsen cells has facilitated a vibrational assignment for monomeric MoF_5 based on a trigonal bipyramid (D_{3h}) structure.

Albers, J., Deutch, J. M., **On the rate equation description of spectral lines,** *Chem. Phys.* **1,** No. 2, 89-98 (Mar./Apr. 1973).

Key words: Correlation function; density expansion; kinetic equations; Langevin equation; rate equations; scattering theory.

We present a derivation of an exact, low-density equation of motion for the generating operator $G_{ij}(t) = \exp(iLt)|j\rangle\langle i|$. For the case of foreign gas pressure broadening, the equation for $G_{ij}(t)$ may be used to obtain an exact rate equation for the line amplitude operator. Under certain well-defined approximations, this rate equation reduces to the form of an equation proposed by Gordon. The origin of the linear density term is considered. We discuss the implications of the use of only completed collisions to describe the spectrum.

Anderson, R. L., **The high temperature stability of platinum resistance thermometers,** (Proc. 5th Symp. on Temperature, Its Measurement and Control in Science and Industry, Washington, D.C., June 21-24, 1971), Paper in *Temperature, Its Measurement and Control in Science and Industry,* H. H. Plumb, Editor-in-Chief, **4,** Part 2, 927-934 (Instrument Society of America, Pittsburgh, Pa., 1972).

Key words: Chemical changes in platinum resistance thermometers; high temperature platinum resistance thermometers; physical changes in platinum resistance thermometers; stability of platinum resistance thermometers.

Some of the chemical and physical parameters that affect the stability of platinum resistance thermometers have been studied, particularly at temperatures near the gold point (1064 °C). A simplified form of resistance thermometer sensor was designed to aid in these studies. The new design, designated as the "steeple," allowed the fabrication of some thermometers from single crystals. Measurements were made of the resistance at the triple point of water after the thermometers had been held above 1000 °C for extended periods. Further information on the aging of platinum wires at high temperatures was obtained with the scanning electron microscope. Some of the results are shown to be applicable to standard thermometers when used above 400 °C.

Aras, N. K., Zoller, W. H., Gordon, G. E., Lutz, G. J., **Instrumental photon activation analysis of atmospheric particulate material,** *Anal. Chem.* **45,** No. 8, 1481-1489 (July 1973).

Key words: Air pollution; atmospheric particulate material; electron linac; photon activation analysis.

Concentrations of fourteen elements in atmospheric particulate matter have been measured by irradiation of the samples with

bremsstrahlung from electrons of 35 MeV from the NBS electron linac and observation of γ rays from the reaction products with Ge(Li) detectors. The elements routinely observed by this nondestructive method are: Na, Cl, Ca, Ti, Cr, Ni, Zn, As, Br, Zr, Sb, I, Ce, and Pb. Several other elements such as Fe, Se, Rb, and Y are marginally observable. Although, in general, instrumental photon activation analysis (IPAA) is less sensitive than instrumental neutron activation analysis (INAA), with IPAA one can measure concentrations of several elements that are difficult or impossible to measure in urban particulates with INAA, especially Ti, Ni, As, I, and Pb. Measurements of Ni, As, and Pb are quite important because of their known toxicities.

Armstrong, G. T., **Calorimetric reference materials—status of the primary standard,** *Proc. 1st Int. Conf. on Calorimetry and Thermodynamics, Warsaw, Poland, Aug. 31-Sept. 4, 1969*, pp. 261-267 (Polish Scientific Publishers, Warsaw, Poland, 1971).

Key words: Benzoic acid; calorimetric reference materials.

Reference materials for reaction calorimetry are briefly reviewed. The value of 26434 Jg^{-1} for the energy of combustion of the primary standard, benzoic acid, has been confirmed by three recent careful determinations, and give this value a very sound basis. Any future investigations leading to a possible change in this value will require extremely careful documentation of precision and accuracy of measurement. Possible sources of systematic error are discussed.

Arvidson, J. M., Durcholz, R. L., Reed, R. P., **Compressive properties of polyurethane and polystyrene foams from 76 to 300 K,** (Proc. 1972 Cryogenic Engineering Conf., Boulder, Colo., Aug. 9-11, 1972), Paper E-4 in *Advances in Cryogenic Engineering* **18,** 194-201 (Plenum Press, New York, N.Y., 1973).

Key words: Compression; foams; temperature.

The compressive properties of 4 different polyurethane foams and 2 polystyrene foams have been measured at 300, 195 and 76 K. Similar to tensile properties, the Young's modulus, yield strength, and compressive strength increased with decreasing temperature, while the elongation to fracture decreased. An approximate linear dependence on density was found for Young's modulus in compression and the proportional limit. Longitudinal specimens were usually stronger than transverse specimens. Specimens pulled in tension were considerably stronger than specimens loaded under compression, but these differences diminished at lower temperatures.

Atkinson, G. H., Laufer, A. H., Kurylo, M. J., **Detection of free radicals by an intracavity dye laser technique,** *J. Chem. Phys.* **59,** No. 1, 350-354 (July 1, 1973).

Key words: Absorption; flash photolysis; free radicals; laser; spectra.

A new technique for the detection of free radicals inside the cavity of a dye laser is described. This intracavity absorption phenomenon has two important advantages: (1) It has the potential for quantitative detection suitable for kinetic studies of transient chemical species and (2) it has a high degree of sensitivity. In the present work, the technique is shown to be at least as sensitive as, and most probably several orders of magnitude more sensitive than, previous methods for the detection of transients. It is presently a powerful tool for obtaining high resolution spectra as well as obtaining precise information about the energy distribution of transient species produced photolytically or kinetically. Spectra for both NH_2 and HCO (produced flash photolytically) are presented.

Barnes, I. L., Murphy, T. J., Gramlich, J. W., Shields, W. R., **Lead separation by anodic deposition and isotope ratio mass spectrometry of microgram and smaller samples,** *Anal. Chem.* **45,** No. 11, 1881-1884 (Sept. 1973).

Key words: Anodic deposition; isotopic analysis; lead; mass spectrometry.

A method is reported for the separation by anodic deposition and subsequent analyses by isotope ratio mass spectrometry of small samples of lead from a variety of matrices. The combined procedure is applicable to samples containing from 10 μg to less than 10 ng of lead and the electrodeposition is more than 95% efficient at these levels. Only a few elements interfere with the deposition, most notably iron and cerium, and procedures for removing the interfering elements are given. The optimum conditions for the anodic deposition of lead as PbO_2 were studied. The mass spectrometric procedure described permits a precision of 0.1% (95% limit of error) or better for the measured isotopic ratios.

Barnes, J. D., **Neutron inelastic scattering study of the "rotator" phase transition in n-alkanes,** (Proc. 5th Symp. on Neutron Inelastic Scattering, Grenoble, France, Mar. 6-10, 1972), Chapter in *Neutron Inelastic Scattering*, pp. 287-299 (International Atomic Energy Agency, Vienna, Austria, 1972).

Key words: n-Alkanes; n-nonadecane; neutron inelastic scattering; phase transition; rotational diffusion; rotator phase.

Many n-alkanes exhibit a solid-solid phase transition a few degrees below their melting points. Such characteristics of the phase transition as transition temperatures, volume change on transition, and heats of transition are very sensitive to chain length in these materials. To characterize the role which molecular motions play in this phase transition, inelastic neutron scattering experiments were carried out on the Fermi chopper time-of-flight spectrometer at the National Bureau of Standards Reactor. Experiments were performed on n-nonadecane at temperatures of 77, 291, 297, 301 and 307 K and on n-eicosane at 301 K. Momentum transfers ranged between .42$Å^{-1}$ and 3.3 $Å^{-1}$ for 2.467 Å neutrons. The full width at half maximum of elastically scattered neutrons was found to be 1.58 ps^{-1} from measurements of scattering from vanadium ($\Delta\lambda/\lambda = 4.6\%$). 297 K and 301 K are above the temperature of the "rotator" phase transition for n-nonadecane. The spectra taken under these conditions consist of a broadened elastic peak superimposed on a continuous spectrum arising from the vibrational modes of the system. The broadening of the elastic peak is found to depend on momentum transfer and is analysed in terms of models involving rotational diffusion of the molecule about the long axis of the chain. The data at 307 K, where the material is molten, reveal a further increase in the quasi-elastic component of the scattering.

Bedford, R. E., Ma, C. K., Barber, C. R., Chandler, T. R., Quinn, T. J., Burns, G. W., Scroger, M., **New reference tables for platinum 10% rhodium/platinum and platinum 13% rhodium/platinum thermocouples,** (Proc. 5th Symp. on Temperature, Its Measurement and Control in Science and Industry, Washington, D.C., June 21-24, 1971), Paper in *Temperature, Its Measurement and Control in Science and Industry*, H. H. Plumb, Editor-in-Chief, **4,** Part 3, 1585-1602 (Instrument Society of America, Pittsburgh, Pa., 1972).

Key words: Blackbodies; calibrations; optical pyrometer; platinum resistance thermometer; platinum-rhodium vs platinum thermcouples; reference tables; thermometric fixed points.

New reference tables for platinum 10 percent rhodium/platinum and platinum 13 percent rhodium/platinum thermocouples have been prepared as a result of a cooperative program among the National Bureau of Standards (USA), the National Physical Laboratory (UK), and the National Research Council (Canada). High purity platinum wires ($\alpha \geq 1.3924 \times 10^{-3}$) and alloy wires of as closely as possible 10 percent and 13 percent rhodium composition, respectively, were supplied by seven American and British manufacturers, from which thirty-two Pt10Rh/Pt and thirty-six Pt13Rh/Pt thermocouples were constructed. Primary calibrations below 1064.43 °C were performed at NBS and NRC; primary calibrations above 1064.43 °C were done at

NPL; thermocouple intercomparisons over the whole temperature range were done at NBS and NRC. The reference tables derive from polynomials fitted, by means of least squares orthogonal polynomial techniques, to a selected group of thermocouples of each type.

Birky, M. M., **Calorimeter for laser energy measurements,** *Appl. Opt.* **10,** No. 1, 132-135 (Jan. 1971).

Key words: Calorimeter; energy; laser; neodymium; ruby.

A calorimeter enclosed in a constant temperature environment has been constructed to measure the output energy of a conventional mode ruby or neodymium laser. The calorimeter was designed according to the measurement theory and has an estimated uncertainty of ±2% in the range 5J to 100J. The time-temperature curves were analyzed according to the theory with the aid of a computer program.

Brower, W. S., Parker, H. S., Roth, R. S., **Synthesis of mercury bismuth sulfide $HgBi_2S_4$,** *Mater. Res. Bull.* **8,** 859-862 (1973).

Key words: Bismuth; mercury; sulfides; synthesis.

The compound $HgBi_2S_4$ was found to be the only phase present, other than the end members, in mixtures of HgS and Bi_2S_3. The compound is apparently a new structure type with monoclinic symmetry, space group C2, Cm or C2/m $a = 14.179$, $b = 4.0555$, $c = 13.986$ Å, $\beta = 118°13.8'$.

Brown, W. C., Buchanan, C. J., **A study of the strength capabilities of children ages two through six,** *NBSIR 73-156,* 56 pages, (Aug. 7, 1973). (Available as COM 73-11286 from the National Technical Information Service, Springfield, Va. 22151.)

Key words: Children; children's strength; pull; push; safety; strength; squeeze; test methods; toys; toy safety; twist.

The Child Strength Study was conducted to provide information which can be used to develop reliable and realistic standards and test methods for children's toys. The study was conducted on over 550 children in the Washington Metropolitan area, and included both black and white children with varying economic and social backgrounds.

Four test devices were used to measure the forces exerted by children when pushing, pulling, twisting, and squeezing. Quantitative relationships were found to exist between these four types of measurements. The study also provided quantitatively precise and useful information about the effects of age and sex on the strength capability of children two through six years old. The results of the study are exhibited in tables of averages, standard deviations, coefficients of variation, and 95th percentiles for each age and sex group tested. A number of graphs are also included for a quick appraisal of the test results.

Brown, W. E., **Solubilities of phosphates and other sparingly soluble compounds,** Chapter 10 in *Environmental Phosphorus Handbook*, E. J. Griffith, A. Beeton, J. M. Spencer and D. T. Mitchell, Eds., pp. 203-239 (John Wiley & Sons, Inc., New York, N.Y., 1973).

Key words: Calcium carbonates; calcium phosphates; hydroxyapatite; limnetic phosphate; phase diagrams; phosphate pollution; solubility.

Solubilities of five calcium phosphates, $Ca_5(PO_4)_3OH$, $\beta - Ca_3(PO_4)_2$, $Ca_9H_2(PO_4)_6)5H_2O$, $CaHPO_4$, and $CaHPO_4 \cdot \frac{1}{2}H_2O$ must be considered as factors that may limit the concentrations of calcium and orthophosphate ions in natural waters. In the three-dimensional plot pH vs $[Ca(OH)_2]$ and $[H_3PO_4]$ for all solutions in the ternary system, $Ca(OH)_2$-H_3PO_4-H_2O, one obtains a surface that (i) has an important bearing on the positions of the isotherms for the five calcium phosphates and the fact that the isotherms have negative slopes, and (ii) is a consequence of the fact that H_3PO_4 is a polybasic, weak acid.

The phase diagram for the ternary system can be expanded to approximate a four component system in which the effects of all other components are incorporated into a single variable which is a measure of their net basicity or acidity. This diagram should have considerable value in the interpretation of field data. Lines of constant pH on this diagram can be used to determine whether a solution is undersaturated or supersaturated with respect to the salt under consideration. Other lines on this diagram define compositions along which the chemical potentials of $Ca(OH)_2$, H_3PO_4 and the various calcium phosphate salts are all constant.

Potential diagrams (− log of the activity of $Ca(OH)_2$ plotted vs that of H_3PO_4) are useful for establishing (i) the degree of saturation of a given solution with respect to anyone or all of the calcium phosphates, and (ii) the Ca/P ratio of the saturating solid phase.

A variety of theoretical and experimental factors must be taken into account in the design of solubility measurements and in the interpretation of results. Their application to calcium phosphates and other sparingly soluble salts of polybasic acids is described.

Burns, G. W., Hurst, W. S., **Studies of the performance of W-RE type thermocouples,** (Proc. 5th Symp. on Temperature, Its Measurement and Control in Science and Industry, Washington, D.C., June 21-24, 1971), Paper in *Temperature, Its Measurement and Control in Science and Industry*, H. H. Plumb, Editor-in-Chief, **4,** Part 3, 1751-1766 (Instrument Society of America, Pittsburgh, Pa., 1972).

Key words: Beryllium oxide; ductility; emf-temperature relationship; microstructure; thermocouple drift; W-Re alloys; W-Re type thermocouples; W-Re thermoelements.

The effect of exposure of bare-wire and BeO-insulated commercial W-Re thermocouple materials to high temperatures in gaseous environments has been investigated. The temperature range of interest has been primarily 2000 to 2400 K, and the investigations have been confined to thermocouple wires of 0.25 mm diameter. With high temperature exposure of the bare thermoelements, an initial shift in the emf-temperature relationship of the exposed thermoelements versus an unexposed "as received" thermoelement was exhibited, and thereafter no discernible drift occurred with exposure in environments of Ar, He, H_2 or N_2 for periods up to 1000 hours. Aging studies were performed to determine the time-temperature parameters of the shift. Thermoelements were examined for metallurgical structural changes and chemical changes by conventional methods. In the temperature range of interest, grain growth was inhibited in the chemically doped W-3 percent Re alloy, and excellent room temperature ductility was retained subsequent to the exposure. The compatibility of high purity (in excess of 99.8 percent), sintered BeO insulators with the thermoelements differed, depending upon whether the BeO-insulated thermoelement assemblies were self-heated electrically or heated in a furnace; in tests in argon environments, highly reliable performance occurred when the assemblies were heated in a furnace. BeO-insulated W-3 percent Re vs W-25 percent Re thermocouples, constructed with degassed and aged materials, exhibited drifts equivalent to about 3 mK/h during 1000 hours of exposure at 2073 K in argon while in the presence of tantalum.

Canfield, L. R., Johnston, R. G., Madden, R. P., **NBS detector standards for the far ultraviolet,** *Appl. Opt.* **12,** No. 7, 1611-1617 (July 1973).

Key words: Detectors; far ultraviolet; ion chamber; photodiodes; radiometry; thermopile.

A program at NBS leading to the realization of practical, stable transfer detector standards for the far ultraviolet is reviewed. Three basic detector types, one covering the region of 584-1216 Å and the other two covering the region of 1164-2537 Å, are described. Examples of these detectors have been calibrated at NBS and distributed

to laboratories throughout the United States and Europe, where they are being used as primary radiometric calibration references in a variety of far-uv experiments.

Cataland, G., Plumb, H. H., **The realization of low temperature fixed points on the NBS acoustical and the NBS-1955 temperature scales,** (Proc. 5th Symp. on Temperature, Its Measurement and Control in Science and Industry, Washington, D.C., June 21-24, 1971), Paper in *Temperature, Its Measurement and Control in Science and Industry*, H. H. Plumb, Editor-in-Chief, **4,** Part 1, 183-193 (Instrument Society of America, Pittsburgh, Pa., 1972).

Key words: Acoustical thermometry; e-H_2 NBP-e-H_2 TP fixed points; neon NBP.

The normal boiling and triple points of equilibrium hydrogen have been realized and related to the NBS (1955) temperature scale. From isotherms that were determined with the NBS acoustical thermometer, values of T(acoustical) can be associated with the above fixed points and also with the normal boiling point.

Cezairliyan, A., **A high-speed (millisecond) system for studies of phase transitions and thermophysical properties of electrical conductors above 2000 K,** *Proc. Int. Conf. on Etude des Transformations Cristallines a Haute Température, Odeillo, France, Sept. 27-30, 1971*, No. 205, 25-32 (Centre National de la Recherche Scientifique, Paris, France, 1972).

Key words: High-speed methods; high temperature; phase transitions; refractory metals; thermophysical properties.

A high-speed system is described for conducting studies on phase transitions, and for measuring selected thermophysical properties of electrical conductors at temperatures above 2000 K. The system can measure specific heat electrical resistivity, hemispherical total emittance, and melting point in subsecond duration experiments. Temperature measurements are made with a millisecond resolution photoelectric pyrometer. Experimental quantities are recorded with a high-speed digital data acquisition system. The entire system has a time resolution of approximately 0.4 millisecond. An experiment simulating the conditions of phase transitions is described. Results of measurements on solid-liquid phase transitions in niobium, molybdenum, and tungsten are presented. High-speed measurements of selected thermophysical properties of niobium, molybdenum, tantalum, and tungsten are summarized. Sources and magnitudes of errors are discussed.

Cezairliyan, A., **Measurement of the heat capacity of graphite in the range 1500 to 3000 K by a pulse heating method,** (Proc. 6th Symp. on Thermophysical Properties, Palm Springs, Calif., Aug. 1973), Paper in *Proceedings of the 6th Symposium on Thermophysical Properties*, P. E. Liley, Ed., pp. 279-285 (American Society of Mechanical Engineers, New York, N.Y., 1973).

Key words: Graphite; heat capacity; high-speed measurements; specific heat; thermodynamics.

Measurement of the heat capacity of a grade of graphite (AXM-5Q, POCO) in the temperature range 1500 to 3000 K by a subsecond-duration, pulse-heating technique is described. The smoothed results for a single specimen corresponding to two different heating rates are in agreement within 0.1% on the average. The smoothed results for two different specimens are in agreement within 0.6%. The heat capacity of graphite in the temperature range 1500 to 3000 K based on the present results is expressed by the following function (standard deviation = 0.5%):

$$c_p = 19.12 + 4.236 \times 10^{-3} T - 5.919 \times 10^{-7} T^2,$$

where T is in K and c_p is in J $mol^{-1}K^{-1}$. The inaccuracy of the reported results is estimated to be not more than 3%.

Cezairliyan, A., **Measuring transient high temperatures by optical pyrometry,** (Proc. 5th Symp. on Temperature, Its Measurement and Control in Science and Industry, Washington, D.C., June 21-24, 1971), Paper in *Temperature, Its Measurement and Control in Science and Industry*, H. H. Plumb, Editor-in-Chief, **4,** Part 1, 657-664 (Instrument Society of America, Pittsburgh, Pa., 1972).

Key words: High-speed measurements; high temperature; pyrometry; radiation; temperature measurement.

Various pyrometric (optical) methods, using photoelectric and photographic detectors, are described for measuring high temperatures. Emphasis is placed on techniques of measuring transient temperature of solids above approximately 1500 K with subsecond (upper millisecond to upper microsecond) resolution. Advantages and limitations of the various methods are discussed and estimates of uncertainties are given. Examples of application of the high-speed temperature measurement methods to various fields of investigations, including determination of thermophysical properties, is presented.

Churney, K. L., West, E. D., Armstrong, G. T., **A cell model for isoperibol calorimeters,** *NBSIR 73-184*, 100 pages (Apr. 1973). (Available as COM 73-11110 from the National Technical Information Service, Springfield, Va. 22151).

Key words: Calorimetry; energy equivalents; energy measurement; heat transfer; internal energy measurement; isoperibol calorimeters; measurement theory.

A calorimeter can be modeled as a large number of volume elements or cells in each of which the temperature may be considered uniform, and each of which can store heat and exchange heat with other cells. Application of the first law of thermodynamics to this set of cells leads to representations of the usual calorimetric equations for internal energy change expressed in terms of measurable or estimatable heat capacities, heat transfer coefficients, temperatures, and work terms for the individual cells. Analysis of the results yields a framework within which most of the design and measurement problems of isoperibol calorimeters can be treated.

Cohen, J., Edelman, S., Vezzetti, C. F., **Pyroelectricity and piezoelectricity in oriented films of polyvinyl fluoride and polyvinylidene fluoride,** (Proc. Conf. on Electrets, Charge Storage and Transport in Dielectrics, Miami Beach, Fla., Oct. 8-13, 1972), Paper in *Electrets, Charge Storage and Transport in Dielectrics*, Martin M. Perlman, Ed., pp. 505-516 (The Electrochemical Society, Inc., Princeton, N.J., 1973).

Key words: Piezoelectricity; poling; polyvinyl fluoride; polyvinylidene fluoride; pyroelectric coefficient; pyroelectricity.

Improved pyroelectric and piezoelectric activities have been produced in films of polyvinyl fluoride (PVF) and polyvinylidene fluoride (PVF_2). The phenomena are ascribed to orientation of dipoles normal to the plane of the film. Activity is developed or enhanced by applying intense electrical fields across the films at elevated temperatures and cooling to room temperature with the field still applied (poling). The PVF_2 films are usually stretched before poling, and this is found to increase both pyroelectric and piezoelectric effects. Room temperature pyroelectric coefficients for these materials have been estimated from measurements of voltage responsivity, and pyroelectric coefficients comparable to that of triglycine sulfate (TGS) have been obtained. Observations of the correlation between the thermal radiation effects and the piezoelectric activity suggest that the former are pyroelectric. A method has been developed to study the poling process.

Corliss, E. L. R., **Remark on "Fixed-scale mechanism of absolute pitch,"** *J. Acoust. Soc. Amer. Letters to Editor* **53,** No. 6, 1737-1739 (June 1973).

Key words: Absolute pitch sense; audition; auditory memory; hearing; musical acoustics; pitch recognition.

Several aspects of this author's subjective experiences concerned with perception of pitch are at variance with the experiences reported by Paul T. Brady, *J. Acoust. Soc. Am.* **48**, 883-887 (1970). In particular, my recognition is not tied to a specific scale (though, of course, nomenclature must be); the precision of recognition shows little fluctuation, if any; and changes in tuning do not influence the recognition of pitch, although such changes may influence the performance of remembered music and the ease of transposition. Tonal memory overrides motor memory for the performance of music learned on instruments tuned to initially different keys.

Craw, A. R., **A comparison of several methods for forecasting U.S. traffic fatalities,** *NBSIR 73-189*, 45 pages (May 1973). (Available as COM 73-11173 from the National Technical Information Service, Springfield, Va. 22151.)

Key words: Exponential smoothing; forecasting; time-series; traffic fatalities.

This is a second report to the Mathematical Analysis Division of the National Highway Traffic Safety Administration (NHTSA) on the subject of forecasting annual highway fatalities. This report concerns a comparison of several time series analysis programs based on exponential smoothing and nondecompositional methods currently employed by NHTSA for projecting the annual *traffic* fatalities for the entire U.S. Several methods of data aggregation are studied.

It is found that there is some advantage in using lumped (pooled) data for each region aggregated either quarterly or half yearly, and using the Sum of Regional estimates to estimate the national value.

Also, there does not appear to be any great difference in the results obtained using the nondecompositional methods and those obtained by time-series analysis programs based on exponential smoothing methods.

Estimates for the 1972 and 1973 national traffic fatalities by a variety of methods were made. For 1973 the estimates ranged from a low of 54186 to a high of 55994, with a mean of 55055.

Craw, A. R., **Analyses for decision in the office of flammable fabrics: the level of the standard,** *NBSIR 73-182*, 90 pages, (Apr. 1973). (Available as COM 73-11284 from the National Technical Information Service, Springfield, Va. 22151.)

Key words: Children's sleepwear; decision analysis; flammable fabrics; probability assessment; standards; utility theory.

The fundamentals of a single-stage decision problem are discussed and illustrated in the problem: The Level of the Standard for Children's Sleepwear, originally discussed by M. Tribus. Outcomes are identified, and various potential measures of disutility are discussed.

Given a particular alternative is in effect one must assign the conditional probabilities of arriving at each outcome. This process is aided by introducing intermediate events (extending the conversation). For the children's sleepwear problem this is done by considering for each of two age groups and three income levels the probability tree with branches: alternatives (a), technology (T), nightwear (N), additional cost to the consumer (C), Use (U) or non-use (u), existence of a hazard (H), exposure (E), ignition (I), burn (B) and burn-severity (B_i), survival (S) or death (D) and body image (I_d).

Attention is given to the preliminary assignment of each of the conditional probabilities needed. Suggestions are made as to sources of information. Much of the needed information is not available, especially that dealing with the social and behavioral aspects of the problem. The concept of exposure to an ignition hazard, for which an operational definition does not exist, is discussed.

Craw, A. R., Ku, R., **The sensitivity of certain indices associated with two-vehicle accidents,** *Accident Anal. Prev.* **5**, 137-146 (1973).

Key words: Highway traffic accidents; indices; sensitivity analysis.

This study describes in mathematical terms a procedure employed by the National Highway Traffic Safety Administration of the Department of Transportation for the analysis of two-vehicle accidents. The procedure contains an Assignment Rule in which one of the involved driver-vehicle combinations is assigned to the class of active involvement and the other driver-vehicle combination is assigned to the class of passive involvement. Once case of interest is the Random Assignment Rule, and this is contrasted with the results of a Fixed Assignment Rule. Results are derived that show the effect on specific indices of (1) errors in assignment and (2) a Composite Assignment Rule (a mixture of Fixed and Random Rules).

Cruz, J. E., Rogers, E. H., Hiester, A. E., **Continuous liquid level measurements with time-domain reflectometry,** (Proc. 1972 Cryogenic Engineering Conf., Boulder, Colo., Aug. 9-11, 1972), Paper H-4 in *Advances in Cryogenic Engineering* **18**, 323-327 (Plenum Press, New York, N.Y., 1973).

Key words: Coaxial probe; emptying rate; fill rate; liquid level; time domain reflectometer.

A time domain reflectometer is considered a closed-loop, one dimensional radar system. Applying the principle of time domain reflectometry to the detection of cryogenic liquid levels, measurements on the order of ±0.3% of total liquid level probe length are possible.

The time domain reflectometer liquid level measurement is independent of liquid density variations and is simple to calibrate and operate. Construction of the liquid level sensing probe is described.

Daney, D. E., McConnell, P. M., Strobridge, T. R., **Low-temperature nitrogen ejector performance,** (Proc. 1972 Cryogenic Engineering Conf., Boulder, Colo., Aug. 9-11, 1972), Paper L-4 in *Advances in Cryogenic Engineering* **18**, 476-485 (Plenum Press, New York, N.Y., 1973).

Key words: Cryogenic ejector; ejector; ejector pump; jet pump; low temperature refrigeration; refrigeration.

The primary objective of the test program reported here was to obtain a nitrogen ejector to replace the Joule-Thomson valve in a Joule-Thomson refrigerator. The desired primary nozzle inlet conditions were 200 atm and 161 K with a flow rate of 16.6 g/s, and the required entrainment ratio was 0.145. In an attempt to find a near optimum ejector for the above conditions, and in order to obtain a more general knowledge of low temperature nitrogen ejector performance, the tests were run over a range of operating conditions. The primary nozzle supply pressure ranged from 35 to 200 atm with a temperature near 161 K. The discharge pressure varied from 1.2 to 1.6 atm, and the entrainment ratio varied from 0.0 to 0.5. Combinations of three primary nozzles with three mixing sections resulted in a range of 118 to 365 for the ratio of the mixing tube area to the primary nozzle throat area. For the design conditions given above, a suction pressure of 0.27 atm was obtained. This corresponds to a liquid nitrogen saturation temperature of 67.7 K.

Dhez, P., Ederer, D. L. **Photoionization resonance profile parameters of the 3s3p $^1P_1$ two-electron excitation in He I,** *J. Phys. B: At. Mol. Phys.* Letter to Editor **6**, L59-L64 (Apr. 1973).

Key words: Autoionization; cross section; Fano parameters; helium; photoionization; resonance profile.

The cross section profile of the 3s3p $^1P_1$ two-electron excitation has been measured in He I. The cross section was assumed to have the form

$$\sigma(E)=C(E)+\frac{(E-E_0)\frac{1}{2}\Gamma a+(\frac{1}{2}\Gamma)^2 b}{(E-E_0)^2+(\frac{1}{2}\Gamma)^2}$$

where the adjustable parameters a, b, $1/2\Gamma$ and E_0 were determined by a least squares fitting process. The parameter values obtained in the experiment were: $a = 0.86 \pm 0.16$ cm^{-1}, $b = 0.27 \pm 0.13$ cm^{-1}, $1/2\Gamma = 65.9 \pm 7.0$ meV, $E_0 = 69.919 \pm 0.007$ eV. The Fano parameters q and σ_a were determined from a and b and had the values 1.36 ± 0.20 and 0.32 ± 0.08 cm^{-1} respectively.

Edelsack, E. A., Kropschot, R. H., Olien, N. A., Olsen, J. L., **A Directory of European Low Temperature Research,** *Cryogenics* **13,** No. 3, 132-133 (Mar. 1973).

Key words: Cryogenics; European low temperature research.

The publication of a Directory of Low Temperature Research in seventeen European countries is described. The Directory contains the names of some three hundred researchers, their addresses, telephone numbers, and brief descriptions of their research interests. Information for obtaining free copies of the Directory is included.

Eisen, H., Rosenstein, M., Silverman, J., **Electron dosimetry using Chalkley-McLaughlin dye-cyanide thin films,** (Proc. Int. Symp. on Dosimetry in Agriculture, Industry, Biology and Medicine, Vienna, Austria, April 1972), Paper in *Dosimetry in Agriculture, Industry, Biology and Medicine*, pp. 615-625 (International Atomic Energy Agency, Vienna, Austria, 1973).

Key words: Calorimetry; depth dose; dose distributions; dye films; electron beams; interface; Monte Carlo transport; stopping power; thin films.

The purpose of this work was to measure electron energy deposition profiles in a variety of absorbing materials and to evaluate the Chalkley-McLaughlin radiochromic dye-cyanide film dosimeter. Information of this type is useful for effective utilization of electron beams in industry and medicine where adjustments in sample thickness, electron beam energy, angle of electron beam incidence, and backing materials may provide more advantageous beam utilization. Experimental depth-dose distributions were determined for broad beams of 2.00 MeV electrons incident on polystyrene, aluminium, copper, tin, gold, and several two-layer slab absorbers. Data were obtained for both semi-infinite and finite homogeneous absorbers at incident beam angles ranging from 0 (normal incidence) to 75 degrees. Radiochromic dye-cyanide films were used as solid-state cavity dosimeters, with an experimental reproducibility of $\pm 6\%$ (2σ). The stopping power ratio necessary to convert from film dose to absorber dose was evaluated several ways. Depth-dependent stopping power ratios, obtained by accounting for the changing electron energy spectrum with absorber depth by two methods, were compared with a constant stopping power ratio for each material. The difference between the constant ratio and a depth-dependent ratio was 1% to 2% for aluminium, 3% to 5% for copper, 3% to 7% for tin, and 3% to 8% for gold. The data demonstrate the decrease in the depth-dose distribution and the total absorbed dose in finite slabs as compared to equivalent layers in semi-infinite slabs. The effect of the atomic number of the absorber and the angle of beam incidence on the shape of the energy deposition profile is also demonstrated. The data for the two-component slab absorbers illustrate the modification of the depth-dose profile in a finite slab of material if a different material is placed adjacent to it. From the dose received by a film placed at the interface, the surface doses at that position were estimated using the material-to-film stopping-power ratio appropriate for each material. The data are compared to theoretical depth-dose profiles obtained using Monte Carlo transport codes. The agreement is generally between 5% to 10% for homogeneous cases and in most cases better than 10% for the two-component cases.

Eisenhower, E. H., **Safety recommendations in ANSI documents,** (Proc. Symp. on Radiation Safety and Protection in Industrial Applications, Washington, D.C., Aug. 16-18, 1972), *DHEW Pub.* No. (FDA) 73-8012, H. F. Klein, Ed., pp. 240-252 (U.S. Department of Health, Education, and Welfare, Public Health Service, Food and Drug Administration, Bureau of Radiological Health, Rockville, Md., Oct. 1972).

Key words: Radiation safety; radiography; voluntary standards; x rays.

This paper discusses American National Standards relating to safety in industrial applications of ionizing radiation. It includes methods by which voluntary standards are produced, and outlines approval procedures required for designation as an American National Standard. The structure and relevant activities of Standards Committee N43, of the American National Standards Institute (ANSI) are described. Maximum permissible dose equivalent values recommended by the National Council on Radiation Protection and Measurements are presented as the basis for requirements in ANSI standards. Existing and future standards of interest to radiation safety in industrial applications are outlined.

Ely, J. F., Hanley, H. J. M., Straty, G. C., **Analysis of the pressure virials and Clausius-Mossotti function for polyatomic gases,** *J. Chem. Phys.* **59,** No. 2, 842-848 (July 15, 1973).

Key words: Clausius-Mossotti function; dielectric virial coefficients; m-6-8 potential; polarizability; polyatomic gases; pressure; second virial coefficients; quadrupole moment; statistical mechanics.

Statistical mechanical equations for the second pressure virial coefficient and the second and third dielectric virial coefficients for quadrupolar molecules are evaluated using the *m*-6-8 potential function. The results are compared with experimental data for nitrogen and fluorine. An approximate value for the quadrupole moment of fluorine is estimated. Agreement between theory and experiment is generally good.

Evans, J. P., **High temperature platinum resistance thermometry,** (Proc. 5th Symp. on Temperature, Its Measurement and Control in Science and Industry, Washington, D.C., June 21-24, 1971), Paper in *Temperature, Its Measurement and Control in Science and Industry*, H. H. Plumb, Editor-in-Chief, **4,** Part 2, 899-906 (Instrument Society of America, Pittsburgh, Pa., 1972).

Key words: Freezing point; gold point; high temperature; platinum resistance thermometer; standard thermocouple; temperature scale.

During the past decade a number of investigators have worked on various aspects of high temperature platinum resistance thermometry with the aim of developing thermometers suitable for use as interpolating instruments on a practical temperature scale up to the gold point. Long-time stability studies have been made of thermometers employing several designs and a variety of insulating and protecting materials; factors affecting the use of thermometers for temperature measurement have been investigated; new electrical instruments, using both direct and alternating current, have been developed to facilitate the measurement of thermometer resistance; and the investigation of metal freezing points as fixed points for calibrating thermometers has been extended to higher temperatures. An intercomparison of standard thermocouples and high temperature platinum resistance thermometers has shown that a practical temperature scale based on resistance thermometry can be realized at least an order of magnitude more precisely than a scale based on thermocouples, and several workers have suggested interpolation schemes for resistance thermometer scales. This paper reviews recent developments in high temperature platinum resistance thermometry, its current status, and some of the problem areas that need further attention.

Feldman, A., Horowitz, D., Waxler, R. M., **Laser damage in materials,** *NBSIR 73-119*, 52 pages (Feb. 1973). (Available as AD 757789 from the National Technical Information Service, Springfield, Va. 22151.)

Key words: Absorption coefficient; damage threshold; electrostrictive self-focusing; electrostriction; Kerr effect; laser damage; nonlinear index of refraction; self-focusing; thermal self-focusing.

The relative contributions of the Kerr, electrostrictive, and thermal effects to the self-focusing thresholds of borosilicate crown glass, fused silica, and dense flint glass have been estimated from an analysis of damage threshold data for linearly polarized and circularly polarized radiation. The measurements were made with a Nd:glass laser operating in the TEM_{oo} mode with a temporal pulse width of 25 ns. The Kerr effect appears to be the largest effect. The thermal effect is also significant. The electrostrictive effect is smallest. Reasonable values of absorption coefficient are calculated from the thermal contribution. The results are in qualitative agreement with the work of others. Self-focusing data obtained with linearly polarized and circularly polarized radiation are presented for yttrium aluminum garnet (YAG) and five commercial Nd:doped laser glasses. The YAG data agree with the theory of self-focusing. Near the threshold the laser glass data appear to indicate intrinsic damage rather than self-focusing. Differences between the various laser glasses are small. Self-focusing data obtained in dense flint glass with a longer focal length lens are also presented. An electro-optic shutter actuated by a laser triggered spark gap is discussed.

Ferguson, J. B., **Summary of flame spread and smoke generation tests conducted for operation BREAKTHROUGH,** *NBSIR 73-228*, 27 pages (July 1973). (Available as PB 222425 from the National Technical Information Service, Springfield, Va. 22151.)

Key words: Carpets; flame spread; kitchen cabinets; Operation BREAKTHROUGH; smoke generation; wall and ceiling.

This document is a listing of the flame spread and smoke generation results of a range of materials that were tested under the Operation BREAKTHROUGH housing evaluation program. The test results reported here were obtained under differing conditions and should not be considered the results of a comprehensive and unified research program for evaluation of interior finish materials. Tables of test results and a brief discussion of the results are presented for walls, ceilings, kitchen cabinets and floor coverings.

Fickett, F. R., **Properties of nonsuperconducting technical solids at low temperatures,** *Proc. 4th Int. Conf. on Magnet Technology*, Brookhaven National Laboratory, Upton, N.Y., Sept. 19-22, 1972, pp. 498-516 (Atomic Energy Commission, Washington, D.C., 1972).

Key words: Composite materials; electrical properties; mechanical properties; metals; plastics; review; thermal properties.

A number of physical and mechanical properties of materials used in low temperature applications are described with references to both theory and compiled data. These properties, which fall into three main groups, thermal, electrical, and mechanical, are given for pure metals, alloys, and a few nonmetals. In essence, this paper is a review of concepts and available data for low temperature engineering applications of nonsuperconductors.

Finkel, P. W., Rowen, J. W., **Clinical laboratory performance analysis using proficiency test statistics,** *NBSIR 73-197*, 61 pages (June 1973). (Available as COM 73-11253 from the National Technical Information Service, Springfield, Va. 22151.)

Key words: Accuracy; CLIA '67; clinical chemistry; hematology; microbiology; precision; proficiency testing.

The proficiency testing aspects of the Clinical Laboratory Improvement Act of 1967 program were assessed. The overall ability of licensed or volunteer laboratories to accurately determine mean values for any of the 13 constituents was not significantly altered during the first two years of program operation. However, the variability of the laboratories has decreased over the two-year period. It appears that the program has increased consistency of laboratory performance.

The general level of laboratory capability seemed to be independent of involvement in state-supported or voluntary proficiency testing programs other than the CDC program and of whether the working supervisor had a B.S., M.S., Ph.D., or M.D. degree. Choice of analytical method did significantly affect performance. Although insufficient evidence was available to make a definitive statement, the data do not appear to support arguments favoring establishment of method-dependent reference group target values.

Finally, it appears that consideration should be given to alternative sampling methods, such as reduced or skip-lot sampling, for those constituents which appear to present no analytical challenge to the licensed and volunteer laboratories. Greater emphasis might then be placed on those constituents which give the laboratories the most difficulty (cholesterol and creatinine, for example).

Flynn, D. R., **Inter-Noise 72 Panel: Noise measurement—problems, perils and pitfalls,** *Noise/News* **2,** No. 1, 7-9 (Jan.-Feb. 1973).

Key words: Acoustics; noise measurements; sound levels.

This short paper discusses some of the problems involved in noise measurements. It is pointed out that noise measurement standards should specify environmental and operational constraints in addition to precise, accurate measurement and operational procedures. A few examples are given of sources of significant measurement errors. The Measurement Assurance Programs of NBS are briefly described as a means that has been used in other disciplines to improve measurements in a total system context.

Fraker, A. C., Ruff, A. W., **The effect of solution pH on the saline water corrosion of titanium alloys,** (Proc. 2d Int. Conf. on Titanium, Boston, Mass., May 2-5, 1972), Paper in *Titanium Science and Technology*, R. I. Jaffee and H. M. Burte, Eds., **4,** 2655-2663 (Plenum Publishing Corp., New York, N.Y., 1973).

Key words: Corrosion; electron microscopy; pressure; salt water; titanium.

The initial stages of corrosion attack on several titanium alloys in saline water solutions have been studied. Transmission electron microscopy and electron diffraction were used to study the corrosion films formed on the exposed surfaces of thin foil specimens and to determine their degree of crystallinity and composition. The corrosion sensitivity of each material to pH variation was studied. Six different alloys were examined over the range 100-200 °C in a Hastelloy-C pressure vessel containing the 3.5 wt. pct. NaCl solution. Sulfuric acid, hydrochloric acid and sodium hydroxide were added singly to the saline solution for individual tests with pH values ranging from 1.8 to 12.5. We find that the surface oxide composition changes with different solution pH values. The oxide covering the surface after exposing in neutral and acid solutions does not occur in alkaline solutions. Examples of local pitting attack were found to occur at both high and low pH values but were more frequent when specimens were corroded in the alkaline solutions.

Fraker, A. C., Ruff, A. W., Yeager, M. P., **Corrosion of titanium alloys in physiological solutions,** (Proc. 2d Int. Conf. on Titanium, Boston, Mass., May 2-5, 1972), Paper in *Titanium Science and Technology*, R. I. Jaffee and H. M. Burte, Eds., **4,** 2447-2457 (Plenum Publishing Corp., New York, N.Y., 1973).

Key words: Alloys; biological; corrosion; electron microscopy; implant; saline solution; titanium.

This study intends to determine corrosive effects of saline and organic solutions on several titanium alloys for potential use as biological implant materials. Experimental techniques included electrochemical measurements and thin foil transmission electron microscopy and diffraction. The effects of varying alloy composition, method of specimen preparation, and different organic and salt solutions were studied. Thin foil transmission electron microscopy was used to examine surfaces of specimens exposed to salt solutions containing albumin, cystine, alanine and uric acid.

Franzen, D. L., **Continuous laser-sustained plasmas,** *J. Appl. Phys.* **44,** No. 4, 1727-1732 (Apr. 1973).

Key words: Gas breakdown; laser; plasma.

Continuous plasmas sustained by a focused high-power CO_2 laser are described. The power required for maintaining a cw plasma following preionization has been determined for Xe, Kr, and Ar, and attempted for Ne and He. Measurements indicate the noble gases with the lowest ionization potentials have the lowest sustaining thresholds. Radiative properties of some of the plasmas were studied with calorimetric techniques. Under certain conditions, more than half of the incident laser radiation can either be scattered or absorbed by the plasma. A major loss mechanism for the plasma is shown to be radiation in the visible and ultraviolet. Spectra of low-pressure Xe plasmas indicate the presence of ultraviolet transitions with a high contrast over the continuum.

Frenkiel, F. N., Klebanoff, P. S., **Probability distributions and correlations in a turbulent boundary layer,** *Phys. Fluids* **16,** No. 6, 725-737 (June 1973).

Key words: Boundary layer; correlations; higher-order moments; high-speed computing; hot-wire anemometry; probability distributions.

One-dimensional and joint probability density distributions for longitudinal components of turbulent velocities as well as higher-order correlations are measured in a turbulent boundary layer on a flat plate using hot-wire anemometry and high-speed computing methods. The effect of the nonlinear response of the hot-wire is taken into account. Data pertaining to the general nature of the turbulent boundary layer are presented and comparison is made between the measured correlations and those corresponding to a Gaussian probability distribution of turbulent velocities as well as to non-Gaussian distributions of the Gram-Charlier type. Similar comparisons are made of the measured one-dimensional and joint probability distributions. Probability distributions in the boundary layer are also compared to those measured downstream of a grid. The closure of the tails of the probability distribution and its effect on the accuracy of the measurements of higher-order moments is considered.

Fröhlich, C., Geist, J., Kendall, J., Sr., Marchgraber, R. M., **The Third International Comparisons of Pyrheliometers and a comparison of radiometric scales,** *Sol. Energy* **14,** 157-166 (1973).

Key words: International Pyrheliometric Scale; irradiance; pyrheliometer; World Meteorological Organization.

The Third International Comparisons of Pyrheliometers organized by the World Meteorological Organization and the Davos Observatory were held in September 1970 at Davos and Locarno. For this purpose the intensity of solar radiation was measured simultaneously by the standard radiometers (Ångström compensation and silver-disc pyrheliometers) from all over the world. For meteorological use the intensity values refer to the International Pyrheliometric Scale 1956 represented by the reference instruments of the Davos Observatory and of the Swedish Meteorological and Hydrological Institute at Stockholm. At the same time measurements were performed by two instruments rendering an absolute value of high accuracy. These sophisticated instruments have been constructed by Kendall and Geist respectively.

A fully-automatic data acquisition system together with a computer was used to compare simultaneously the 22 Ångström Pyrheliometers and to monitor the auxiliary measurements necessary for defining the state of the atmospheric conditions specified by a turbidity coefficient of $0'03 < m\beta < 0'3$. The intensity values covered a range of 55-100 mW/cm². The results show a significant difference between the two radiometeric scales. The intensity value deduced from the absolute measurement is about 2 percent higher than the value based on the International Pyrheliometric Scale.

Fromhold, A. T., Jr., Kruger, J., **Space-charge and concentration-gradient effects on anodic oxide film formation,** *J. Electrochem. Soc.* **120,** No. 6, 722-729 (June 1973).

Key words: Anodization; corrosion; oxidation.

Numerical computations illustrate the effects of space charge and a concentration gradient on the steady-state mobile-defect concentration profile and the kinetics of anodic film formation. The position-dependence of the concentration of mobile defects producing growth is shown to vary with current density and film thickness. Of especial interest is a series of curves illustrating the total electrostatic potential developed across the oxide as a function of thickness for growth under constant current conditions. Space charge is shown to have the capability of being a critical factor in retarding the growth rate of the anodic film.

Furukawa, G. T., Bigge, W. R., Riddle, J. L., **Triple point of argon,** (Proc. 5th Symp. on Temperature, Its Measurement and Control in Science and Industry, Washington, D.C., June 21-24, 1971), Paper in *Temperature, Its Measurement and Control in Science and Industry*, H. H. Plumb, Editor-in-Chief, **4,** Part 1C, 231-243 (Instrument Society of America, Pittsburgh, Pa., 1972).

Key words: Argon; fixed point; triple point; temperature scale.

The average triple-point (TP) temperature of two argon cells was determined to be 83.7997_7K, the two cells being within 0.38 mK of each other and the estimated uncertainty of the value being ±0.5 mK. (The uncertainty includes imprecision of the measurements and possible systematic errors.) The temperature value is based on thermometers calibrated in terms of the NBS-1955 temperature scale adjusted to the International Practical Temperature Scale of 1968 (IPTS-68). The value of temperature obtained by extrapolating the deviation function, $\Delta W_4(T)$, specified for the temperature interval 90.188 K to 273.15 K by the IPTS-68, is about 0.3 mK lower. The argon TP is recommended as a defining fixed point to replace the oxygen normal boiling point.

Furukawa, G. T., Riddle, J. L., Bigge, W. R., **Investigation of freezing temperatures of National Bureau of Standards tin standards,** (Proc. 5th Symp. on Temperature, Its Measurement and Control in Science and Industry, Washington, D.C., June 21-24, 1971), Paper in *Temperature, Its Measurement and Control in Science and Industry*, H. H. Plumb, Editor-in-Chief, **4,** Part 1D, 247-263 (Instrument Society of America, Pittsburgh, Pa., 1972).

Key words: Fixed point; freezing point; standards; tin; tin point.

The intercomparison of freezing points was made on selected samples of tin from two series of standards that are nominally 99.9999 (6N) and 99.999 (5N) percent pure. The freezing point of each tin-point cell prepared from the samples is reproducible within 0.05 mK from freeze to freeze; the freezing points of the cells from each series agree with each other within ±0.1 mK. The freezing points of the 5N standard are on the average 0.5 mK lower than those of the 6N standard. On the basis of the chemical purity information on the samples,

the freezing-point of the 6N samples is expected to be within less than ±0.7 mK of the freezing point of 100 percent pure tin.

Furukawa, G. T., **Vapor pressures of ^{20}Ne and ^{22}Ne,** (Proc. 5th Symp. on Temperature, Its Measurement and Control in Science and Industry, Washington, D.C., June 21-24, 1971), Paper in *Temperature, Its Measurement and Control in Science and Industry*, H. H. Plumb, Editor-in-Chief, **4**, Part 1B, 127-135 (Instrument Society of America, Pittsburgh, Pa., 1972).

Key words: Fixed point; ^{nat}Ne; ^{20}Ne; ^{22}Ne; neon; vapor pressure.

The results of the vapor-pressure measurements with pure neon isotopes ^{20}Ne and ^{22}Ne are described. The measurement precision is ±0.1 to ±0.2mK. The vapor pressures of ^{nat}Ne calculated from the law for ideal solutions and the data on the pure neon isotopes are in agreement with the observed values on ^{nat}Ne within about ±0.5 mK. A table of normal boiling point temperatures as a function of composition of "^{nat}Ne" is given.

Gadzuk, J. W., Lucas, A. A., **Field-emission tails and tunneling lifetimes,** *Phys. Rev. B* **7**, No. 11, 4770-4775 (June 1, 1973).

Key words: Field emission; surfaces; tunneling.

Recent observations of high- and low-energy tails in field-emission energy distributions can be interpreted in terms of quasi-stationary-state single-particle tunneling. This imposes a restriction on the observable range of energies in such studies. The tails result from the predicted breakdown of the transfer Hamiltonian theory of tunneling when fourth-order terms in the perturbation expansion of the tunneling matrix element become large. The tunneling lifetimes $\sim 10^{-12}$ sec required to fit the experimental data are consistent with both the *RC* time constant discussed by Thornber, McGill, and Mead and also a simple intuitive picture. Alternate theories of tunneling lifetimes are critically evaluated.

Garvin, D., **Chemical kinetics data survey IV. Preliminary tables of chemical data for modelling of the stratosphere,** *NBSIR-203*, 95 pages, (May 1973). (Available as COM 73-11288 from the National Technical Information Service, Springfield, Va. 22151.)

Key words: Atmospheric chemistry; chemical kinetics; data evaluation; energy transfer; gas phase; high temperature air chemistry; ion-molecule reactions; optical absorption cross sections; photochemistry; quantum yield; rate constants.

Chemical kinetic and photochemical data for gas phase reactions pertinent to the chemistry of the stratosphere are presented in four tables. These tables give recommended values and also cite recent experimental work. They give data in the following subject areas: chemical reactions and photochemistry of neutral species, energy transfer reactions, high temperature air reactions, and ion-molecule reactions.

Garvin, D., **Chemical kinetics data survey V. Sixty-six contributed rate and photochemical data evaluations on ninety-four reactions,** *NBSIR 73-206*, 121 pages, (May 1973). (Available as COM 73-11262 from the National Technical Information Service, Springfield, Va. 22151.)

Key words: Atmospheric chemistry; chemical kinetics; data evaluation; gas phase reactions; optical absorption cross sections; photochemistry; quantum yields; rate constants.

This report records the data evaluations contributed to the Climatic Impact Assessment Program chemical kinetics survey during the period Nov. 1972-Apr. 1973 by various kineticists and photochemists. Data are included on reactions of $O(^1D)$, $O(^1S)$, $O_2(^1\Delta)$, CH_3ONO, CH_3O, CH_3O_2, H_2O_2, HO_2, SO, SO_2 and the H_2-N_2-O_2 system.

Garvin, D., Hampson, R. F., **Evaluated rate and photochemical data for modeling of the stratosphere,** (Proc. 2d Conf. on Climatic Impact Assessment Program, Cambridge, Mass., Nov. 14-17, 1972), *DOT Report* No. TSC-OST-73-4, 12 pages (Transportation Systems Center, Department of Transportation, Cambridge, Mass., 1972).

Key words: Atmospheric chemistry; chemical kinetics; data evaluation; nitrogen oxides; ozone; photochemistry; stratosphere; water.

Three important types of input data for studies of the chemistry of the stratosphere are rate constants, absorption coefficients, and quantum yields for elementary processes. About 135 of these data items are needed for studies that will define the chemistry of the stratosphere. These data are being obtained both by experiment and by review and evaluation of existing measurements.

The data-evaluation program has two parts: evaluation by a group at NBS, and a cooperative survey by a large number of gas kineticists. The evaluated data now available are summarized in a table. The possible interactions among 42 species that may be present in the stratosphere are displayed on a reaction grid. Where possible the importance of a reaction and the status of its data are indicated.

Pollutants introduced into the stratosphere will interact with the existing complex $O_3/O_2/NO_x/HO_x$ photolytic system. Laboratory studies of the O_3/O_2 and O_3/H_2O_2 photolytic systems and rate measurements in an $O/O_3/NO_x$ system illustrate the types and magnitudes of effects to be expected.

Garvin, D., **Progress in rate evaluations,** (Proc. 7th Thermochemistry Working Group, Interagency Chemical Rocket Propulsion Group, Cleveland, Ohio, Apr. 9-11, 1969), *CPIA Pub. 189*, **I**, 109-118 (Chemical Propulsion Information Agency, Johns Hopkins University, Applied Physics Laboratory, Silver Spring, Md., Aug. 1969).

Key words: Art of evaluation; chemical reactions; quality control measures; rate constants; rate evaluations.

A survey is given of recent activities in the area of evaluation of rates of chemical reactions. The problem of quality control is discussed. A recent evaluation of rates of reactions of oxygen is used to illustrate the uses of evaluated data and conclusions that can be drawn from them. A plan for expanding evaluation efforts is offered.

Geist, J., **New NBS scale of irradiance,** *Appl. Opt.* **12**, No. 4, 907-908 (Apr. 1973).

Key words: Electrically calibrated detectors; irradiance; total irradiance.

This letter presents a short report on the new NBS scale of total irradiance that was recently realized with an electrically calibrated detector. The results of intercomparisons of two such detectors as well as a comparison of the new scale with the old scale as maintained at NBS are presented.

Geist, J., **Theoretical analysis of laboratory blackbodies. 1: A generalized integral equation,** *Appl. Opt.* **12**, No. 6, 1325-1330 (June 1973).

Key words: Blackbody; holrahm radiation; radiometry; thermal radiative transfer.

The integral equations describing radiative equilibrium in a blackbody cavity are presented. Solving these equations in terms of the power sources in the furnace surrounding the cavity is not practical. However, if provisions are made for measuring the temperature over some surface between the power sources and the cavity interior, the analysis is feasible. This restriction and some realistic assumptions lead to a single, linear, inhomogeneous integral equation that approximately describes the interaction of the cavity geometry, the

thermal radiative properties of the cavity wall, and the temperature gradients within the cavity in reducing the quality of the blackbody. The formulation is general enough to accomodate realistic reflectance and temperature distributions for high quality blackbodies, and the accuracy of calculations based upon it will probably not be limited by approximations involved in its derivation, but by the present state of the art in the knowledge of the thermal radiative properties of materials.

Geltman, S., **Free-free radiation in electron-neutral atom collisions,** *J. Quant. Spectrosc. Radiat. Transfer* **13,** 601-613 (June 1973).

Key words: Bremsstrahlung; elastic scattering; free-free radiation.

Free-free absorption coefficients are calculated for the electron-neutral atom systems involving He, C, N, O, Ne, Ar, Kr, and Xe. The calculations are based upon model atomic potentials which have been adjusted to fit experimental scattering cross sections or electron affinities. Some angular distributions are presented and thermal averages are evaluated in the ranges $\lambda = 0.5 - 20\ \mu m$ and $T = 500 - 20{,}000$ K.

Ginnings, D. C., Reilly, M. L., **Calorimetric measurement of thermodynamic temperatures above 0 °C using total blackbody radiation,** (Proc. 5th Symp. on Temperature, Its Measurement and Control in Science and Industry, Washington, D.C., June 21-24, 1971), Paper in *Temperature, Its Measurement and Control in Science and Industry*, H. H. Plumb, Editor-in-Chief, **4,** Part 1, 339-348 (Instrument Society of America, Pittsburgh, Pa., 1972).

Key words: Blackbody; calorimeter; ice point; steam point; Stefan-Boltzmann law; thermodynamic temperature scale.

Using the Stefan-Boltzmann law, a thermodynamic temperature can be determined by measuring the ratio of blackbody radiation at the unknown temperature to that at the triple point of water. This measurement requires no knowledge either of radiation constants or of geometry. For the above measurements, there has been developed a heat-flow calorimeter operating at liquid helium temperatures in which extremely small powers can be accurately measured. The radiant power absorbed by the calorimeter is measured by substituting known electrical power; if these powers are equal the substitution results in no change in the temperature of the calorimeter.

The calorimeter was originally intended for measuring the thermodynamic temperature of the melting point of gold, but as a check on its performance, measurements are being made of the ratio of radiation at 100 °C to that of 0 °C (IPTS-68). Performance tests show the calorimeter to be sensitive to a change of about 0.002 °C in the temperature of the radiator with the chosen aperture system. There is now in progress an investigation of possible errors of the measurements, including any effect of diffraction.

Gonano, R., **Isothermal comparisons of He^3 and He^4 vapor pressures,** (Proc. 5th Symp. on Temperature, Its Measurement and Control in Science and Industry, Washington, D.C., June 21-24, 1971), Paper in *Temperature, Its Measurement and Control in Science and Industry*, H. H. Plumb, Editor-in-Chief, **4,** Part 1, 121-126 (Instrument Society of America, Pittsburgh, Pa., 1972).

Key words: Helium; pressure measurement; temperature scale; vapor pressure.

Isothermal measurements of He^3 and He^4 vapor pressures are being made in order to compare proposed vapor pressure scales in the region 0.90 to 3.32 K. Preliminary results in the range 1.40 to 3.25 K show that the currently accepted scales, T_{62} and T_{58}, are in close agreement with each other as was intended during the construction of T_{62}. Observed differences are less than 0.6 mK (rms deviation = 0.22 mK), which is within the experimental uncertainty of the present comparison. No systematic pattern is detectable in the deviations. A comparison of germanium resistance thermometers calibrated on the NBS Provisional Scale 2-20 (1965) with the vapor pressure scales shows that $T_{2\text{-}20} - T_{vp}$ ranges from 6 mK at 2.3 K to 10 mK at 4.2 K, in agreement with other published values. We also discuss the techniques used to reduce or eliminate the effects on vapor pressure measurements of the aerostatic and thermomolecular pressure gradients and of the heat load due to superfluid film flow.

Grabner, L., Wong, E. Y., **Zeeman effect of no-phonon $^4A_{2g}$ - $^4T_{2g}$ transition of Cr^{3+} in TiO_2,** *Phys. Rev. B* **8,** No. 3, 1032-1037 (Aug. 1, 1973).

Key words: Cr^{3+} in TiO_2; identification of excited state; $^4A_{2g}$-$^4T_{2g}$ transition; Zeeman effect.

The site symmetry of Cr^{3+} in TiO_2 is D_{2h} which splits the cubic (O_h) $^4T_{2g}$ state into $^4B_{1g}$, $^4B_{2g}$, and $^4B_{3g}$. Spin-orbit interaction further splits these states into six Kramers doublets all of symmetry Γ_5^+. Previous optical work on TiO_2: Cr^{3+} established the lowest-lying sharp lines at 12685 and 12732 cm^{-1} as no-phonon lines of magnetic dipole character. It proposed these lines as due to transitions between the $^4A_{2g}$ ground state and two of the above six states. The present report extends this work by a Zeeman study, in emission, at 4 K of the line at 12685 cm^{-1}. The results are: The Zeeman splitting of this line identifies the excited state of this transition as the $M_s = \pm 3/2$ spin-orbit component of an orbital state consisting of 77% $^4B_{2g}$, 17% $^4B_{1g}$, and 6% $^4B_{3g}$ with an effective $g = 1.73$. Furthermore, the line at 12732 cm^{-1} is identified as the $M_s = \pm 1/2$ spin-orbit component by its effect in second order in the magnetic field on the Zeeman pattern of the line at 12685 cm^{-1}. For the excited state the spin is quantized along the x direction of the magnetic axes while for the ground state it is quantized along the z direction. The reason for spin quantization along the x axis is discussed.

Guildner, L. A., Anderson, R. L., Edsinger, R. E., **Effects of sorption on the realization of the thermodynamic scale,** (Proc. 5th Symp. on Temperature, Its Measurement and Control in Science and Industry, Washington, D.C., June 21-24, 1971), Paper in *Temperature, Its Measurement and Control in Science and Industry*, H. H. Plumb, Editor-in-Chief, **4,** Part 1E, 313-322 (Instrument Society of America, Pittsburgh, Pa., 1972).

Key words: Gas thermometer; sorption; steam point; thermodynamic temperature scale.

The NBS Gas Thermometer is of the constant volume type. It has a 450 cm^3 platinum-20% rhodium bulb connected by a 0.9 mm internal diameter tube to a diaphragm at room temperature. The measured quantities contribute an estimated uncertainty of 5 parts per million. The gas thermometer has such stability that, upon return to the fiducial temperature, the pressure is reproduced within one or two parts per million for periods of a week or more. This stability is attributed to a marked reduction of sorption effects achieved by the following: (1) The thermometer bulb is subjected to prolonged pumping at high temperatures prior to measurements. (2) With most of the contaminants removed by this procedure, and the use of very pure helium as a thermometric fluid, there is too little active gas left to produce erratic results from sorption. The value of the temperature at the steam point on the thermodynamic Celsius scale has been determined as 99.973 °C. A final certainty is not assigned.

Hall, J. L., Bordé, C., **Measurement of methane hyperfine structure using laser saturated absorption,** *Phys. Rev. Lett.* **30,** No. 22, 1101-1104 (May 28, 1973).

Key words: Hyperfine spectrum; laser stabilization; methane; spectoscopy.

With optical resolution above 10^{10}, we study hyperfine structure in the methane vibration-rotation line at 3.39 μm. Doppler-generated

crossing resonances were observed in addition to the resolved $\Delta F = 0$ and -1 lines. Splittings in both ground and excited states were determined. Differential saturation of such hyperfine structure will lead to an intensity-dependent shift in many molecularly stabilized lasers.

Hamilton, C. A., **Analog-computer studies of mixing and parametric effects in Josephson junctions,** *J. Appl. Phys.* **44,** No. 5, 2371-2377 (May 1973).

Key words: Analog; Josephson junction; mixing; parametric.

Analog-computer studies are made on a variety of mixing and parametric effects in Josephson junctions. The predictions of the constant-voltage model are compared with the more general behavior of a junction in a resistive circuit. A simple approximate method is developed for calculating frequency conversion efficiency and the matching condition for a junction operating in the oscillator mixer mode. A similar calculation is made for the second mode of operation, in which an external local oscillator is used. In either of these modes, frequency conversion gain is possible even in a purely resistive circuit. The conditions for parametric amplification without frequency conversion are also studied and it is found that gain occurs only when the self-oscillation frequency is near the signal frequency.

Hastie, J. W., **Mass spectrometric studies of flame inhibition: Analysis of antimony trihalides in flames,** *Combust. Flame* **21,** 49-54 (1973).

Key words: Antimony trihalides; flame inhibition; flames; mass spectrometry.

The chemistry of $SbBr_3$ and $SbCl_3$ in 1 atm premixed fuel rich CH_4-O_2 and CH_4-O_2-N_2 flames has been studied. Using line-of-sight mass spectrometric techniques, concentration profiles were obtained for the major species SbX_3, HX, CH_3X, X, Sb, and SbO, where X = Br or Cl. Reaction mechanisms are indicated and their relation to flame inhibition discussed. Evidence for a negligible perturbation of the flame kinetics by the sampling procedure is given.

Hauge, R. H., Margrave, J. L., Hastie, J. W., **Infrared spectra of matrix isolated ZrF_2, ZrF_3, and ZrF_4,** *High Temp. Sci.* **5,** 89-96 (1973).

Key words: Entropy; geometry; infrared spectra; matrix isolation; stability; ZrF_2, ZrF_3, ZrF_4, CaF_2.

By using the multiple Knudsen cell technique the equilibrium species ZrF_2, ZrF_3, and ZrF_4 have been produced and isolated in rare gas solid matrices. From infrared spectra, the antisymmetric stretch frequencies have been assigned for each species. Isotope shift measurements indicate a $120° \pm 4°$ bond angle for the C_{2v}-ZrF_2 species, the symmetry being verified by the observation of the symmetric stretch frequency. The results are compared with those of the Ti-F and similar systems. The measured frequencies and bond angle of ZrF_2 were used to determine the entropy and FEF data for ZrF_2 at various temperatures.

Heinrich, K. F. J., **Errors in electron probe microanalysis,** *Proc. of the Seminar on Quantitative Analysis with Electron Microprobes and Secondary Ion Mass Spectrometry, Jülich, Germany, Oct. 18-20, 1972,* pp. 68-79 (Mar. 1973).

Key words: Data reduction; electron probe; errors; microanalysis; x-ray measurement.

Errors in quantitative electron probe microanalysis are due to errors in the measurement of relative characteristic x-ray intensities and in the interpretation of the experimental measurements. The random errors in the x-ray measurement include those due to Poisson's statistics, but other sources must not be excluded from consideration. Systematic errors may be committed in the estimation of coincidence losses (dead-time) and background. Those arising in the evaluation of the data may be due to the theoretical models, or to the parameters and constants which enter the calculation. Satisfactory models require adjustment to empirical measurements, and improvement in the accuracy of electron probe microanalysis requires the performing of critical experiments which can lead to further adjustment of the models. It is also important to adjust the conditions of measurement so as to minimize the effects of uncertainties and errors in models and parameters.

Heinrich, K. F. J., **The application of Monte-Carlo calculations in electron probe microanalysis,** *Proc. of the Seminar on Quantitative Analysis with Electron Microprobes and Secondary Ion Mass Spectrometry, Jülich, Germany, Oct. 18-20, 1972,* pp. 149-155 (Mar. 1973).

Key words: Data reduction; electron probe; Monte-Carlo calculations; thin layers.

The simulation of electron trajectories by means of the Monte-Carlo calculations offers an attractive alternative to the conventional data reduction procedures in electron probe microanalysis. It is particularly flexible with regard to specimen geometry, and should be very useful for the analysis of thin films and similar materials. However, as in the conventional procedures, approximations and empirical adjustments are necessary for the development of a useful model. The experiences derived from such a model can in turn be used to improve the conventional algebraic correction schemes.

Hessel, M. M., Lucatorto, T. B., **The rotating heat-pipe oven; a universal device for the containment of atomic and molecular vapors,** *Rev. Sci. Instrum.* **44,** No. 5, 561-563 (May 1973).

Key words: Heat pipe; indium iodide; laser application; sodium; spectroscopic application.

A new type of heat-pipe oven has been developed that uses centrifugal force as a return mechanism for the condensed vapors in contrast to capillary return forces for the conventional heat-pipe oven. Since this new oven is no longer limited to materials that wet wicks, it can be used to contain *any* material that does not react with the walls of the containing vessel. We describe the operation of this oven with sodium and InI even when the InI is solid. Spectroscopic and laser applications of the "rotating" heat-pipe oven are discussed.

Hsieh, C., Thomson, R., **Lattice theory of fracture and crack creep,** *J. Appl. Phys.* **44,** No. 5, 2051-2063 (May 1973).

Key words: Creep of crack; fracture; lattice theory.

A quasianalytic solution for the atomic displacements of a discrete two-dimensional lattice containing a crack is obtained. We assume that the force laws are linear up to a critical displacement when the bond snaps, which is the basic assumption of the lattice static approximation. When compared to the classic Griffith continuum description, new results are: (i) a predicted and observable lattice trapping of the crack, (ii) difficulties with the interpretations of the crystal surface energy in a cleavage experiment, and (iii) a predicted characteristic crack creep phenomenon under external constant stress. The present theory shows how two separate "surface energies" are inferred from the stress to open and to close a crack, and on our model these energies differ from one another by a large factor of 5.7. The thermodynamic "surface energy" is not related to either of these quantities. Experimental verification of the lattice trapping of cracks is thought to be most readily and directly obtained by observations of the creep of a crack under high vacuum conditions.

Hudson, R. P., Pfeiffer, E. R., **Temperature scale for cerous magnesium nitrate,** (Proc. 5th Symp. on Temperature, Its Measurement and Control in Science and Industry, Washington, D.C. June 21-24, 1971), Paper in *Temperature, Its Measurement and Con*

trol in Science and Industry, H. H. Plumb, Editor-in-Chief, **4**, Part 2, 1279-1285 (Instrument Society of America, Pittsburgh, Pa., 1972).

Key words: Cerous magnesium nitrate; low temperature; magnetic temperature; temperature scale; thermometry.

Below 1 K, cerous magnesium nitrate (CMN) should obey the Curie Law over a wide temperature range and show deviations only in consequence of the dipolar coupling between ions. The susceptibility deviation should be accounted for by a very small Curie-Weiss θ (theoretical value, 0.27 mK) and the entropy should vary as $\ln 2 - AT^{-2} + BT^{-3} - CT^{-4} + \ldots$, with theoretical values now available for A, B and—somewhat less firmly based —C. These show that representation of S(T) by the term in A alone is justifiable only above 0.1 K. We present experimental values for A, B, and C arising from recent measurements together with new results for the magnetic temperature, T*, scale derived from γ-ray heating calorimetry.

Huggett, C., **Carpet flammability and the NBS corridor fire program,** *ASTM Stand. News* **1**, No. 5, 16-20 (May 1973).

Key words: Carpets; corridor fires; fire test; flammability; floor coverings.

The NBS corridor fire program was designed to study the effects of configuration, fuel loading and distribution, ventilation, and other design parameters on the spread of fire through corridors in multiple occupancy buildings. A fully instrumented 8 ft × 8 ft × 30 ft corridor is used to carry out full-scale experiments. Fires are started in a connecting 8 ft × 8 ft × 9 ft fire room and the rate and intensity of fire spread in the corridor is observed.

Floor coverings have received special attention during the initial phase of the program. With a sufficiently intense room fire source, fire can spread rapidly over the surface of a carpet in the corridor, even with noncombustible wall and ceiling surfaces. Radiative energy transfer to the carpet surface appears to be the controlling mechanism. When the carpet starts to burn, additional energy feedback causes an accelerated propagation down the corridor. The fire spread is characterized in terms of critical energy input necessary to cause propagation, rate of fire spread, and energy contribution of the carpet to the fire.

Results of typical experiments are described. Preliminary experiments relating to the development of a test method to assess the hazard potential of floor coverings in building, based on a critical energy concept, are described.

Hust, J. G., Clark, A. F., **A survey of compatibility of materials with high pressure oxygen service,** *Cryogenics* **13**, No. 6, 325-336 (June 1973).

Key words: Compatibility data; high pressure; oxygen; safety; survey.

The literature on high pressure oxygen compatibility has been surveyed in order to present the existing state of knowledge. Searches have been conducted of NASA and NBS data retrieval systems. In addition, many individuals, active in the field, were contacted in order to retrieve useful unpublished information. Compatibility data, such as mechanical impact, pneumatic impact, ignition temperature, and flash-and-fire point, were compiled for pressures above 200 bar (2×10^7 Nm^{-2}). Lower pressure data were included if they were useful for extrapolation to pressures above 200 bar. These data, too numerous to be given here, are available from the authors. Brief descriptions of the trends of these data are given. Recommendations for additional high pressure studies are included.

Hust, J. G., Powell, R. L., Sparks, L. L., **Methods for cryogenic thermocouple thermometry,** (Proc. 5th Symp. on Temperature, Its Measurement and Control in Science and Industry, Washington, D.C., June 21-24, 1971), Paper in *Temperature, Its Measurement and Control in Science and Industry*, H. H. Plumb, Editor-in-Chief, **4**, Part 3, 1525-1535 (Instrument Society of America, Pittsburgh, Pa., 1972).

Key words: Cryogenics; thermocouples; thermometry.

Accurate cryogenic thermocouple thermometry is only possible if care is taken in material selection, general experimental design, thermocouple calibration and assembly, and measurement techniques. After several years' research on both calibration and usage of thermocouples, we have developed procedures and tests that minimize experimental temperature errors and give realistic estimates of the inaccuracies.

Some material selection criteria are listed and recommendations are given for a few common experimental conditions. Simple experimental systems are described that may be used for tests to determine static or dynamic short range inhomogeneities, variability and interchangeability of different lots, and deviations from standard values. Methods for adding corrections to the standard tables are also given.

Good design criteria and methods of thermocouple assembly can lead to significant improvement in accuracies. Specific topics of discussion include reference junction placement, thermal tempering, heat conduction and radiation shielding, electrical connections, and electrical shielding.

Jacox, M. E., Milligan, D. E., **Matrix isolation study of the vacuum-ultraviolet photolysis of methanol. The infrared spectrum of the CH_2OH free radical,** *J. Mol. Spectrosc.* **47**, No. 1, 148-162 (July 1973).

Key words: CH_2OH; force constants; infrared spectrum; matrix isolation; methanol; vacuum-ultraviolet photolysis.

Infrared studies of the products of the 1470 Å photolysis of normal and isotopically substituted methanol isolated in argon and nitrogen matrices at 14 °K have provided evidence for the stabilization of a significant yield of CH_2OH. Assuming a slightly nonplanar structure for the molecule, it has been possible to obtain an approximate valence-force potential field which provides a reasonable fit to virtually all of the data. The C-O bond of CH_2OH is slightly stronger than that of methanol, and the torsional barrier is significantly greater, in accord with previous electron spin resonance observations. There is no evidence for the production or stabilization of CH_3O in the matrix. CH_2OH undergoes photodecomposition upon exposure to radiation in the 2300-2800 Å spectral region, leading to a growth in the HCO absorptions.

Jones, F. E., **Air density and helicopter lift,** *Joint Army-Navy Aircraft Instrumentation Research, JANAIR Report No. 721201*, 54 pages (Available as AD 754420 from the National Technical Information Service, Springfield, Va. 22151, Jan. 1973).

Key words: Air density; helicopter lift; ideal gas law.

An analysis has been made of ideal and real gas equations as they apply to the calculation of air density in the region of interest for helicopter flight. The uncertainties in calculated air density due to uncertainties in measurements of temperature, pressure and humidity have been investigated and estimates have been made of measurement accuracies which would be required to enable calculation of air density with a desired relative uncertainty. A reference system has been assembled to provide measurements of temperature, pressure and dew-point temperature aboard a helicopter. This system is to be used in making calculations of reference air density for flight tests of a system for computing hover lift margin and several devices for measuring air density. The effects on hover lift margin, defined by a simple equation, of relative uncertainties in air density and power have been investigated. Nuclear statistics as they apply to "direct" mea-

525-013 O - 74 - 6

surements of air density by application of nuclear radiation are discussed.

Kamper, R. A., Simmonds, M. B., Adair, R. T., Hoer, C. A., **Quantum mechanical measurement of rf attenuation,** *Proc. 1972 Applied Superconductivity Conf., Annapolis, Md., May 1-3, 1972*, pp. 696-700 (IEEE, Inc., New York, N.Y., 1972).

Key words: Josephson effect; quantum interference; rf attenuation; rf measurements; superconductivity.

We have used a broadband Superconducting QUantum Interference Device (SQUID), operating at a frequency of 9 GHz, as a sensor of current at lower radio frequencies. The periodic nature of the response of the SQUID enabled us to measure variations in rf attenuation directly. The results of such a measurement were in agreement with the NBS Calibration Service to within ±0.004 dB over a dynamic range of 40 dB. We also discuss other applications of this SQUID to rf measurements.

Kamper, R. A., **Survey of noise thermometry,** (Proc. 5th Symp. on Temperature, Its Measurement and Control in Science and Industry, Washington, D.C., June 21-24, 1971), Paper in *Temperature, Its Measurement and Control in Science and Industry*, H. H. Plumb, Editor-in-Chief, **4**, Part 1, 349-354 (Instrument Society of America, Pittsburgh, Pa., 1972).

Key words: Absolute temperature; thermal noise; thermometry.

This survey covers various techniques which have been developed to estimate relative or absolute temperatures by measuring various parts of the spectrum of thermal noise at frequencies in the microwave range and below. It includes a report of the author's own work on absolute noise thermometry in the millikelvin range of temperature.

Keplinger, M. S., **The case for invisible copies,** *Proc. 33d Annual Meeting of the American Society for Information Science, Philadelphia, Pa., Oct. 11-15, 1970*, **7**, 241-243 (1970).

Key words: Computers; copyright; information storage and retrieval; infringement; input; intellectual property; proprietary rights.

The problem of control of the use of copyrighted works in computerized information storage and retrieval systems is discussed. It is concluded that such input may be considered copyright infringement under the current Copyright Revision Bill as interpreted through the teachings of recent court decisions, as well as being an infringement under the current copyright statute.

Kirchhoff, W. H., **Microwave spectroscopy,** *Chem. Eng. News* **47**, 88-98 (Mar. 24, 1969).

Key words: Dipole moment; microwave spectroscopy; molecular rotation; molecular structure; qualitative analysis; quantitative analysis.

A review of microwave spectroscopy is presented with special emphasis on its applications to problems of chemical interest. The fundamental concepts of molecular rotation are discussed using classical mechanics, and the relationship of molecular structure and forces with the molecular rotation is presented. The quantum mechanical model is then presented with sufficient detail to understand the nature of rotational spectroscopy. The Stark effect and its dependence on the molecular dipole moment is briefly described. Recent instrumental advances as well as the application of microwave spectroscopy to quantitative and qualitative analysis are mentioned.

Koonce, C. S., **Enhancement effects: Theory,** (Proc. of a Summer Course on The Science and Technology of superconductivity, held at Georgetown University, Washington, D.C., Aug. 13-26, 1971), Paper in *The Science and Technology of Superconductivity*, W. D. Gregory, W. N. Mathews, Jr., and E. A. Edelsack, Eds., **1**, 389-403 (Plenum Press, New York, N.Y., 1973).

Key words: Dielectric function; superconductor; transition metal; transition temperature.

A discussion of which modifications of normal state properties such as phonon frequencies and electronic density of states as a function of energy are likely to enhance the superconducting transition temperature will be given. A discussion of the methods of modification of the material properties such as alloying, doping applying pressure and forming thin films will also be given.

Koonce, C. S., **Theory of superconducting semiconductors,** (Proc. of a Summer Course on The Science and Technology of Superconductivity, held at Georgetown University, Washington, D.C., Aug. 13-26, 1971), Paper in *The Science and Technology of Superconductivity*, W. D. Gregory, W. N. Mathews, Jr., and E. A. Edelsack, Eds., **1**, 373-387 (Plenum Press, New York, N.Y., 1973).

Key words: Energy gap equation; semiconductors; superconductor; transition temperature.

The BCS theory of superconductivity will be applied to degenerate semiconductors. Methods of calculating superconducting properties of degenerate semi-conductors will be compared with methods used to calculate superconducting properties of metals. The normal state properties of degenerate semiconductors which are important in determining the superconducting properties will be discussed.

Kruger, J., **Application of ellipsometry to electrochemistry,** Chapter in *Advances in Electrochemistry and Electrochemical Engineering*, R. H. Muller, Ed., **9**, 227-280 (John Wiley & Sons, Inc., New York, N.Y. 1973).

Key words: Corrosion; electrochemistry; electropolishing; ellipsometry; electrodeposition.

A review of the application of ellipsometry to electrochemistry is given which considers the electrochemical phenomena of passivation and corrosion, electroadsorption, electrodeposition and electropolishing. The ellipsometry of bare surfaces and gaseous adsorption as related to electrochemistry is discussed. Both the advantages and limitations of the techniques are considered. Over a hundred references are cited.

Kuriyama, M., **Dynamical diffraction equations for imperfect crystals,** *Z. Naturforsch.* **28a**, No. 5, 622-626 (1973).

Key words: Canonical transformation; dynamical diffraction; imperfect crystal.

The ray theory of Kato and Kambe for imperfect crystals is derived in a formal way from a general dynamical theory of diffraction. This development together with the results from a previous paper concerning Takagi's equation (the wave theory) helps to clarify the meaning and limits of various phenomenological theories that have been extended to an imperfect crystal from the dynamical diffraction theory for a perfect crystal.

LaFleur, P. D., **Retention of mercury when freeze-drying biological materials,** *Anal. Chem.* **45**, No. 8, 1534-1536 (July 1973).

Key words: Freeze-drying; lyophilization; mercury; mercury loss; methylmercury; nuclear activation analysis; phenylmercuric acetate.

The retention on freeze-drying of three compounds of mercury tagged with mercury-203 and fed to experimental animals, has been measured. The compounds employed in the investigation were methylmercuric chloride, phenylmercuric acetate and mercuric nitrate. The retention of mercury was determined radiometrically on

individual tissues and on blood and feces. The effect of prefreezing the samples, prior to the lyophilization cycle, was also studied.

LaVilla, R. E., **$M_{2,3}$-Region x-ray emission spectrum from gaseous krypton,** *Phys. Rev. A.* **8,** No. 2, 1143-1145 (Aug. 1973).

Key words: Double electron single vacancy process; final state configuration interaction; krypton; $M_{2,3}$ x-ray emission; single electron double vacancy process.

The $M_{2,3}$ x-ray emission spectrum of gaseous krypton excited by direct electron bombardment has been recorded with a scanning single-flat crystal spectrometer. The most prominent spectral features are two peaks at 187 and 203 eV, with the 187-eV peak having an extended low-energy tail. This low-energy tail is attributed to double-electron single-vacancy transitions owing to the strong mixing of the final-state configuration $4s4p^6\ ^2S$ with the even levels $4s^24p^4ns\ ^2S$ and $4s^24p^4nd\ ^2S$. The 203-eV peak is identified as probably the single-electron double-vacancy $M_{2,3}M_{2,3} \rightarrow M_{2,3}N_1$ multiplet complex.

Leasure, W. A., Jr., Rubin, A. I., Fath, J. M., Fisher, R. L., Flynn, D. R., **Fundamentals of noise: Measurement, rating schemes, and standards,** *Environmental Protection Agency Report No. NTID300.15,* 163 pages (Available as PB 206727 from the National Technical Information Service, Springfield, Va. 22151, Dec. 31, 1971).

Key words: Acoustics; environmental pollution; noise; sound.

This report is intended to serve as an introduction to noise, including the inter-relationship between physical measures and psychological responses. The basic principles of sound generation and propagation are discussed as well as the measurement of both the physical attributes of noise and the effects of noise on people. The suitability and effectiveness of various noise exposure rating schemes, used to estimate or predict the effects of noise on man, are discussed and critiqued. Included are sample calculations of sound level, loudness level, and perceived noise level for five selected spectra. The need is stressed for inclusion of well-defined environmental and operational requirements into measurement procedures for those devices where the noise produced is dependent on the surroundings and the operation of the device. Also presented are a glossary of pertinent acoustic terminology and a compilation of existing standards related to noise, including a brief description of the intent and scope of each.

Lee, R. D., Kostkowski, H. J., Quinn, T. J., Chandler, P. R., Jones, T. P., Tapping, J., Kunz, H., **Intercomparison of the IPTS 68 above 1064 °C by four national laboratories,** (Proc. 5th Symp. on Temperature, Its Measurement and Control in Science and Industry, Washington, D.C., June 21-24, 1971), Paper in *Temperature, Its Measurement and Control in Science and Industry,* H. H. Plumb, Editor-in-Chief, **4,** Part 1, 377-393 (Instrument Society of America, Pittsburgh, Pa., 1972).

Key words: International temperature scale; pyrometry; standards; temperature.

The International Practical Temperature Scale above the melting point of gold, as realized and maintained with high precision photoelectric pyrometers at NBS, NPL, NSL and PTB, has been intercompared. Six specially selected tungsten strip lamps, four vacuum and two gas, were used in the intercomparison. Determinations were made at a number of brightness temperatures from 1064 to 1700 °C and at 2200 °C with the laboratories agreeing to within a few tenths of a degree up to 1700 °C and 2.0 °C at 2200 °C.

Lee, T. G., Huggett, C., **Interlaboratory evaluation of the tunnel test (ASTM E 84) applied to floor coverings,** *NBSIR 73-125,* 56 pages, (Mar. 1973). (Available as COM 73-11189 from the National Technical Information Service, Springfield, Va. 22151.)

Key words: ASTM E 84; building materials; carpets; fire tests; flame spread tests; interlaboratory evaluation; round robin; statistical analysis; test method standard.

Results of an interlaboratory evaluation of the ASTM E 84 tunnel test method involving eleven laboratories and nine materials, including four carpets, are reported. Data on flame spread, smoke, and fuel contribution are analyzed statistically. Selected physical characteristics of each tunnel are tabulated and compared relative to specifications in the test method. The between-laboratory coefficient of variation (reproducibility) in flame spread classification (FSC) was found to range from 7 to 29% for the four carpets and from 18 to 43% for the other materials tested. The between-laboratory coefficients of variation for smoke developed and fuel contribution ranged from 34 to 85% and from 22 to 117% respectively for all materials tested. The causes of higher variability in smoke and fuel contribution measurement between laboratories is not definitely known but may reasonably be attributed to variations in tunnel construction, maintenance, and operation, in the location of photometers, and in the mounting of thermocouples in different laboratories. Some variability of results may possibly be due to variation in test specimens. Variation in construction and measurement techniques among tunnels may be minimized by updating the test method standard.

Le Neindre, B., Tufeu, R., Bury, P., Sengers, J. V., **Thermal conductivity of carbon dioxide and steam in the supercritical region,** *Ber. Bunsenges. Physik. Chem.* **77,** No. 4, 262-275 (1973).

Key words: Carbon dioxide; critical phenomena; steam; thermal conductivity; transport properties.

The thermal conductivity of carbon dioxide and steam has been measured as a function of temperature and density using a concentric cylinder method. Earlier measurements of the thermal conductivity of CO_2, obtained with a parallel plate method, covered a range of temperatures from 25 to 75 °C and revealed the existence of an anomalous thermal conductivity in the critical region. In this paper the experimental temperature range for the thermal conductivity of CO_2 is extended to 700 °C. The high temperature data enable us to determine a "background" thermal conductivity needed for a quantitative analysis of the anomalous thermal conductivity in the critical region. In addition, we provide experimental evidence that the thermal conductivity of steam exhibits an anomalous increase in the critical region similar to the behavior observed for the thermal conductivity of CO_2.

Lew, H. S., **The effect of impact loadings on the performance of wood joist subflooring systems,** *NBSIR 73-187,* 49 pages (May 1973). (Available as PB 221188 from the National Technical Information Service, Springfield, Va. 22151.)

Key words: Concentrated loads; deflection; floor hardboard; housing; impact energy; Operation BREAKTHROUGH; plywood; subfloors; underlayment; wood; wood joists.

This report presents the results of an experimental study of wood-joist subflooring systems subjected to impact load. Six different types of subflooring systems were tested following the test method described in the ASTM Standard Methods (ASTM Designation E-72). The magnitude of impact load was varied by dropping a 60-lb bag from different heights.

A concentrated static load of 400 lb was applied to the subfloor after it was exposed to impact load. It is suggested that the deflection under this concentrated load be used as a measure of the impact resistance of the subfloor.

Liebman, J. F., **On the electron affinity of perfluorocycloalkanes and perfluoroalkanes,** *J. Fluorine Chem.* **3,** 27-33 (1973/74).

Key words: Electron affinity; fluorocarbons; orbital; perfluoroalkanes; perfluorocycloalkanes.

There is an increasing body of evidence showing that perfluorocycloalkanes have a higher electron affinity than their open chain analogs, the perfluoroalkanes. A new molecular orbital model is presented to explain these results and compared with the electrostatic model of Mittal and Libby. Explicit experiments are suggested which would allow comparison of the two models.

Linsky, J. L., **A recalibration of the quiet sun millimeter spectrum based on the moon as an absolute radiometric standard,** *Solar Phys.* **28,** No. 2, 409-418 (Feb. 1973).

Key words: Millimeter absolute radiometry; millimeter solar continuum; solar chromosphere.

The solar millimeter continuum between 1 and 20 mm is recalibrated using observations of the average lunar brightness temperature at the center of lunar disk and new Moon brightness temperatures. The solar data are placed on a common scale according to the average lunar brightness temperature distribution proposed by Linsky. A least-squares parabolic regression curve is proposed for the solar millimeter continuum. A small departure from this regression curve near 8 mm may indicate the existence of an absorption feature.

Lozier, D. W., Maximon, L. C., Sadowski, W. L., **A bit comparison program for algorithm testing,** *Comput. J.* **16,** No. 2, 111-117 (May 1973).

Key words: Algorithm testing; bit comparison testing; computer algorithm; mathematical function subroutines.

In view of the increasingly important role of the computer in scientific calculations, the development of computer algorithms for elementary and special functions has been given a great deal of attention. The development of algorithms cannot be divorced from their evaluation, for a computer algorithm is judged solely on the basis of its performance characteristics. These include storage requirements, speed and accuracy. The present paper will deal only with the accuracy aspect of algorithm testing. The other two aspects must be evaluated in the context in which the algorithm is used. In this paper by an algorithm we mean a computer algorithm, i.e., an implementation of a mathematical algorithm in a specific environment. The environment is taken to include factors that may affect the algorithm, e.g., the operating system under which the program is run and hardware algorithms for arithmetic operations. Whereas in some instances mathematical algorithms have been successfully used to locate hardware malfunctions that were not traceable by normal trouble shooting tests, any malfunctions of the software or hardware will not be considered here to be part of the environment.

Maienthal, E. J., **Determination of trace elements in metals by differential cathode ray polarography,** *Amer. Lab.*, pp. 25-33 (1972).

Key words: Alloys; analyses; cast irons; differential cathode ray polarography; high purity materials; metals; steels; trace elements.

Some of the recent applications of cathode ray polarography at NBS to the determination of a number of trace elements in different metal matrices will be discussed. Some of the elements could be determined directly with no separations. The elements determined included aluminum, antimony, copper, cadmium, iron, lead, bismuth, and tellurium in matrices such as steels, high temperature alloys, white cast irons, brasses, bronzes, and high purity metals. The results will be compared with those obtained by other techniques.

Maki, A. G., Sams, R. L., Olson, W. B., **Infrared determination of C_0 for phosphine via perturbation-allowed $\Delta|k-l|=\pm 3$ transitions in the $3\nu_2$ band,** *J. Chem. Phys.* **58,** No. 10, 4502-4512 (May 15, 1973).

Key words: Forbidden transitions; ground state splitting; infrared spectrum; perturbation allowed transitions; phosphine; rotational constants.

The $3\nu_2(A_1)$ and $4\nu_2 - \nu_2(A_1)$ infrared bands of PH_3 have been measured with high resolution. In the $\nu_2=3$ state an interaction between the K and $K\pm3$ levels gives rise to perturbation allowed $\Delta K=3$ transitions through a weak high order interaction. Since only one component of the $K=3$ levels is of the proper symmetry to interact with the $K=0$ levels there is a splitting of the $K=3$ levels. Also detectable is the splitting of the $K=3$ levels of the ground vibrational state. The measurements have been combined with microwave measurements to give accurate values for the ground state rotational constants B_0, C_0, D_0^J, D_0^{JK}, D_0^K, H_0^J, H_0^{JJK}, and H_0^{JKK}. The absence of observable inversion effects sets an upper limit of about 0.02 cm^{-1} for the inversion splitting of the $4\nu_2$ level.

Martin, W. C., **Some aspects of the energy-level structures of lanthanide atoms and ions,** *Opt. Pura Apl.* **5,** No. 3, 181-191 (1972).

Key words: Atomic spectra; energy levels; rare earths.

The development of our understanding of some main features of these structures is reviewed, and the present degree of completeness of the analyses and theoretical interpretations of the spectra is indicated. Energy differences of the type $4f^{N-1}nl(6s^M) - 4f^N(6s^M)$(with each configuration represented by its lowest level) are of special importance, both for the analyses of a number of the spectra and for the interpretation of certain basic data for metals and compounds of these elements. The general behavior of such differences as a function of N is understood, and the resulting graphs are very similar to the d-shell energy-difference graphs studied by Catalán, Rohrlich, and Shenstone, and by Racah. The data confirm striking regularities among the f-shell graphs, first used by Racah, that yield predictions of unknown system differences and, for third and higher spectra, of inonization energies ($M=0$, $n=\infty$).

McCamy, C. S., Pope, C. I., **Redox blemishes—their cause and prevention,** (Proc. National Microfilm Association, Boston, Mass., May 7, 1969), *J. Microgr.* **3,** No. 4, 165-170 (June 1970).

Key words: Archival records; microfilm; redox blemishes.

A type of small spots and character-associated defects on some microfilm were investigated by a variety of techniques. The blemishes result from the displacement of image silver by an oxidation-reduction reaction caused by peroxides and other gaseous products of degradation of the paper cartons in which the films are stored. A method of producing blemishes for test purposes was developed. Recommendations cover the materials, processes, and storage conditions for microfilm preservation of records of permanent value.

McCamy, C. S., Pope, C. I., **The stability of silver-gelatin images,** (Proc. 2d Int. Congress on Reprography, Cologne, Germany, Oct. 25-31, 1967), Paper A3-1 in Section A3 of *Reprographie* **II,** 112-115 (Verlag Dr. Othmar Helwich, Darmstadt, Germany und Wien, Austria, 1969).

Key words: Aging blemishes; blemishes, microfilm; film storage; microfilm; microfilm image stability.

Though microfilm has been in commercial use in the United States for 40 years, recent observations of blemishes on film have occasioned a re-evaluation of factors affecting long-term stability. Six types of blemishes appear to be the result of oxidation-reduction reactions initiated by gaseous reactants. These reactants are traceable to the cardboard containers in which reels of film have been stored. Statistical analysis of data gathered by 100 film inspectors supports this conclusion. Laboratory experiments ruled out biological causes. Experiments prove the existence of oxidizing and reducing

agents, formaldehyde, and formic acid in the atmosphere within cardboard containers. Appropriate films, properly processed and stored in inert containers, at a relative humidity under 40 percent and temperature under 21 °C, should be as durable as the best record paper.

McCamy, C. S., **Properties of photographic films related to information recovery,** *SPIE Seminar Proc. on Image Information Recovery, Philadelphia, Pa., Oct. 24-25, 1968,* **16,** 11-19 (Society of Photo-Optical Instrumentation Engineers, Redondo Beach, Calif., 1969).

Key words: Image processing; photographic films; photographic information.

New concepts, terminology, and symbolic notation simplify the precise treatment of optical density, which is the fundamental quantity in information recovery. The resolving power of optical and photographic systems may be treated as discrete or statistical, visual or instrumental and may be a guide to information capacity. The photographic spread function is the key to understanding image formation. The ambiguity of the modulation transfer function requires recourse to more rigorous analytic methods. Granularity, spatial effects of processing, temporal effects, and dimensional stability are important considerations in information recovery.

McCamy, C. S., **The evaluation and manipulation of photographic images,** Chapter in *Picture Processing and Psychopictorics,* A. Rosenfeld and B. S. Lipkin, Eds., 57-74 (Academic Press, Inc., New York, N.Y., 1970).

Key words: Image evaluation; image manipulation; image optics; photography.

The scientific use of photography in the study of the psychophysics of images requires a knowledge of the techniques employed in specifying the characteristics of optical and photographic systems and the available techniques for manipulating photographic images. The primary measure of the photographic effect is *optical density*, a quantity which depends on the method of measurement in a complex way. The photographic process is quantitatively characterized by sensitometry. Image structure is characterized by resolving power, spread function, modulation transfer function, pupil function, acutance, and granularity. Photographic images may be manipulated by various forms of dodging, masking, and special processing.

McClenon, R., **General purpose scientific document code operations under Exec 8,** *NBSIR 73-198,* 21 pages, (May 1973). (Available as COM 73-11289 from the National Technical Information Service, Springfield, Va. 22151.)

Key words: Character codes for scientific text; computerized text processing; NBS computer system; scientific text; users manual.

Operating procedures for the use of the General Purpose Scientific Document Code text handling system are described. These apply to the use of the system on the NBS 1108 computer under control of the Exec 8 supervisor. Control cards, file definition and handling, compilation of routines and execution of programs are described. Examples of typical runs are given. The report is a manual for users of the system.

McLaughlin, W. L., Bjergbakke, E., **Electrochemical dosimetry using ferric-fluoride ion complex formation,** (Proc. Int. Symp. on Dosimetry in Agriculture, Industry, Biology and Medicine, Vienna, Austria, Apr. 1972), Paper in *Dosimetry in Agriculture, Industry, Biology and Medicine,* pp. 383-396 (International Atomic Energy Agency, Vienna, Austria, 1973).

Key words: Dosimetry; electrochemistry; ferric-fluoride complex; ferrous sulfate solutions; fluorides; Fricke dosimeter; ion selective electrodes; lanthanum fluoride; potentiometry.

Irradiated aqueous ferrous sulphate solutions containing fluoride ions can be analysed for ferric ion yield by means of electrochemical potentiometry. For certain applications this approach has advantages over the usual method of spectrophotometric determination of ferric ion concentration, which also varies linearly with absorbed dose up to about 40 krad: (1) Small dosimeter volumes down to 10 microlitres are functional; (2) Solid gels may be used, thus allowing for thin-film geometries; (3) The potentiometric method permits real-time (current readings) or integrated (EMF readings) measurement of radiation dose. The electrochemical analysis of ion-complex yield is fairly simple. A fluoride ion electrode of the solid-state type serves as an ion-selective sensor. The electrochemical potential (or its rate of change in some instances) between the fluoride ion electrode and the reference electrode is then read on a pH-meter. Since the Fe^{3+} cation complex with F^- is not passed by the lanthanum fluoride crystal membrane at the end of the electrode probe, and since the free F^- ion concentration diminishes linearly with dose up to about 40 krad (corresponding to approximately 0.4m*M* Fe^{3+} ion concentration at pH 2.7), the dose or dose rate can be determined from readings of linear change in millivoltage or rate of change of millivoltage. For cobalt-60 gamma-ray irradiation of a 1.00m*M* solution of Fe^{2+} and F^- made to pH 2.7 with H_2SO_4, the G-value of Fe^{3+} -F^- complex formation is 13.7 $\pm$0.3 per 100 eV energy absorbed. This G-value is in good agreement with the initial G-value 13.75 of the Fricke dosimeter at pH 2.74.

McLaughlin, W. L., Hjortenberg, P. E., Radak, B. B., **Absorbed-dose measurements with thin films,** (Proc. Int. Symp. on Doismetry in Agriculture, Industry, Biology and Medicine, Vienna, Austria, April 1972), Paper in *Dosimetry in Agriculture, Industry, Biology and Medicine,* pp. 577-597 (International Atomic Energy Agency, Vienna, Austria, 1973).

Key words: Absorbed dose; calorimetry; cavity theory; depth dose; dosimetry; dye dosimeters; electron beams; gamma rays; plastic dosimeters; radiochromic dyes; thin films.

Thin films of plastic, coatings, papers, ceramics, emulsions, cleaved crystals, microtomed gel sections, and metal foils have all been used with advantage to measure large radiation absorbed doses. The three most successful methods of relating the radiation effects in the film to the dose are: Calorimetry, which measures temperature rise; photometry, which measures changes in light emission, transmission or reflection; and electrometry, which measures electrical changes such as variations in resistivity, e.m.f., current, etc. The chief problems in making good measurements of radiation dose or dose rate with thin films are: (1) quality control of the dosimeter itself; (2) discontinuity problems, that is, how the energy imparted to a thin probe is related to energy imparted to surrounding matter; (3) meaning of the calibration, that is, how the radiation effect in the film material is related to the absorbed energy as a function of spectrum dose rate, temperature, etc. The first of these can be dealt with effectively by control of film thickness, chemical composition and environmental influences. The second is often more complicated, especially if the thin probe differs appreciably in absolute density and atomic number from its surroundings, since proper application of cavity theory may be difficult for some geometrical arrangements. The third problem is usually the most difficult of all, because the radiation effect in a thin material used as a dosimeter often depends on many variables leading to systematic errors in dose interpretations. In this work, methods are given for calibrating in electron beams the radiation response of thin-film dosimeters calorimetrically, accounting for the sources of error cited above. The calibration procedures include the use of appropriate cavity-theory correction factors needed to relate the response of the thin probe of one material held in another medium. Finally, a suitable film dosimeter material is described. It consists of radiochromic dye films, which can measure doses from about 10^4 to 10^8 rad in various media under different irradiation conditions.

McLaughlin, W. L., Kosanić, M., Draganić, I. G., **Extending the response of the pararosaniline dye system,** (Proc. Int. Symp. on Dosimetry in Agriculture, Industry, Biology and Medicine, Vienna, Austria, Apr. 1972), Paper in *Dosimetry in Agriculture, Industry, Biology and Medicine*, pp. 362-366 (International Atomic Energy Agency, Vienna, Austria, 1973).

Key words: Dosimetry; dyes; gamma rays; nitrobenzene; oxidation; pararosaniline cyanide; radiochromic dyes; triphenylmethane dyes.

Organic solutions of triphenylmethane dye precursors, particularly pararosaniline cyanide (4, 4', 4'' -triamino-triphenylacetonitrile) and hexa (hydroxyethyl) pararosaniline cyanide (4, 4', 4''-tris- (di-β-hydroxyethylamino) triphenylacetonitrile, have been used successfully in measuring gamma-ray absorbed doses in the range from 1 to 100 krad. With conventional slightly acidified and aerated ether alcohol solutions of the dye precursors, the optical density read at the absorption maximum in the visible portion of the spectrum increases linearly with dose up to about 100 krad. Saturation and bleaching of the solutions at doses between 100 and 200 krad limit the usefulness of these liquid systems. A recent study has been performed at the Boris Kidric Institute of Nuclear Sciences and the Danish Atomic Energy Commission, Research Establishment Risø, for the purpose of making chemical adjustments in the solutions so that higher absorbed doses may be measured with a linear optical density-versus-dose response.

Meijer, P. H. E., **Calculations on the specific heat and the susceptibility of interacting spin systems,** (Proc. 5th Symp. on Temperature, Its Measurement and Control in Science and Industry, Washington, D.C., June 21-24, 1971), Paper in *Temperature, Its Measurement and Control in Science and Industry*, H. H. Plumb, Editor-in-Chief, **4**, Part 1, 1267-1278 (Instrument Society of America, Pittsburgh, Pa., 1972).

Key words: Dipole-dipole interactions; low temperature salts; specific heat; susceptibility.

The corrections on the specific heat and susceptibility due to dipole-dipole interactions in a number of low temperature compounds are calculated. A general description of the method is given, followed by a short discussion of the properties of the most used low temperature compounds. Eight representative salts were chosen and the deviations from the ideal specific heat and susceptibility in second and third order were determined.

Milligan, D. E., Jacox, M. E., **Infrared spectroscopic evidence for the stabilization of HAr_n^+ in solid argon at 14 K,** *J. Mol. Spectrosc.* **46**, No. 3, 460-469 (June 1973).

Key words: Argon reactions; $H(^2S)$ reaction with Ar: HAr_n^+; infrared spectrum; interstitial H atom spectrum; matrix isolation; proton affinity; vacuum ultraviolet photolysis.

Absorptions which have been observed at 905 and at 644 cm^{-1} upon 1216-Å photolysis of hydrogen- and deuterium-containing compounds, respectively, in an argon matrix correspond well with similar absorptions reported in studies of the trapped products of a glow discharge through $Ar:H_2$ and $Ar:D_2$ mixtures. Evidence is presented supporting the assignment of these two absorptions to HAr_n^+ and to DAr_n^+ rather than to interstitial H and D atoms trapped in octahedral sites in the argon lattice.

Mitchell, R. A., Woolley, R. M., Chwirut, D. J., **Composite-overlay reinforcement of cutouts and cracks in metal sheet,** *NBSIR 73-201*, 96 pages, (Feb. 1973). (Available as COM 73-11121 from the National Technical Information Service, Springfield, Va. 22151.)

Key words: Adhesively bonded joints; composite materials; composite-overlay reinforcement; contour plotting; cracks, reinforcement of; cutouts, reinforcement of; debond analysis, progressive; finite element analysis; joints, adhesively bonded; nonlinear analysis, shear; reinforcement, composite overlay; reinforcement, cutouts and cracks; shear analysis, nonlinear.

Finite element computer programs were developed for the planform analysis and the longitudinal cross-section analysis of metal sheet reinforced by adhesively bonded overlays of composite material. The analyses articulate the separate responses of the metal sheet, the composite overlays, and the adhesive layers. All materials are assumed to be orthotropic and linear elastic, with the provision that nonlinear interlaminar shear deformation can be approximated by a series of stepwise-linear solutions. The computer programs were developed specifically for the study of three general configurations: (1) a sheet with a reinforced cutout; (2) a sheet with a reinforced cutout with two symmetrical transverse cracks, within the sheet, radiating away from the cutout edge; and (3) a sheet with a reinforced transverse crack. The programs are also suitable for the study of bonded lap joints. The principal output of the computer programs is a set of contour plots of stress and strain fields throughout the sheet, the overlays, and the adhesive layers. A series of laboratory tests was conducted to demonstrate the validity of the analyses. Strains measured on the surfaces of specimens representing the general configurations studied were, for the most part, in good agreement with strains predicted by the finite element analyses. Significant correlations between certain failure modes and the stresses computed by the finite element analyses were apparent. Similarities between the modes of failure under static and fatigue loading were also evident.

Mittag, K., **Kapitza conductance and thermal conductivity of copper niobium and aluminum in the range from 1.3 to 2.1 K,** *Cryogenics* **13**, No. 2, 94-99 (Feb. 1973).

Key words: Aluminum; copper; heat transfer; Kapitza conductance; niobium; superfluid helium; thermal conductivity.

The Kapitza conductance and thermal conductivity of ofhc-copper, niobium, ultra high purity aluminium, and of the aluminium alloy 6061 Al have been measured in the temperature range from 1.3 to 2.1 K, yielding both quantities in the same steady state experiment. The temperature dependence of the Kapitza conductance, h_0, was between $T^{3.3}$ and $T^{4.6}$ for the different samples, which is higher than the most frequently observed T^3 dependence. The magnitude of h_0 for both ofhc-copper and aluminium agrees well at 1.9 K with an empirical prediction, but for niobium it is a factor of two to four lower than the value predicted. At 1.9 K, h_0 is higher by a factor of two for an annealed and chemically polished niobium sample than for an untreated sample. The thermal conductivity measured from ofhc-copper and 6061 Al as in good agreement with the value calculated from the resistivity of these materials and the Wiedemann-Franz law. The measured thermal conductivity obtained for an annealed niobium sample is a factor of 2.8 higher than the highest published value.

Molino, J., **Perceiving the range of a sound source when the direction is known,** *J. Acoust. Soc. Amer.* **53**, No. 5, 1301-1304 (May 1973).

Key words: Audition and ranging; physiological and psychological acoustics; psychophysics; space perception.

A modification is proposed in Hirsch's equation for determining the range of a sound source of unknown strength [H. R. Hirsch, J. Acoust. Soc. Am. **43**, 373-374 (1968)]. The modified formula applies to the case where the direction of the sound source is known. Greene's comments on Hirsch's letter are investigated for their ability to predict the limitations on the resolution obtainable in human auditory ranging [D. C. Greene, J. Acoust. Soc. Am. **44**, 634 (1968)]. In a brief experiment, two subjects were unable to make distance judgments for sustained pure-tone sources over ranges of 3 to 48 ft.

Moore, R. T., **Penetration tests on J-SIIDS barriers,** *NBSIR 73-223*, 86 pages, (June 4, 1973). (Available as COM 73-11120 from the National Technical Information Service, Springfield, Va. 22151.)

Key words: Barrier penetration; intrusion resistance; physical security.

A series of penetration tests were made on three simulated arms rooms which incorporated a variety of structural barriers which were intended to be representative of the broad range of construction likely to be encountered in existing arms rooms.

The observed penetration times varied from 1.3 minutes for a double-planked wooden wall, 11.31 minutes for an eight-inch thick, reinforced concrete wall and up to 18.27 minutes for a GSA Class 6 vault door. All penetrations were made with portable readily available tooling and produced acoustical or vibrational or both types of disturbances which are readily detectable.

The test results provide a basis for estimating the time in which response to an intrusion alarm must occur in order to adequately safeguard an arms room, a computer room or any other sensitive area.

Moriarty, J. E., **City I: Player's Manual,** *NBSIR 73-110*, 149 pages (Mar. 1973). (Available as COM 73-11191 from the National Technical Information Service, Springfield, Va. 22151.)

Key words: City; computer; directors; economic; games; government; metropolitan; players; sectors; simulation; social; urban.

City I is an operational simulation game in which participants make economic, government, and social decisions affecting a hypothetical metropolitan area. Through the use of a computer, the simulated urban system responds to the participant's decisions as any real city would. Each player in City I is assigned to a team which shares an economic and governmental role. This manual describes the player details for the economic and government sectors along with general information required for game play. It is one of three manuals necessary for game play. (Player's Manual, Director's Manual, Computer Operator's Manual). Each of these manuals are designed to be used for reference and by themselves will not describe enough details for a complete game play.

Negas, T., **The $SrMnO_{3-x}$-Mn_3O_4 system,** *J. Solid State Chem.* **7,** 85-88 (1973).

Key words: Nonstoichiometry; phase equilibria; $SrMnO_{3-x}$-Mn_3O_4 system; $SrMn_3O_{6-x}$.

Phase relations were determined in the $SrMnO_{3-x}$-Mn_3O_4 system at elevated temperatures in air using quenching, gravimetric, and x-ray diffraction techniques. The system contains one intermediate compound, $SrMn_3O_{6-x}$ ($0 \leq x \leq 0.10$ between 900-1200 °C), which decomposes to $SrMnO_{3-x}$ plus Mn_3O_4 near 1215 °C. The existence of an oxygen deficient $SrMnO_{3-x}$ having the hexagonal 4-layer structure was confirmed. Crystals of perovskite-like $SrMnO_{3-x}$ ($x < 0.25$) were grown from its primary field located in the system.

Okabe, H., Splitstone, P. L., Ball, J. J., **Ambient and source SO_2 detector based on a fluorescence method,** *J. Air Pollut. Contr. Ass.* **23,** No. 6, 514-516 (June 1973).

Key words: Air pollutant; detector, fluorescence; SO_2.

The principle of this detector is based on the measurement of the intensity of the ultraviolet fluorescence of SO_2 produced by absorption of the Zn 2138 Å or Cd 2288 Å line. The fluorescence intensity was found to be linear from 0.1 to 500 ppm of SO_2 in air with the Zn lamp and from 0.1 to 1600 ppm with the Cd lamp. The detection limit at present is about 20 ppb. There is no detectable interference from O_3, H_2S, NO_2, CO_2, CO, or H_2, although the presence of a large concentration of CS_2 (500 times as much as SO_2) NO (500 times) or C_2H_4 (4000 times) interferes with the measurement. The presence of 2 percent H_2O reduces the signal by 25 percent, while up to 1 percent CH_4 has almost no effect.

Olien, N. A., Sarkes, L. A., **Keeping up with LNG—a new literary awareness service helps to do the job,** *Amer. Gas Ass. Mon.* **55,** No. 7-8, 29 and 31 (July-Aug. 1973).

Key words: Current awareness services; information retrieval; information systems; Liquefied Natural Gas; methane; methane mixtures.

A description is given of the methods used by the Cryogenic Data Center in covering the current published and patent literature. The services provided to the Cryogenic industry are also discussed. The *Liquefied Natural Gas Quarterly* which has been published since 1970 is covered in detail. It is noted that nearly 2,000 articles, papers, reports, and patents dealing with LNG have been listed in the twelve issues of the quarterly published to date. A series of comprehensive bibliographies on LNG, methane, and methane mixtures is also described.

Omont, A., Smith, E. W., Cooper, J., **Redistribution of resonance radiation. I. The effect of collisions,** *Astrophys. J.* **175,** No. 1, Part 1, 185-199 (July 1972).

Key words: Collisional depolarization; level degeneracy; redistribution functions; resonance radiation.

The techniques of modern line-broadening theory are used to investigate the scattering of polarized radiation in the rest frame of an atom undergoing collisions. The formulation explicity includes both elastic and inelastic (quenching) collisions. When the lower state has zero width, a form for the redistribution function similar to that of Zanstra is obtained, but with the redistribution in the neighborhood of the resonance line being caused solely by elastic collisions. In the limit of no collisions, but with both levels of finite lifetime, the result of Weisskopf and Woolley is obtained. The effect of level-degeneracy is also explicitly included; in this case the results are a function of the polarization of the light and the different relaxation rates for the multipolar components of the atomic states.

Omont, A., Smith, E. W., Cooper, J., **Redistribution of resonance radiation. II. The effect of magnetic fields,** *Astrophys. J.* **182,** No. 1, Part 1, 283-300 (May 15, 1973).

Key words: Irreducible tensor formalism; magnetic fields; resonance radiation.

Previously obtained results for scattering of radiation in the presence of collisions are restated in a density matrix formalism which employs an irreducible-tensor description of the radiation field. This formalism is particularly useful for problems associated with radiative transfer theory. The redistribution is then extended to include the effect of a weak magnetic field. By averaging over a finite bandwith which is on the order of the Doppler width, simplified expressions of physical significance for the scattering in the Doppler core and the Lorentz wings are obtained. Expressions are also obtained for the corresponding source function of radiative transfer theory.

Orcutt, R. H., **Interlot density variation of a siloxane manometer fluid,** *J. Vac. Sci. Technol.* **10,** No. 4, p. 506 (July-Aug. 1973).

Key words: Diffusion pump fluid; micromanometry; silicone.

The mean value of density for six samples of a siloxane manometer fluid is 1.06311 g/cm^3 with an estimated standard deviation of 11×10^{-5} g/cm^3 for the lot-to-lot variation in density of this fluid. From this result it is concluded that for use of this material in manometry to the 0.01% level the density of the actual fluid used must be determined.

Peiser, H. S., Corruccini, R. J., Newman, S. B., **Standardization and measurement services in Turkey,** *NBSIR 73-172*, 90 pages (Oct. 14-28, 1972). (Available as COM 73-11175 from the National Technical Information Service, Springfield, Va. 22151.)

Key words: AID; assistance; economics; LDC's (less developed countries); measurement services; standardization; survey; Turkey.

The survey of standardization and measurement services for developing industries in Turkey has been carried out by NBS with funding by AID, with participation by representatives of Ecuador and Korea, and under the guidance of the Turkish Standards Institute. The Survey Team spent two weeks in Turkey where it inspected representative laboratories and plants, and had discussions with leaders of Government, the USAID Mission, principal universities and industry. The Report describes the preparation for the Survey, a summary of the economy of the country soon to be a full member of the European Common Market, notes on Turkish science and technology and the independent Turkish Standards Institute recognized by law as the national standards body. Issues addressed are 1) Standards Development, 2) Test Methodology, 3) Product Certification, 4) Product Testing, 5) Calibration, 6) Weights and Measures Control, 7) Export Control, 8) Quality Control, 9) Consumer Protection, 10) Industrial Extension, 11) Building Codes, 12) International Contacts, and 13) Publications. The principal conclusion is that the Turkish economy would benefit from a strengthening of standardization and measurement services. Appropriate recommendations are offered.

Peiser, H. S., Coyle, T. D., Eby, R. K., **A report on a survey in Korea on standardization and measurement services in support of industrialization goals of Korea.** *NBSIR 73-185*, 41 pages, (June 19-30, 1972). (Available as COM 73-11287 from the National Technical Information Service, Springfield, Va. 22151.)

Key words: AID; assistance; economics; LDC's (less developed countries); measurement services; standardization; survey; Korea.

The survey of standardization and measurement services for developing industries in Korea has been carried out by NBS with funding by AID, participation by representatives of Ecuador and Turkey, and under the guidance of the Korean Ministers for Commerce and Industry, and for Science and Technology. The Korean Director of the Survey was backed by six Korean Survey Team members and seven senior staff. The Survey Team spent two weeks in Korea where it inspected representative laboratories and plants, and had discussions with leaders of government, the USAID Mission, principal universities and industry. The report describes the preparation for the Survey, a summary of the economy of the country, notes on Korean science and technology, and relevant Korean institutions and laws. Nineteen problems were identified as of concern to national capability for standardization and measurement services. A summary description is given of the various existing and needed functions that Korean government should provide. The idea is endorsed to create a single agency to address all these functions.

Peterson, R. L., **Kinks in the magnetophonon oscillations of semiconductors,** *Phys. Rev. B* **7,** No. 12, 5405-5408 (June 15, 1973).

Key words: Magnetophonon effect; semiconductors; transport theory.

Exact expressions for the discontinuities in the magnetic field derivative of the longitudinal drift mobility at the magnetophonon resonance and pseudoresonance fields are given for nonpolar semiconductors with combined optic- and acoustic-phonon scattering of carriers. The reasons for the discontinuities are discussed in physical terms.

Pierce, E. T., Kelly, K. L., McPherson, M. A., Howett, G. L., Booker, R. L., **Emergency vehicle warning devices: Interim review of the state-of-the-art relative to performance standards,** *LESP-RPT-0501-00*, 73 pages. Available as PB 211938 from the National Technical Information Service, Springfield, Va. 22151, (U.S. Department of Justice, Law Enforcement Assistance Administration, National Institute of Law Enforcement and Criminal Justice, Washington, D.C., May 1972).

Key words: Action; communication; conspicuity; controlled environment; effectiveness; flashing lights; guidelines; information; laboratory testing; people; response; sirens; standards.

This interim progress report describes the activities carried out, from the initiation of the program through July 1971, concerning the preparation of performance standards for emergency vehicle warning devices (lights and sirens). A partial survey of present standards and specifications indicated that there now are very few meaningful performance standards for emergency warning lights and essentially none for sirens. Brief descriptions of those standards which were found are included. Manufacturer's literature on available warning devices rarely includes meaningful quantitative data on the physical performance characteristics of either lights or sirens. The program strategy described in this report includes (a) quantitative physical characterization of the spectral content, directionality, level, and time duration of the signals from a representative sampling of emergency vehicle warning equipment; (b) literature and laboratory study of the effectiveness of representative signals in alerting drivers to an emergency situation requiring appropriate reactions; and (c) development of draft standards. In conjunction with the physical characterization of lights and sirens, examples are given of the type of data which will be taken and detailed descriptions are given of the facilities which will be used for these measurements. A discussion is given of the various factors which influence the effectiveness of warning signals. It is proposed to study both the time elapsing between the occurrence of a signal and the completion of the required response (complex reaction time) and the distance at which an observer first notices and correctly interprets a signal (recognition distance). Performance standards can then be prepared which are clearly related to the appropriate human responses.

Pike, R. G., Hay, R. E., Clifton, J. R., Beeghly, H. F., Mathey, R. G., **Nonmetallic coatings for concrete reinforcing bars,** *Public Roads* **37,** No. 5, 185-197 (June 1973).

Key words: Chlorides; concrete; corrosion; epoxy coatings; organic coating; steel reinforcing bars.

The study reported here was conducted to determine the feasibility of using organic coatings, especially epoxies, to protect steel reinforcing bars embedded in concrete from corrosion accelerated by chloride ions.

Coatings were evaluated on the basis of their chemical and physical durabilities as well as their protective qualities. In this study, attention was also directed to the application methods and surface preparation of the steel reinforcing bars. Four different materials appear to be suitable for such coatings.

Powell, C. J., **Contrasting valence-band Auger-electron spectra for silver and aluminum,** *Phys. Rev. Lett.* **30,** No. 23, 1179-1182 (June 4, 1973).

Key words: Aluminum; Auger electron transitions; electronic density of states; final state effects; silver; transition probabilities.

Measurements of the $L_{2,3}VV$ (V=valence) Auger spectrum of aluminum and the $M_{4,5}VV$ Auger spectrum of silver cannot be simply related to the valence-band density of states. The data for Al indicate a strong energy variation of the transition probability. For silver, the position and shape of the Auger spectrum are associated with multiplet splitting of localized double-d-hole final states.

Powell, C. J., **High-resolution measurements of Auger-electron and photoelectron structure in the secondary-elec-**

tron energy distributions of aluminum, nickel and copper, (Proc. Int. Conf. on Inner Shell Ionization Phenomena and Future Applications, Atlanta, Ga., Apr. 17-22, 1972), Paper in *Proceedings of the International Conference on Inner Shell Ionization Phenomena and Future Applications*, R. W. Fink, S. T. Manson, J. M. Palms and P. V. Rao, Eds., CONF-720404, 1, 743-756 (U.S. Atomic Energy Commission, Technical Information Center, Oak Ridge, Tenn., Jan. 1973).

Key words: Aluminum; Auger-transitions; copper; electronic density of states; nickel; photoelectron energy distribution; secondary-electron energy distribution; x-ray photoemission.

Measurements are reported of selected structure in the secondary electron energy distributions of evaporated aluminum, nickel and copper. The specimens were bombarded with 3 keV electrons and the secondary structure was measured with a resolution of 0.1 eV. For each metal, attention was given primarily to data that could give information on the valence-band density of states.

Attempts were made to observe the $AlKL_{2,3}M$ Auger-electron energy distribution expected at about 1470 eV. Structure was, however, observed with a high-energy edge of 1485.9 ± 0.5 eV and a breadth of 8-9 eV. This structure was interpreted as being due to photoemission of valence electrons by internally generated Kα x-rays and was similar to uv photoelectron distributions and to the calculated density of states. Inelastic scattering of the photoelectrons obscures the expected $AlKL_{2,3}M$ structure.

Auger electron peaks in the ranges 730-800 eV and 820 to 865 eV were measured in the energy spectra for nickel and copper, respectively. Structure was observed in the $L_3M_{2,3}M_{4,5}$ transition which could be associated in part with solid-state effects and in part with the final atomic states of each element. Density-of-states data could not be derived from the Auger spectra without more detailed knowledge of the final states expected after the Auger transition of interest.

Powell, R. L., Hall, W. J., Hust, J. G., **The fitting of resistance thermometer data by orthogonal functions,** (Proc. 5th Symp. on Temperature, Its Measurement and Control in Science and Industry, Washington, D.C., June 21-24, 1971), Paper in *Temperature, Its Measurement and Control in Science and Industry*, H. H. Plumb, Editor-in-Chief, **4**, Part 2, 1423-1431 (Instrument Society of America, Pittsburgh, Pa., 1972).

Key words: Numerical analysis; orthogonal functions; resistance thermometer.

Analyses of highly accurate thermal data require sophisticated fitting methods so that expensively obtained experimental precision will not be negated by inadequate mathematical techniques. This article describes fitting methods using orthogonal functions that have been used for several years to fit many types of data, including germanium resistance curves. The method is a generalization and extension of ideas suggested earlier by Lanczos for fitting noisy data. The method usually cleanly separates noise from the fundamental signal in a straightforward manner, allowing one to avoid either an oscillating overfit or an inaccurate underfit. The procedure consists of five parts: (1) transformation of variables so that the curve is as linear as possible in the transformed variables; (2) weighting of data to satisfy the Gauss-Markoff conditions with the weighting function inversely proportional to the experimental variance; (3) orthogonal function generation and coefficient determination using Gram-Schmidt type algorithms developed by Bjorck; (4) separation of noise coefficients from the fundamental signal coefficients based on their different dependence on the number of terms; and (5) calculation of smoothed data using the proper number of coefficients.

Powell, R. L., **Revision of the standard reference data for thermocouples,** (Proc. 5th Symp. on Temperature, Its Measurement and Control in Science and Industry, Washington, D.C., June 21-24, 1971), Paper in *Temperature, Its Measurement and Control in Science and Industry*, H. H. Plumb, Editor-in-Chief, **4**, Part 3, 1579-1584 (Instrument Society of America, Pittsburgh, Pa., 1972).

Key words: Standard Reference Data; thermocouples.

Revision of the International Practical Temperature Scale requires that there be changes for all accurately tabulated thermophysical values. Revised reference data for thermocouples have been generated in a cooperative program between groups of the National Bureau of Standards in Boulder and Gaithersburg. The new reference data reflect not only revisions in the temperature scale, but also slight changes in the materials themselves and improvements in data fitting methods. A new NBS monograph that contains tables, analytic expressions, various approximations, and explanatory text has been prepared. A general discussion of the project and some specific examples will be given.

Quinn, T. J., Lee, R. D., **Vacuum tungsten strip lamps with improved stability as radiance temperature standards,** (Proc. 5th Symp. on Temperature, Its Measurement and Control in Science and Industry, Washington, D.C., June 21-24, 1971), Paper in *Temperature, Its Measurement and Control in Science and Industry*, H. H. Plumb, Editor-in-Chief, **4**, Part 1, 395-411 (Instrument Society of America, Pittsburgh, Pa., 1972).

Key words: Pyrometry; source; temperature; tungsten.

This paper describes the changes which take place in a piece of tungsten strip as it is outgassed and aged during the processing of a vacuum tungsten strip lamp. It is shown that by paying sufficient attention to the cleaning of the tungsten and the glass bulb, and to the outgassing and aging of the tungsten, a very stable strip lamp can be produced. Results are given of a series of stability tests from 1064 to 1500 °C of a group of lamps made in this way at NBS.

Reader, J., **Comment on: How to mount a Pellin-Broca prism for laser work,** *Appl. Opt.* **12**, No. 7, 1405 (July 1973).

Key words: Pellin-Broca prism; spectroscope.

It is shown that a recently published mounting for constant deviation prisms is equivalent to one published in 1917. An example of the use of this mounting for a plane grating spectrograph at NBS is given.

Reed, R. P., Arvidson, J. M., Durcholz, R. L., **Tensile properties of polyurethane and polystyrene foams from 76 to 300 K,** (Proc. 1972 Cryogenic Engineering Conf., Boulder, Colo., Aug. 9-11, 1972), Paper E-3 in *Advances in Cryogenic Engineering* **18**, 184-193 (Plenum Press, New York, N.Y., 1973).

Key words: Foams; low temperature; tensile properties.

The tensile properties of 17 different polyurethane foams and 2 polystyrene foams have been measured at 300, 195 and 76 K. The Young's modulus, yield strength and tensile strength increased with decreasing temperature, while the elongation decreased. Strength and Young's modulus were found to be approximately linearly dependent on temperature; however, at low temperatures the density dependence was greater. Specimens whose long axis was cut parallel to the cell rise direction were stronger than those whose long axis was cut normal to the cell rise direction. Comparisons between foam tensile and compressive properties are presented in the accompanying paper.

Reichard, T. W., Greene, W. E., Jr., Cattaneo, L. E., Masters, L. W., **Structural tests on housing components of glass fiber reinforced polyester laminate,** *NBSIR 73-188*, 98 pages (Apr. 1973). (Available as PB 221183 from the National Technical Information Service, Springfield, Va. 22151.)

Key words: Adhesive bond; aging; composites; compression; flexure; glass fiber; housing system; innovations; laminate;

Operation BREAKTHROUGH; racking; reinforced plastics; reinforced polyester; sustained loading; tensile shear.

This report describes a series of structural evaluation tests performed on housing components made with a glass fiber reinforced polyester (FRP) laminate. The components tested were: (1) the FRP laminate used for the facings and the corrugated core of the basic panel; (2) the adhesive bond between the facing and core; (3) typical wall panels; and (4) typical roof panels. Test data include: (1) the effect of temperature and moisture on the tensile and compressive strength of the FRP laminate; (2) the effect of temperature, accelerated aging and sustained loads on the tensile shear strength of the facing-to-core polyester adhesive bond; (3) the short-term strength of the wall panels under compressive and in-plane shear loading; (4) the long-term strength of the wall panels under sustained compressive loading; and (5) the short-term and long-term performance of the roof panels under flexural loading.

Reno, R. C., Swartzendruber, L. J., **Origin of Mössbauer linewidth in stainless steel,** (Proc. 18th AIP Conf. on Magnetism and Magnetic Materials, Denver, Colo., Nov. 28-Dec. 1, 1972), Paper in *Magnetism and Magnetic Materials*, C. D. Graham, Jr., and J. J. Rhyne, Eds., No. 10, 1350-1353 (American Institute of Physics, New York, N.Y., 1973).

Key words: Hyperfine fields; perturbed angular correlation, Mössbauer effect; stainless steel.

The hyperfine interactions which broaden the Mössbauer effect (ME) spectrum in austenitic stainless steel have been investigated with the aid of ^{57}Fe time-differential perturbed angular correlations (TDPAC). The TDPAC measurements reveal a distribution of electric field gradients at the ^{57}Fe nuclei with a mean value corresponding to a Mössbauer splitting of 0.14 mm/s. This splitting is not sufficient to explain the total line width and isomer shifts are invoked to account for the remaining width.

Robertson, A. F., Rappaport, M. W., **Fire extinguishment in oxygen enriched atmospheres,** *NASA CR-121150*, 60 pages (National Aeronautics and Space Administration, Washington, D.C., Feb. 1973).

Key words: Controlled atmospheres; extinguishing; fire extinguishers; fires; halons; oxygen; spacecraft cabin atmospheres; water.

Current state-of-the-art of fire suppression and extinguishment technique in oxygen enriched atmosphere is reviewed. Four classes of extinguishment action are considered: cooling, separation of reactants, dilution or removal of fuel, and use of chemically reactive agents. Current practice seems to show preference for very fast acting water spray applications to all interior surfaces of earth-based chambers. In space, reliance has been placed on fire prevention methods through the removal of ignition sources and use of nonflammable materials. Recommendations are made for further work related to fire suppression and extinguishment in oxygen enriched atmospheres, and an extensive bibliography is appended.

Roder, H. M., **A new phase transition in solid hydrogen?,** *Cryogenics Letter to Editors* **13,** No. 7, 439-440 (July 1973).

Key words: Hydrogen; phase transition.

Available but often discordant data on PVT, dielectric constant, specific heat, velocity of sound, and melting pressures are interpreted to indicate the possibility of a transition in solid hydrogen. This structural change, suggested by others previously, has not yet been investigated as thoroughly as the corresponding transition in solid helium.

Rosenstock, H. M., Larkins, J. T., Walker, J. A., **Interpretation of photoionization thresholds: Quasiequilibrium theory and the fragmentation of benzene,** *Int. J. Mass Spectrom. Ion Phys.* **11,** 309-328 (1973).

Key words: Appearance potential; benzene; photoionization; quasiequilibrium theory.

Quasiequilibrium theory has been applied to the parent ion fragmentation of benzene. Assuming uniform excitation energy transfer in the fragmentation threshold region and applicability of the step-function photoionization threshold law, it is possible to calculate fragment photoionization threshold curves in good agreement with experiment. It is concluded that the unimolecular decomposition occurs via two independent pairs of competing reactions. One pair of reactions leads to the formation of $C_6H_5^+$ and $C_6H_4^+$, and involves the benzene ion ground state. The other pair of reactions, leading to $C_4H_4^+$ and $C_3H_3^+$ involves the first excited state of $C_6H_6^+$ lying 2.25 eV above the ground state, or an open chain isomer having a similar heat of formation. At threshold the $C_6H_5^+$ ion has a phenyl ion structure, the $C_3H_3^+$ ion a cyclopropenyl ion structure and the $C_4H_4^+$ ion may have a cyclobutene ion structure. A heat of formation of ~ 100 kcal/mol is derived for the benzyne molecule, in good agreement with semi-empirical estimates. Kinetic shift effects on the fragmentation thresholds are found to be important. Some difficulties are encountered in the comparison of relative abundances of parent ion metastable transitions to the relative abundances of the daughter ions near threshold. The calculated energy dependence of the unimolecular rate of formation of $C_4H_4^+$ ion is in good agreement with experiment. However, the weak energy dependence of the rate of formation of $C_6H_6^+$ found experimentally cannot be explained. Suggestions for further work are outlined.

Roth, R. S., Parker, H. S., Brower, W. S., Waring, J. L., **Phase equilibria, crystal chemistry and crystal growth of alkali oxide-metal oxide systems,** (Proc. NATO sponsored Advanced Study Institute, Belgirate, Italy, Sept. 1972), Paper in *Fast Ion Transport in Solids*, pp. 217-232 (North-Holland Publ. Co., Amsterdam, The Netherlands, 1973).

Key words: Alkali oxides; crystal chemistry; crystal growth; phase equilibria; system $LiTaO_3$-Ta_2O_5; system $NaTaO_3$-Ta_2O_5; system $KTaO_3$-Ta_2O_5.

In view of the recently discovered properties of the sodium ion in β-alumina, it is of some scientific and practical importance to review the chemistry of alkali ions in oxide systems in general. From a practical point of view, however, the number of systems of interest will necessarily be severely limited. For commercial utilization of ionic conductivity it is necessary to limit systems to those which will contain little or no electronic conductivity and therefore do not contain an element which is easily reduced during the synthesis. For fast ion transport it is probably advantageous to have an alkalai ion in a "non-stoichiometric" crystallographic position. Attention will be concentrated on methods of study of alkali oxide-tantalum oxide systems as applied to the search for new crystallographic phases which may be of interest.

New results are presented of phase equilibria studies in the systems Li_2O, Na_2O and K_2O with Ta_2O_5 and Li_2O with Nb_2O_5. In addition preliminary results will be discussed of the ternary systems involving the binaries with MoO_3. These ternary systems have been utilized for flux-growth of single crystals of many of the new phases in the binary systems. Each of the Ta_2O_5 systems has at least one interesting non-stoichiometric phase which deserves further study for conductivity properties. A phase in the Li_2O-Ta_2O_5 system has the structure of the low-temperature form of Ta_2O_5, the Na_2O-Ta_2O_5 system contains a phase with a "tetragonal-bronze"-like structure and the K_2O-Ta_2O_5 system has both "tetragonal-" and "hexagonal-bronze"-like phases. In the sub-system Ta_2O_5-$KTaO_3$ eleven distinct phases have been found where only two were previously known.

Roszman, L. J., Hooper, C. F., Jr., **Distribution of the time-dependent microfield in a plasma,** *Phys. Rev. A* **7,** No. 6, 2121-2130 (June 1973).

Key words: Distribution; Holtsmark; ion dynamics; microfield; plasma; time-average.

The theory of the distribution of the time average of the time-dependent microfield in a quantum plasma taken over a finite time interval is introduced and developed. The short- and long-time limits are derived. The Wigner phase-space representation is employed to derive the correct distribution for a classical plasma and to establish a formalism which can be used for low-order quantum corrections. Numerical results are presented for a classical gas of charged noninteracting particles. It is found that for time-averaging intervals, which are larger than the time it takes a particle traveling with the average thermal velocity to cross the ion-sphere radius, the distribution deviates from the corresponding Holtsmark distribution for the quasi-static model.

Rubin, A. I., **The social impact of noise: A survey of medical, psychological, and social consequences,** *Environmental Protection Agency Report No. NTID300.11,* 25 pages (Available as PB 206724 from the National Technical Information Service, Springfield, Va. 22151, Dec. 1971).

Key words: Noise; noise sources; social impact.

Noise is an environmental pollutant which shares many characteristics with other pollutants—its levels are increasing, more and more people are being affected; its consequences are medical, psychological and social. Man has been successful in producing labor-saving devices used during work and play as well as to provide many forms of transportation. However, an associated by-product is increasingly in evidence as the machines have become more powerful, namely *Noise.* Whereas only midcity areas, heavy industries and communities near airports were formerly recognized as being "special" problems because of the noise levels associated with them; this is no longer true. Intrusive noise pervades the home, industry and most recreation areas now since, where man has moved, he has taken his machines with him. This pervasiveness of noise has led to actions by individuals, groups, and many levels of government to "do something about the problem." Among the methods attempted have been regional planning, zoning ordinances, government standards and regulations, and individual law suits. Thus far these approaches have not been successful. The number of people exposed to hazardous noise levels is increasing, the quality of our auditory environment is being degraded, and the social impact of noise may substantially contribute to other problems in our society.

Rupp, N. W., **Intermediary base and cementation,** Chapter 5 in *Operative Dentistry,* L. Baum, Ed., pp. 59-72 (W. B. Saunders Co., Philadelphia, Pa., 1973).

Key words: Cementation; intermediary base; pulp protection; retention; temporary cementation.

This is a literature review of the dental cements currently being used for intermediary bases and cementation. Clinical applications of the various cements are discussed relative to physical properties and biological response of tooth tissues. Some recently introduced materials are included.

Schneider, S. J., Levin, E. M., **Polymorphism of K_2CO_3,** *J. Amer. Ceram. Soc.—Discussions and Notes* **56,** No. 4, 218-219 (1973).

Key words: DSC; DTA; high temperature x-ray; K_2CO_3; phase transformation; polymorphs.

The polymorphism of K_2CO_3 was investigated by differential thermal analysis, differential scanning calorimetry and high temperature x-ray diffraction techniques. The data indicate that K_2CO_3 is dimorphic with a 2nd order transformation from a monoclinic form to a hexagonal modification occurring at 420 ± 5 °C. Unit cell dimensions as a function of temperature and a representative x-ray powder pattern of hexagonal K_2CO_3 are given.

Schooley, J. F., **Enhancement effects,** (Proc. Summer Course on The Science and Technology of Superconductivity, held at Georgetown University, Washington, D.C., Aug. 13-26, 1971), Paper in *The Science and Technology of Superconductivity,* W. D. Gregory, W. N. Mathews, Jr., and E. A. Edelsack, Eds., **1,** 405-428 (Plenum Press, New York, N.Y., 1973).

Key words: High transition temperature; pressure effects; proximity effect; superconductive alloys; superconductive compounds; superconductivity.

Superconductivity research has had as one of its continuing aims the production of high-transition-temperature materials. This situation arises from the realization that superconductivity can be applied to transportation, communication, power transmission, and instrumentation on a wider and more efficient basis, the higher the transition temperature. Many of these applications will be discussed during this course by several of the lecturers.

In this lecture, I will discuss various ways in which experimenters have attempted to generate high transition temperatures.

Schooley, J. F., Soulen, R. J., Jr., **The use of superconductors to provide fixed points on a cryogenic temperature scale,** (Proc. 5th Symp. on Temperature, Its Measurement and Control in Science and Industry, Washington, D.C., June 21-24, 1971), Paper in *Temperature, Its Measurement and Control in Science and Industry,* H. H. Plumb, Editor-in-Chief, **4,** Part 1, 169-174 (Instrument Society of America, Pittsburgh, Pa., 1972).

Key words: Fixed points; OSRM; superconductive devices; superconductive transition temperature; superconductivity; temperature scale.

It is suggested that reproducible superconductive transition temperatures be used as fixed points for temperature scales below 10K. The superconductive transitions of lead, indium, aluminum, zinc, and cadmium have been found to be as narrow as one millikelvin and reproducible to less than one millikelvin. It is planned that devices incorporating these elements will be made available through the NBS Office of Standard Reference Materials.

Schooley, J. F., **Superconductors in Thermometry,** (Proc. Summer Course on The Science and Technology of Superconductivity held at Georgetown University, Washington, D.C., Aug. 13-26, 1971), Paper in *Science and Technology of Superconductivity,* W. D. Gregory, W. N. Mathews, Jr., and E. A. Edelsack, Eds., **2,** 625-630 (Plenum Press, New York, N.Y., 1973).

Key words: Critical magnetic field; heat capacity; Josephson junctions; noise thermometry; superconductive fixed points; superconductivity; thermometry.

Various properties of superconductors show monotonic temperature dependences, so that in principle they may be used as thermometric parameters. Other properties can be utilized in devices which find convenient application in thermometry. Of the many possible examples, we will examine several which have found some actual use either as thermometers or detectors in thermometry.

Schroder, I. G., **Emission of long-range α-particles in the subthermal-, thermal- and resonance-neutron fission of ^{239}Pu,** *Nucl. Phys.* **A195,** 257-268 (1972).

Key words: Alpha-particle; emission; fission; neutron; reactor; ^{239}Pu.

An investigation has been made of the possible dependence of the binary-to-ternary fission ratio as well as of the energy distribution of the long-range α-particles emitted in the low-energy fission of ^{239}Pu

on the energy of the incident neutron. To this effect a number of relative measurements have been made using three neutron filters covering, respectively, the subthermal-, thermal- and resonance-neutron regions. Furthermore, a measurement of the binary-to-ternary fission ratio has been performed for a reactor beam. The results obtained show no variation in the binary-to-ternary fission ratio or in the energy of the long-range α-particles for the energy intervals considered to within the precision of these measurements. The measurement with the reactor beam yielded a value of the binary-to-ternary fission ratio of 412 ± 11.

Siu, C. I., Ellis, W. M., Kusuda, T., **Test of a polyester composite wall panel for moisture accumulation and potential removal of moisture through venting,** *NBSIR 73-220*, 18 pages (May 1973). (Available as PB 222437 from the National Technical Information Service, Springfield, Va. 22151.)

Key words: Composite wall panel; condensation; humidity; moisture; pressure; temperature.

A polyester composite exterior wall panel was exposed to accelerated winter temperature and humidity conditions for the purpose of determining performance with respect to moisture accumulation and release as a result of pressure and temperature differences. No moisture condensation within the wall system was detected from visual examinations made at various times of the testing period; no significant increase in gross weight of the wall was found from the direct weighings of the wall system. Results also indicate that a wet insulation in such a wall system is unlikely to be dried out by natural thermal action and convective motion.

Slattery, W. J., **Standards information for your company,** *Stand. Eng.* **25,** No. 3, p. 22, (June 1973).

Key words: Company; information; standardization; standards.

The Standards Information Services Section of the National Bureau of Standards (NBS-SIS) maintains the largest reference collection of engineering and related standards, specifications, test methods, codes and recommended practices in the United States. From its original holdings of several thousand standards, NBS-SIS now maintains an extensive reference collection of over 122.000 standards issued by U.S. industry associations, federal and state governmental organizations, and foreign national and international standardizing bodies. NBS-SIS serves primarily as a referral activity by identifying sources of standards, and directing inquirers to the respective standards-issuing organizations to obtain copies of standards. By means of a computer-produced Key-Word-In-Context (K-WIC) Index, more than 4,000 inquiries are answered a year. Although the majority of these requests have to date come from agencies of the U.S. Federal Government, the staff is particularly interested in receiving an increase in the number of inquiries from the corporate sector. NBS-SIS also compiles computer-produced indexes designed to assist companies and other industry groups, government organizations and anyone interested in information on standards. Requests for information may be made by personal visit, telephone or letter.

Smith, R. L., Phelan, R. J., Jr., **Limitations of the use of vacuum photodiodes in instruments for the measurement of laser power and energy,** *Appl. Opt.* **12,** No. 4, 795-798 (Apr. 1973).

Key words: Biplanar vacuum photodiodes; lasers; laser energy measurements; laser power measurements; vacuum photodiodes.

The effect of the variation in the area sensitivity upon the calibration of instruments incorporating biplanar vacuum photodiodes for the measurement of laser power and energy is discussed. A technique for the measurement of the area sensitivity is described, and the experimental results for several tubes are given. At the present time it would appear to be difficult to use biplanar vacuum photodiodes in devices to measure laser energy or power.

Somes, N. F., **Abnormal loading on buildings and progressive collapse,** *NBSIR 73-221*, 76 pages (May 1973). (Available as PB 220849 from the National Technical Information Service, Springfield, Va. 22151.)

Key words: Abnormal loading; building; codes; design criteria; multistory; progressive collapse; risk; stability; standards; strength; United States.

The document is an interim report of ongoing studies at the National Bureau of Standards. It defines the several aspects of abnormal loading on buildings and the problem of progressive collapse. It documents the extent to which present U.S. Codes and Standards address the problem.

Abnormal loadings are identified, classified and discussed with regard to their characteristics and frequencies of occurrence. The report reviews the state of international knowledge of the characteristics of abnormal loadings and the response of buildings and building elements to these loadings. The latter includes discussion of several incidents in which multistory buildings have collapsed progressively.

Using currently available statistics an estimate is made of the combined frequency of abnormal loadings on residential buildings in the U.S. For buildings susceptible to progressive collapse, the corresponding risk of fatality is compared with the levels of risk that society will generally accept. The risk is further compared with the risk of mortality associated with fire in residential buildings, an area of considerable public concern and expenditure.

It is concluded that U.S. standards-writing bodies should adopt appropriate rational criteria as soon as possible to reduce the risks of progressive collapse. There are several areas in which criteria might be introduced to reduce the risk of progressive collapse. These are discussed; particular attention is given to the philosophies behind the structural criteria implemented in the USA and other countries.

Soulen, R. J., Jr., Schooley, J. F., **Superconducting transition widths and reproducibilities,** (Proc. XIIIth Int. Congress of Refrigeration, Washington, D.C., Aug. 27-Sept. 3, 1971), Paper in *Progress in Refrigeration Science and Technology* **1,** 399-403 (Avi Publ. Co., Inc., Westport, Conn., 1973).

Key words: Superconductivity; thermometry, transition temperature.

As part of a program to investigate the possibility of utilizing superconductive transitions as reference points on a cryogenic temperature scale, we are examining the transitions of samples with different purities and with various metallurgical histories. In our initial efforts, we examined the transition widths of Pb, Sn, In, Al, Ga, Zn and Cd wires using short mutual inductance coils to avoid end effects. As we reported at the XII Int. Conf. on Low Temperature Physics, all but the Sn and Cd samples showed transition widths of 10^{-3} K or less, and repeated examination of the widths over an extended period of temperature cycling showed no drift or broadening of the five narrow transitions larger than 10^{-3} K.

We are now preparing samples of Pb, In, Al, Zn and Cd with various impurities and with various forming and annealing procedures in order to determine the practical boundary conditions for obtaining a given transition temperature and transition width. We are attempting to extend this study to low temperature (Ir, $T_c \approx 0.1$ K) and high-temperature (Nb_3X, V_3Si, $T_c = 15 - 20$ K) materials, although intitial experiments show transition widths of $0.1 - 0.3$ K for the latter.

Smith, R. L., Honda, T., **Impulse rise and fall times of biplanar vacuum photodiodes,** *Appl. Opt.* **12,** No. 7, 1606-1610 (July 1973).

Key words: Biplanar vacuum photodiodes; impulse fall time; impulse rise time; laser pulses.

The impulse rise and fall times of biplanar vacuum photodiodes are experimentally investigated by the use of a single ultrashort laser pulse from a train of mode-locked pulses. It was confirmed that the impulse rise time is a function of the photoelectrons' transit time from photocathode to anode, and that the impulse fall time is 2.2 times the capacitance of the photodiode and the resistive component of the load.

Straty, G. C., Younglove, B. A., **Velocity of sound in saturated and compressed fluid oxygen,** *J. Chem. Thermodyn.* **5,** No. 3, 305-312 (May 1973).

Key words: Compressed liquid; compressibility; saturated liquid; sound velocity oxygen; specific heat ratio.

In a continuing effort to generate accurate thermodynamic and transport properties of cryogenic fluids, we have measured the velocity of sound in saturated liquid oxygen from 58 to 150 K and in compressed fluid oxygen along isotherms from 70 to 300 K at pressures to 34 MPa. The results have been used along with previously measured p, ρ, T results to obtain the isentropic compressibility and the heat capacity ratio, and to examine the quality of the p, ρ, T data by comparison of the measured velocities with velocities calculated from these data.

Sugar, J., **Ionization energies of the neutral actinides,** *J. Chem. Phys.* **59,** No. 2, 788-791 (July 15, 1973).

Key words: Actinium; americium; berkelium; californium; curium; einsteinium; fermium; ionization energy; mendelevium; neptunium; nobelium; plutonium; protactinium; thorium; uranium.

Values for the ionization energies of the neutral actinides have been derived by utilizing interpolated spectral properties of these atoms. The results in electron volts are Ac: 5.17(12); Th: 6.08(12); Pa: 5.89(12); U: 6.05(7); Np: 6.20(12); Pu: 6.06(2); Am: 5.993(10); Cm: 6.09(2); Bk: 6.30(9); Cf: 6.41(10); Es: 6.52(10); Fm: 6.64(11); Md: 6.74(12); No: 6.84(12).

Sullivan, D. B., **Precise electrical measurements at low temperature,** *Proc. 1972 Applied Superconductivity Conf., Annapolis, Md., May 1-3, 1972,* pp. 631-639 (IEEE, Inc., New York, N.Y., 1972).

Key words: Fundamental constants; Josephson effect; precise electrical measurements; superconductivity.

The application of low temperature phenomena to electrical metrology is reviewed. The review includes a number of recent developments which involve measurement systems based on the quantum of magnetic flux as well as adaptations of classical concepts to low temperature devices. Quantities considered include radio frequency current, infrared frequency, and direct current and voltage. Concepts for secondary emf standards are also discussed.

Swartzendruber, L. J., Evans, B. J., **Local interactions and spin transfer mechanisms in the Heusler-type alloys $Pd_{1+x}MnSb$ and $Pd_2MnSb_{0.9}Sn_{0.1}$,** (Proc. 18th AIP Conf. on Magnetism and Magnetic Materials, Denver, Colo., Nov. 28-Dec. 1, 1972), Paper in *Magnetism and Magnetic Materials,* C. D. Graham, Jr., and J. J. Rhyne, Eds., No. 10, 1369-1373 (American Institute of Physics, New York, N.Y., 1973).

Key words: Alloys; antimony; hyperfine fields; manganese; Mössbauer effect; palladium, tin.

The magnetic hyperfine fields at ^{121}Sb, $H_{eff}(Sb)$, in the Heusler-type alloys $Pd_{1+x}MnSb$ are found to be strongly dependent on x, varying from about 600 kG for $x=1$ to about 300 kG for $x=0$. As x is decreased from unity, the single unique value observed in Pd_2MnSb is replaced by a distribution in $H_{eff}(Sb)$, with an average value which decreases in a regular manner with the number of Pd vacancies. In $Pd_2MnSb_{0.9}Sn_{0.1}$, $H_{eff}(Sn)$ is found to be similar in magnitude to $H_{eff}(Sn)$ in Pd_2MnSn. Both these results indicate that local spin transfer mechanisms are important in determining the magnitude and sign of H_{eff} at the Sb site in Heusler-type alloys.

Tilford, C. R., **A fringe counting laser interferometer manometer,** *Rev. Sci. Instrum.* **44,** No. 2, 180-182 (Feb. 1973).

Key words: Fringe counting; laser interferometer; manometer.

A prototype standard mercury manometer using a fringe counting laser interferometer to measure the differential height of the mercury columns has been built and successfully operated. The 10.6 μ wavelength radiation from a CO_2 laser and specially treated manometer tubes have been used to reduce the effect of disturbances on the mercury surface so that reliable operation of the manometer is possible.

Tsai, D. H., MacDonald, R. A., **Second sound in a solid under shock compression,** *J. Phys. C: Solid State Phys. Letter to Editor* **6,** L171-L175 (1973).

Key words: Crystalline solid; iron; molecular dynamics; second sound; shockwave; thermal relaxation; three dimensions.

The propagation of a strong shock wave in a perfect, three-dimensional crystalline lattice is studied by means of molecular-dynamical calculations. The results show that behind the shock front there is a region of thermal relaxation which increases with time. The thermally relaxed region, therefore, propagates with a velocity lower than that of the shock front. It is believed that the wave-like propagation of this thermally equilibrated region is a natural extension of second sound from the conventional low-temperature, low-pressure régime to the high-temperature, high-pressure régime. The implication of this phenomenon on *PVT* calculations from shock-wave data is discussed briefly.

Waterstrat, R. M., Dickens, B., **The crystal structure of V_3Rh_5,** *J. Less-Common Metals* **31,** 61-67 (1973).

Key words: Atomic ordering; crystal structures; intermetallic compounds; rhodium alloys; vanadium alloys.

The crystal structure of the phase V_3Rh_5 has been elucidated. The unit cell is orthorhombic with $a=5.420$ Å, $b=9.276$ Å, $c=4.320$ Å and $Z=2$; the space group is either $Cm2m$ or $Cmcm$. The structure is close-packed and contains both ordered and disordered atomic sites. It is intermediate between the structures of the Cu_3Au and CuAu types except that it possesses a two-layer stacking sequence.

Waterstrat, R. M., Manuszewski, R. C., **The chromium-rhodium constitution diagram,** *J. Less-Common Metals* **32,** 331-343 (1973).

Key words: Chromium alloys; constitution diagram; equilibrium diagram; phase diagram; rhodium alloys.

The Cr-Rh alloy system has been studied over the entire composition range by metallography, X-ray diffraction and electron microprobe methods. There are two intermediate phases in this system. The ϵ phase has a hexagonal close-packed structure and is stable over a broad composition range from about 20 at.% Cr at 900 °C to 68 at.% Cr at 1475 °C. The β phase possesses a $Cr_3Si(A15)$ type structure and is stable over a narrow composition range from about 77 to 78 at.% Cr. The location of the face-centered cubic (γ Rh) to hexagonal close-packed (ϵ phase) transition is strongly temperature dependent. Precipitation of a metastable hexagonal close-packed structure occurs during rapid cooling of the body-centered cubic (α-Cr) solid solution. A peritectic reaction exists at 1700 ± 10 °C, a eutectic reaction occurs at 1475 ± 10 °C, and peritectoid reaction is located at 1265 ± 12 °C.

Wells, J. S., **A stabilized HCN laser for infrared frequency synthesis,** *IEEE Trans. Instrum. Meas. IM-22*, No. 2, 113-118 (June 1973).

Key words: HCN laser; infrared frequency synthesis; laser frequency measurements; laser stabilization; laser metrology; phase locked laser.

Infrared frequencies have recently been synthesized in suitable diodes up to 88 THz with accuracies of parts in 10^9. Stabilized lasers are necessary in order to make frequency measurements of higher accuracy. The hydrogen-cyanide laser is the lowest frequency basis laser used in these synthesis schemes, and its stabilization has been the subject of recent interest. The laser is stabilized by locking it to a phase-locked microwave reference chain. Two servo loops are utilized. The first loop is a relatively slow frequency-lock loop with the correction applied to a piezoelectric-translator driver. This loop not only accommodates thermal expansion of the laser, but also serves as an acquisition aiding loop for the second servo. The latter is a phase-locked system with the correction applied to the laser discharge current controller. Data regarding the system stability are presented.

Zimmerman, J. E., Siegwarth, J. D., **Portable helium dewars for use with super-conducting magnetometers,** *Cryogenics* **13,** No. 3, 158-159 (Mar. 1973).

Key words: Dewar; gas shielded; helium; liquid; magnetometer; multilayer insulated.

Simple helium dewars have been constructed using gas-cooled radiation shields and multilayer aluminized plastic insulation. They will retain one litre of liquid for up to 40 hours. The shields may be made mostly non-conducting so the dewar can be used with ultrasensitive superconducting magnetometers. For most other applications thin sheet metal such as copper or aluminium is suitable for the shields.

**Publications with prices and SD Catalog numbers may be purchased directly from the Superintendent of Documents, U.S. Government Printing Office, Washington, D.C. 20402 (foreign: one-fourth additional). Microfiche copies are available from the National Technical Information Service (NTIS), Springfield, Va. 22151. Reprints from outside journals and the NBS Journal of Research may often be obtained directly from the authors.*

U. S. GOVERNMENT PRINTING OFFICE : 1974 O - 525-013

UNITED STATES
GOVERNMENT PRINTING OFFICE
PUBLIC DOCUMENTS DEPARTMENT
WASHINGTON, D.C. 20402

OFFICIAL BUSINESS
PENALTY FOR PRIVATE USE $300

POSTAGE AND FEES PAID
U.S. GOVERNMENT PRINTING OFFICE
375

JOURNAL OF RESEARCH of the National Bureau of Standards
A. Physics and Chemistry

Vol. 78A, No. 1 Jan.–Feb. 1974

SJRA UNIVE300UA R 1
UNIVERSITY MICROFILMS INC
ATTN SERIALS SECTION
300 NORTH ZEEB RD
ANN ARBOR MI 48106

Contents

Page

Thermophysical measurements on iron above 1500 K using a transient (subsecond) technique. Ared Cezairliyan and J. L. McClure. 1

Measurement of melting point, normal spectral emittance (at melting point) and electrical resistivity (near melting point) of some refractory alloys. Ared Cezairliyan. 5

Comparative density measurements for solid specimens weighing a few milligrams. A. D. Franklin and J. R. Donaldson. 9

A density scale based on solid objects. Horace A. Bowman, Randall M. Schoonover, and C. Leon Carroll. 13

Geometrical considerations in the measurement of the volume of an approximate sphere. Daniel P. Johnson. 41

Note on diffusion of vapor into flowing gas. Daniel P. Johnson. 49

Theoretical analysis of miscibility gaps in the alkali-borates. Pedro B. Macedo and Joseph H. Simmons. 53

Publications of the National Bureau of Standards. 61

Library of Congress Catalog Card Number: 62–37059

For sale by the Superintendent of Documents, U.S. Government Printing Office, Washington, D.C. 20402. (Order by SD Catalog No. C 13.22/sec.A:78/1). Single copy price varies. This issue $3. Subscription price $17.00 a year; $4.25 additional for foreign mailing.

UNITED STATES GOVERNMENT PRINTING OFFICE, WASHINGTON : 1974